University of Navarra

Faculty of Science

ANALYSIS OF THE REGENERATIVE POTENTIAL OF THE INDUCED PLURIPOTENT STEM CELLS IN A MODEL OF ACUTE MYOCARDIAL INFARCTION IN MICE

DOCTORAL THESIS

Olalla Iglesias García

Pamplona, February 2013

University of Navarra

Faculty of Science

ANALYSIS OF THE REGENERATIVE POTENTIAL OF INDUCED PLURIPOTENT STEM CELLS IN A MODEL OF ACUTE MYOCARDIAL INFARCTION IN MICE

A dissertation by **Olalla Iglesias García** in partial fulfillment of the requeriments for the degree of Doctor of Molecular and Cellular Biology by the University of Navarra.

This work has been conducted under our supervision at the Area of Cell Therapy, Division of Oncology, CIMA, University of Navarra.

We thereby authorize its presentation to the Thesis Committee for evaluation.

Pamplona, February 2013

Dr. Felipe Prósper Cardoso   Dra. Beatriz Pelacho Samper

Director   Co-director

No son los vestíbulos de mármol los que proporcionan la grandeza intelectual, sino el alma y el cerebro del investigador

Alexander Fleming
Premio Nobel de Medicina
1945

A la memoria de mi abuela Petra

ACKNOWLEDGEMENTS

A Sulay y Pablo, por vuestro apoyo y ayuda y por los grandes momentos vividos en Colonia.

A mis amigas de la facultad, Maria José, Ana, Carolina, Inma, Ana A., Ana M., Maite LL., Maite M., Lucía e Irene, por todos los buenos momentos, por hacer que mis años en Salamanca hayan sido unos de lo mejores de mi vida y porque aunque hayan pasado los años seguimos siendo grandes amigas.

A mis hermanos Ivo y Millán, gracias por cuidarme.

A mi hermana Nadia, porque sabes que no me gusta decirte cuñada, gracias por formar parte de mi vida.

A mi sobrino Ivito, gracias por existir, porque me alegras el día, porque eres mi tesoro.

A Sandra por cuidar de mis padres.

A mis padres porque, si hay unos padres perfectos, vosotros lo sois. Gracias papá, gracias mamá, por los esfuerzos que habéis hecho para que pudiera formarme, por inculcarme los valores de la vida, por vuestra generosidad y humildad, por demostrarme vuestro amor cada día. Os quiero más que a nada en este mundo.

A mi familia canaria, Miriam, Fernando, David y Dani, gracias por hacerme sentir en el paraíso y por quererme.

Al amor de mi vida, mi alegría, mi felicidad. Fer, gracias por cruzarte en mi camino, porque me sacaste del círculo y ahora vamos hacia delante juntos. Gracias por quererme, entenderme, valorarme, porque junto a ti los malos momentos no existen, y haces que el tiempo se pare.

A mi abuela Petra, mi ángel de la guarda que supo transmitirme el amor por la vida y por la ciencia, por su generosidad, porque siempre daba todo y nunca esperaba nada a cambio. Por su sabiduría, por enseñarme que se viene a la vida para ser útil a los demás, porque me enseñó que con esfuerzo e ilusión todo es posible. Te llevo siempre en mi corazón.

TABLE OF CONTENTS

ABREVIATIONS

αMhc: Alpha myosin high chain

βMhc: Beta myosin high chain

α-SMA: Alpha-smooth muscle actin

5-AZA: 5-azacytidine

A-83-01: TGFβ inhibitor

AA: Ascorbic acid

ABCA1: ATP-binding cassette transporter

ACAT1: Acetyl-coA cholesterol acyltransferase 1

ADSC: Adipose derived stem cells

AKT: Serine/threonine-specific protein kinase

ALS: Amyotrophic lateral sclerosis

ANP: Atrial natriuretic peptide

AP: Action potential

APD50: Action potential duration at 50% repolarization

APD90: Action potential duration at 90% repolarization

Aread: End-diastolic area

Areas: End-systolic area

bFGF: Basic fibroblast growth factor

BM-MNCs: Bone marrow-derived mononuclear cells

BMPs: Bone morphogenetic proteins

BNP: Brain natriuretic peptide

BSA: Bovine serum albumin

C/Ebpα: CCAAT/enhancer-binding alpha

C/Ebpβ: CCAAT/enhancer-binding beta

Cacna1c: L-type calcium channel

cDNA: Complementary deoxyribonucleic acid

CDy1: Testis specific chromodomain protein y1

cMLCK: Cardiac myosin light chain kinase

CMs: Cardiomyocytes

CPC: Cardiac progenitors cells

CpG: cytosine-phosphate guanine

CPP: Cell-penetrating peptide

cTnT: Cardiac troponin T

CVD: Cardiovascular diseases

CVF: Collagen volume fraction

Cx43: Connexin 43

Davi: Left ventricule internal diameter at apical level

Dbvi: Left ventricule internal diameter at basaline level

DKK1: Dickkopf 1 homolog

DMD: Duchene muscular dystrophy

DMEM HG: High glucose Dulbeccos´s modified eagle medium

DMEM: Dulbeccos´s modified eagle medium

DMSO: Dimethyl sulfoxide

Dmvi: Left ventricule internal diameter at middle level

DNA: Deoxyribonucleic acid

EBs: Embryoid bodies

ECM: Extracellular matrix

ECs: Endothelial cells

EDTA: Ethylenediaminetetraacetic acid

EF% simp: Ejection fraction using Simpson´s rule

EF% tei: Ejection fraction using Teichholz

EF: Ejection fraction

EFG: Epidermal growth factor

EMINLIN2: Elastin microfibril interf 2

END-2: Endoderm-like cell line

eNOS: Endothelial nitric oxide synthase

EPCs: Endothelial progenitors cells

ErbB: Erytroblastic leukaemia viral oncogene homolog tyrosine kinase membrane receptor

Erk: Extracellular signal-regulated kinase

ESC: Embryonic stem cells

ESC-CMs: Cardiomyocytes derived from embryonic stem cells

ESC-ECs: Endothelial cells derived from embryonic stem cells

ESRRB: Orphan nuclear receptor ERRbeta

FAC% long: Fractional area change measured in a long-axis

FAC% short: Fractional area change measured in a short-axis

FAC: Fractional area change

FAK: Focal adhesion kinase

FBS: Fetal bovine serum

FGF: Fibroblast growth factor

Flk-1: Fetal liver kinase 1

FS% tei: Fractional shortening using Teichholz

FS: Fractional shortening

G-CSF: Granulocyte colony-stimulating factor

GFP: Green fluorescent protein

GMEM: Glasgow minimum essential medium

GSK3: Glycogen synthase kinase 3

Hcn1: Potassium/sodium channel

HD: Huntington´s disease

hESC: Human embryonic stem cells

hESC-CMs: Cardiomyocytes derived from human embryonic stem cells

HGF: Hepatocyte growth factor

hiPS: Human induced pluripotent stem cells

HR: Heart rate

hTERT: Human telomerase reverse transcriptase

IA: Infarcted area

IGF-1: Insulin-like growth factor 1

IHD: Ischemic heart disease

IL: Interleukin

INS: Insulin

iPS: Induced pluripotent stem

iPS-CMs: Cardiomyocytes derived from induced pluripotent stem cells

Isl1: Islet1

KDR: Kinase insert domain receptor

Klf4: Krüppel-like factor 4

LAD: Left anterior descending coronary artery

LDL: Low-density lipoproteins

LI-BEL: Low insulin, bovine serum albumin, essential lipids media

LIF: Leukemia inhibitory factor

LV: Left ventricle

LVA: Left ventricular area

MAPK: Mitogen-activated protein kinase

MCP-1: Monocyte chemoattractant protein-1

MDP: Maximal diastolic potential

Mef2c: Myocyte-specific enhancer factor 2C

MEFs: Mouse embryonic fibroblasts

MEK: Mitogen-ativated enzyme kinase

mESC: Mouse embryonic stem cells

mESC-CMs: Cardiomyocytes derived from mouse embryonic stem cells

MI: Myocardial infarction

miPS: Mouse induced pluripotent stem cells

miPS-CMs: Cardiomyocytes derived from mouse induced pluripotent stem cells

Mlc2a: Myosin light chain 2 atrial

Mlc2v: Myosin light chain 2 ventricular

MMPs: Matrix metalloproteinases

mRNA: Micro-ribonucleic acid

NaB: Sodium butyrate

NO: Nitric oxide

NPC: Neural progenitors cells

NRG-1: Neuregulin protein 1

NSCs: Neural stem cells

o/n: Overnight

Oct3/4: Octamer-binding transcription factor 3/4

OSKM: Oct3/4, Sox2, Klf4, c-Myc

p.c.: post coitum

PB: Phosphate buffer

PBS: Phosphate buffer saline

PDK1: Pyruvate dehydrogenase kinase 1

PEG: Poly ethylene glycol

PI3K: Phosphatidylinositol-3-kinase

PLGA: poly-lactic-co-glycolic

PLLA: Poly-l-lactic acid

Pln: Phospholamban

qPCR: Quantitative polymerase chain reaction

R/T: Room temperature

RAAS: Renin-angiotensin-aldosterone system

rhNRG-1β: Recombinant human neuregulin protein 1β

RNA: Ribonucleic acid

ROS: Reactive oxygen species

RPMI: Roswell Park Memorial Institute medium

RT: Reverse transcription

Ryr2: Ryanodine receptor 2

SAHA: Suberoylanilide hydrozamic acid

Sca1: Stem cell antigen 1

SCF: Stem cell factor

SDF-1: Stromal derived factor-1

siRNA: Small-interfering RNA

SIRPA: Signal regulatory protein α

Sm22α: Smooth muscle 22 alpha

Sox2: SRY (sex determining region Y)-box 2

SV: Stroke volume

SV40 LT: Simian vacuolating virus 40 large T antigen

SVF: Stromal vascular fraction

TBS: Tris buffer saline

TGF-β: Transforming growth factor-β

TIMPs: Inhibitors of metalloproteinases

TLR: Toll-like receptor

TNF-α: Tumoral necrosis factor-α

Tri-P: Tricell patch

TSA: Trichostatin A

Utf-1: Undifferentiated embryonic cell transcription factor 1

VCAM1: Vascular cell adhesion molecule 1

VD: Volume in diastole

VEFG: Vascular endothelial growth factor

Vmax: Maximal upstroke velocity

VPA: Valproic acid

VS: Volume in systole

vWF: Von Willebrand factor

Wnt: Wingless

Wnt3a: Wnt family protein

INTRODUCTION

1. CARDIOVASCULAR DISEASE: EPIDEMIOLOGY, DISEASE AND THERAPY

1.1. Epidemiology and risk factors

Cardiovascular diseases (CVD) constitute the first cause of morbidity and mortality worldwide and represents approximately 30% of all deaths (**Figure I1**), being the myocardial infarction (MI) responsible for nearly half of them. Unfortunatelly, predictions are not favorable and it is estimated that by 2030, almost 24 million people will die from cardiovascular diseases, representing 42% of global deaths (In: www.who.int/mediacentre/factsheets). The major risk factors associated with ischemic heart disease (IHD) are tobacco and alcohol consumption, hypertension, high cholesterol, obesity, diabetes and physical inactivity [1] that can be also associated with non-modifiable factors like aging, family history, gender and ethnic origin.
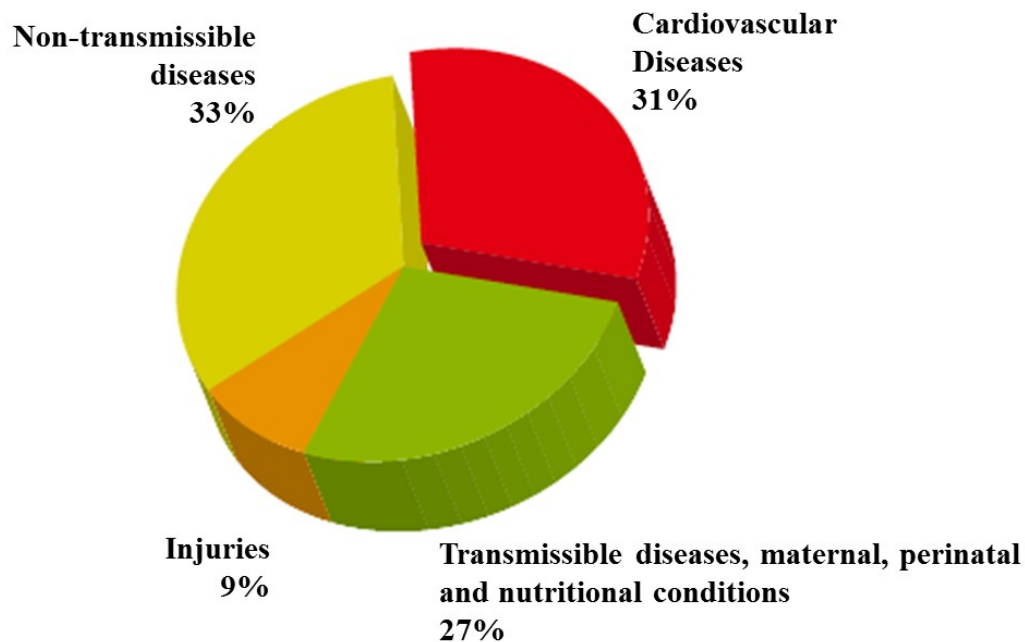
Figure I1. Distribution of major causes of death including cardiovascular diseases (CVD). (Image taken from Global Atlas on Cardiovascular Disease Prevention and Control. World Health Organization, 2011).

1.2. Myocardial infarction pathology

MI is induced when cholesterol plaques or thrombi partially or totally block the arteries, limiting the blood supply to the heart and thereby preventing the required oxygen and nutrients from reaching the heart tissue (**Figure I2**). Over time, the damage becomes irreversible and it is accompanied by cell death and tissue necrosis. A compensatory mechanism of tissue remodeling is activated and a fibrotic scar that avoids heart rupture substitutes the damaged area. With time, this process becomes a chronic maladaptive response that leads to contractile dysfunction, arrhythmias and heart failure [2].

The atherosclerosis represents the principal cause of vascular occlusion [3] (**Figure I2**). This phenomenon occurs due to chronic inflammation of the arterial vessels in response to irritative stimuli. Arterial endothelial cells express adhesion molecules that capture leukocytes on their surfaces.
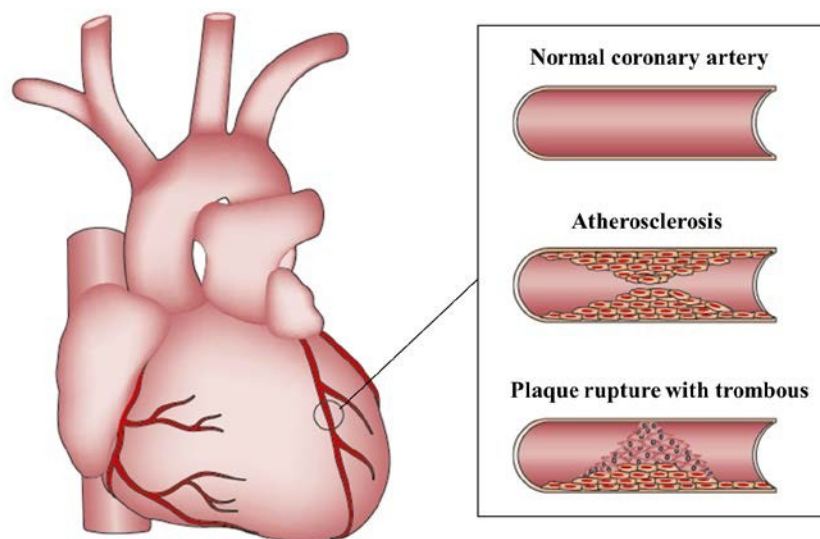
Figure I2. Atherosclerosis in coronary arteries. Atherosclerosis plaques grow in the coronary artery blocking the blood flow. Ruptures of the fibrous cap of the plaque expose thrombogenic material to the circulation and induce thrombus formation in the lumen of the vessel, provoking the isquemic cardiac process (Image modified from *Thygesen K et al. Nat Rev Cardiol, 2012*).

Changes in the endothelial permeability and in the extracellular matrix (ECM) composition promote the entry and retention in the artery wall of cholesterol-containing-low-density lipoproteins (LDL) particles together with the migration of

inflammatory cells to the lumen of the artery, which leads to the release of matrix metalloproteinases (MMPs) by fibroblast-like cells that promote the degradation of the ECM. Finally, these processes lead to the rupture of the atherome plaque by activating thrombus formation and fibrin accumulation, which provoke a partial or total occlusion of the vessel and ischemia of the tissue supplied by that vessel.

Since the heart presents strict metabolic requirements and, in anoxic conditions, it is not capable to produce enough energy to maintain its functionality, the constant supply of oxygen is essential [4]. Thus, in ischemic conditions, a cascade of events initiates within 10 seconds of occlusion that include: cessation of aerobic metabolism, depletion of creatine phosphate, anaerobic glycolisis onset and accumulation of products of anoxic metabolism. After 60 seconds of ischemia, the cardiomyocytes (CMs) lose their contractile capacity and in few minutes, cell ultrastructural changes like mitochondrial swelling start. After 40-60 minutes the damage is irreversible, with marked sarcolemmal damage and abnormal mitochondria density and four-six hours later, the necrosis of the cardiac muscle is already evidenced.

The acute loss of myocardium results in the activation of remodeling mechanisms, which initiates and subsequently modulates reparative changes that include dilatation, hypertrophy and collagen scar formation. Ventricular remodeling may continue for weeks, months or years until the distending forces are counterbalanced by the tensile strength of the collagen scar. All these compensatory mechanisms can be divided in three phases: 1) inflammatory phase; 2) formation of granulation tissue or proliferative phase and 3) scar maturation phase (**Figure I3**).

1) Inflammatory phase: After CMs death, their intracellular content is released, initiating an inflammatory response by activation of compensatory mechanisms of the innate immunity. The complement cascade is activated [5], reactive oxygen species (ROS) are generated in the ischemic myocardium and Toll-like receptor (TLR) signalling pathways are activated inducing the release of numerous inflammatory cytokines like the tumoral necrosis factor-α (TNF-α), the interleukins (IL)-1β and IL-6 [6] and chemotactic active molecules such as the monocyte chemoattractant protein-1 (MCP-1) or the stem cell factor (SCF) [7]. These biological reactions are involved in the time-course of remodeling after the ischemic episode and induce important structural and functional changes in the CMs [8, 9]. On the other hand, the release of inflammatory cytokines induces also activation of the MMPs [10] and collagen

deposition, which contribute to the structural changes and tissue repair of injured myocardium. The activated MMPs degrade the ECM, disrupting the fibrillar collagen network and allowing the inflammatory cells to migrate into the damaged tissue to remove the necrotic CMs [11]. Infarct expansion occurs within hours of CMs injury and with time, results in wall thinning and abnormal ventricular dilation, causing the elevation of diastolic and systolic wall stress.
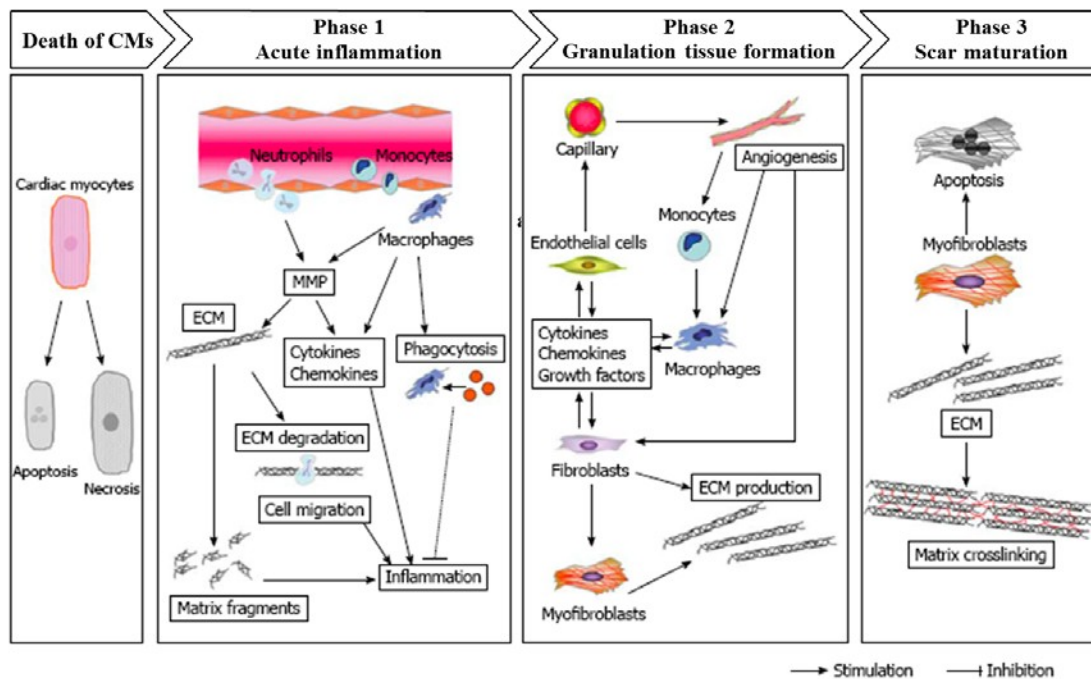
Figure I3. Phases of cardiac remodeling after MI (Image adapted from *Matsui Y et al. Worl J Biol Chem, 2010*).

2) Formation of granulation tissue or proliferative phase: During this stage, several mechanisms are activated to induce the revascularization of the damaged tissue. Cardiac endothelium and inflammatory cells activate the release of chemoattractant factors such as the stromal derived factor-1 (SDF-1) or the IL-8 [12] that are involved in the recruitment of vascular progenitors to the injured area. Among these progenitors, it has been demonstrated in mice that the attraction of monocytes that express low levels of Ly-6C (low) promote tissue healing via myofibroblasts accumulation, formation of new blood vessels and collagen deposition [13]. Accumulation of fibroblasts and monocytes into the injured area promotes the formation of deposits of fibronectin allowing the creation of a second matrix and inducing the release of anti-inflammatory

cytokines such as the transforming growth factor-β1 (TGF-β1) [14], IL-10 [15] and the tissue inhibitors of MMPs (TIMPs). These low-molecular-weight proteins form high affinity complexes with the activated MMPs, inhibiting them [16] and neutralizing collagen degradation to allow the beginning of the third phase.

3) Scar maturation phase: During infarct scar maturation, the provisional matrix deposited during early remodeling phases is stabilized. Myofibroblasts play an important role in this stage by releasing TIMPs that inhibit the degradation of the ECM and induce deposition of new collagen fibers that contribute to the scar formation and prevent ventricular dilatation and heart rupture [17]. Moreover, circulatory hemodynamics are disturbed triggering the activation of the sympathetic adrenergic system, stimulating catecholamine synthesis and activating the rennin-angiotensin-aldosterone system (RAAS) that leads to the production of atrial and brain natriuretic peptides (ANP and BNP). The natriuretic peptides will reduce intravascular volume and systemic resistance, normalizing ventricular dilatation and finally improving pump function [18].

Thus, cardiac remodeling process includes a cascade of molecular and cellular mechanisms that modulates reparative changes to maintain the functionality of the heart. However, the very modest regenerative capacity of the adult cardiac tissue can not prevent the presence of the scar in the myocardium and the deleterious progress of the injured heart, being necessary exogenous cells/factors to facilitate a positive heart remodeling.

1.3. Evaluation of left ventricular function in myocardial infarction

Early expansion of the infarcted zone is associated with left ventricle (LV) dilation which is caused by the increase of regional wall stress [18]. Between one half to one third of the patients experience progressive post-infarction heart dilatation with distortion of ventricular geometry and secondary mitral regurgitation [19]. Quantitative bi-dimensional transthoracic echocardiography is routinely performed to characterize the heart remodeling associated with these cardiomyopathies [20, 21], LV end-diastolic and end-systolic volumes and LV mass being estimated to predict adverse cardiovascular follow-up events, including recurrent infarction, ventricule arrhythmias, mitral regurgitation and heart failure [21].

Pig and rodent MI animal models are commonly used to provide new insights into the physiology and treatment of cardiovascular diseases. In these models, infarction is tiggered by the temporary or permanent occlusion of the left anterior descending (LAD) coronary artery and cardiac function determined by echocardiography or magnetic resonance imaging (MRI) is impaired [22-27]. For rodent models, specific high-resolution echocardiographic equipment like the Vevo 770 (VisulaSonics, Toronto, Canada) is available [28], providing a fast and inexpensive alternative to magnetic resonance imaging.

Evaluation of the LV systolic function is usually performed by measuring common parameters like the volume in diastole (VD), volume in systole (VS), fractional shortening (FS%) and ejection fraction (EF%) [29]. Both ventricular volumes VD and VS are required to calculate the FS% and EF% parameters. FS% corresponds to the fraction of any diastolic dimension that is lost in systole and EF% represents the volumetric fraction of blood pumped out of the ventricule. Both parameters are used to estimate myocardial contractility. Damage to the muscle of the heart, such as that provoked after MI, compromises the heart´s ability to perform as an efficient pump and therefore, a reduced EF% and FS% are observed that indicate a worsening of cardiac function. On the other hand, the LV function can also be measured as the percentage of change in the left ventricular cross-sectional area between diastole and systole (fractional area change, FAC%), which has been found to correlate well with the EF% both in normal situations and when disease is present [30]. These parameters are routinely calculated using the Teichholz method [31], which assumes that the left ventricular cavity can be represented as a 3D ellipsoid of revolution. However, this might not be a reasonable assumption when the LV adopts the complex shapes caused by the regional wall motion abnormalities that are common after MI. Therefore, an alternative approach to calculating EF% exists, which is based on the shape independent Simpson´s rule [22, 32, 33], where the 3D geometry of the heart is taken into account as the LV endocardial border is traced in multiple slices both in systole and diastole and the volumes are computed from these tracings.

1.4.   Treatment of myocardial infarction: Stem cell therapy

Medical advances at the pharmacological, interventional and surgical levels have greatly improved, significantly decreasing the rate of mortality at the acute stage of the disease and prolonging the patient's life expectancy. However, despite this progress, the current treatments are not able to regenerate the diseased heart and cannot offer a definitive cure. In the most severe cases, heart transplantation is the only option, but it presents the concomitant limitations of immunocompatibility and donor unavailability. In view of this worrisome scenario, new alternative options based on the application of gene (reviewed in [34]), protein (reviewed in [35]) and stem cells therapies (reviewed in [36]) have been intensively researched. Hopes have been placed in stem cell research (**Figure I4**), considering it a promising therapy that could exert not only a protective but a regenerative effect.
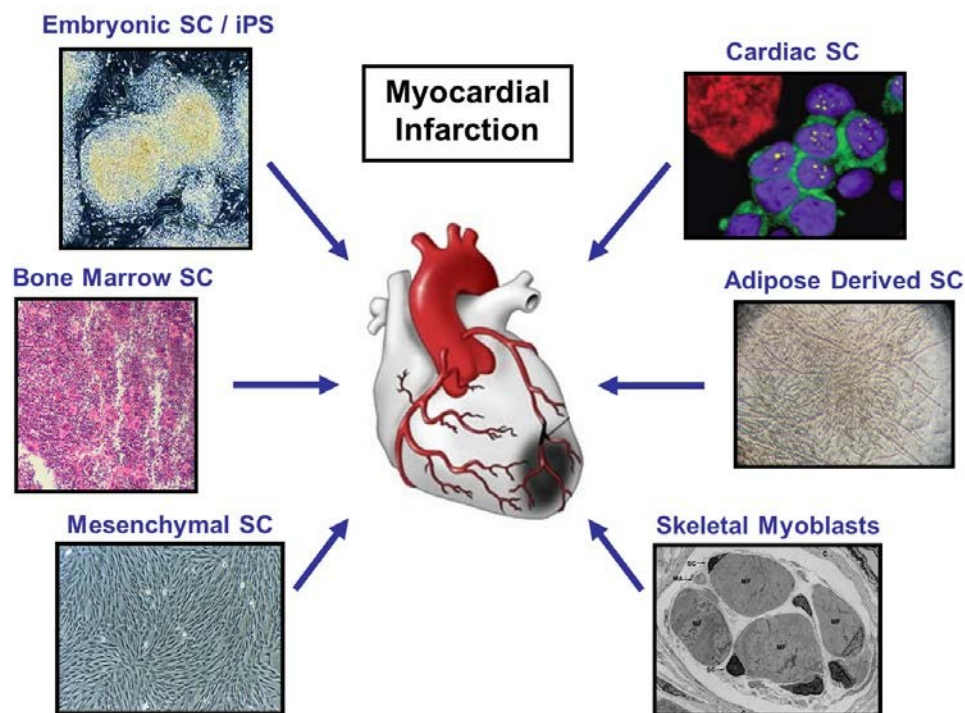
Figure I4. Stem cell therapy for treating myocardial infarction. Many stem cell (SC) populations have been tested for cardiac regeneration, going from the most undifferentiated ones, the embryonic stem cells (ESC) or the recently discovered induced pluripotent stem (iPS) cells, to stem cells derived from adult tissues like the bone marrow, the adipose tissue or the skeletal and cardiac muscle.

Interestingly, it is now known that the main mechanism of action of the transplanted cells was not the initially expected, and a trophic effect instead of a direct

contribution to the tissue after *in vivo* differentiation, has been described as the principal one that benefits the heart. In fact, despite the reported ability of some adult stem cell populations to *in vitro* differentiate towards the cardiovascular lineages of the heart, cardiac *in vivo* contribution has been only demonstrated for few cell populations, such as those derived from the stromal vascular fraction (SVF) of the adipose tissue [37, 38] or the ones derived from the cardiac tissue (reviewed in [39]). Cardiac progenitor cells (CPC) were first described by Dr. Anversa and colleagues and were phenotypically characterized by the expression of the cKit marker in mice. Their *in vitro* and *in vivo* differentiation potential towards cardiac and vascular cells was reported together with their therapeutic potential after implantation in a murine model of acute MI [40-42]. Surprisingly, another cell population defined by the opposite phenotype, Sca-1$^+$ cKit$^-$, was also indentified and its cardiac differentiation potential when transplanted into the ischemic heart was demonstrated too [43]. Other populations like the Sca-1$^+$/cKit^{LOW}/Abcg-2$^+$ cells [44], Islet-1$^+$ cells [45, 46] and the *in vitro* derived cardiospheres [47, 48] have been described. However, despite the positive effects exerted by the cited populations *in vivo*, a limited self-renewal potential and an inefficient differentiation towards cardiomyocytes (CMs) have been generally described. Moreover, the cardiac progenitor population has not been well defined yet, since there is no consensus for its specific phenotype. A similar limitation has been found for the SVF, where, despite the fact that a certain cardiomyogenic potential has been demonstrated [49], no specific markers have been yet elucidated to define it. On the other hand, embryonic stem cells (ESC) have shown the greatest cardiac differentiation potential [50-52] although important limitations such as their tumoro- and immunogeneicity together with the ethical issues derived from their human embryonic origin, have hampered their clinical use. Finally, the discovery of the so-called induced pluripotent stem (iPS) cells [53] has emerged as an exciting alternative, as these closely resemble ESC in terms of global genetic profile, long-term self-renewal capacity and *in vitro* and *in vivo* differentiation potential (including differentiation towards the cardiovascular lineages). Moreover, iPS cells also present the advantage that they can be derived with relative straightfordwardness from adult cells, bypassing the ethical and immunogenic concerns of ESC.

2. INDUCED PLURIPOTENT STEM CELLS

2.1. Discovery and generation of iPS cells

Although the cell differentiation process was believed to be irreversible, in 2006, the laboratory of the current Nobel prize winner Dr. Yamanaka reported the generation of embryonic stem-like cells from somatic cells that were named as "induced pluripotent stem cells" or iPS cells [53]. Cell de-differentiation was initially induced by retroviral transduction of several factors involved in pluripotency and self-renewal of ESC. Initially, a total of 24 genes were selected and over-expressed in different combinations, being finally restricted to only four of them, *Oct3/4*, *Klf4*, *Sox2* and *c-Myc* (OSKM) as those necessary for reprogramming the mouse adult fibroblast into iPS cells. One year later, human iPS (hiPS) generation was also reported by using the same combination of factors [54-56] or a different one (*Oct3/4*, *Sox2*, *Nanog* and *Lin-28*) [57]. The generated iPS cells presented similar morphological and genetic properties than ESC [58-60], including the capacity to *in vitro* and *in vivo* differentiate towards cell types derived from any of the three germ layers. Confirming that potential, their contribution to teratomas when injected into immunodepressed mice, and to chimeras when injected into the embryo, was also demonstrated [53, 54, 59]. On the other hand, despite the similarity of the iPS cells to ESC, differences in gene expression signatures [61], DNA methylation patterns [62] and efficiency degree in differentiating to specific lineages [63] have been also evidenced.

Importantly, the protocol developed for iPS derivation has been proved to be quite reproducible and, with minor modifications, iPS have been already generated from many other species than mouse, including human [54, 55, 64], non-human primate [65], pig [66, 67], rat [68, 69], rabbit [70], dog [71], marmoset [72], sheep [73] and bird [74] among others (**Table I1**). Also, many cell types have been assayed with success for iPS derivation, including pancreatic β cells [75], neural stem cells (NSC) [76, 77], post-mitotic neurons [78], mature B lymphocytes [79], keratinocytes [56, 80], stomach and liver cells [81], amniotic fluid-derived cells [82], CD34^{+} hematopoietic stem cells [83, 84], cord blood-derived cells [85, 86], melanocytes [87, 88], adipose stem cells [89, 90], hepatocytes [91] and dental pulp-derived stem cells [92]. This unexpectedly consistent method of deriving pluripotent cells from almost every tissue has demonstrated the striking plasticity of the cells, independently of their origin and differentiation stage,

and, importantly, it has also offered a new pluripotent stem cell source that could be autologously applied, bypassing the immune and ethical issues derived from the use of human embryos.

Table I1. Methods for iPS cell generation. Legend: **O**: Oct3/4; **S**: Sox2; **K**: Klf4; **M**: c-Myc; **N**: Nanog; **L**: Lin28

Method	Species	Cell types	Factors	Efficiency	Advantages	Disadvantages	Ref.
Retroviral	Mouse, human, rat, pig, rhesus monkey, rabbit, avian, dog, sheep, marmoset	Fibroblasts, neural stem cells, astrocytes, stomach cells, liver cells, keratinocytes, amniotic cells, blood cells, adipose cells, hepatocytes	OSKM, OSK, OSN, OK, OS, OM, O	~ 0.01-0.5%	Relatively efficient	Multiple integrations and incomplete silencing	[53, 54, 56, 64, 93-96]
Lentiviral	Mouse, human	Fibroblasts, keratinocytes, cord blood cells, adipose derived stem cells, amniotic cells	OSKM, OSNL	< 0.1–1%	Relatively efficient	Multiple integrations and incomplete silencing	[55, 57, 97]
Inducible lentiviral	Mouse, human, pig	Fibroblasts, β cells, keratinocytes, peripherial blood cells, melanocytes	OSKM, OSKMN	< 0.1–1%	Relatively efficient and time-controlled factor expression	Multiple integrations, requires transactivator expression	[79, 80, 98]
Transposon	Mouse, human	Fibroblasts	OSKM	< 0.1%	Reasonable efficiency and no genomic integration	Screening of excised lines is laborious	[99]
lox-P-flanked lentiviral	Mouse, human	Fibroblasts	OSK	< 0.1-1%	Relatively efficient and excisable (no integration)	Screening of excised lines is laborious, loxP sites remain in genome	[100, 101]
Adenoviral	Mouse, human	Fibroblasts and liver cells	OSKM	< 0.001%	No integration	Low efficiency	[97, 102]
Plasmid	Mouse, human	Fibroblasts	OSNL	< 0.001%	Only occasional integration	Low efficiency and rare vector integration	[103]
Sendai virus	Human	Fibroblasts	OSKM	< 1%	No integration and high transfection efficiency	Sequence sensitive to RNA replicase	[104]
Episomal vectors	Human	Fibroblasts	OSNL, OSNLKM	< 1%	High transfection efficiency	Posibility of random integration	[105]
Protein transduction	Mouse, human	Fibroblasts	OSKM, OS	< 0.001%	No integration, no DNA single transduction	Low efficiency	[106-108]
RNA transfection	Human	Fibroblasts	OSKM, OSKML	< 1%	No integration and high transfection efficiency	Multiple cycles of transfections needed	[109]
microRNA	Human	Adipose stromal cells and fibroblasts	mir-200c, mir-302s, mir-369s	< 0.1%	No integration and faster reprogramming	Low efficiency	[110, 111]

2.2. iPS generation methodology

2.2.1. Viral-based methods

As already mentioned, iPS cells were originally generated by retroviral transduction of the transcription factors OSKM. However, this combination is not exclusive and others such as *Oct3/4*, *Sox2*, *Nanog* and *Lin28* [57, 85] have been demonstrated to be similarly efficient. Interestingly, in an attempt to minimize the risk of chromosomal disruption and to simplify reprograming, several studies have demonstrated that a more reduced set of reprogramming factors can be enough to generate iPS cells. Transduction of only three factors *Oct3/4*, *Sox2* and *Nanog* [96] or *Oct3/4*, *Sox2* and *Klf4* [93] induce also iPS cells formation, demonstrating that the oncogenen *c-Myc* is dispensable for the reprogramming process. iPS cells have been also generated with just two factors, combining *Oct3/4* with *Klf4* [77, 95, 112], *c-Myc* [77] or *Sox2* [86, 94] and these combinations have been even further reduced to *Oct3/4* alone when reprogramming NSC [113], as they already endogenously express *Sox2* and *c-Myc*.

2.2.2. Non-integrative methods

Although the integrated viruses are transcriptionally silenced following reprogramming, the risk of tumor formation due to spontaneous reactivation of the viral transgenes or undesired viral transgene insertions that could activate oncogenes expression, constitutes the major limitation of this technology. Other strategies for iPS generation are therefore being studied (**Figure I5**), including the use of non-integrative vectors such as adenoviruses [97, 102], RNA-based Sendai viruses [104], episomal vectors [105, 114], DNA plasmids encoding the reprogramming factors [103, 115], excisable vectors [99-101], mRNA [109] and microRNAs [110, 111]. In addition, direct protein transduction has been also assayed by directly delivering the four reprogramming proteins (OCT3/4, SOX2, KLF4 and c-MYC) into the cells. For that purpose, proteins were previously fused with a cell-penetrating peptide (CPP) that contained a high proportion of basic amino acids that allowed overcoming the cell membrane barrier [106, 107]. In addition to this, a single transfer of ES cell-derived extract proteins was also assayed [108], demonstrating the reprogramming induction of

adult somatic cells, although, in this case, with a much lower reprogramming efficiency (**Table I1**).

SOMATIC CELLS

Integrative

- Retrovirus
- Lentivirus
- Inducible lentivirus

Non-integrative

- Adenovirus
- Plasmid
- Episomal vectors

Chemical compounds Growth factors

Excisable

- Transposon
- Floxed lentiviral

DNA free

- Sendai virus
- Protein
- RNA transfection
- microRNA

INDUCED PLURIPOTENT STEM CELLS
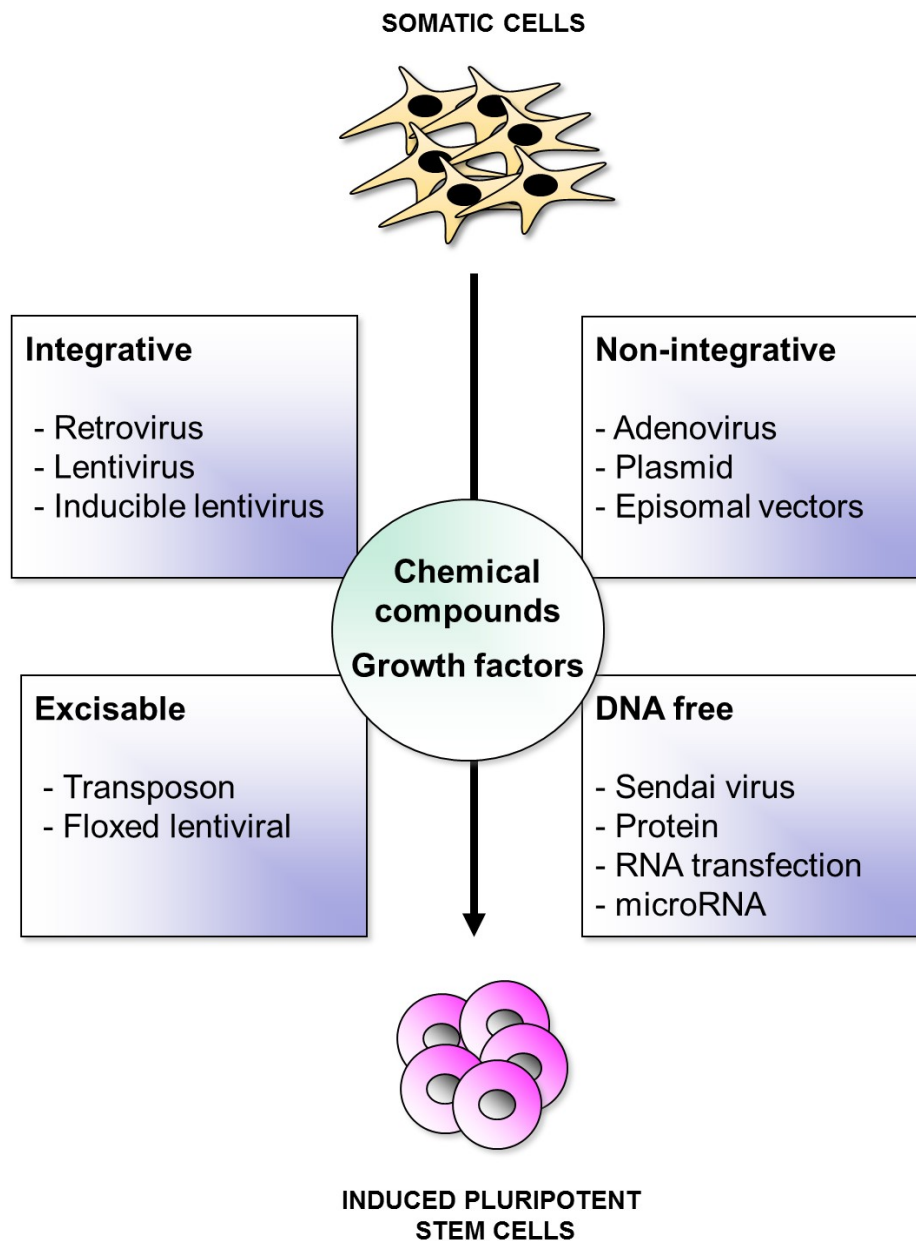
Figure I5. Approaches for cellular reprogramming. Somatic cells can be reprogrammed to induced pluripotent stem (iPS) cells by retroviral or lentiviral transduction of pluripotent transcription factors. Other strategies have also been studied for iPS generation including the use of non-integrative vectors such adenovirus, sendavirus, plasmid vectors, recombinant proteins and microRNAs transfections. iPS cells can be also generated by excisable vectors like the piggyback transposons and floxed lentivirus. Also, use of chemical compounds and growth factors have been shown to enhance cell reprogramming reducing the number of reprogramming factors needed.

2.2.3. Increasing efficiency of cell reprogramming

In general, the reprogramming of somatic cells is a slow and inefficient process that has been estimated at approximately 0.01% when following standard viral method protocols and an even lower percentage when using non-viral methods such as protein, plasmid and adenoviral-based protocols (about 0.001%). Other methods have improved this rate by using excisable (about 0.1%) or RNA transfection (about 1%) systems, although still remain quite low (**Table I1**). Thus, efforts have been made to improve iPS reprogramming efficiency, inducing the expression of different transcription factors or adding several chemical compounds that could promote pluripotency and self-renewal (**Table I2**). In early experiments, increased reprogramming efficiency was obtained in human fibroblasts when retroviral vectors encoding human telomerase (hTERT) and the SV40 large T antigen (SV40 LT) were supplemented to the four transcription factor (OSKM) vector cocktail [55, 116]. These additional factors play an important role in cell transformation and senescence [117, 118], which could prevent cellular apoptosis, and thereby improve the reprogramming efficiency. This greater induction was also achieved in human fibroblasts by co-expression of the *Utf-1* factor with the reprogramming factors OSKM, along with siRNA knock-down of *p53* [119]. Activation of *p53* leads to cell cycle arrest, so its silencing could overcome the cellular senescence process and render a more efficient process in terms of reprogrammed cell numbers. *Utf-1* expression, which is a target gene for the *Oct3/4* and *Sox2* complex [120], may also activate other downstream genes important for promoting reprogramming. Another transcription factor involved in self-renewal and pluripotency, the *Esrrb* factor, regulates the expression of *Klf4* and acts as a transcriptional activator of *Oct3/4*, *Sox2* and *Nanog* reprogramming factors [121, 122], also enhancing the reprogramming process [123]. In addition to these factors, the activation of the Wnt signaling pathway by the soluble Wnt3a molecule also promoted the generation of iPS cells in the absence of *c-Myc* [124] (Table 2). The Wnt signaling pathway is involved in the maintenance of pluripotency in ESC [125, 126] through the inhibition of GSK3 (that causes the subsequent translocation of β-catenin into the nucleus where it interacts with TCF proteins that regulate the expression of key ESC transcription factors) [127]. Moreover, iPS cells have been shown to be efficiently derived from mouse embryonic and adult fibroblasts by viral delivery of a single reprogramming factor (*Oc3/t4*) when combined with the BMP4, BMP7 and BMP9 proteins [128].

Furthermore, addition of chemical compounds can also enhance cell reprogramming or replace core reprogramming factors. Among them, the DNA methyltransferase inhibitors, which induce DNA demethylation, and the histone deacetylase inhibitors, that cause a relaxation of the DNA/histone complex through histone acetylation, can favor the reactivation of silenced genes. Some extensively used molecules are the 5-aza-cytidine (5-AZA) [129, 130], the trichostatin A (TSA), the suberoylanilide hydrozamic acid (SAHA) [130] (among the DNA methyltransferase inhibitors) and the valproic acid (VPA) (among the histone deacetylase inhibitors) [94]. Also, the inhibitor of the G9a histone methyltransferase, BIX-01294 (BIX), has been demonstrated in mouse fibroblasts [131] and neural progenitors cells (NPC) [132] to be effective for cell reprogramming. G9a histone methyltransferase represses *Oct3/4* expression [133] and therefore BIX could induce the reactivation of *Oct3/4*. Furthermore, the combination of BIX with another chemical compound, the L-calcium channel agonist BayK8644 (BayK), has significantly enhanced the reprogramming of mouse embryonic fibroblasts (MEFs) in the absence of *Sox2* and *c-Myc* [131]. The mechanisms of action of BayK still remain unclear. Moreover, the manipulation of other signaling pathways involved in self-renewal and pluripotency has been also reported, like the MEK and GSK3 ones, which could be inhibited by the PD0325901 and CHIR99021 molecules respectively, promoting iPS growth from mouse NSC [112] and mouse NPC [132]. Moreover, inhibition of the transforming growth factor-β (TGF-β) signaling with the A-83-01 inhibitor can co-operate in the reprogramming of mouse and human fibroblasts and rat liver progenitors by enabling a faster and more efficient generation of iPS cells [68]. Interestingly, iPS cells can be also derived by exogenous expression of *Oct3/4* alone if combined with the mentioned molecules PD0325901 and A-83-01 or others like PS48 (an activator of PDK1 that leads downstream AKT activation) and sodium butyrate (NaB) (an histone deacetylase inhibitor) [134]. Moreover, hypoxic cultivation or supplementation with ascorbic acid (AA) has also been found to increase the reprogramming efficiency [135, 136] (**Table I2**).

Table I2. Factors and chemical compounds used to increase cell reprogramming efficiency. Legend: **O**: Oct3/4; **S**: Sox2; **K**: Klf4; **M**: c-Myc; **M***: N-Myc; **N**: Nanog; **L**: Lin28; **Fbs**: Fibroblasts; **mFbs**: mouse fibroblasts; **hFbs**: human fibroblasts; **NPC**: neural progenitors cells; **NSC**: neural stem cells

Molecules		Biological Function	Infected cell types	Transcription Factors	Effects in cell reprogramming	Ref.
Factors	**SV40 LT**	SV40 large T antigen used for cell transformation	Fibroblasts	OSKM*	Enhance the efficiency by 23-70 fold in both human adult and fetal Fbs	[116]
		"	"	OSM*	Increase the efficiency by 55 fold in comparison with OSKM* (able to replace K)	[116]
		"	"	OS	Increase the efficiency by 9 fold in comparison with OSKM* (able to replace N and L)	[116]
	hTERT	Human telomerase reverse transcriptase, involved in cellular senescence	Fibroblasts	OSKM	Increase the efficiency by 3 fold in comparison with OSKM	[55]
	p53 siRNA, Utf-1	Tumor supressor, ESC specific transcription factor	Fibroblasts	OSKM	Enhance the reprogramming by 100 fold in comparison with OSKM	[119]
	Esrrb	Orphan nuclear receptor, involved in ESC self-renewal and pluripotency	Fibroblasts	OSM, OS	Replace K transcription factor	[123]
	Wnt3a	Cell signaling molecule involved in the regulation of cell fate and patterning during embryogenesis	Fibroblasts	OSK	Potentiates iPS generation by 20 fold in the absence of M	[124]
	BMPs	Growth factors that belong to the TGF-β family involved in embryonic development	Fibroblasts	OS, O	Fibroblasts reprogramming in absence of K and M and with O alone	[128]
Chemical compounds	**5-AZA**	DNA methyltransferasa inhibitor	Fibroblasts	OSKM, OSK	Enhance the reprogramming by 4 fold with OSKM. Increase the efficiency by 10 fold with OSKM and by 3 fold with OSK	[129], [130]

Molecules		Biological Function	Infected cell types	Transcription Factors	Effects in cell reprogramming	Ref.
Chemical compounds	**VPA**	Histone deacetylase inhibitor	Fibroblasts	OSKM, OSK, OS	More than 100 fold increase efficiency with OSKM in mFbs. Enhance the efficiency by 50 fold increase with OSK in mFbs and by 10 fold in hFbs. VPA replace K and M	[130]
	TSA, SAHA	Histone deacetylase inhibitors	Fibroblasts	OSKM	15 fold increase in efficiency with TSA and by 2 fold increase with SAHA	[130]
	BIX-01294	G9a histone methyltransferase inhibitor	Fibroblasts, NPC	OK, SKM	Enhance efficiency by 5 fold increase in mFbs and 8 fold in comparison with OK. In mNPC, BIX replaces O	[131, 132]
	BayK8644	L-type calcium agonist	Fibroblasts	O	In combination with BIX-01294 increase efficiency by 15 fold in absence of S and M	[131]
	PD0325901, CHIRR99021	Inhibitor of MEK signaling Inhibitor of GSK3 pathway	NSC, NPC	OK	Both chemicals compounds plus LIF promote growth of iPS cells	[112, 132]
	PS48, NaB, A-83-01	PS48: activator of PDK1 NaB: histone deacetylase inhibitor A-83-01: TGF-β inhibitor	Keratinocytes, HUVECs, amniotic cells	O	Induce cell reprogramming when combined with O + PD032590	[116, 134]
		″	Liver progenitors, fibroblasts	OSK, OSNL	A-83-01 in combination with LIF and PD0325901 and CHIRR99021 induce iPS generation in rat liver progenitors with OSK and in hFbs with OSNL	[68]
	Ascorbic acid	Antioxidant	Fibroblasts	OSKM, OSK	Increases the efficiency of iPS generation by reducing p53 levels	[136]

Finally, specific microRNAs that regulate the cell cycle in the ESC have also been successfully tested in combination with *Oct3/4*, *Sox2* and *Klf4* retrovirus. Transfection of miR-291-3p, miR-294 or miR-295 into MEFs consistently increased the number of iPS colonies [137]. Moreover, the addition of the single miR-294 with the three reprogramming factors (without *c-Myc*) increased the efficiency of reprogramming at similar rates than those obtained with the four transcription factors.

2.3. Genetic and epigenetic profile of iPS cells

Despite the initial excitement due to the ES-like features of the iPS cells, deeper molecular analysis have revealed relevant differences between iPS cells and ESC, mainly related to aberrant gene expression. Incomplete silencing of somatic genes in cells undergoing reprogramming, weak activation of ESC specific pluripotency genes and unspecific aberrations distinct from either the cell of origin or ESC, have been detected. Comparison of the methylation marks of ESC and iPS cell genome has also revealed significant variations. A thorough screening of cytosine-phosphate-guanine (CpG) islands in iPS cells identified aberrantly reprogrammed loci, with different methylation patterns from those of their parental fibroblast and ESC [138]. Also, a recent study showed significant reprogramming differences in CpG methylation and histone modifications compared to ESC and other iPS cells [139]. Similar consistent differences have been observed in miRNA expression between human ESC (hESC) and human iPS (hiPS) cells [140]. Also, two other studies that compared the global gene expression of ESC and iPS cells consistently identified the persistence of donor cell gene expression in iPS cells [141, 142]. Furthermore, one interesting study showed that iPS and ESC clones have overlapping variations in gene expression and that both cell types are clustered together. A meta-analysis of published gene expression data sets on ESC and iPS cell lines from four different laboratories (with multiple iPS clones derived using various methods of generation) showed that the different clones clustered according to the lab of origin rather than to their identity or method of derivation [143]. These data strongly argue that differences in culture conditions, including those that inherently exist across multiple laboratories, influence the gene expression signatures of both ESC and iPS cells. Interestingly, it seems that these differences are more characteristic of early-passage iPS clones and can be evened out with extended culture, bringing them transcriptionally closer to ESC in later passages [144].

On the other hand, it has been suggested that due to this aberrant gene expression, a putative immune response could happen even after autologous transplantation. A recent work from Zhao and collaborators has shown that whereas ESC derived from C57/B6 mice did induce teratoma formation without any evident immune rejection, iPS cells derived from the same mouse strain failed to form teratomas due to rapid rejection provoked by a T cell dependent immune response [145]. Global gene expression analysis of ESC and iPS-derived teratomas revealed overexpression of teratoma-related genes in the iPS, responsible for the immune rejection. However, controversy has arisen regardind these findings and a recent study has reported the limited/none immunogenicity of skin and bone marrow-derived iPS. Immunogeneicity levels induced by ten different iPS clones were similar to what was detected with seven different ESC clones-derived cells and formation of stable grafts in skin and bone marrow after transplantation of the iPS differentiated cells were detected in both cases [146].

2.4. Differentiation potential of iPS cells

Numerous protocols, most of them based on previous ESC differentiation methods, have been followed to guide the *in vitro* differentiation of mouse iPS (miPS) and hiPS cells towards diverse cell types, including CMs and hematopoietic cells [147, 148], vascular cells (endothelial cells (ECs) and smooth muscle cells (SMC)) [148, 149], adipocyte and osteoblast cells [150], macrophages and dendritic cells [151], hepatocytes [152], retinal cells [153] and neurons [154] among others, demonstrating their pluripotency. Also, their *in vivo* differentiation potential has been confirmed in different animal models. To give one example, rat iPS cells were able to generate rat pancreas when injected into mouse blastocysts that were deficient in an essential pancreas development gene [155] and also, undifferentiated iPS cells differentiated towards cardiac and vascular cells after transplantation into the ischemic rodent heart [156]. However, despite the proven pluripotency of the iPS cells, differentiation towards specific cell types can be affected by the origin and epigenetic characteristics of the derived iPS, which can be more prone to differentiate towards specific cell types. Although the molecular mechanisms are not well understood yet, this issue is explained by the fact that iPS present residual DNA methylation signatures characteristic of their somatic tissue of origin, which can favor their differentiation towards lineages related to the donor cell [157-159]. For example, it has been shown that iPS cells derived from

non-hematopoietic cells exhibit a residual methylation at loci required for hematopoietic cell fate, which results in a reduced blood differentiation potential *in vitro* [158]. Also, human retinal pigmented epithelial cells present a greater tendency to differentiate back into this cell type than ESC or iPS cells that have been derived from other tissues [159]. Furthermore, it has been shown that iPS derived from different somatic cell types are transcriptionally distinguishable. Specifically, in an interesting study from Dr. Polo and colleagues it was demonstrated how iPS cells generated from tail tip fibroblasts, splenic B cells, bone marrow derived granulocytes and skeletal muscle precursors, exhibited gene expression patterns from their cells of origin, confirming that iPS cells retain a transcriptional memory of their previous state of differentiation [157]. More recently, it has been demonstrated that iPS cells generated from human pancreatic islet β-cells present a greater ability to *in vitro* and *in vivo* differentiate into insulin-producing cells than ESC and isogenic non-β-cells, which correlates with the fact that β-cell-derived iPS kept open the chromatin structure at key β-cells genes [160]. In view of this data, it might be relevant to ascertain which cell lines are the best sources of iPS cells for each cell lineage specification and to elucidate the best way to select such iPS cell lines for specific differentiation.

In addition, it has been also suggested that the differentiation efficiency of iPS cells might depend on the number of reprogramming factors, although it is not clear which combination could be the best, as contradictory results have been obtained. The study of Dr. Löhle and colleagues demonstrated that an omission of reprogramming factors in NSC derived from iPS cells could significantly decrease the efficiency of their differentiation [161]. A lower functional maturity was detected in the neural cells obtained after differentiation of iPS that had been generated by overexpression of one or two transcription factors than from the ones derived from the four-transcription factors-iPS. In constrast, cardiac differentiation was most consistently induced when performed with three factor-derived iPS cells than from four-factors iPS where a poor and inconsistent differentiation towards the cardiac lineage was observed [162]. In view of these contradictory results, it is obvious that to reach a clear conclusion, it will be necessary to perform more specific and detailed molecular studies that establish whether these differences are really due to the number of factors initially overexpressed in the somatic cells or are just related to specific reprogramming differences in each derived iPS clone.

3. CARDIOMYOCYTE DIFFERENTIATION FROM PLURIPOTENT STEM CELLS

The generation of cardiac cells represents a key issue for therapeutic application CVD. Despite the proven differentiation capacity of many stem cell populations towards different lineages (including the vascular ones), a robust differentiation towards functional cardiac cells has not been shown for many of them. Cardiac progenitors present in the heart have been described, as the main adult tissue cell source but their *in vivo* cardiac differentiation potential after their *in vitro* expansion does not sufficiently contribute to heart tissue repair. On the other hand, although a much more robust cardiac differentiation capacity has been shown for ESC (reviewed in [163]), its clinical use is not contemplated. Thus, the discovery of iPS cells as a new source for cardiac cells has opened new perspectives for the establishment of future autologous myocardial cell-replacement therapies. The spontaneous capacity of mouse [147], human [164] and pig [165] iPS cells to differentiate towards the cardiac lineage has been already demonstrated, differentiating towards CMs with a similar gene expression and functional properties than ESC derived-CMs [166, 167]. Also, undifferentiated iPS cells contribute to the cardiac tissue after differentiating towards cardiovascular cells *in vivo* [156]. However, as it could be expected, due to their embryonic characteristics, cells also exert a tumorogeneic potential [156]. To bypass this serious limitation and, also, to enrich the cardiac population to populate the heart, cardiac cells have been *in vitro* derived from hiPS to be then injected into the heart [168]. Retention of the transplanted cells within the infarcted heart and an induction of heart positive remodeling after ischemic damage has been shown. Importantly, no tumor formation has been reported although very careful long-term studies are required to confirm this. Furthermore, for future clinical use, very stringent conditions for CMs selection would be required to contemplate their application in patients. To this end, several fluorescent dies and antibodies have already been developed. For example, the CDy1 die labels undifferentiated cells [169] where a mitotracker red dye labels mitochondrias with a much higher fluorescence intensity in cardiac than in undifferentiated cells [170], allowing separation of cardiac cells from undifferentiated cells without loosing cell viability. Also, antibody detection of proteins present in the CMs membrane such elastin microfibril interf 2 (EMINLIN2) [171], the signal regulatory protein α (SIRPA) [172] and VCAM1 [173] have been reported as useful cardiac markers. In any case,

despite the fact that cardiac cells can be successfully derived and selected from iPS cells, optimization of the existing protocols is needed, as the rendered differentiated CMs present poor levels of maturation [174] with high interline variability [164, 167, 175]. Another suitable option is the derivation of cardiovascular progenitors, which have been successfully differentiated from iPS cells. In particular, Isl1$^+$ cardiovascular progenitors have been differentiated from miPS cells and have demonstrated an *in vivo* contribution towards cardiovascular lineages without teratoma formation [176]. Also, iPS-derived Flk-1$^+$ progenitors cells have been shown to engraft in the heart tissue and to differentiate towards mature cardiac and vascular cells, improving the heart function after their transplantation into an acute model of MI in mice [177].

3.1. Enhancing cardiac differentiation with cytokines and small molecules

Many protocols have been tested with ESC to specifically induce cardiac differentiation (reviewed in [178]) (**Table I3**), that have been also later applied for iPS specification. Initially, co-culture with the cell line END-2 was reported as a successful method for CMs derivation, as this cell line was derived from the visceral endoderm and plays an inductive role in the cardiac differentiation of the adjacent mesoderm [179]. Also, by emulating embryo development, stem cells have been sequentially treated with specific growth factors required for the different stages in heart formation. Highly purified CMs have been generated from hESC by sequential treatment with Activin A and BMP4 [51]. A combination of other growth factors such as Activin A and FGF2 [180] or BMP4 and FGF2 [181] have also been used to increase cardiac differentiation efficiency in hESC and hiPS cell lines. In the same way, hiPS cells have been also successfully differentiated towards CMs after treatment with Activin A, BMP-4, basic fibroblast growth factor (bFGF) and AA [168]. Elliot and co-workers also demonstrated a highly efficient cardiac differentiation protocol for ESC that used BMP4 and Activin A in combination with Wnt3a, SCF and vascular endothelial growth factor (VEGF) in hESC [182]. In addition, sequential application of some of these cytokines (Activin A and BMP4) together with bFGF to a cell monolayer cultured over matrigel was highly effective for inducing cardiac differentiation of hESC and hiPS cells [183]. Also, other growth factors such as BMP2 and FGF-10, were shown to enhance cardiac differentiation in both ESC and iPS cells [184, 185]. In contrast, inhibition of BMP signaling was also reported to induce CMs differentiation from mouse ESCs [186],

suggesting that transient suppression of BMP signaling might be necessary during CMs specification. Furthermore, manipulation of the Wnt/β-catenin signaling pathway, which is required for mesoderm formation and heart development, can induce cardiac specification [187]. An early treatment with the agonist Wnt3a has been shown to increase hESC cardiac differentiation [188] and also, activation of the Wnt/β-catenin signaling by treatment with GSK3 inhibitors such CHIR99021 has been reported to promote cardiac differentiation of hESC and hiPS cells [189]. On the other hand, the inhibiton of the Wnt pathway by late addition of DKK1 can induce cardiac specification in ESC too [190]. Other groups have induced cardiac differentiation of hESC [191, 192] and hiPS cells [193] by treatment with the Wnt signaling inhibitors IWR-1 or IWP-4. A time-dependent action through the Wnt/β-catenin pathway explains these apparently contradictory results, with early activation required for cardiac differentiation and inhibition needed for later specification of cardiac precursors [187]. The biphasic role of TGFβ has also been studied. Inhibition of TGFβ/Activin/Nodal and BMP signaling using the molecules SB431542 and dorsomorphin promoted cardiac differentiation in ESC and iPS cell lines [194], whereas an early inhibition of TGFβ signaling produced complete inhibition of cardiac differentiation in ESCs [195, 196]. On the other hand, Notch signaling (reviewed in [197]) also plays a critical role in cardiac differentiation by negatively regulating the Wnt/β-catenin pathway [198]. Thus, sustained inhibition of Notch signaling by the γ-secretase inhibitor (GSI) promoted cardiac mesoderm specification [199]. Finally, other factors like the Neuregulin-1 (NRG-1) have been shown to induce cardiac differentiation of ESC [200, 201].

In addition, inhibitors of BMP have been shown to enhance the cardiac differentiation from mouse ESC (mESC) [202] and AA has been also tested in ESC [203] and iPS cells [204] showing formation of mature CMs with sarcomeric organization and enhanced responses to β-adrenergic and muscarinic stimulations. Other molecules, including DMSO [205], G-CSF [206], and cyclosporin-A [207] have been identified to induce and enhance the generation of CMs from mouse and human pluripotent stem cells.

Table I3. Current methods for cardiac differentiation of pluripotent stem cells. Legend: **BMP4**: bone morphogenic protein 4; **FGF2**: fibroblast growth factor 2; **VEGFA**: vascular endothelial growth factor A**; DKK1**: dickkopf homolog 1; **FGF10**: fibroblast growth factor 10; **IWR-1**: WNT signaling inhibitor; **SB431542**: TGF-β/activin/nodal signaling inhibitor; **dorsomorphin**: BMP signaling inhibitor; **CHIR99021**: GSK3 signaling inhibitor; **SCF**: stem cell factor, **IWP-4**: WNT signaling inhibitor; **bFGF**: basic fibroblast growth factor; **FBS**: fetal bovine serum; **GMEM**: Glasgow Minimum Essential Medium; **DMEM**: Dulbecco´s Modified Eagle Medium; **RPMI**: Roswell Park Memorial Institute medium; **RPMI/INS**: RPMI based-media supplemented with insulin; **B27**: media supplement; **LI-BEL**: low insulin, bovine serum albumin, essential lipids media; **Stem Pro34**: serum-free medium from Invitrogen; **RPMI-INS**: RPMI based-media without insulin.

Method	Differentiation format	Mesoderm induction	Cardiac specification	Cardiomyocyte differentitiation	References
Embryoid Body (EB) formation	**Suspension EB**	Activin A, BMP4, FGF2	VEGFA, DKK1	VEGFA, FGF2	[190]
		FGF10	FBS/GMEM	FBS/GMEM	[185]
		BMP4	IWR-1	FBS/DMEM	[193]
		Activin A, BMP4, FGF2	VEGFA, DKK1, SB431542 dorsomorphin	VEGFA, FGF2	[194]
		Activin A, BMP4, FGF2	IWR-1	Triiodothyronine	[192]
		CHIR99021	RPMI/FBS	RPMI/FBS	[189]
	Forced aggregation EB	Activin A, FGF2	FBS/DMEM	FBS/DMEM	[180]
		BMP4, FGF2	FBS/RPMI	RPMI/INS	[181]
		Activin A, BMP4, FGF2, VEGFA, SCF	LI-BEL	LI-BEL	[182]
Cell Monolayer	**Simple Monolayer**	Activin A, BMP4	RPMI/B27	RPMI/B27	[51]
		Activin A, BMP4, FGF2	VEGFA, DKK1	VEGFA, FGF2	[173]
		Activin A, BMP4, FGF2, VEGFA, SCF	LI-BEL	LI-BEL	[182]
		Activin A, BMP4	IWR-1 or IWP-4	RPMI/B27	[191]
		Activin A, BMP4, bFGF Ascorbic acid	StemPro-34	StemPro-34	[168]
	Matrix sandwich	Activin A, BMP4, bFGF	RPMI-INS	RPMI/B27	[183]

3.2. Neuregulin-1 protein: role in cardiac development and cell differentiation

NRG-1 protein belongs to the epidermal growth factor (EGF) family and it is the only neuregulin known to be an important regulator of both cardiac development and postnatal function (reviewed in [208]). NRG-1 can be further divided into three types. Type I and type II neuregulins are released to nearby cells after proteolytic processing, signaling in a paracrine manner [209] whereas mature type III neuregulin remain anchored to the cell-membrane and signal to adjacent cells in a juxtacrine manner [210]. By alternative splicing, the extracellular EGF-like domain gives rises to the α and β isoforms which differ in their binding activity, exhibiting the β isoforms 10-100 fold times more activity than the α isoforms [211] and being only the β variants biologically active on CMs [212]. NRG-1 isoforms exert their biological effect through the erytroblastic leukaemia viral oncogene homolog (ErbB) tyrosine kinase membrane receptors ErbB-2, ErbB-3 and ErbB-4. These three receptors are critical for heart development [213-215] (**Figure I6**) whereas ErbB-3 expression is lost in the adult heart [216].
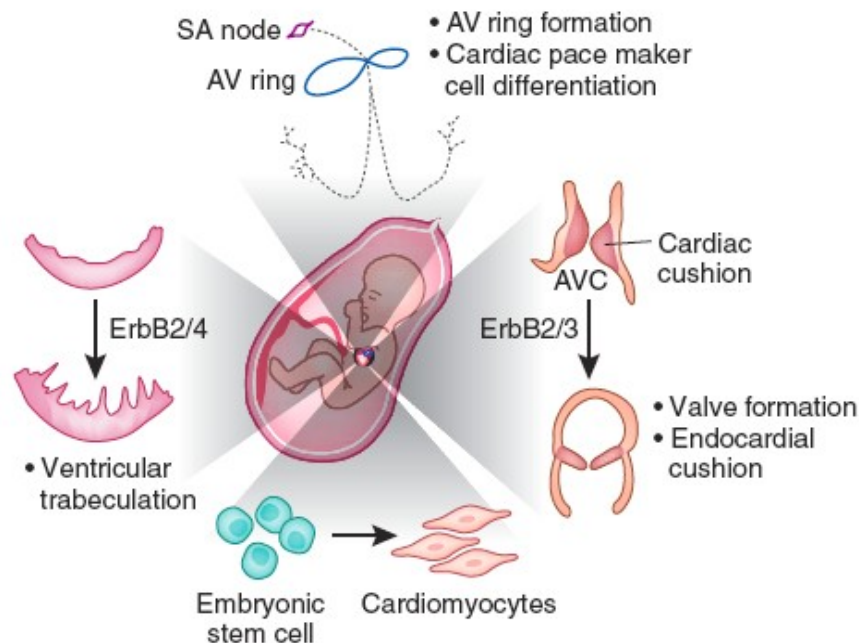
Figure I6. Role of Neuregulin-1 in cardiac development (Image taken from *Odiete O et al. Circ Res, 2012*).

NRG-1 ligands are produced by the microvascular ECs present in the myocardium in response to stress conditions [217]. In CMs, NRG-1 binds to the ErbB-4 receptor, which dimerizes with ErbB-2, leading to multiple cellular responses like the survival and proliferation of neonatal [216] and adult CMs [216, 218, 219]. NRG-1 protein exerts multiple effects on cardiac function including cell survival, proliferation and calcium uptake among others by activation of multiple signalling cascades (**Figure I7**).
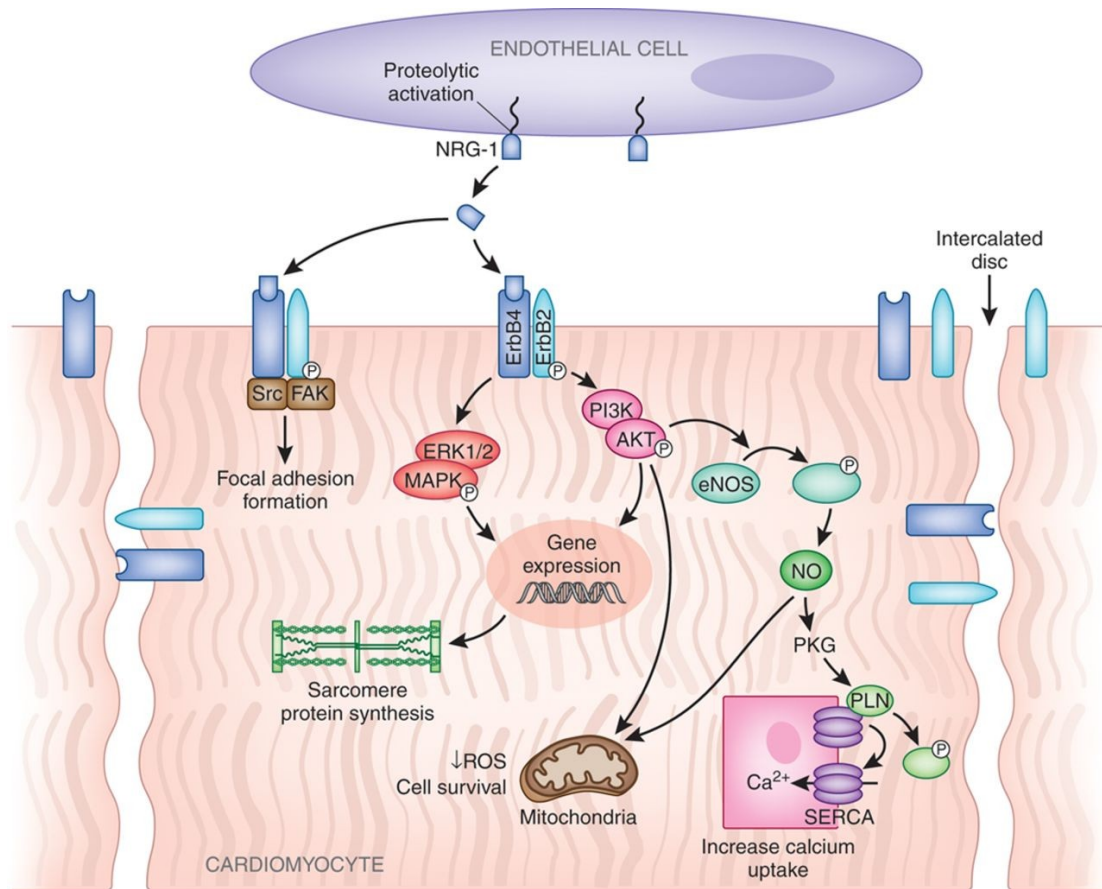
Figure I7. Neuregulin-1 signaling cascade in cardiomyocytes. NRG-1 is expressed in the microvascular endothelium and the ErbB-2 and ErbB-4 receptors are expressed in ventricular cardiomyocytes. NRG-1 protein exerts multiple effects on cardiac function by activation of multiple signalling cascades, including the phosphatidylinositol-3-kinase (PI3K)/protein kinase B (Akt), extracellular signal-regulated kinase (Erk) 1/2, mitogen-activated protein kinase (MAPK), phosphatidilinositol-3-kinase (PI3K)/protein kinase B (Akt) and Src/focal adhesion kinase (FAK) pathways (Image taken from *Odiete O et al. Circ Res, 2012*).

NRG-1 is involved in myocardial structure preservation by activation of the Src/FAK (Focal Adhesion Kinase) pathway and up-regulation of the cMLCK, a cardiac-specific myosin light-chain kinase that controls muscle contraction and sarcomeric organization [217, 220]. Also, NRG-1 regulates calcium homeostasis implicated in myocyte relaxation [221] and also exerts anti-adrenergic effects through nitric oxide (NO) synthesis via the endothelial NO synthase (eNOS), reducing heart overload [222]. Other NRG-1 effects include indirect paracrine angiogenic effects on ECs through the induction of VEGF-A release [223] and an anti-atherosclerotic effect by reducing the cholesterol acyltransferase 1 (ACAT1) and increasing the ATP-binding cassette transporter A-1 (ABCA1) expression in monocyte-derived macrophages [224]. Importantly, NRG-1β stimulates differentiation of embryonic CMs into cells of the cardiac conduction system with an increase in pacemaker current density, and transforms fetal CMs into cardiac pacemaker-like cells [225]. Moreover, it has been also demonstrated the capacity of NRG-1 to induce cardiac differentiation of ESC, significantly increasing the number of beating embryoid bodies (EBs) derived from murine ESC which up-regulated the expression of specific cardiac genes such as *Nkx2.5*, *Gata4*, *αMhc*, *βMhc* and *Actinin* [200]. Interestingly, it has been shown that NRG-1β can also modulate the ratio of nodal to working-type cells in differentiating hESC. The inhibition of NRG-1β/ErbB signalling greatly enhanced the proportion of cells with nodal phenotype, while the treatment with additional exogenous NRG-1β increased the fraction of working-type cells [201]. Thus, by manipulating NRG-1β/ErbB signaling, it might be possible to generate enriched working-type CMs for their use in infarct repair therapy.

Furthermore, many *in vivo* studies have established the therapeutic potential of NRG-1, showing a positive effect on heart function and survival. In rats with heart dysfunction, intravenous doses of recombinant human NRG-1β (rhNRG-1β) improved cardiac function and increased capillary density in the fibrotic peri-infarct area [226]. Similar beneficial effects on cardiac function were reported in models of anthracycline and virally induced cardiac injury in mice where the rhNRG-1β administration similarly improved cardiac contractility and relaxation [226, 227]. Moreover, under pathological conditions, NRG-1β induces *in vivo* proliferation of differentiated CMs and promotes myocardial regeneration and decreased hypertrophy, leading to improved function after MI in mice [228]. In other MI animal models, it has been also demonstrated the benefit

of NRG-1 on cardiac function, contributing to improve ventricular remodeling and reducing mitochondrial dysfunction, CMs apoptosis and oxidative stress [229, 230]. In addition, administration of exogenous NRG to endothelium-specific NRG knockout mice, fully reversed the effects of endothelium-selective NRG deletion after MI, leading to a significantly smaller infarct size. This data supports the idea that endothelium-derived NRG protects the heart against ischemic injury [231].

Thus, all these beneficial effects on the biology of the heart suggest that NRG-1 protein may provide a molecular strategy to promote cardiac regeneration. Finally, two recent clinical assays have been carried out in Australia and China [232, 233]. Patients with heart failure received daily intravenous infusions of the EGF domain rhNRG-1β for 10 days. Three months later, improved cardiac function was observed, demonstrating that treatment with NRG-1β in patients with cardiac dysfunction can produce favourable hemodynamic effects.

3.3.   Partial and direct cell reprogramming for cardiac differentiation

Even though methods for safe and efficient iPS cells derivation are being rapidly developed, their tumorigenic potential remains as a major limitation for clinical applications. Overcoming this problem will require careful optimization of methods for differentiation, isolation, and/or characterization of the cells to be transplanted. In this regard, a protocol allowing differentiation of murine embryonic fibroblasts into CMs through an initial partial de-differentiation proved to be a fast and efficient manner for cardiac cell production (**Figure I8**) and was first described by Dr. Efe and coworkers. Briefly, fibroblasts were transduced with four reprogramming factors (OSKM) and cultured in reprogramming media (without LIF cytokine and with an inhibitor of the JAK-STAT pathway) for nine days before they were induced for cardiac differentiation via BMP4 treatment [234]. Along the same lines as this new method, a similar partial reprogramming protocol was successfully followed to generate neural progenitors [235] and NSC [236]. Thus, with this unique strategy, induction of a transitory or parcial undifferentiated state could favor cell specification towards a concrete differentiated cell type. There would be still a risk of acquiring a pluripotent state with tumorogeneic potential, so a third option is being also tested, which is the direct reprogramming of a somatic cell into an alternative adult cell, in this case, without inducing a total or partial cell de-differentiation first. In fact, direct reprogramming is not a new concept. It has

been long known since it was established that, for example, exogenous expression of *MyoD* can directly convert murine fibroblasts into skeletal muscle cells [237]. Also, B cells can be reprogrammed into macrophages by enforced expression of *c/Ebpα* and *c/Ebpβ* transcription factors [238] and T cell progenitors reprogrammed to macrophages and dendritic cells by inducing *c/Ebpα* and *Pu.1* transcription factor expression [239]. Other groups have also demonstrated that fibroblasts can be directly derived towards different cell types like macrophages [240], neuronal cells and NSC [241, 242], blood progenitors cells [243] and hepatocytes [244, 245] by overexpression of defined sets of transcription factors combined with different chemical molecule treatments. Furthermore, direct lineage conversion of terminally differentiated hepatocytes into functional neurons has been also shown, demonstrating that lineage reprogramming is possible between cell types derived from different germ layers [246]. Moreover, within the cardiovascular field, reprogramming of fibroblasts into functional ECs has been also recently reported. Human fibroblasts were transduced with the OSKM reprogramming factors for four days and then treated with VEGF to induce endothelial differentiation. Interestingly, increased angiogenesis and blood flow was observed after their transplantation in a hindlimb ischemia mouse model [247]. Moreover, direct transdifferentiation of mouse mesoderm to beating CMs was achieved through over-expression of two transcription factors, *Gata4* and *Tbx5*, and a cardiac-specific subunit of BAF chromatin-remodeling complexes, Baf60c [248]. All these findings show the possibility of modifying the global gene expression pattern of the cells and, more importantly, it demonstrates their unexpectedly great plasticity. Making a step forward, a recent report has described successful *in vitro* transdifferentiation of somatic cells into functional CMs [249]. For this, Dr. Srivastava and colleagues found that over-expression of only three transcription factors, *Gata4*, *Mef2c* and *Tbx5* in cardiac or dermal fibroblasts was sufficient for reprogramming into CMs (**Figure I8**). Importantly, this capacity was also shown *in vivo* following local delivery of these three transcription factors [250-252] and the effect was enhanced by addition of thymosin β4 [253]. Fibroblast-derived cells expressed CMs markers, showed sarcomeric organization, became binucleated, presented contractile potential and were electrically coupled. Moreover, a smaller infarct size and improved cardiac function was detected in the treated animals three months post-infarction. Similar, *in vivo* reprogramming of endogenous cardiac fibroblasts into CMs was also recently reported after

overexpression of *Gata4*, *Hand2*, *Mef2c* and *Tbx5* [251]. Although this new approach holds promise, it might require optimization since a recent study found that CMs generated using this technique (with Gata-4, Mef2c, and Tbx5) failed to express typical cardiac genes, showed incomplete functional maturation, and displayed poor survival after transplantation in a model of MI [254].
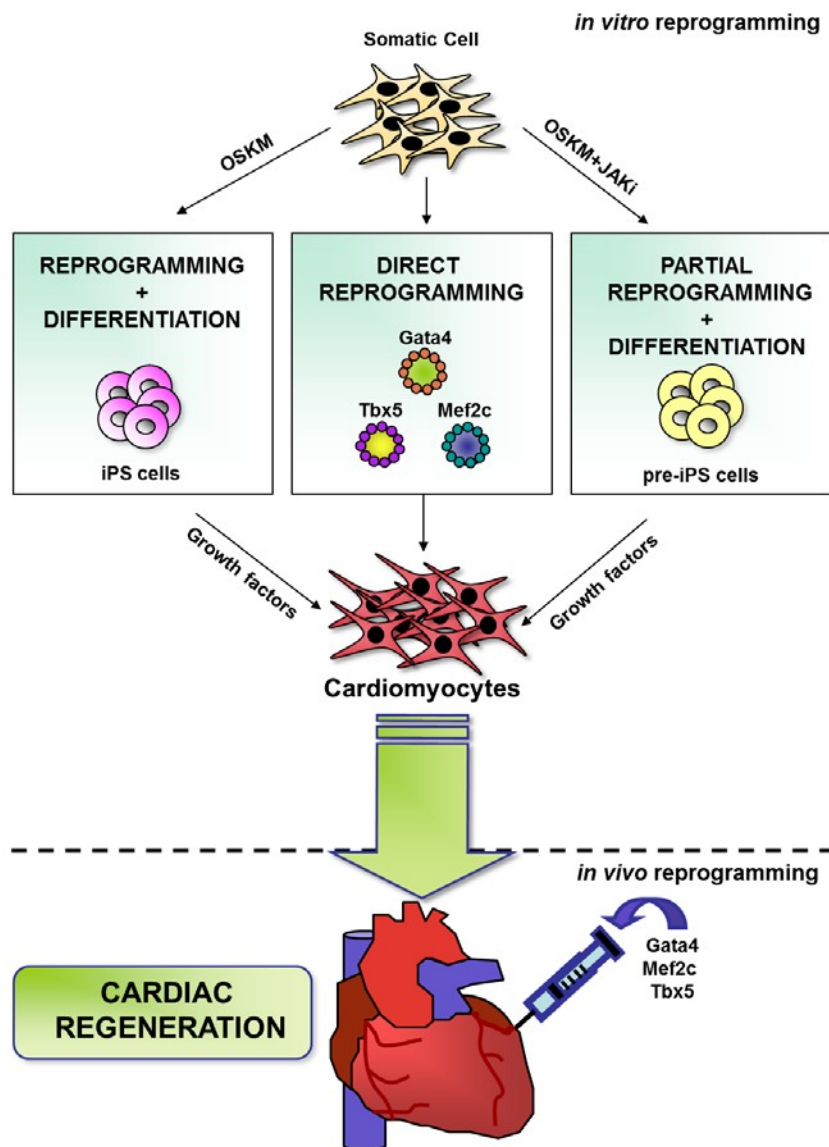
Figure I8. Strategies for cardiac regeneration therapy. Cardiomyocytes (CMs) can be successfully derived from iPS cells by *in vitro* treatment with different cytokines and cardiac growth factors. Moreover, a partial reprogramming protocol from somatic cells through over-expression of *Oct3/4*, *Sox2*, *Klf4* and *c-Myc* but without clonal isolation of iPS cells and following cardiac differentiation has been demonstrated to be a fast and relatively efficient manner for CMs generation. Furthermore, CMs can be directly obtained from a somatic cell without first coming into a pluripotent state, by over-expression of cardiac transcription factors. New discoveries have shown that resident non-myocytes in the murine heart can be reprogrammed into cardiomyocyte-like cells *in vivo* by local delivery of *Gata4*, *Mef2c* and *Tbx5* transcription factors.

Finally, microRNA-mediated transdifferentiation is also plausible. A single transfection of the mirRNAs 1, 133, 20, and 499 has been shown to directly convert cardiac fibroblasts into CMs. Moreover, this was demonstrated both *in vitro* and *in vivo*, following delivery of these mirRNAs to ischemic mouse myocardium. The resulting CMs showed expression of typical mature cardiac markers and sarcomeric organization, and exhibited spontaneous calcium transients [255]. Taken together, these findings are extremely encouraging as they offer the possibility of reprogramming heart endogenous fibroblasts into functional CMs. However, the efficiency of direct reprogramming remains very low and must be improved for future regenerative use.

4. iPS CELLS FOR APPLICATION IN CARDIAC DISEASE

Despite the unquestionable scientific and therapeutic potential of iPS cells, additional research and optimization will be required to enable future clinical application of this technology. In fact, it is essential that we acquire a deeper understanding of technical and biological aspects related to iPS cells generation and differentiation and standardization of cell transdifferentiation protocols, as well as the complex genetic and epigenetic mechanisms of cell reprogramming. Other practical limitations such as the improvement of *in vivo* cell engraftment and survival degree (a generally observed caveat in stem cell therapy) need also to be solved. In order to circumvent this last issue, new strategies such as the co-transplantation of iPS cells with other cell types that could favor their survival in heart tissue, are being assayed. Thus, it has already been demonstrated that co-transplantation of ESC and mesenchymal stem cells (MSC) into the ischemic heart can provide better functional preservation than a single-cell treatment [256]. MSC can act in a paracrine manner (reviewed in [257]) secreting growth factors that would favor cell survival and also enhance different tissue regenerative processes like tissue revascularization [258] and positive tissue remodeling [259]. Furthermore, MSC might modulate the immune response [260], which could allow the stabilization of the transplanted cells. In fact, it has been shown in a preclinical pig model of MI that the co-administration of hiPS cells with MSC considerably increased the hiPS cell retention in the myocardium [261]. In this study, cell engraftment was detected 15 weeks post-injection and iPS-derived ECs were found integrated into the cardiac vasculature.

Furthermore, it has become clear that combining these therapies with tissue engineering techniques allowing the creation of cell sheets and patches, can increase stem cell survival and boost therapeutic action (reviewed in [262]). Indeed, creation of human cardiac cell sheets using hiPS cells was recently reported, and hiPS derived-CMs sheets displayed spontaneous and synchronous beating and electrical transmission between cell layers [263]. Moreover, transplantation of stem cell populations within bioengineered scaffolds has led to greater improvement of cardiac function in animal MI models [264, 265] and has even allowed for the generation of engineered human cardiac tissue [266]. For example, a recent report has shown the benefit of transplanting a matrix composed by a mixture of SSEA1$^+$ cardiac progenitors derived from nonhuman primate ESC and adipose derived stem cells (ADSC), providing new differentiated CMs and exerting a trophic support, respectively [267]. Also, when hESC derived-CMs and vascular cells were seeded onto poly-l-lactic acid (PLLA) scaffolds, a highly vascularized cardiac tissue with structural, molecular and functional cardiac properties was generated *in vitro*. In another recent study, a functional improvement was shown in a porcine model of MI after transplantation of a fibrin scaffold patch seeded with hESC-derived ECs and SMC [268]. Also, other relevant reports on myocardial tissue engineering have been published showing the benefit of scaffold-free myocardial constructs transplantation. Dr. Stevens and colleagues created heart patches by combining hESC derived-CMs, endothelial and stromal cells that markedly enhanced tissue vascularization and survival after their transplantation into rodent hearts [269]. Similar positive effects were reported in the context of the use of an ESC-derived cardiac tissue sheet in a rat model of MI [270]. Also, based on this knowledge, tissue patches have been created with cardiovascular cells derived from iPS. Thus, the generation of a three-dimensional (3D) human cardiac tissue patch by combining collagen type I and hESC-derived and also hiPS derived-CMs has also recently been reported [271]. CMs showed alignment and proliferation within the collagen 3D matrix when subjected to mechanical stress. Also, formation of a vascular network within the bioengineered human cardiac tissue was demonstrated when ECs and stromal cells were co-cultured with the CMs. Moreover, when cardiac constructs were transplanted into immunodefficient rat hearts, human myocardium survived and formed grafts that closely resembled the host myocardium. Other studies have been reported, showing the functional benefit derived from the use of an iPS-derived cardiac tissue in mouse [272] and pig [273] models of MI. Dai and colleagues showed the efficacy of transplantating a

tricell pacth containing iPS derived-CMs, ECs and MEFs in an infarcted mouse model, which led to improved the cardiac function and attenuated the degree of adverse tissue remodeling fibrosis [272]. Interestingly, the therapeutic benefit of hiPS derived-CMs sheets in a porcine model of MI was also reported [273], resulting in significantly improved cardiac function and attenuated left ventricular remodeling following ischemic damage. Importantly, few surviving cells were found when hiPS cell-derived CM grafts were monitored eight weeks after transplantation, and no teratoma formation was observed. This report suggests that iPS-derived cardiac tissue could be therapeutically effective and safe for their use in cardiac regeneration therapy. Moreover, a recent study has reported the mechanical integration of hESC-derived CMs in a pig model of MI [274], demonstrating cell integration with synchronized contractions within the host myocardium four weeks after their transplantation, reducing susceptibility to arrhythmia and preserving mechanical function. Therefore, combining different cell populations and using tissue-engineering platforms might result in improved engraftment and survival of the transplanted cells, subsequently boosting their therapeutic effects.

5. iPS CELLS FOR TREATING DISEASE AND DRUG TESTING

The potential use of iPS-derived cells for the treatment of disorders has not only been shown in animal models of cardiac disease but also in others like Parkinson, spinal cord injury or muscular dystrophy. The group of Dr. Werning demonstrated that neurons derived from reprogrammed fibroblasts functionally integrated into the brain and improved symptoms of parkisonian rats [275]. Also, Dr. Tsuji and coworkers showed that iPS-derived neurospheres differentiated into the neural lineages after their transplantation into the damaged spinal cord, promoting locomotor function recovery [276]. Similar transplantation strategies have been performed in a mouse model of muscular dystrophy. Myogenic precursors were derived from hiPS cells and were transplanted into the dystrophic mouse muscle, engrafting and differentiating towards myofibers that significantly improved muscle contractility [277]. On the other hand, iPS cells have been proven to be useful for repairing disease caused by mutations. In a pioneer study, it was demonstrated that iPS cells could exert a therapeutic effect in an animal model of sickle cell anemia [278]. In this work, iPS cells were generated from hematopoietic cells isolated from a transgenic mouse that carried the β-globin gene

mutation that was then repaired by gene specific targeting. Afterwards, directed differentiation of the repaired iPS cells into hematopoietic progenitors was performed and transplantation of these progenitors into the transgenic mouse led to the rescue of the disease phenotype. In addition, phenotypic correction of hemophilia A in mice transplanted with iPS derived-endothelial progenitors cells has been also demonstrated [279] and genetic correction has also been applied to iPS cells derived from patients with disorders like Fanconi anaemia disease [280]. Patient-derived fibroblasts could be repaired by transduction with lentiviral vectors encoding the *Fanca* gene and next be reprogrammed into iPS cells with a normal phenotype, deriving, when differentiated, towards functional hematopoietic progenitor cells. Furthermore, genetic correction of Huntington´s Disease (HD) in fibroblast-derived iPS cells, has also recently been reported [281]. hiPS cells derived from HD patient fibroblasts could be corrected by the replacement of the mutation in the huntingtin gene by homologous recombination, with a persistence of the correct genotype in the differentiated neurons, both *in vitro* and *in vivo*. Finally, targeted gene correction has also been shown in iPS cells derived from patients with Duchenne muscular dystrophy (DMD) [282], laminopathy disorders [283], Wilson´s disease [284], granulomatous [285] and β-thalassemia disease [286].

In addition to their regenerative capacity, iPS cells can constitute also an important tool for modeling cardiac diseases, allowing to study the molecular mechanisms involved in different syndromes and to test specific drug targets (**Figure I9**). Several laboratories have already addressed the efficacy of drugs or small molecules for correcting or improving the disease phenotype for familial dysautonomia [287], spinal muscular atrophy [288] and Rett syndrome [289]. Thus, for example, the group of Dr. Lee and colleagues [287] derived iPS cells from patients with familial dysautonomia, a rare genetic disorder of the peripherial nervous system caused by a mutation in the *Ikbkap* gene and, after drug screening with different compounds, showed that the disease phenotype could be partially repaired by kinetin, a plant hormone. Similarly, drug screening in amyotrophic lateral sclerosis (ALS) patient-specific iPS cells, identified the anacardic acid (a histone acetyltransferase inhibitor) as a compound that could prevent the motor neuron degeneration [290].
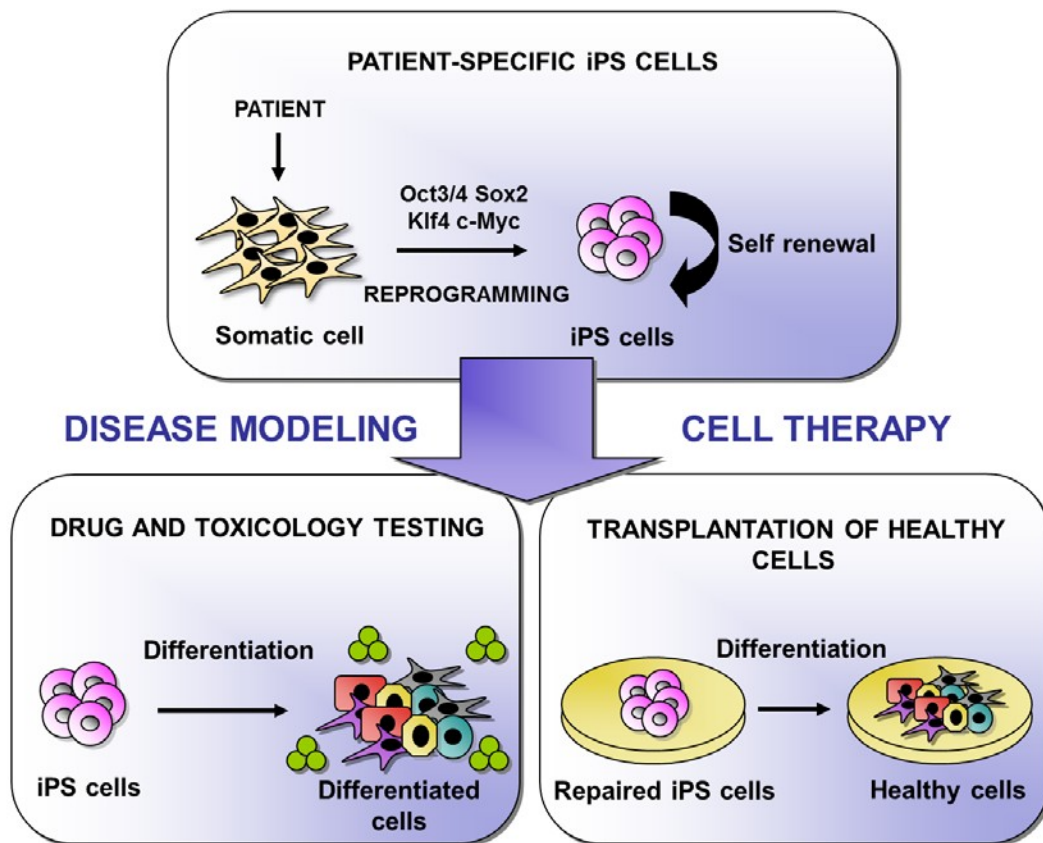
Figure I9. Clinical applications of iPS cells. Generation of iPS cells from somatic cells have broadened the horizon for regenerative therapy as these cells present the potential to model and treat human disease. Patient-specific iPS cells can be derived from somatic cells by ectopic expression of the transcription factors *Oct3/4*, *Sox2*, *Klf4* and *c-Myc*, to be next *in vitro* differentiated towards the desired cell subtype, allowing to model the patient´s disease and to screen potential drugs. Alternatively, iPS cells derived from a patient with a known mutation could be genetically repaired and, once corrected, undergo differentiation into the desired cell type to be transplanted into the patient. The derivation of iPS cells presents great potential for stem cell therapy but it is necessary to generate a reproducible differentiation system for the establishment of patient specific disease models, for drug screening and target validation and for the establishment of future autologous cell-replacement therapies.

The generation of iPS cells from patients having genetic cardiac disorders has already been shown too. For instance, iPS cells have been derived from patients with LEOPARD syndrome, and the *in vitro*-derived CMs presented the disease phenotype [291]. Also, hiPS cell-derived CMs from patients with long-QT syndrome displayed the characteristic electrophysiological signatures of the disease [292-295]. Similar findings were observed for human iPS cell-derived CMs from patients with familial dilated cardiomyopathy and Brugada syndrome [296, 297]. Using these cells as a model, studies have analyzed the potential therapeutic efficacy of drugs or small molecules for correcting cardiac disease phenotypes. In this regard, it was reported that CMs derived

from long-QT syndrome iPS cells were susceptible to catecholamine-induced tachyarrhythmia, and that the effects of isoprenaline, which exacerbated the disease phenotype, could be attenuated by treatment with β-adrenergic receptor blocker [292]. Moreover, type-II long-QT syndrome has also been modeled using iPS-derived CMs [293], which were used to evaluate the therapeutic potency of existing and new pharmacological agents. It was identified that the long-QT behavior of the CMs was aggravated by potassium channel blockers, whereas nifedipine (a calcium channel blocker) and pinacidil (an agonist of ATP-sensitive potassium channels) ameliorated the long-QT syndrome phenotype, as shown by decreased duration of action potentials and elimination of arrhythmias. Finally, catecholaminergic polymorphic ventricular tachycardia (CPVT) was also studied using hiPS cells, and the arrhythmogenic disease phenotype could be abrogated following treatment with dantrolene, a drug effective on malignant hyperthermia [298]. Thus, important advances are likely to stem from the use of iPS cell-related disease models, which can be utilized to study mechanisms of cardiac pathogenesis, to identify cardiotoxic effects of drugs, and to characterize the protective effects or optimal doses of therapeutic agents.

In summary, the ability to induce a pluripotent state in somatic cells offers attractive new therapeutic options and provides possible tools for obtaining a deeper understanding of human disease. Although the use of iPS cells seems ideal for regenerative medicine, there are many aspects of this technology that need to be improved and assessed before clinical application becomes a reality. Indeed, optimization of non-integrative methods for cell reprogramming, cell differentiation/selection protocols, and *in vivo* functionality will be required prior to clinical translation of these techniques. In this regard, direct reprogramming or transdifferentiation strategies, which can allow generation of progenitors and mature cells from human somatic cells without establishing initial pluripotency, might lead to safer protocols. These approaches could avoid the danger associated with residual pluripotent stem cells that are capable of forming teratomas. In any case, greater efforts should be made to improve current standard approaches and to better understand the molecular processes involved in cell reprogramming. Furthermore, new bioengineering strategies could increase the efficacy of iPS cell-derived transplants by improving their engraftment, survival, and functionality in tissues. Also these techniques offer the possibility of creating tissue patches *in vitro* that could be transplanted into injured

organs to mediate repair. Finally, this technology can be used to generate reproducible systems that model patient-specific disease, facilitating drug screening and target validation.

Taken together, the reprogramming of somatic cells into iPS cells offers exciting new tools that can be used to gain molecular insight into cardiac diseases and the potential to develop novel regenerative therapies.

HYPOTHESIS AND OBJECTIVES

The generation of induced pluripotent stem (iPS) cells represents a great promise for cardiovascular research and therapeutic applications. The ability of iPS cells to differentiate into cardiomyocytes has been recently described although their immature phenotype has been revealed by electrophysiological studies.

Interestingly, it has been described the importance of NRG-1β protein in heart development as well as its role in ESC cardiac differentiation and cardiomyocytes survival and proliferation.

Thus, the **hypothesis** of our study is that NRG-1β protein may provide a molecular strategy to promote cardiac specification and maturation in iPS cells and that iPS-derived cardiomyocytes could contribute to the regeneration of damaged heart tissue after myocardial infarction.

Based on these premises, this thesis attempts to fulfill the following **objectives**:

1. To generate and characterize clones of iPS cells from adult fibroblasts derived from an αMHC-GFP transgenic mouse.

2. To analyze the *in vitro* differentiation potential of iPS cells into cardiac cells and determine the role of the NRG-1β protein in cardiac specification and maturation.

3. To establish an optimized acquisition and analysis protocol for echocardiographic evaluation of heart left ventricle remodeling, in a mouse model of myocardial infarction.

4. To study the regenerative potential of the iPS-derived cardiomyocytes in a model of acute myocardial infarction in mice.

MATERIAL AND METHODS

1. GENERATION OF INDUCED PLURIPOTENT STEM CELLS

1.1. Mouse tail fibroblasts isolation

Mouse fibroblasts were isolated from the tail of 6-8 weeks old αMHC-GFP DBA/2J female mice (generously donated by Dr. LJ. Field, Indianapolis University, Indiana, United States) (ethical protocol #099-09 approved by the University of Navarra, Institutional Committee on Care and Use of Laboratory Animals). The tail was longitudinally cut to separate the skin from the bone, and the dermis cut into 1 cm pieces and subjected to mechanical and enzymatic digestions (4 rounds of 15 minutes with 4 mg/ml of Collagenase-I (Gibco) at 37°C). After centrifugation (600 x g, 10 minutes), the cells were resuspended in standard culture D10 media (DMEM HG (Gibco), 10% Fetal Bovine Serum (FBS) (Biochrom) 1% L-glutamine (Gibco) and 1% penicillin-streptomycin (Biowhittaker)) supplemented with 10 ng/ml of basic fibroblast growth factor (bFGF) (Sigma-Aldrich) and maintained in culture for 7 days in 0.1% gelatin (Sigma) coated dishes at 37°C in 5% CO_2 and humidified atmosphere. The bFGF concentration was gradually reduced (10 – 1 ng/ml) until the day before use. Cells were passaged every 2-3 days at a splitting ratio of 1:4 and used within three passages to avoid replicative senescence.

1.2. Mouse embryonic fibroblasts isolation, expansion and irradiation

DBA/2J mice embryos of 14.5-15.5 days post coitum (p.c.) were extracted from their placenta and surrounding membranes and dissected to remove the limbs, brain, internal organs and guts (ethical protocol #110-10 approved by the University of Navarra, Institutional Committee on Care and Use of Laboratory Animals). The embryos were washed with DMEM and subjected to 3-4 cycles of mechanical and enzymatic digestions with 0.5% Trypsin: 2 g/L EDTA (Gibco) for 10 minutes at 37°C and occasional mixing by vortex. Pooled supernatants were collected and filtered through a 40 μm nylon cell trainer (BD) to remove debris. Cells were centrifuged at 600 x g for 10 minutes and the pellet resuspended in D10 media plus 2 ng/ml of bFGF (Sigma). Cells were splitted every 2-3 days at a 1:3 ratio for a maximum of three passages before use (**Figure M1A**).

MEFs at passage 3 were irradiated at 50 Gy in a GammaCell irradiator (Gammacell 3000 Serial #375 Irradiator, MDS Nordion). No changes in cell viability were detected after irradiation. Next, cells were centrifugated (600 x g, 5 minutes) and frozen in freezing media (50% FBS and 10% of dimethyl sulfoxide (DMSO) (Sigma) in DMEM) at a cellular density of 2.5×10^6 cells/cryovial. Cells were immediately stored at -80 ºC in freezing containers (Nalgene) and transferred the next day to liquid nitrogen tanks for long-term storage. When needed, frozen cells were thawed and plated at a cellular density of 4×10^4 cells/cm^2 onto 0.1% gelatin coated dishes the day before use (**Figure M1B**).
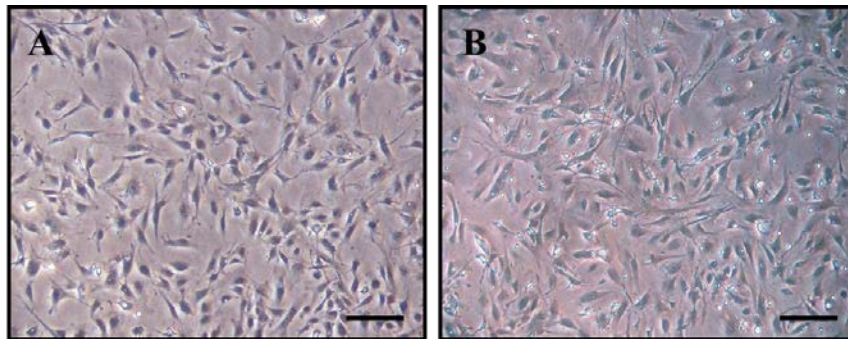
Figure M1. Mouse embryonic fibroblasts (MEFs) for iPS cell culture. A) Embryonic fibroblasts from mice embryos (14.5 p.c.) at passage 2. **B)** Irradiated embryonic fibroblasts at passage 3. Scale bars: 100 µm.

1.3. Retroviral infection and iPS cell generation

For virus production, Plat-E packaging cells (Cell Biolabs) were expanded in 1 µg/ml puromycin (Sigma) and 10 µg/ml blasticidin S (Fluka)-supplemented D10 medium at a splitting ratio of 1:4 - 1:6. The addition of puromycin and blasticidin-S allows the positive selection of those cells containing the structural genes *gag-pol* and *env* along with resistance genes against the two drugs. A day before transfection, Plat-E cells were plated in 100 mm Petri dishes at a cellular density of 1×10^5 cells/cm^2 in D10 media without puromycin and blasticidin-S. To transfect Plat-E cells 27 µl of the Fugene 6 transfection reagent (Roche) was added to 300 µl DMEM, mixed gently, and incubated for 5 minutes at room temperature (R/T). Nine micrograms each of the pMXs plasmids individually containing the reprogramming factors Oct3/4, Sox2 and Klf4 (Addgene) was added to the Fugene-DMEM mix and incubated for 15 minutes at R/T

(**Figure M2**). Finally, the complete transfection mix was added dropwise into the medium of Plat-E cells (10 ml) and incubated overnight (o/n) at 37ºC, 5% CO_2.
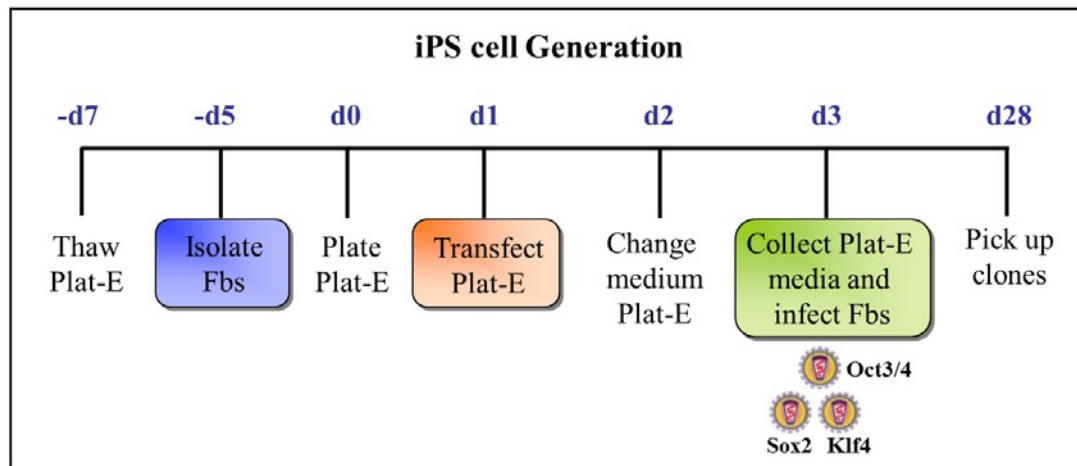
Figure M2. iPS cells generation protocol. iPS cells were obtained from adult fibroblasts (Fbs) derived from the mouse tail. Plat-E cells were transfected with retrovirus carrying the reprogrammning factors Oct3/4, Sox2 and Klf4. Equal amounts of each retrovirus supernatant were mixed and transferred to the fibroblasts (passage 2-3). Three weeks post-infection, some iPS clones started to appear and at day 28 were selected and maintained in culture onto irradiated embryonic murine fibroblast feeders.

Twenty-four hours after transfection, the media was replaced and the virus-containing supernatant collected after another 24 hours. Supernatants were filtered through a 0.45 µm pore size filter and supplemented with 4 µg/ml polybrene (Sigma). Equal amounts of each retrovirus supernatant were mixed and transferred to the fibroblasts (passage 2-3) at 2 ml/well (**Figure M3A**). Cells were incubated o/n at 37ºC, 5% CO_2. A pMXs-GFP vector (Addgene) was used as control for transfection (**Figure M3B**).

On days 1 and 2 post-infection, media was replaced with fresh D10 media and at day 3, standard media was switched to iPS media (DMEM HG (Gibco), 15% Knock-out serum replacement (Gibco), 1% nonessential amino acids (BioWhittaker), 1% penicillin-streptomycin (BioWhitakker), 1% L-glutamine (Gibco), 0.1 mM β-mercaptoethanol (Gibco) and 10^3 units/ml leukemia inhibitory factor/LIF (Chemicon)). From this day on, media was changed every day. Three weeks after infection, defined colonies started to appear and at day 28 each individual iPS colony was isolated and disaggregated into single cells by treatment with 0.5% Trypsin: 2 g/L EDTA (Gibco)

for 30 minutes at 37°C. iPS clones were then transferred onto a 24-well plate coated with MEFs and maintained in iPS culture media. After one week, colonies were passaged onto feeder coated 6-well plates and from there on, frozen and characterized in the following passages. Cells were split every 2-3 days at a ratio of 1:6 – 1:8, depending on cell density and not allowing a confluence greater than 80% in any case. The media was changed every day. When spontaneous differentiation became apparent, cells were split at a ratio of as high as 1:12 to rescue the cultures. When it was impossible to reverse the differentiation, undifferentiated iPS colonies were individually picked-up in the same manner as in picking-up colonies during an iPS derivation experiment.
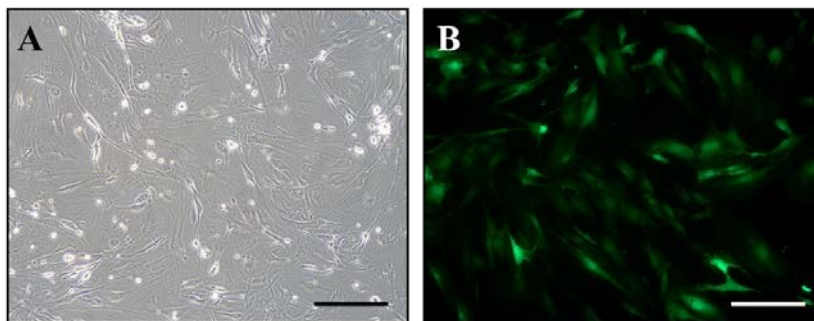
Figure M3. iPS cell generation after tail fibroblasts retroviral infection. A) Tail fibroblasts from 6 week-old mice at passage 1. **B**) Tail fibroblasts infected with GFP as control for infection. Scale bars: 50 μm.

2. CHARACTERIZATION OF iPS CELLS

2.1. RNA isolation, reverse transcription and quantitative PCR

Total RNA from iPS cells was extracted using the Ultraspect total RNA isolation kit (Biotecx Laboratories). Two million cells were homogenized with 1 ml of Ultraspect reagent and mixed with 200 μl of chloroform. After centrifugation, the aqueous layer was collected and RNA precipitated with an equal volume of 2-propanol and washed and dissolved in DEPC-treated water. RNA yield was measured using a NanoDrop spectrophotometer (Thermo Scientific). Next, samples were treated to remove genomic DNA contamination with the Turbo DNA free kit (Ambion). One-ten μg of RNA were mixed with a Turbo DNase Buffer and 1 μl of Turbo DNase in a final volume of 50 μl and then incubated at 37ºC for 30 minutes. Next, 5 μl of 10X DNase Inactivation

Reagent was added to the samples and incubated 2 minutes at R/T. After centrifugation at 10000 x g for 90 seconds, the RNA was collected and the inactivation reagent removed. The RNA yield was again measured with a NanoDrop spectrophotometer.

Purified RNA was next reverse transcribed into complementary DNA (cDNA) using the Superscript II Reverse Transcription Kit (Invitrogen). One µg of RNA was mixed with 5 µl of random hexamers (100 ng/µl) in a final volume of 20 µl and a preliminary annealing step performed (70ºC for 10 minutes and 25ºC for 10 minutes). For the cDNA synthesis, a master mix was prepared with 8 µL 5X First Strand Buffer, 4 µl of 0.1 M DDT, 2 µl of 10 mM dNTPs, 1 µl of RNAsa OUT, 1 µl of SuperScript II enzyme and 4 µl of distilled water. Finally, 20 µl of the master mix was added to the first reaction mix (annealing step) for cDNA synthesis (25ºC for 10 minutes, 37ºC for 45 minutes, 42ºC for 45 minutes and 70ºC for 15 minutes). Retrotranscription was performed in a 2720 Thermal Cycler (Applied Biosystems, Foster City, CA, USA). cDNA solutions were finally diluted to a final volume of 160 µl with distilled water.

Two microliters of the diluted cDNA solution was added to each quantitative PCR (qPCR) composed of 6 µl 10X Syber Green Master Mix (Applied Biosystems), 0.5 µl of 5 µM forward primer (Sigma), 0.5 µl of 5 µM reverse primer (Sigma) and 3 µl of PCR-grade water. The qPCR reactions were carried out in the 7300 real-time PCR system (Applied Biosystems) using the following program: Stage I (1 cycle of 50ºC for 2 minutes), Stage II (1 cycle of 95ºC for 10 minutes), Stage III (40 cycles of 95ºC for 15 seconds and 60ºC for 1 minute) followed by a dissociation stage (1 cycle of 95ºC for 15 seconds, 60ºC for 60 seconds, 95ºC for 15 seconds, and 60ºC for 15 seconds).

Mouse *Gapdh* (Applied Biosystems) was used as housekeeping gene. RNA from mouse D3 embryonic stem cell line (ATCC, CRL-1934) was used as positive control to normalize the pluripotent genes and total mouse heart RNA (Clontech) was used as positive control to normalize the cardiac genes. Specific primers were designed by Primer 3 Software (http://primer3.sourceforque.net/) (**Table M1**) with annealing temperatures at 60ºC and in a way that amplicons spanned or encompassed large introns if possible. By nucleotide BLAST (http://blast.ncbi.nlm.nih.gov/Blast.cgi), primers were verified to have not any sequence homology with other transcripts. Primers were tested before their use to verify no dimer formation.

To test for silencing of the retroviral transgenes expressed for cell reprogramming, qPCR was carried out in the same manner but using primers that distinguish between endogenous and total transcripts (total transcripts meaning both endogenous and viral transcripts) as described by Takahashi & Yamanaka [53] (**Table M1**).

Table M1. qPCR primers for stem cell pluripotency markers (**Endo**: endogenous gene expression, **Total**: viral plus endogenous gene expression).

ESC markers	Sense	Antisense
Endo Oct3/4	TAGGTGAGCCGTCTTTCCAC	GGTGAGAAGGCGAAGTCTGA
Endo Sox2	AAGGGTTCTTGCTGGGTTTT	AGACCACGAAAACGGTCTTG
Endo Klf4	ATTAATGAGGCAGCCACCTG	ACGCAGTGTCTTCTCCCTTC
Endo c-Myc	TGAAGGCTGGATTTCCTTTG	TTCTCTTCCTCGTCGCAGAT
Total Oct3/4	CACGAGTGGAAAGCAACTCA	TTCATGTCCTGGGACTCCTC
Total Sox2	ACTTTTGTCCGAGACCGAGA	CTCCGGGAAGCGTGTACTTA
Total Klf4	AAAAGAACAGCCACCCACAC	TGGTAAGGTTTCTCGCCTGT
Nanog	CGCCATCACACTGACATGAG	GAGGCAGGTCTTCAGAGGAA
Ecat-1	TGCCTGGAAGATCCAAAAAG	TGTGCTCTCCATCCTTACCA
Eras	CCTACTGCCCCTCATCAGAC	TTTGTAGGCAAAGCCATTCC
Rex1	CCACTGACCAAAAAGCAGGT	CCACTTGTCTTTGCCGTTTT
Fbx15	TGCCAATTGTTGGGAGTACA	CATGCTGCTTCGTGACAGAT

2.2. Alkaline phosphatase staining

Alkaline phosphatase staining was performed using the Leukocyte Alkaline Phosphatase Kit (Sigma). The cells were fixed 15 minutes at R/T with Zn-Formalin (Thermo Scientific), washed 3 times with PBS and incubated 10 minutes in dark with the alkaline phosphatase solution. Cells were further washed and blue staining (that indicates alkaline phosphatase activity) determined. D3 cell line and MEFs were used as positive and negative controls respectively.

2.3. Immunofluorescence for pluripotent markers

For immunofluorescence staining, iPS cells were plated on gelatin-coated 6-well plates with three 15 mm cover slips each well. After 2 days, cells were fixed with Zn-Formalin (Thermo Scientific) for 10 minutes at R/T and washed thrice with PBS. At this stage, cells could be stored at 4ºC in PBS. For detection of pluripotency markers, cells

were permeabilized with 0.1% Triton X-100 for 30 minutes at R/T and then washed thrice with PBS for 5 minutes each. Primary antibodies (**Table M2**) diluted in 3% bovine serum albumin (BSA) in PBS, were added and incubated during 30 minutes at 37°C. Finally, cover slips were washed thrice with PBS for 5 minutes each, and Cy3-conjugated secondary antibodies (**Table M2**) diluted in the same solution as the primary antibodies were added and incubated during 30 minutes at 37°C in the dark. For nuclear staining, TOPRO-3 (Molecular Probes) was mixed at a 0.02 mM concentration in a solution of PBS:glycerol (1:1). Small drops of mounting medium were added on a glass slide (two per slide) and cover slips were placed upside down on TOPRO-3 to stain. D3 cell line and MEFs were used as positive and negative cell controls respectively. All photographs were taken on a Zeiss LSM 510 META laser confocal microscope (Carl Zeiss, Germany) and analyzed with a computerized system (AIM 4.2, Carl Zeiss, Jena GbmH, Germany).

Table M2. Antibodies used in immunofluorescence techniques for iPS cells characterization.

Type	Antibody	Host	Manufacturer	Catalog No.	Dilution
Primary	Oct3/4	Rabbit	Santa Cruz	sc-9081	1:50
Primary	Nanog	Rabbit	Abcam	Ab80892	1:100
Secondary	Anti-rabbit IgG Cy3-conjugated	Sheep	Sigma-Aldrich	C2306	1:1500
Secondary	Anti-mouse IgG Cy3-conjugated	Sheep	Sigma-Aldrich	C2181	1:1000

2.4. Teratoma formation assay

To test *in vivo* iPS pluripotency, 1 x 10^6 cells were subcutaneously transplanted into the dorsal flanks of 6-8 weeks old Rag2-/-γc-/- male mice (generously donated by Dr.Spits, Academic Medical Center of Amsterdam, Netherlands) (ethical protocol #112-10 approved by the University of Navarra, Institutional Committee on Care and Use of Laboratory Animals). Mouse adult fibroblasts used to generate the iPS cells, non-irradiated MEFs and the mouse embryonic stem cell line D3, were also injected as negative and positive cell controls respectively. Six-eight weeks later, the developed tumours were dissected and fixed in 10% formalin (Thermo Scientific) for 24 hours and processed for paraffin inclusion. Paraffin embedded samples were sectioned and stained

with hematoxylin-eosin following conventional protocols for histological analysis. Presence of differentiated cells representative of the three embryonic germ layers was considered indicative of iPS pluripotency.

3. *IN VITRO* DIFFERENTIATION

3.1. Cardiac differentiation protocol

For iPS cardiac differentiation, iPS cells were previously plated onto 0.1% gelatin coated dishes to eliminate contaminating MEFs. Two days later, iPS colonies were flushed and cultured on Ultra Low Attachment Culture Dishes (Corning) to allow embryoid bodies (EBs) formation (day -5). EBs were maintained in suspension during 5 days in differentiation media (DMEM High Glucose (Gibco) medium supplemented with 10% FBS (Biochrom), 1% L-glutamine (Gibco) and 1% penicillin-streptomycin (Biowhittaker) and afterwards, plated onto gelatin coated dishes (d0) and treated at days 1, 3 and 5 with 1% DMSO (Sigma-Aldrich) or 100 ng/ml NRG-1β protein (ImmunoTools) or the combination of both treatments. One week later, when beating colonies appeared, media was replaced by a specific media for cardiac cells (Claycomb media (Sigma-Aldrich) supplemented with 10% FBS (Biochrom), 1% L-glutamine (Gibco) and 1% penicillin-streptomycin (Biowhittaker)). For determining cardiac differentiation, GFP positive areas (indicative of cardiac specific αMHC expression) were quantified. Twenty random pictures were taken with a 2.5x objective (at day 7 and at day 14) and analyzed with the Analysis FIVE software (Olympus Biosystems GmbH, Germany). Data were expressed as the percentage of GFP positive areas. Finally, beating areas were dissected under the microscope (at day 7 and at day 14) and disagregated by incubation with 0.1% trypsin (Gibco) (diluted in DMEM media plus 2% chicken serum (Gibco)) for 2 hours at 37°C, for their characterization and for the *in vivo* studies.

3.2.   Characterization of iPS-derived cardiomyocytes (iPS-CMs)

3.2.1.   Cardiovascular gene expression

RNA isolation, reverse transcription (RT), and qPCR were performed as described above (See 2.1). Cardiac specific markers were evaluated using the primers indicated in **Table M3** and *Gapdh* (Applied Biosystems) was included as housekeeping gene.

Table M3. qPCR primers for cardiovascular markers.

Cardiac	Sense	Antisense
Mef2c	TGGAGAAGCAGAAAGGCACT	CACTTCTTCACTGCCACAGC
Nkx2.5	CAAGTGCTCTCCTGCTTTCC	GGCTTTGTCCAGCTCCACT
Tbx5	CACCTGGACCCGTTTGGA	CTTTGAACCGAACCCATTATTTTC
Gata4	CTGGAAGACACCCCAATCTC	CACAGGCATTGCACAGGTAG
αMhc	ATGTTAAGGCCAAGGTCGTG	CACCTGGTCCTCCTTTATGG
βMhc	CAACTGGAGGAGGAGGTCAA	TTCCCTCAGCAGGTCACAAT
Mlc2v	ACTATGTCCGGGAGATGCTG	TGGGTAATGATGTGGACCAA
Actinin	TCTCTTCCAGCCCTCTTTCA	ATGGTGGTGCCTCCAGATAG
Ryr2	GCGAGGATGAGATCCAGTTC	CTGCTGTTCTTTGTGGATGG
Hcn1	GTGGAGAAGGAGCAGGAAAG	GACCAAATTTCCAACCATCA
Cacna1c	AGGAAGTTCAAGGGCAAGGT	ATTCATGTTGGCATGAGCTG
Pln	CACTGTGACGATCACCGAAG	TTTCCATTATGCCAGGAAGG
Endothelium		
Cd31	GTCATGGCCATGGTCGAGTA	CTCCTCGGCGATCTTGCTGAA
vWF	TGCCGTTATGATGTTTGCTC	TTCCCACACTGCAGGTACAC
Flk-1	GATGCAGGAAACTACACGGTCA	CATAGGCGACATCAAGGCTTTC
VE-cadherin	ATTGAGACAGACCCCAAACG	TTCTGGTTTTCTGGCAGCTT
Smooth muscle		
Sm22α	CCACAAACGACCAAGCCTTCT	CGGCTCATGCCGTAGGAT
α-SMA	ACTGGGACGACATGGAAAAG	GTTCAGTGGTGCCTCTGTCA
Calponin	ACATCATTGGACTGCAGATG	CAAAGATCTGCCGCTTGGTG

3.2.2.   Immunofluorescence for cardiac markers

For immunofluorescent detection of cardiac markers, day 12-differentiated cells were seeded in chamber slides (Nalgene Nunc International, Naperville, IL) at a density of 60×10^3 cells/cm^2 and 2 days later (day 14 of differentiation) fixed with Zn-Formalin

(Thermo Scientific) for 10 minutes at R/T. After washed with PBS, permeabilized with 0.1% Tween (Sigma) for 15 minutes and blocked with 0.4% Fish Gelatin (Sigma) for 1 hour at R/T, cells were incubated 2 hours at R/T with the primary antibodies diluted in 0.4% Fish Gelatin (**Table M4**). After three washes with 0.1% Tween, Alexa Fluor-594 anti-mouse (Invitrogen), Alexa Fluor-594 donkey anti-rabbit (Invitrogen) and Cy3 donkey anti-goat (Jackson Immunoresearch) secondary antibodies were diluted and incubated at R/T for 1 hour in the dark. For nuclear staining, TOPRO-3 was used. The murine cardiac cell line, HL1 (generously donated by Dr. Claycomb, Louisinana State University Medical Center, USA) and the murine fibroblasts cell line, STO (MMRRC, UC Davis) were used as positive and negative cell controls respectively. All photographs were taken on a Zeiss LSM 510 META laser confocal microscope (Carl Zeiss, Germany) and analyzed with a computerized system (AIM 4.2, Carl Zeiss, Jena GbmH, Germany).

Table M4. Antibodies used for immunofluorescence techniques for characterization of iPS-CMs.

Type	Antibody	Host	Manufacturer	Catalog No.	Dilution
Primary	Cardiac actinin	Mouse	Sigma-Aldrich	A9357	1:100
Primary	Connexin 43	Rabbit	Sigma-Aldrich	C6219	1:500
Primary	Gata-4	Goat	Santa Cruz	sc-1237	1:50
Primary	Titin	Mouse	Hybridoma Bank	Clone 9D10	1:300
Secondary	Anti-mouse Alexa Fluor-594	Goat	Invitrogen	A11032	1:500
Secondary	Anti-rabbit Alexa Fluor-594	Donkey	Invitrogen	A21207	1:500
Secondary	Anti-goat IgG Cy3-conjugated	Donkey	Jackson Immunoresearch	705-166-147	1:500

3.2.3. Transmission electron microscopy

Isolated iPS-CMs were seeded in chamber slides (Nalgene Nunc International, Naperville, IL) at day 12 of differentiation at a density of 60×10^3 cells/cm^2 and 2 days later (day 14) fixed in 3.5% glutaraldehyde for 1 hour at 37 °C. Cells were post-fixed in 2% OsO$_4$ for 1 hour at R/T and stained in 2% uranyl acetate for 2 h at 4°C (dark). Finally, cells were rinsed in 0.1 M sodium phosphate buffer (PB) (pH 7.2), dehydrated in ethanol and infiltrated o/n in Araldite (Durcupan, Fluka, Buchs SG, Switzerland).

Following polymerization, embedded cells were detached from the chamber slide and glued to araldite blocks. Serial semi-thin (1.5 μm) sections were cut with an Ultracut UC-6 (Leica, Heidelberg, Germany) and mounted onto slides and stained with 1% toluidine blue. Selected semi-thin sections were glued (Super Glue, Loctite) to araldite blocks and detached from the glass slide by repeated freezing (in liquid nitrogen) and thawing. Ultrathin sections (0.06 – 0.09 μm) were prepared with the Ultracut and stained with lead citrate.

For electron microscopy studies of the mice hearts, animals were sacrificed, perfused with 0.1 M PB during 5 minutes and with Zn-Formalin / 0.5% glutaraldhehyde (Thermo Scientific) during other 5 minutes. Immediately, hearts were cut in slices of 1.0 mm with the help of a mouse heart slicer matrix (Zivic instruments) and fixed with Zn-Formalin / 0.5% glutaraldhehyde at 4ºC o/n. Slices were saturated in 25% sucrose (4ºC o/n), embedded in O.C.T. compound (Tissue-Tek, Sakura) and snap frozen in nitrogen-cooled isopentane. One hundred micrometer sections were washed in 0.1 M PB, cryoprotected in 25% sucrose and freeze-thawed (3x) in methyl-butane. For immunogold staining, samples were washed in PB, blocked in the solution I (0.3% BSA (Aurion) in PB) for 1 hour at R/T and incubated with a chicken primary anti-GFP antibody (1:200 diluted in blocking solution I; Aves Labs) for 3 days, at 4ºC under mild agitation. After three washes in PB (10 minutes each), sections were incubated in blocking solution II (0.5% BSA and 0.1% fish gelatin (Aurion) in PB) for 1 hour at R/T and incubated next with an anti-chicken goat antibody conjugated to colloidal gold (1:50 diluted in blocking solution II; UltraSmall; Aurion) for 24 hours at R/T under mild agitation. Sections were washed in PB and 2% sodium acetate. Silver enhancement was performed (following Aurion instructions) and washed again in 2% sodium acetate. To stabilize silver particles, samples were immersed in 0.05% gold chloride (10 minutes at 4°C), washed first in sodium thiosulfate and next in PB and postfixed in 2% glutaraldehyde (30 minutes). Sections were contrasted with 1% osmium and 7% glucose and embedded in araldite. Finally, semi-thin 1.5 μm sections were prepared, selected at the light microscope level and re-embedded for ultra-thin sectioning at 70 nm.

All photomicrographs were obtained under a transmission electron microscope FEI Tecnai G2 Spirit (FEI Europe, Eindhoven, Netherlands) using a digital camera Morada (Olympus Soft Image Solutions GmbH, Münster, Germany).

3.2.4. Patch-clamp analysis

To compare the electrophysiological maturation process, cells differentiated in the presence or not of NRG-1β protein were analyzed. Embryoid bodies were generated and differentiated as described above (See 3.1) on PD30 culture dishes (Falcon) coated with 0.1% of gelatine, and the cells were analyzed at day 7 and 14 of differentiation. Beating cells were examined under an inverted fluorescence microscope (Axiovert 200; Zeiss, Oberkochen, Germany), enabling the identification of GFP positive cardiomyocytes. Glass microelectrodes filled with 3 mol/l KCl (resistance: 20-30 MΩ) were used for recordings of intracellular APs. Since the cell layer was to some extent transparent, the tip of the recording electrode could be localized by the inverted microscope used, allowing a specific positioning of the electrode. All recordings were performed at 37ºC. Signals were amplified by a SEC-10LX single electrode clamp amplifier (NPI Electronic, Tamm, Germany, http://www.npielectronic.com/) and acquired with the PULSE software (HEKA, Lambrecht/Pflaz, Germany, htpp://www.heka.com/). AP parameters were analyzed off-line with the Mini Analysis software (Synaptosoft, Decateur, GA, USA, http://synaptosoft.com/).

4. TRANSPLANTATION OF iPS-CMs IN A MOUSE MODEL OF ACUTE MYOCARDIAL INFARCTION IN MICE

4.1. Surgical procedure for induction of myocardial infarction

Eight week old female DBA/2J mice (n=28) (Charles River Laboratories, France) underwent coronary artery ligation [299]. For surgical procedure, animals were anesthetized with 2% isofluorane (Isoflo®, ABBOTT S.A, Madrid, Spain), placed on a heating table in a supine position and endotracheally intubated for mechanical ventilation with supplementary oxygen. During surgery, anesthesia was maintained with a combination of 3% isoflourane and 0.01 mg/kg/ fentanyl (Fentanest, Kern Pharma). A thoracotomy was then performed at the left three intercostal space, the pericardium was opened and the left anterior descendent (LAD) coronary artery ligated with a 7.0 absorbable suture. Myocardial ischemia was confirmed by color change of the left ventricular wall. 10-15 minutes after artery ligation and CMs-iPS at day 7 of differentiation (2×10^5 cells suspended in 10 μl of DMEM) or control medium (10 μl) were injected in 4 points of the peri-infarct area by using a Hamilton syringe (Hamilton,

701N, 10μl). The intercostal incision was closed in layers with a 6.0 absorbable suture, the endotracheal tube removed and spontaneous breathing restored. The animals were kept in a cage, lying on a heating blanket for several hours until recovered from surgery. Enrofloxacin (25 mg/Kg) (Alsir ®, Esteve veterinaria) was added in the drinking water for 7 days to prevent infections and Ketoprofen (Ketofen®, Jesús Guerreo) subcutaneously injected 24 and 48 hours after surgery for analgesia. The survival rate over the course of the experiment was over 90%. Only those animals that survived (n=26) and with an ejection fraction (EF) below 40% (determined by echocardiography, see section 4.2.2) 2 days post-transplantation, were included in the study (n=16). All experiments were performed in accordance with the principles of laboratory animal care formulated by the National Society for Medical Research and the guide for the care and use of laboratory animals of the Institute of Laboratory Animal Resources (Commission on Life Science, National Research Council). All animal procedures were approved by the University of Navarra Institutional Committee on Care and Use of Laboratory Animals (ethical protocol #099-09).

4.2. Echocardiographic studies

For echocardiography procedure, mice were anesthetized with isoflurane (Isoflo®, ABBOTT S.A, Madrid, Spain), at a concentration of 4% (for induction) and 1.5% (for maintenance) in 100% of oxygen. The animal was placed on a heating table in a supine position with the extremities fixed on the table through four electrocardiography leads. The chest was shaved using a chemical hair remover (Veet, Reckitt Benckise, Granollers, Spain). Warmed ultrasound gel (Quick Eco-Gel, Lessa, Barcelona, Spain) was applied to the thorax surface to optimize the visibility of the cardiac chambers. The heart rate (HR) was recorded immediately before the echocardiography study (ethical protocol #099-09 approved by the University of Navarra, Institutional Committee on Care and Use of Laboratory Animals).

Echocardiography was performed using a Vevo 770 ultrasound system (Visualsonics, Toronto, Canada) and measurements for small animals optimized and performed as we have previously described [300]. For iPS-derived CMs or media (control group) treated hearts, echocardiography was performed 2, 30 and 60 days after LAD artery ligation. LV remodeling was quantified according to the guidelines and standards of American Society of Echocardiology, and the Guide to micro-

71

echocardiography study using the Vevo 770 and the Vevo 770® Protocol-Based Measurements and Calculations guide. LV structural analysis was quantified. First volume in diastole (VD) and volume in systole (VS) were calculated using the Simpson´s rule from a long-axis view and four short-axis views at different levels, from the aortic annulus to the endocardial border at the apex level, in both diastole and systole (**Figure M4**).
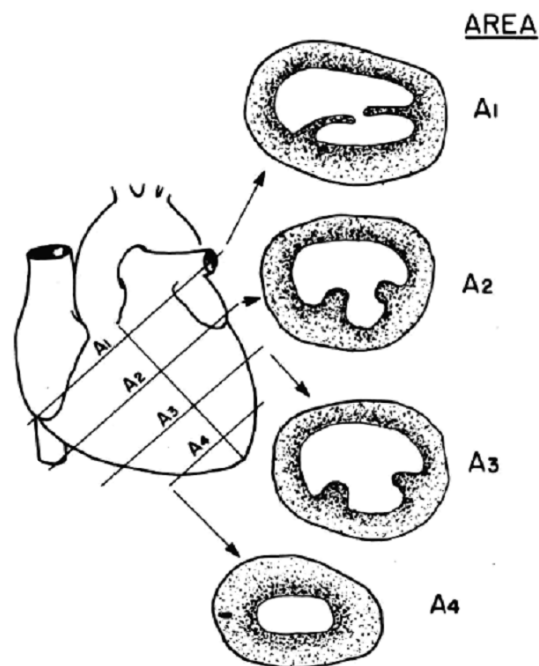
Figure M4. Scheme of area and length measurements performed to obtain Simpson´s measurements.

Stroke volume (SV), fractional shortening (FS%) and ejection fraction (EF%) were calculated according to the following equations: SV=VD-VS, FS%=[(VD-VS)/VD] x 100 and EF%= (SV/VD) x 100. Given the poor definition of the endocardial border on the short-axis view (especially at mid-ventricular and apical levels), that is caused by the apical location of the infarction in our model, the fractional area change (FAC%) was calculated in one paraesternal long-axis (FAC% long) in systole (Areas) and diastole (Aread) following the equation: FAC%= [(Endocardial Aread – Endocardial Areas)/Endocardial Aread] x 100. Long-axis views were acquired using gain settings that optimized the visualization of the endocardial and epicardial walls.

4.3.   Tissue processing and staining

Animals were sacrificed at 1, 2 and 4 weeks (1-2 mice/group) for histological assessment and at 2 months (8 animals/group) for functional and histological assesment. Mice were anesthetized, injected with 100µl of 0.1mM cadmium chloride (Sigma) for diastole cardiac arrest, and perfusion-fixed for 15 minutes with Zn-Formalin (Thermo Scientific) under physiological pressure. The hearts were excised, fixed o/n in Zn-Formalin at 4ºC, and cut in 3 equally sized blocks (apical, mid-ventricular and basal) of 3.0 mm by using a mouse heart slicer matrix (Zivic instruments) (**Figure M5**). Finally, hearts were dehydrated in ethanol 70% (4°C, o/n) and embedded in paraffin.
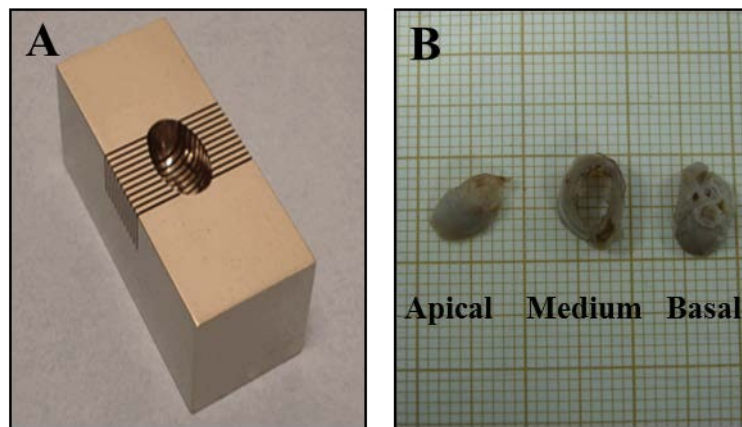
Figure M5. Tissue processing. A) Rodent heart slicer (Zivic Instruments). The heart is located into the slicer hole and two blades (Stanley) inserted (3 mm separated of each other). Once the blades are partially inserted, they are aligned with another one and simultaneously pressed down until the end. **B)** Heart blocks. The blades are raised out and the three heart blocks (apical, mid-ventricular and basal) removed.

For histological analysis, 5 µm serial sections were performed. Cell detection was based upon the presence of GFP positive signals by immnunohistochemical methods using anti-GFP rabbit polyconal antibody (pAb), or anti-GFP chicken pAb diluted in TBS (TBS: Tris 50 mM, NaCl 0.9%, pH: 7.36) for immunofluorescence. Immunolabeling was performed with antibodies against α-Smooth Muscle Actin (α-SMA-Cy3 conjugated), Caveolin-1, Connexin 43 and Cardiac-Troponin (cTnT) (**Table M5**). AlexaFluor-633 rabbit anti-mouse IgG, Alexa Fluor-594 donkey anti rabbit IgG, Alexa Fluor-488 goat anti chicken and Donkey anti rabbit FITC were used as secondary

antibodies (**Table M5**). EnVision[TM]-HRP conjugated system (Dako) was used as secondary reagent for immunohistochemistry. For confocal microscopy, a LSM 510 META (Carl Zeiss, Germany) microscope was used and photographs analyzed with a computerized system (AIM 4.2, Carl Zeiss, Jena GbmH, Germany).

For Sirius Red staining, sections were deparaffinized and immersed for 90 minutes in 0.1% Fast Red (Sigma) diluted in a saturated solution of picric acid, differentiated 2 minutes in 0.01 N HCl (Sigma), dehydrated, and mounted in DPX.

Table M5. Antibodies used for heart tissue staining.

Type	Antibody	Host	Manufacturer	Catalog No.	Dilution
Primary	eGFP	Rabbit	Invitrogen	A11122	1:500
Primary	eGFP	Chicken	Invitrogen	A13970	1:200
Primary	Caveolin-1	Rabbit	Cell signaling	3238	1:125
Primary	α-SMA-Cy3	Mouse	Sigma-Aldrich	6198	1:500
Primary	Troponin I	Mouse	Abcam	ab19615	1:100
Primary	Connexin 43	Rabbit	Sigma-Aldrich	C6219	1:500
Secondary	Anti-chicken Alexa Fluor-488	Goat	Invitrogen	A11039	1:500
Secondary	Anti-mouse Alexa Fluor-633	Rabbit	Invitrogen	A21063	1:400
Secondary	Anti-rabbit Alexa Fluor-594	Donkey	Invitrogen	A21207	1:500
Secondary	Anti-rabbit FITC	Donkey	Jackson Inmunology	711-096-152	1:200

4.4. Morphometric analysis

The infarct size and the tissue fibrosis degree were determined in Sirius Red stained sections. Infarct size was assessed by quantifying images taken from 12 serial heart sections 50 μm apart. Images were analyzed with the *AnalySIS* software and data expressed as a percentage of the ischemic area *versus* the total left ventricle area (LVA). For the quantification of the fibrosis degree, 24 images of the peri-infarct areas were taken from serial heart sections and analyzed with the *AnalySIS* software. Data were expressed as a percentage of the fibrotic area (red) of the peri-infarct zone *versus* the total tissue area.

Quantification of the vascular density was performed in animals sacrificed 2 months post-implantation. For arteriolar area (μm^2), 12 serial sections 50 μm apart were stained with an anti-α-SMA-Cy3 conjugated antibody (**Table M5**) and infarct border images were analyzed by measuring the area occupied by smooth muscle-covered vessels. Pictures were analyzed with software developed with the *Matlab* platform.

5. STATISTICAL ANALYSIS

Normal distribution was analyzed using the Shapiro-Wilk test. All data were expressed as mean ± SD. In case of normal distribution, comparisons between groups were performed using Student's t-test or ANOVA followed by Bonferroni's and Tukey´s HDS post-hoc tests. Non-parametric analysis was performed using Kruskal-Wallis and Mann-Whitney *U* test. Statistical analysis was performed with Prism GraphPad 4.0 and SPSS 11.0 softwares. Differences were considered statistically significant when $P<0.05$.

RESULTS

1. PART ONE: GENERATION OF MOUSE iPS CELLS

1.1. Generation of iPS cells from adult mouse tail fibroblasts

Induced pluripotent stem (iPS) cells were derived following Dr. Yamanaka´s protocol. Adult fibroblasts obtained from the tail of αMHC-GFP transgenic mice were transduced with a combination of three genes involved in stem cell pluripotency (*Sox2*, *Oct3/4* and *Klf4*), using a retrovirus-based approach. Approximately three weeks after infection, several clones started to appear as compact clusters with embryonic stem cell-like morphology. These colonies could be identified by their small, round, and compact morphology and tight, well defined borders, consistent with full reprogramming [301]. Six colonies were picked-up four weeks after infection and expanded into stable clones over an irradiated feeder layer of fibroblasts (MEFs). All the picked-up colonies easily grew to become stable clones. Irradiated MEFs supported the growth of undifferentiated iPS cells more robustly than the murine immortalized fibroblast cell line STO (only 1 clon of 56 picked-up colonies grew to became a stable clone), on which unwanted differentiation occurred more frequently, so all the studies were performed with a MEFs feeder layer. Six independent isolated clones were selected for *in vitro* characterization (**Figure R1**) that could be maintained in culture for at least 25 passages.
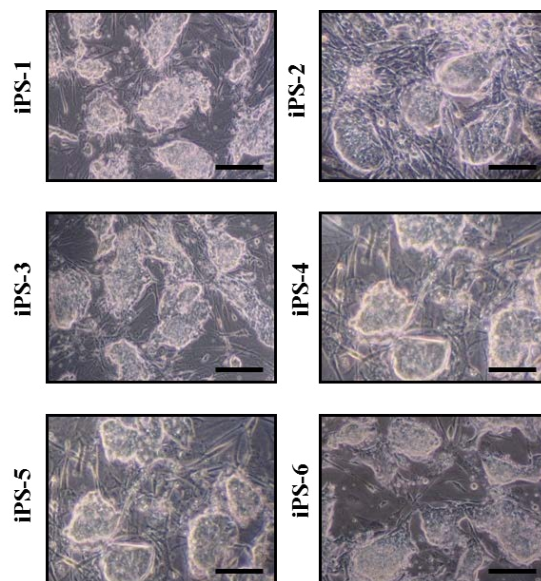
Figure R1. iPS cells morphologically resemble ESC. Morphology of six mouse iPS clones cultured over irradiated embryonic murine fibroblasts (MEFs) at passage 2. Scale bars: 50 μm.

1.2. iPS cells express endogenous ESC markers

One of the key properties of fully reprogrammed iPS clones is the endogenous activation of the core ESC gene regulatory network [301, 302]. Pluripotency of the selected clones was analyzed by qPCR data, showing that all of them expressed high levels of the endogenous pluripotent genes *Oct3/4*, *Klf4*, *Sox2* and other pluripotent genes not included in the reprogramming cocktail such as *Nanog*, *c-Myc*, *Ecat1*, *Eras*, *Fbx15* and *Rex1*, which were in some cases even higher than in the murine embryonic stem cell line D3. Expression of these genes was variable among clones being as an average higher in clone 1 (iPS-1) (**Figure R2**).
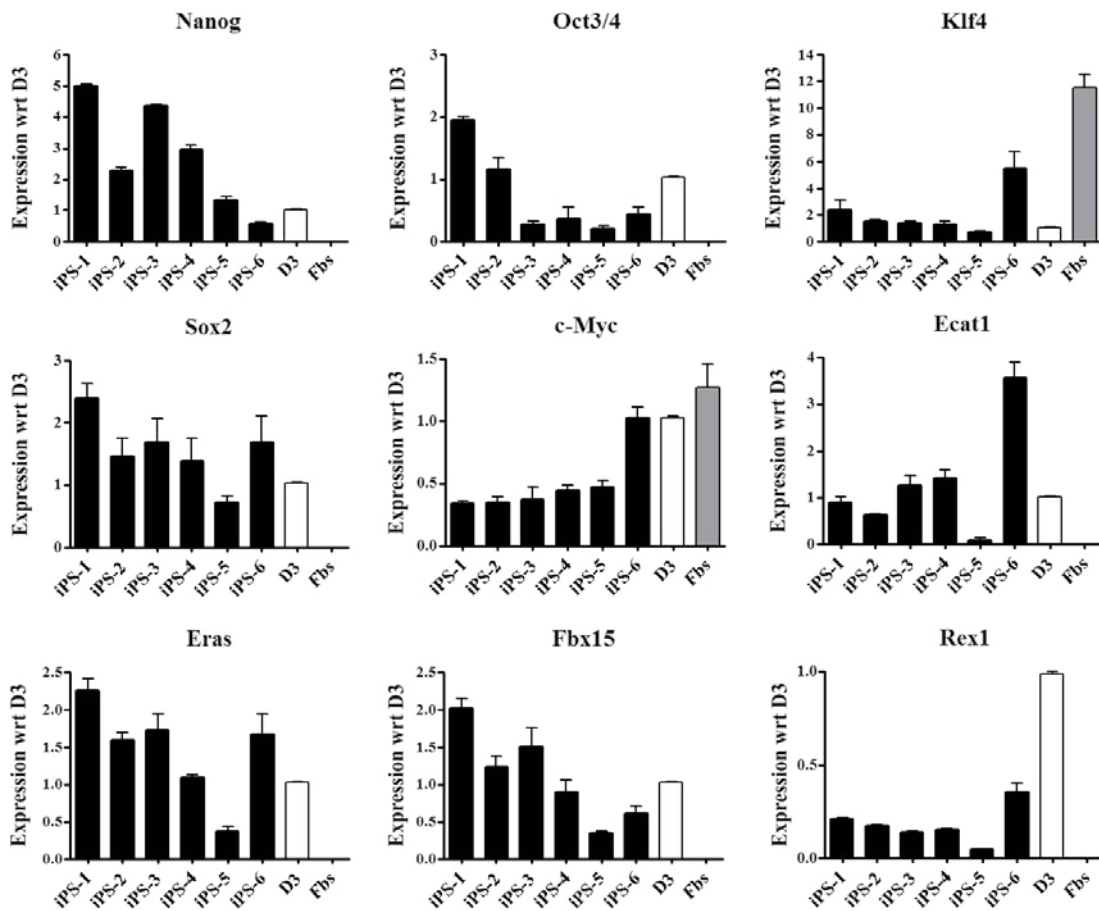
Figure R2. Endogenous gene expression of pluripotency markers measured by qPCR. The six iPS clones expressed genes common to pluripotent cells including *Nanog*, *Oct3/4*, *Klf4*, *Sox2*, *c-Myc*, *Ecat1*, *Eras*, *Fbx15* and *Rex1*. The murine embryonic stem cell line D3 and mouse adult fibroblasts (Fbs) were included as positive and negative controls respectively. Values were represented in comparison with D3 (Expression with respect to (wrt) D3). Data were expressed as mean ± SD.

Protein expression of the key pluripotent markers OCT3/4 and NANOG was analyzed by immunofluorescence together with Alkaline Phosphatase activity. All clones stained for OCT3/4 and NANOG proteins (**Figure R3**). Alkaline Phosphatase activity was also detected in all the clones (**Figure R4**).
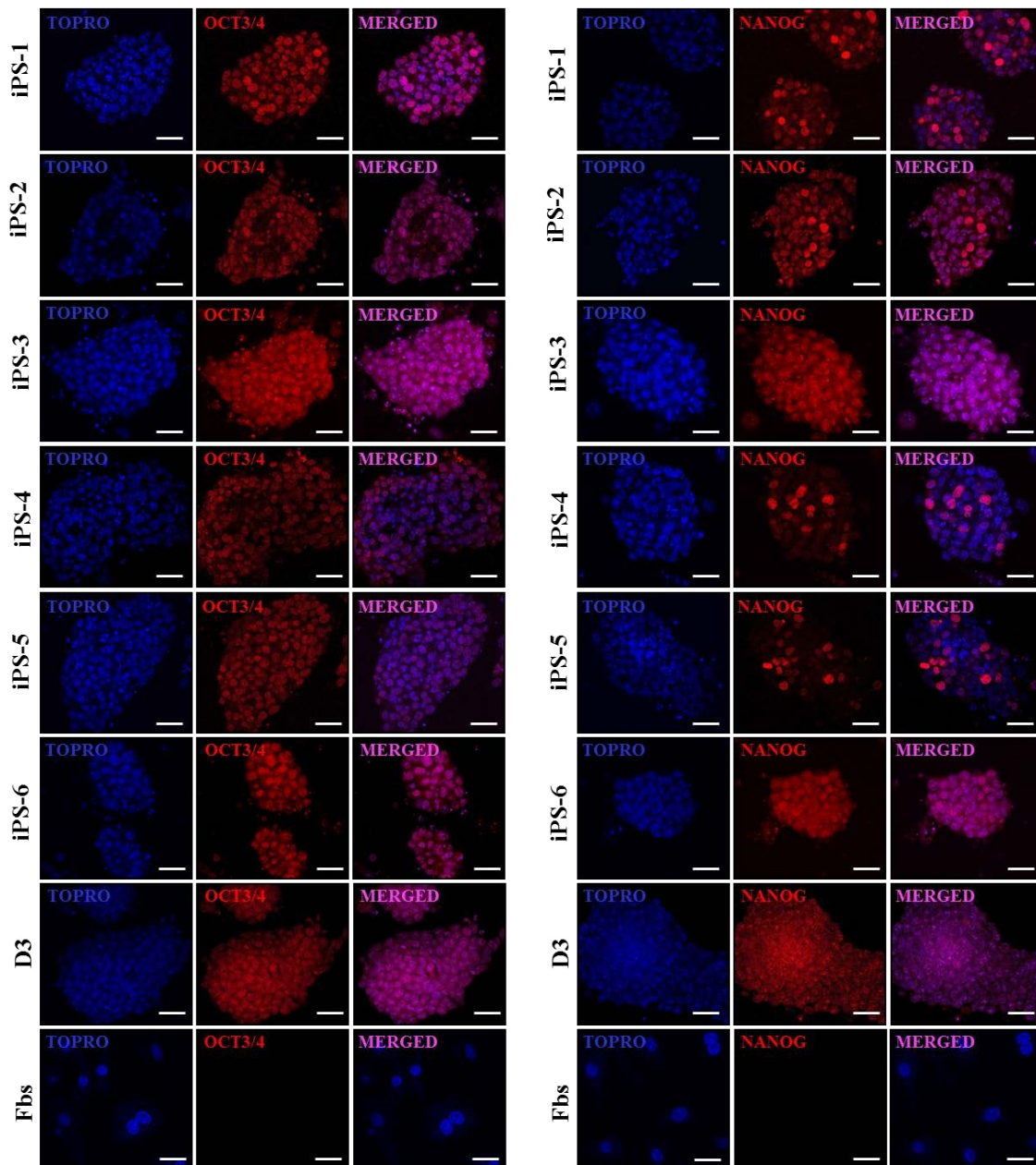
Figure R3. Protein expression of pluripotency markers. Protein expression of OCT3/4 (Cy3: red) and NANOG (Cy3: red) in iPS clones detected by immunoflurescence technique. Mouse embryonic stem cells (D3 cell line) and mouse adult fibroblasts (Fbs) were included as positive and negative controls respectively. Nuclear staining was performed with TOPRO-3 (blue). Scale bars: 50µm.
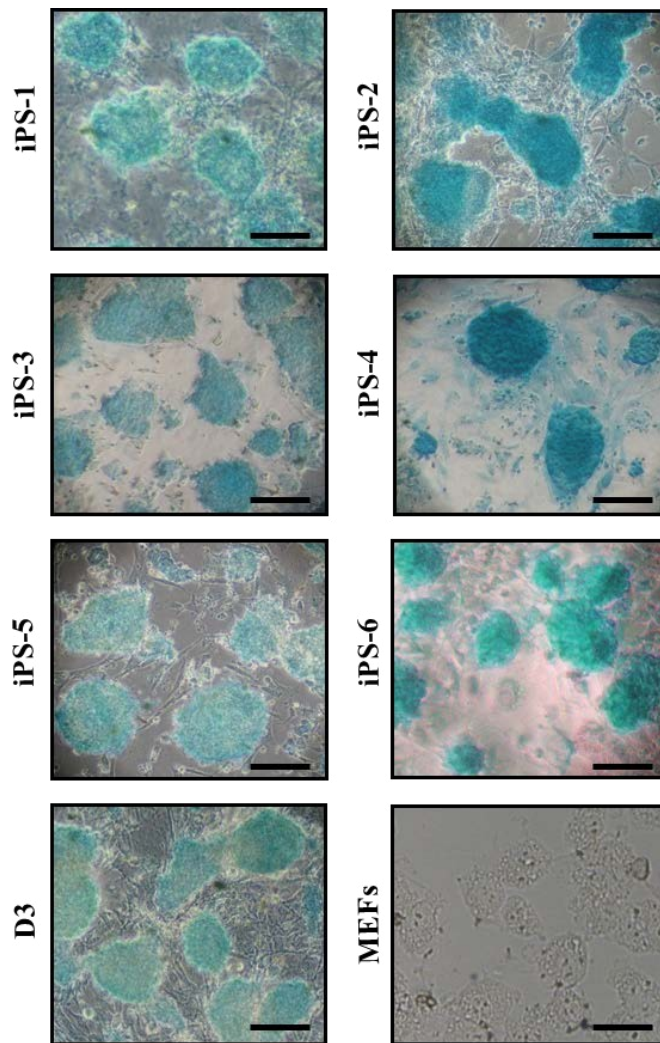
Figure R4. Alkaline Phosphatase staining in iPS clones. AP staining was performed in all the iPS clones, in the mouse embryonic stem cell line D3 (positive control) and in the mouse embryonic fibroblast (MEFs) (negative control). Scale bars: 50 μm (iPS and D3) and 25 μm (MEFs).

1.3.   iPS cells show retroviral silencing

Another mark of fully reprogrammed iPS clones is their capacity to silence the retroviruses introduced and therefore their ability to sustain pluripotency in absence of exogenous factor expression [301]. Thus, qPCR primers were designed to discriminate the endogenous transcripts of the three factors from the total transcripts (viral plus endogenous). The clones iPS-1, iPS-2 and iPS-6 demonstrated retroviral silencing of the three factors confirming the reprogramming of the cells (**Figure R5**). iPS-3, iPS-4 and iPS-5 clones expressed higher levels of total transcripts demonstrating an incomplete reprogramming.
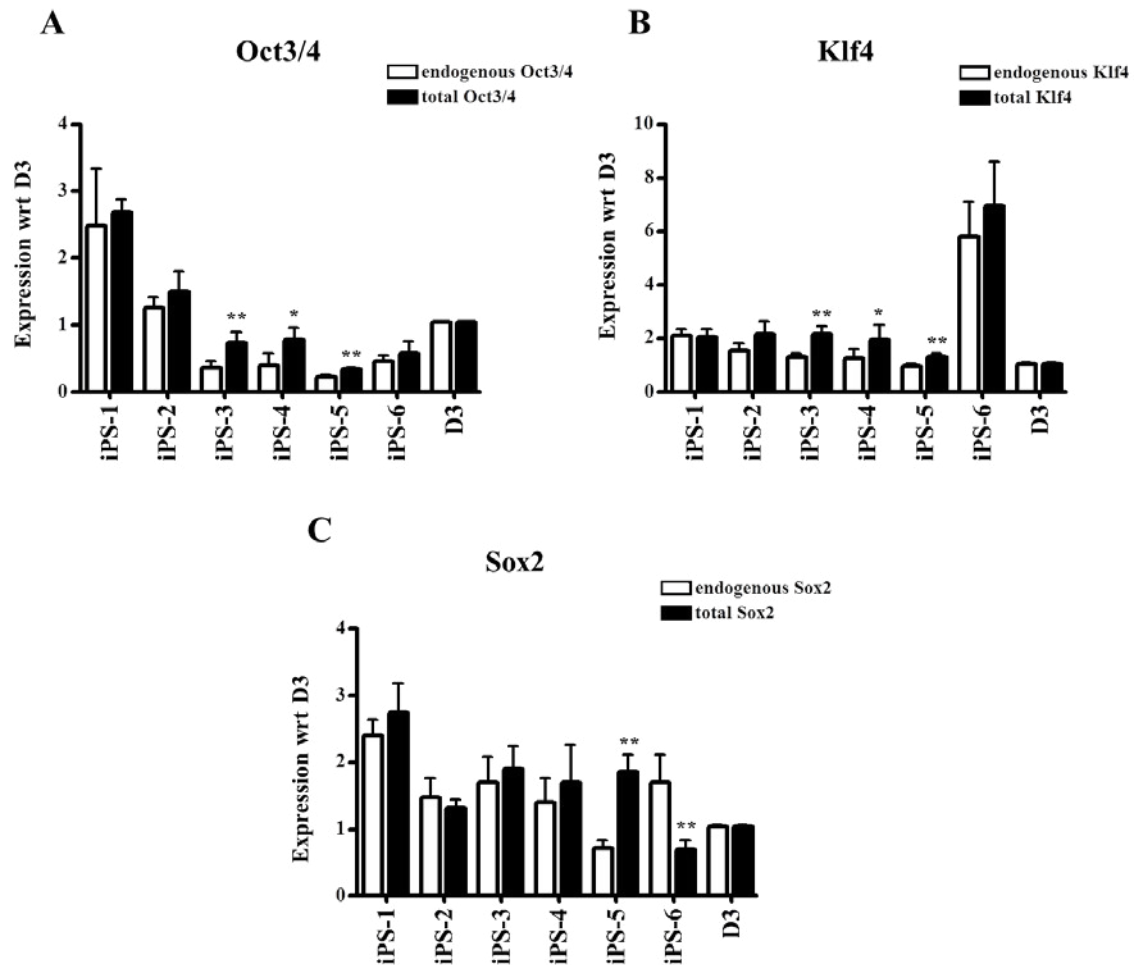
Figure R5. Retroviral silencing in iPS clones. qPCR data showing endogenous and total (viral plus endogenous) expression of the three factors **(A)** *Oct3/4*, **(B)** *Klf4*, and **(C)** *Sox2* in iPS clones analyzed at passage two. High levels of total transcripts in iPS-3, iPS-4 and iPS-5 denote retroviral activity. Total levels did not increased in iPS-1, iPS-2 and iPS-6 clones. Data were expressed as mean ± SD. *$p<0.05$; **$p<0.01$ between endogenous and total expression.

1.4.   iPS cells form teratomas *in vivo*

To test the *in vivo* pluripotency of iPS clones, one million cells of each iPS clone, the mouse embryonic stem cell line D3 and mouse adult fibroblasts, were subcutaneously injected into the dorsal flanks of Rag2$^{-/-}$γc$^{-/-}$ mice. As early as 2-3 weeks after injection, several nodules appeared at the sites of the injection for both ESC and iPS cells whereas no tumor growth was observed in the fibroblasts control group (**Figure R6A**). Histological analysis of 4-8 weeks tumours showed presence of many differentiated cell types that belonged to any of the three germ-layers like glandular epithelia (endoderm), cartilage (mesoderm) and nervous tissue (ectoderm) among others, confirming the pluripotent potential of the iPS clones (**Figure R6B**).
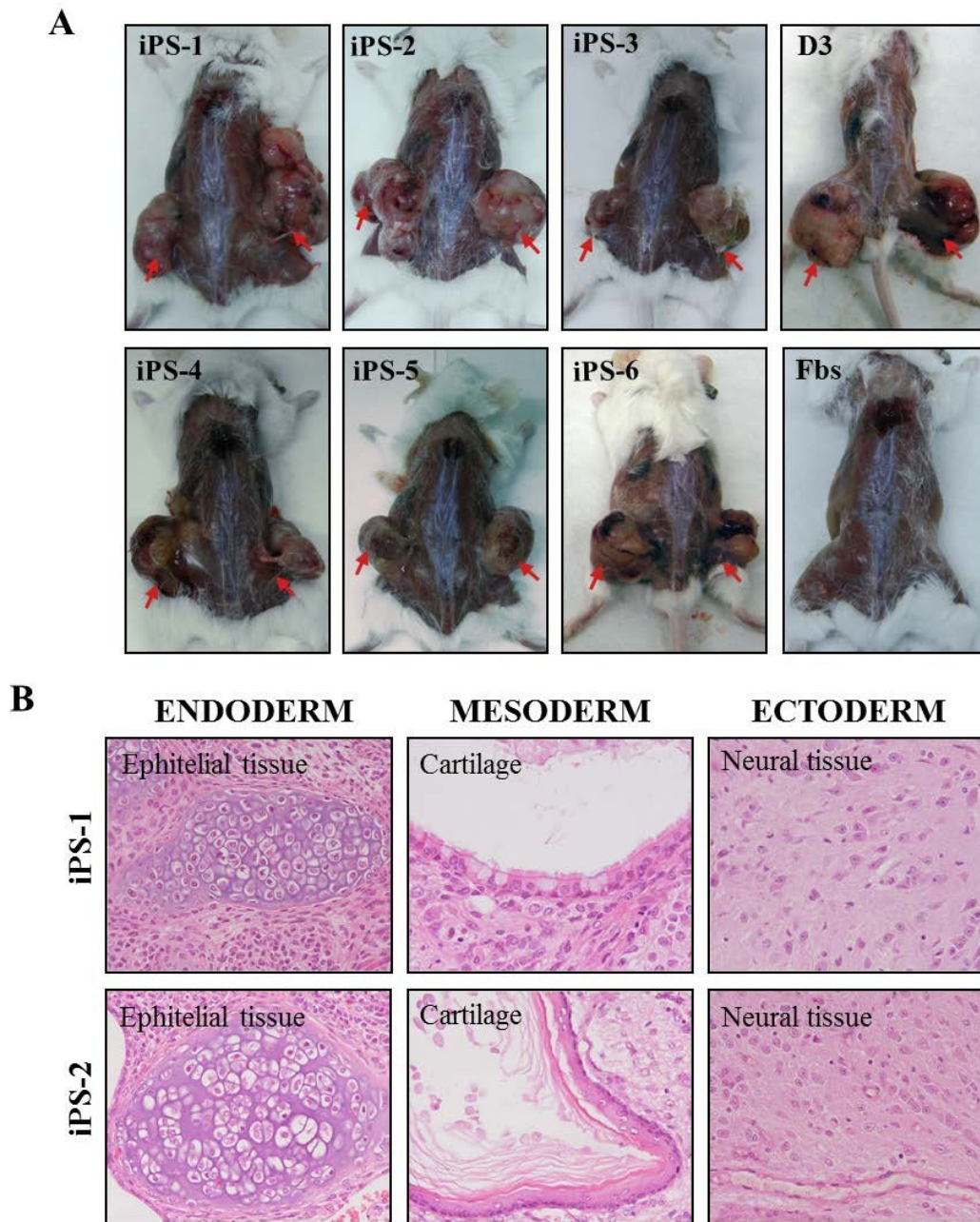
Figure R6. Generation of iPS-derived teratomas. A) One million cells of mouse iPS cells, the mouse embryonic stem cell line D3 and adult fibroblasts (Fbs) were subcutaneously transplanted into the dorsal flanks of Rag2$^{-/-}$γc$^{-/-}$ mice. iPS and D3 cells, but not Fbs, formed large teratomas after 6-8 weeks of injection. **B)** Histological analysis of the iPS-teratomas from iPS-1 and iPS-2 clones in haematoxilin and eosin-stained sections confirmed iPS differentiation towards epithelial tissue (endoderm), cartilage (mesoderm) and neural tissue (ectoderm) among others.

2. CARDIAC DIFFERENTIATION OF MOUSE iPS CELLS

2.1. iPS cardiac differentiation potential

The cardiac differentiation potential of the six iPS clones was analyzed. For that purpose, EBs were generated and initially differentiated by treatment with 1% DMSO (**Figure R7A**). Among the six clones, a consistent cardiac differentiation with GFP positive beating areas was observed for clones iPS-1 and iPS-2 (**Figure R7B**). Lower differentiation potential was observed for the clone iPS-6 which presented smaller GFP positive beating areas (data not shown) and no cardiac differentiated cells were obtained with clones iPS-3, iPS-4 and iPS-5, in which total silencing of the retroviral transcripts has not been achieved. The clones iPS-1 and iPS-2 were selected for further evaluation of their cardiac differentiation potential.
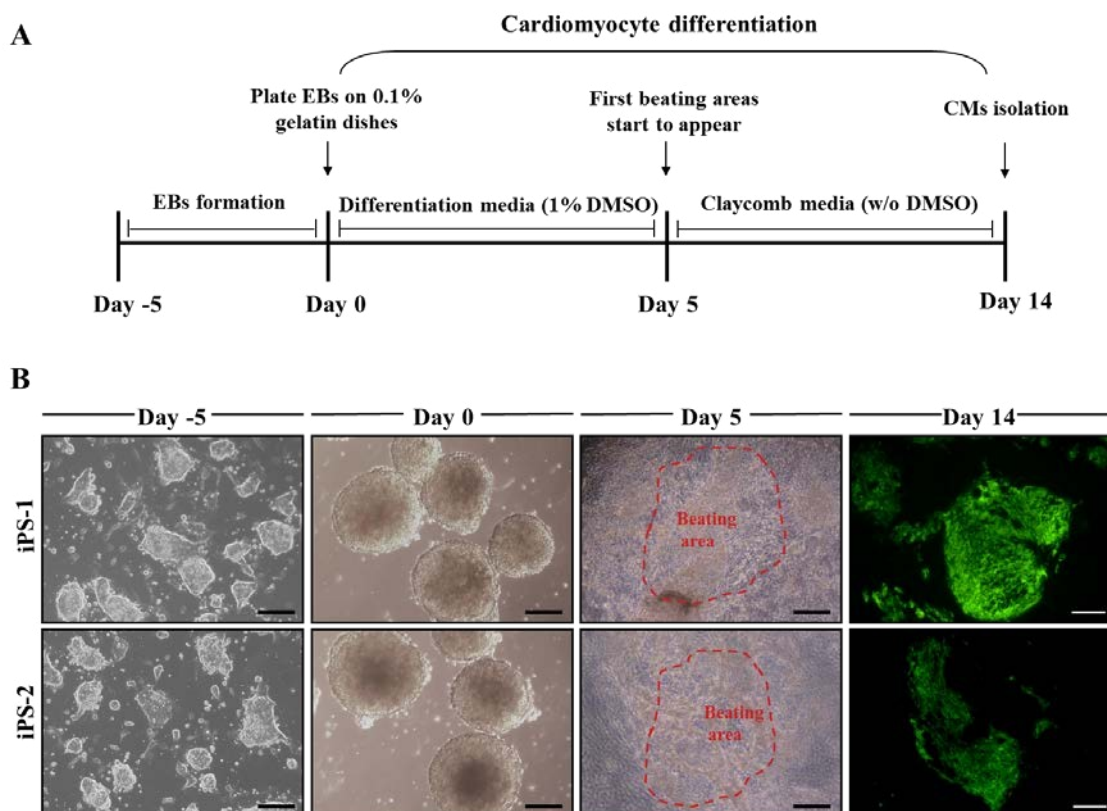
Figure R7. Cardiac differentiation of iPS cells. A) Scheme of iPS cardiac differentiation protocol. **B)** Cardiac differentiation process. iPS clones (day -5) were differentiated into embryoid bodies (EBs) (day 0) and plated on gelatin-coated dishes where they formed several clusters that acquired spontaneous contraction (day 5) (outlined red dotted lines) that were maintained during days (day 14). Beating clusters were GFP positive, which indicated expression of the cardiac αMHC protein and confirmed cardiac differentiation. Scale bars: 150 μm (GFP positive clusters); 100 μm (iPS clones) and 50 μm (EBs and beating clusters).

Five days after plating the EBs, the cells acquired spontaneous contraction that increased over time. Also, presence of GFP positive clusters were detected demonstrating differentiation towards CMs as the expression of the GFP protein is driven under the cardiac specific αMHC-GFP promoter.

Day 14-beating clusters were analyzed after differentiation treatment. First, cardiac gene expression was determined by qPCR, detecting up-regulation of the cardiac genes *Gata4* and *Mef2c* (early expression) and *βMch*, *αMhc*, *Mlc2v* and cardiac *Actinin* (late expression) in both clones, although, as an average, it was higher in the CMs derived from iPS-1 (**Figure R8**). Moreover, in order to evaluate the level of maturation of the cardiac derived cells, the gene expression of specific cardiac channel markers was also analyzed by qPCR at day 14 of differentiation. High levels of L-type calcium channel (*Cacna1c*), Ryanodine receptor (*Ryr2*), potassium/sodium channel (*Hcn1*) and Phospholamban (*Pln*) genes were detected in the clones iPS-1 and iPS-2.

Furthermore, putative differentiation towards other cell types that could contribute to the cardiovascular lineages, like the endothelial and smooth muscle lineages was analyzed. Very low levels were detected after DMSO-cardiac differentiation, indicating a directed specification towards a cardiac phenotype (**Figure R9**).

iPS-1

iPS-2

Early cardiac markers

Early cardiac markers

Late cardiac markers

Late cardiac markers

Channel cardiac markers

Channel cardiac markers

☐ **iPS cells**   ■ **iPS-CMs d14**
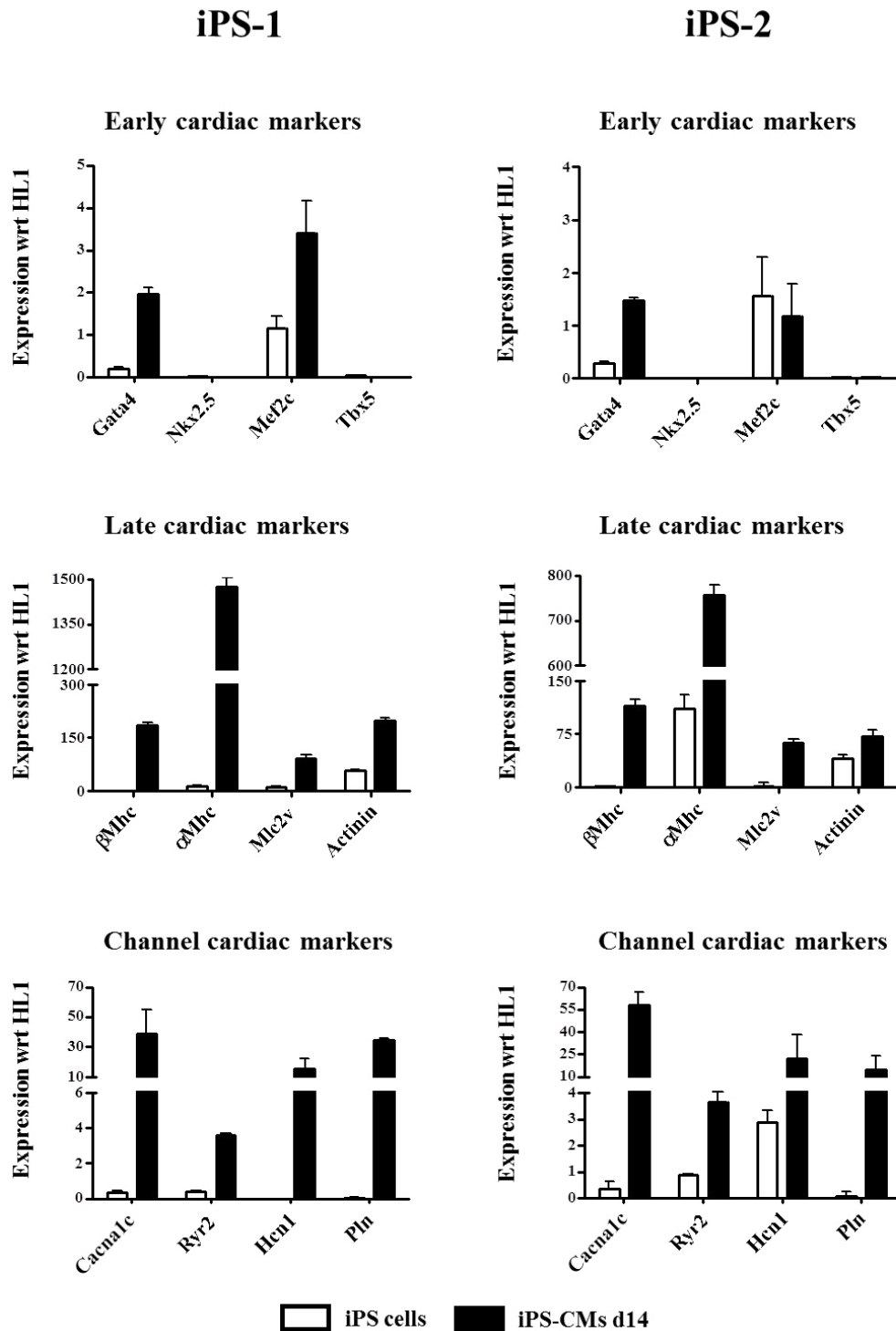
Figure R8. Expression of cardiac markers in differentiated iPS cells. Cardiac specification was analyzed in two different iPS clones (iPS-1 and iPS-2) at day 14 of differentiation. Cardiac gene expression was determined by quantitative PCR. High levels of early cardiac markers (*Gata4* and *Mef2c*) and late cardiac genes (*βMhc*, *αMhc*, *Mlc2v* and cardiac *Actin*in) were detected. Up-regulation of specific cardiac channel markers (*Cacna1c*, *Ryr2*, *Hcn1* and *Pln*) were also detected in the iPS clones. Values were represented in comparison with the murine cardiac cell line HL1 (Expression with respect to (wrt) HL1). Black bars denote cardiomyocytes derived from iPS cells at day 14 of differentiation (iPS-CMs d14) and white bars denote undifferentiated iPS cells (iPS cells). Data were expressed as mean ± SD.
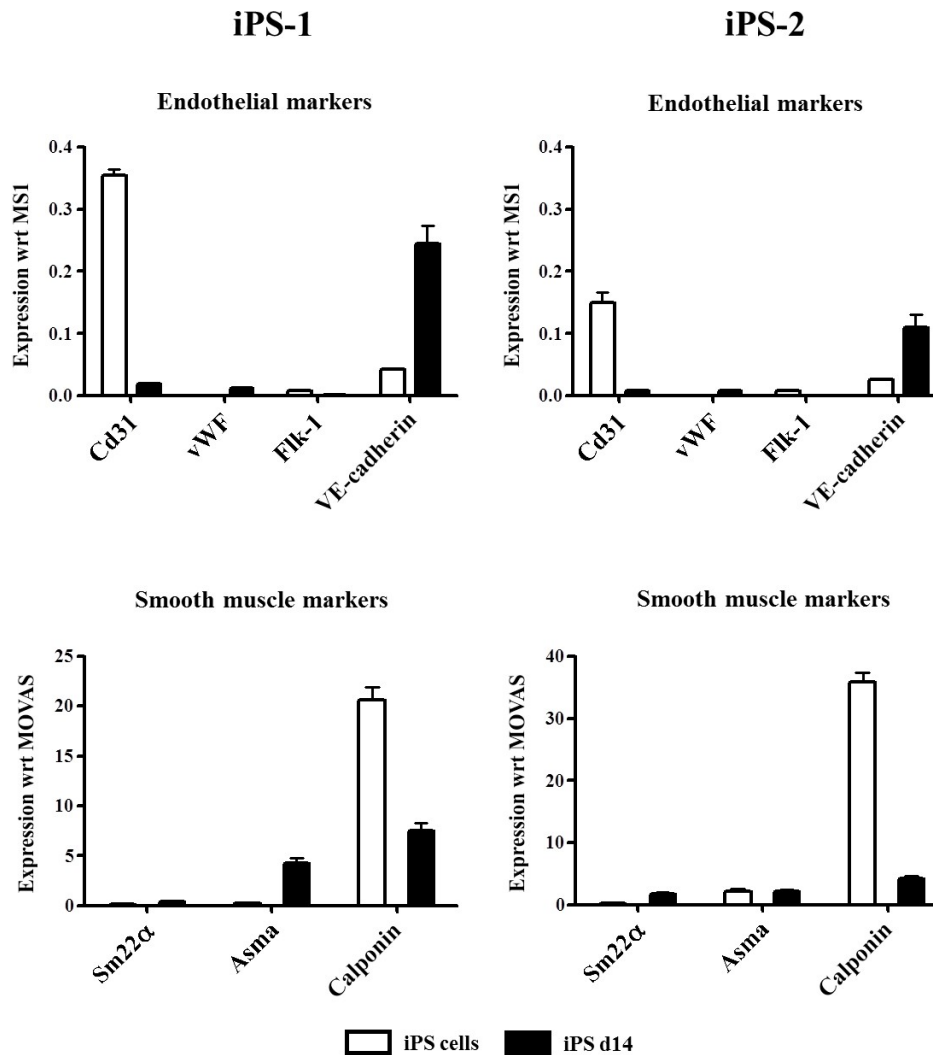
iPS-1

iPS-2

Figure R9. Expression of endothelial and smooth muscle markers in differentiated iPS cells. Endothelial and smooth muscle differentiation was analyzed by quantitative PCR in two different iPS clones (iPS-1 and iPS-2) at day 14 of differentiation. Very low levels of endothelial markers (*Cd31*, *vWF*, *Flk-1* and *VE-cadherin*) and smooth muscle markers (*Sm22α, Asma* and *Calponin*) were detected. Values were represented in comparison with the murine endothelial cell line MS1 (Expression with respect to (wrt) MS1) and the murine smooth muscle cell line MOVAS (Expression with respect to (wrt) MOVAS). Black bars denote cells derived from iPS cells at day 14 of differentiation (iPS d14) and white bars denote undifferentiated iPS cells (iPS cells). Data were expressed as mean ± SD.

Furthermore, cardiac differentiation was analyzed at the protein level and expression of GATA4, TITIN, CONNEXIN43 (CX43) and ACTININ cardiac markers was confirmed by immunofluorescence technique at day 14 of differentiation in both iPS clones (**Figure R10**). Cells were positive for all these markers and expressed GFP also, indicating expression of cardiac αMHC protein and thereby, confirming cardiac specification (**Figure R10**).
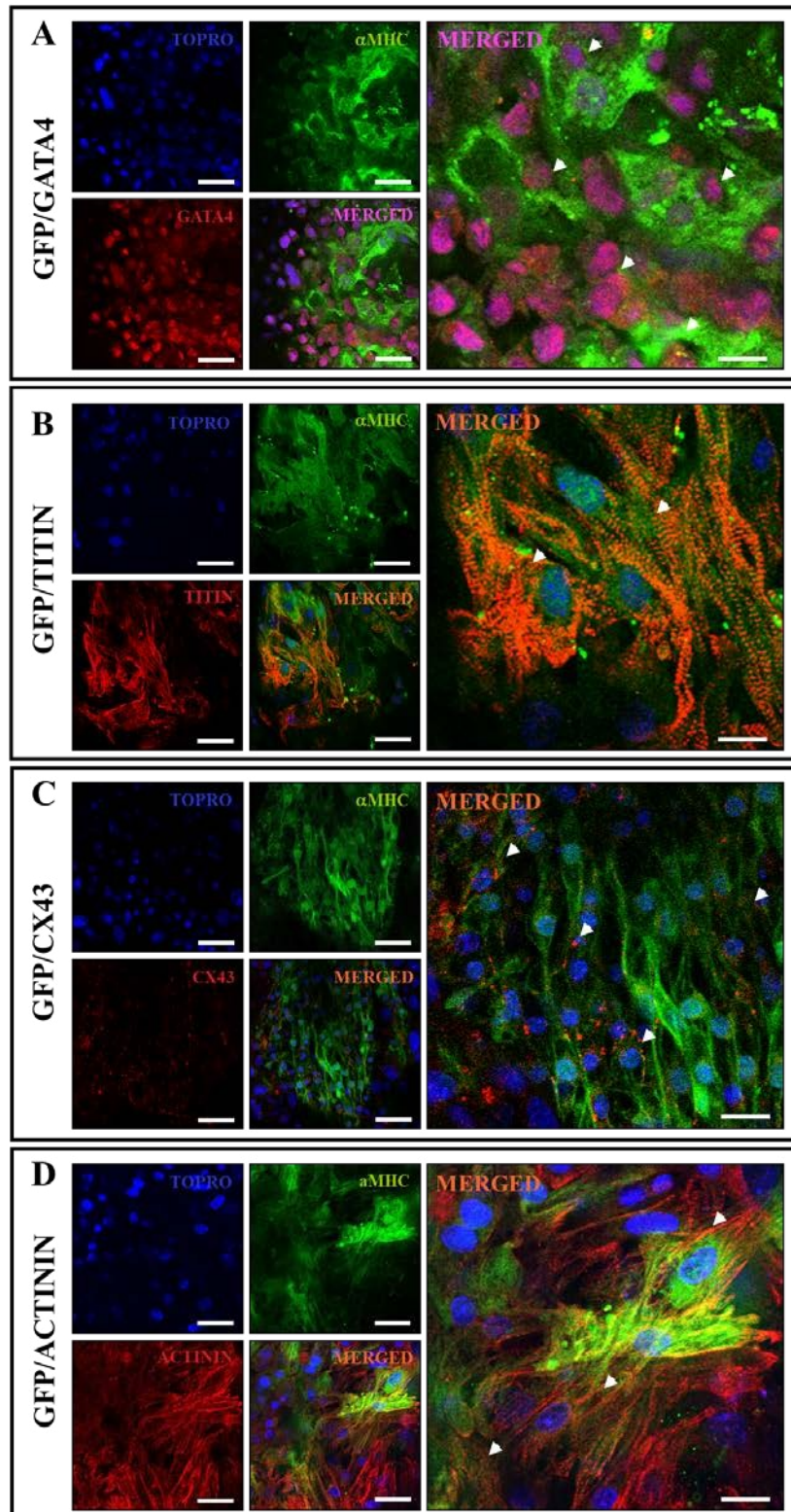
Figure R10. Immunofluorescence detection of cardiac proteins after iPS differentiation. Cardiac differentiation was anlyzed by immunofluorescence in clones iPS-1 and iPS-2 at day 14 of differentiation. Representative images of iPS-1 clone are shown. Cells were stained for GATA4 (Alexa-594: red) **(A)**, TITIN (Alexa-594: red) **(B)**, CX43 (Alexa-594: red) **(C)** and cardiac ACTININ (Alexa-594: red) **(D)**. The cells positive for these markers were also positive for GFP, which indicates cardiac specific αMHC protein expression (arrowheads). Nuclear staining was performed with TOPRO-3 (blue). Scale bars: 50 µm; higher magnification: 10 µm.

Finally, formation of mature CMs was confirmed at the ultrastructural level by transmission electronic microscopy showing a typical sarcomeric organization with organized myofibrils that distributed through out the cytoplasm (**Figure R11**).
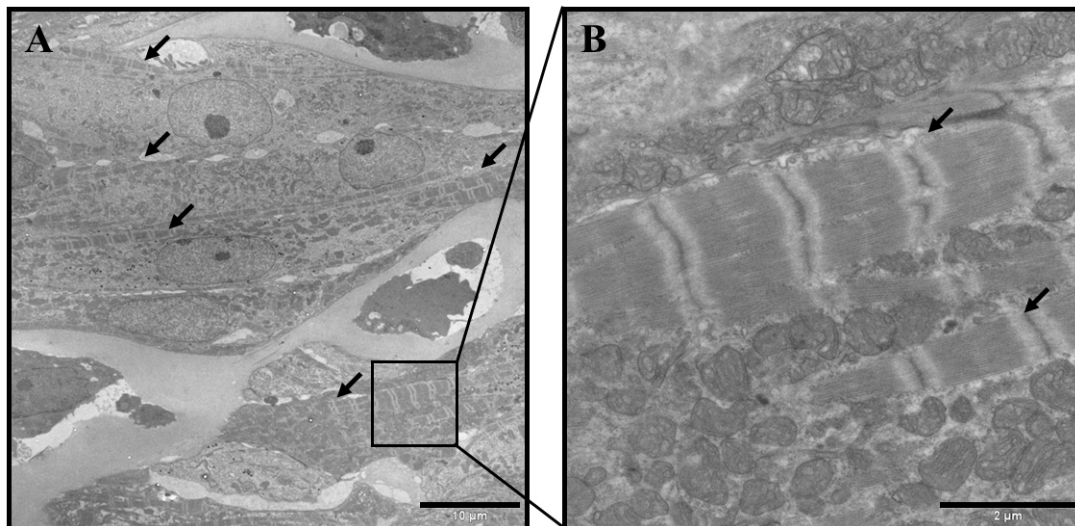
Figure R11. Electron microscopy photographs of iPS-CMs. Cardiac differentiation was also confirmed in clones iPS-1 and iPS-2 at day 14 of differentiation by electronic microscopy. Representative images of iPS-1 clone are shown. A typical sarcomeric organization was observed in the differentiated cells (arrowheads) **(A)**. A higher magnification field shows cardiomyocytes that contained organized myofibrils that distributed trough out the cytoplasm (arrowheads) **(B)**. Scale bars: 10 µm (A), 2 µm (B).

2.2.   Role of NRG-1 β protein in cardiac specification and maturation

2.2.1.   NRG-1β potentiates iPS cardiac differentiation

The effect of the NRG-1β protein in iPS cardiac differentiation and maturation was analyzed as its importance in heart development (reviewed in [208]) as well as its role in ESC cardiac differentiation [200, 201, 225] and CMs survival and proliferation [226, 228, 231] have been previously demonstrated. For such analysis, the clone iPS-1 was selected, as showed the best cardiomyogenic potential.

Cardiac differentiation was analyzed at day 7 and day 14 after treatment with DMSO, NRG-1β or the combination of both treatments. At day 7 of differentiation, the percentage of formed GFP positive areas was significantly greater in the group treated with the combination of DMSO and NRG-1β protein (DMSO+NRG-1β) in comparison with the treatments alone (**GFP$^+$ areas %:** DMSO: $17.7 \pm 3.0\%$ ($p<0.001$ *vs*. NRG-1β),

NRG-1β: 10.3 ± 3.1%; DMSO+NRG-1β: 25.0 ± 3.9% ($p<0.01$ *vs.* DMSO and $p<0.001$ *vs.* NRG-1β) (**Figure R12**). This effect was also observed by day 14 of differentiation. An increase in the GFP areas was detected in the three analyzed groups that was significantly higher in the group treated with DMSO+NRG-1β (**GFP$^+$ areas %:** DMSO: 37.0 ± 4.3% ($p<0.001$ *vs.* NRG-1β), NRG-1β: 19.8 ± 4.4% DMSO+NRG-1β: 44.7 ± 5.7% ($p<0.05$ *vs.* DMSO and $p<0.001$ *vs.* NRG-1β) (**Figure R12**). These results demonstrate the synergic effect of the NRG-1 and DMSO that, when combined, induced a greater cardiac differentiation of iPS than when added alone.
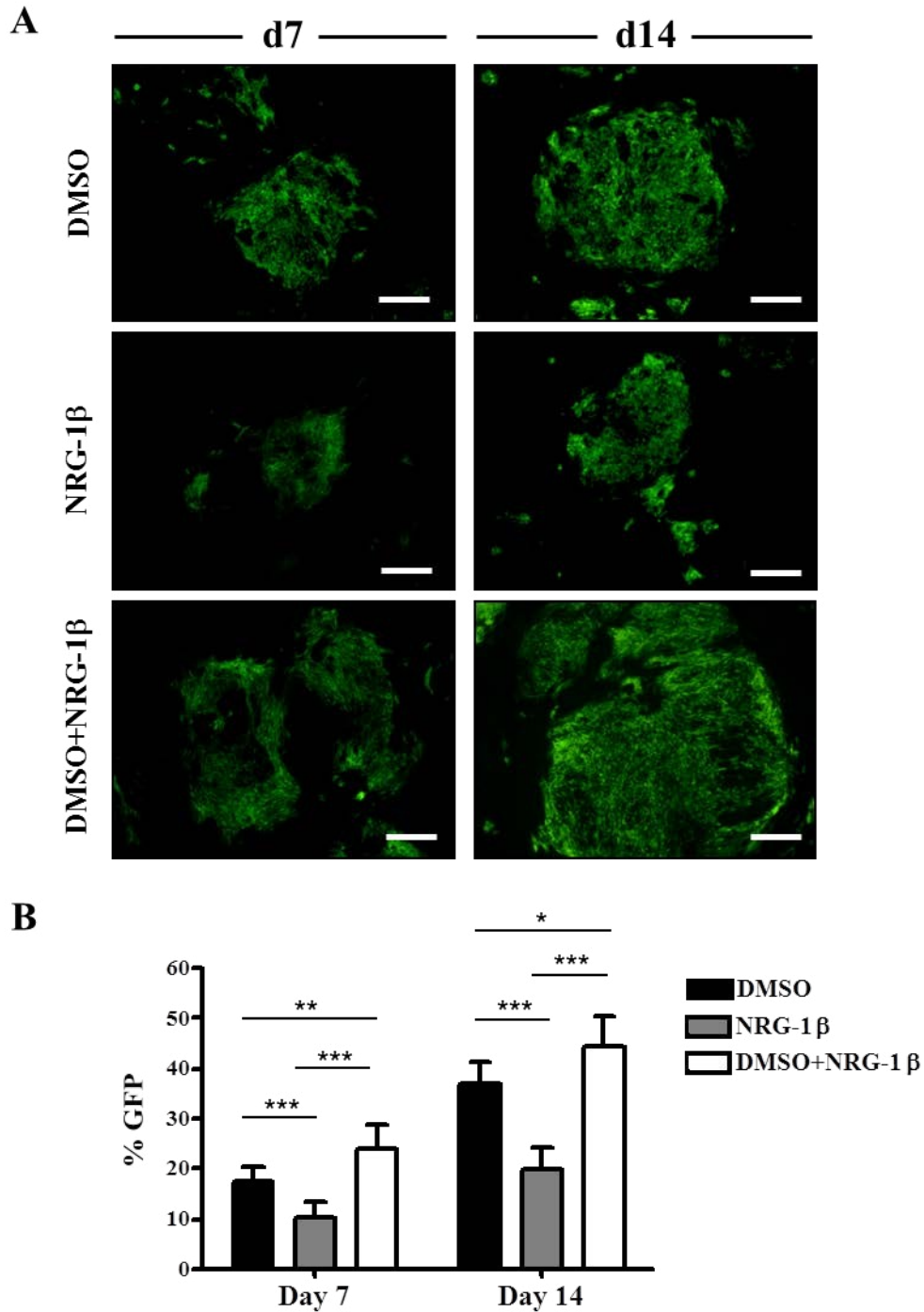
Figure R12. NRG-1β potentiates iPS cardiac differentiation. **A)** GFP positive clusters were detected at day 7 and at day 14 of differentiation. iPS-1 clone was differentiated by treatment with DMSO (1%), NRG-1β (100ng/ml) or with the combination of both treatments. Larger GFP areas were observed when cells were treated with the combination of DMSO and NRG-1β protein. Scale bars: 150 μm. **B)** Quantification of GFP positive areas. GFP positive areas were quantified at day 7 and at day 14 of differentiation. The percentage of GFP positive clusters was significantly higher in the group treated with the combination of DMSO and NRG-1β than with the treatments alone (*$p<0.05$, **$p<0.01$, ***$p<0.001$). Data were expressed as mean ± SD.

2.2.2.   NRG-1β potentiates maturation of iPS-CMs

As contractile properties of the cardiac cells are crucial for functional regeneration, the electrophysiological properties of the iPS-CMs were evaluated by patch-clamp technique. Their specific phenotype (atrial, ventricular or nodal CMs) and maturation state were analyzed at day 7 and 14 of differentiation in the three experimental groups. Intracellular action potential (AP) recordings demonstrated the existence of viable iPS-CMs and revealed ventricular-like action potentials in all the analyzed groups. Not atrial or pacemaker CMs were found indicating a specific differentiation towards a ventricular phenotype. By day 14 of differentiation, the amplitude of AP increased in all the groups that was higher in those ones treated with NRG-1 than in the one treated only with DMSO (**Figures R13 and R14**).
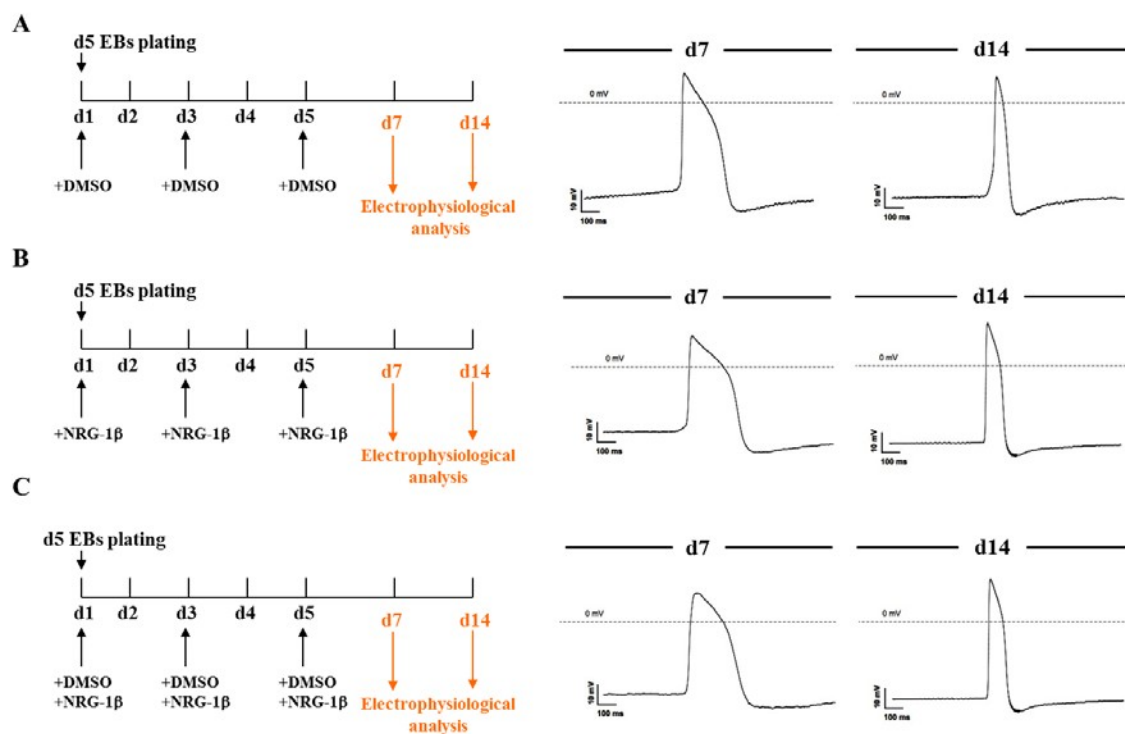
Figure R13. **iPS-CMs phenotype.** iPS cells were differentiated by embryoid body formation and following plating on gelatin-coated dishes. The cells were treated at different time points (1, 3 and 5 day after plating the EBs) with DMSO (1%) **(A)**, NRG-1β (100ng/ml) **(B)** and DMSO+NRG-1β **(C)**. The electrophysiological properties were analyzed at day 7 and day 14 of differentiation. Spontaneous action potential (AP) recordings showed a ventricular-like cardiac phenotype **(A-C)** and a higher action potential amplitude in the group treated with the combination of NRG-1 and DMSO than with the treatments alone, at day 14 of differentiation.
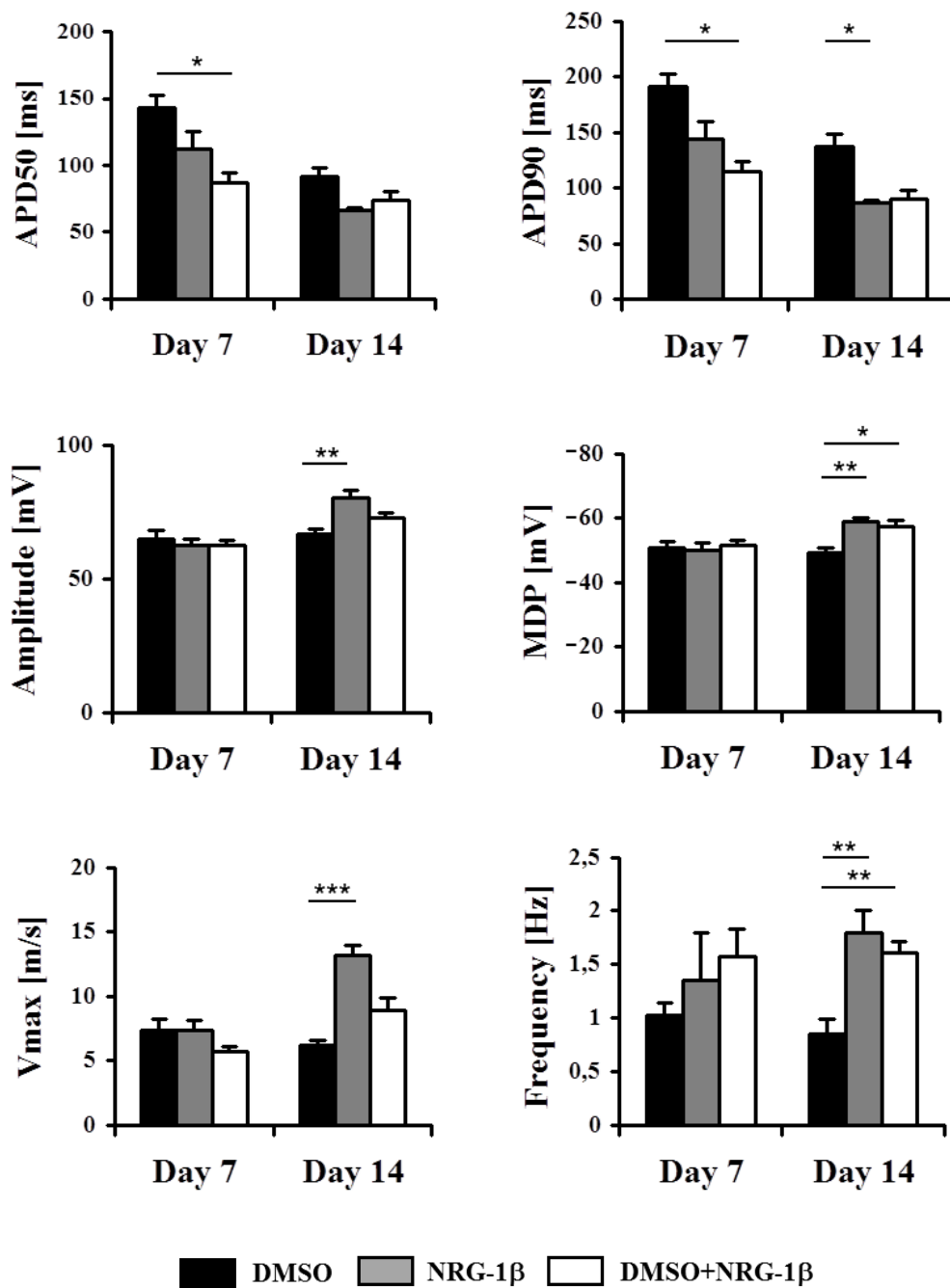
Figure R14. Electrophysiological properties of iPS-CMs. Action potential duration at 50% repolarization (APD50), action potential duration at 90% repolarization (APD90), amplitude, maximal diastolic potential (MDP), maximal upstroke velocity (Vmax) and frequency parameters were measured at day 7 and at day 14 of differentiation. Ten-fourteen measurements were performed in different beating clusters per experimental group. Although AP parameters of iPS-CMs showed typical properties of fetal ventricular-like CMs, maturation of the CMs electrophysiological properties was observed after treatment with NRG-1β protein. Results are shown as mean ± SD. *$p<0.05$, **$p<0.01$, ***$p<0.001$ in comparison with DMSO.

Furthermore, in order to evaluate the effect of NRG-1 protein on the maturation of AP properties of iPS-CMs, the action potential parameters: action potential duration at 50% repolarization (APD50), action potential duration at 90% repolarization (APD90), amplitude, maximal diastolic potential (MDP), maximal upstroke velocity (Vmax) and frequency were also determined (**Figure R14**).

Significant lower values for APD50 and APD90 were detected at day 7 of differentiation in the group treated with DMSO+NRG-1β than in the DMSO group (*p*<0.05 *vs.* DMSO), indicating the formation of CMs with a higher level of maturation. Also, a decrease of APD50 and APD90 was detected in the group treated with NRG-1β, although a statistical significance was not reached. Interestingly, at day 14 of differentiation, the groups treated with NRG-1β (either with or without DMSO) showed lower APD50 and APD90 values (**Figure R14**), with closer APD90 values to the adult host CMs (**APD90**: 136.9 ± 11.7 ms (DMSO); 90.4 ± 7.4 ms (DMSO+NRG1β) and 86.4 ± 2.2 ms (NRG1β) (*p*<0.01 *vs.* DMSO) *vs.* Adult CMs: 83.3 ± 4.5 ms (previously described by *Halbach et al.* [303] and performed in the same conditions), indicating that NRG-1β protein treatment contributed to the cardiac differentiation and maturation process.

Moreover, although at day 7 of differentiation the cells possessed an Amplitude value of fetal cultivated CMs (FCMs) (**Amplitude**: 62.8 mV (FCMs) previously described by *Halbach et al.* [303] and performed in the same conditions), this value increased by day 14 of differentiation, being significantly higher in the group treated with NRG-1β (*p*<0.01 *vs.* DMSO) and closer to the amplitude value of the adult host CMs (**Amplitude**: 66.8 ± 3.0 mV (DMSO); 80.2 ± 3.0 mV (NRG-1β) and 72.8 ± 1.9 mV (DMSO+NRG1β) *vs.* Adult CMs: 87.0 ± 2.6 mV (*See Halbach et al.* [303]) (**Figure R14**). Moreover, MDP and Vmax values also increased by day 14 of differentiation, being higher in the groups treated with NRG-1β (**MDP**: DMSO: -49.1 ± 1.4 mV; NRG-1β: -58.7 ± 1.2 (*p*<0.01 *vs.* DMSO) and DMSO+NRG-1β: -57.1 ± 2.0 (*p*<0.05 *vs.* DMSO); **Vmax:** DMSO: 6.1 ± 0.4 m/s; NRG-1β: 13.1 ± 0.8 m/s (*p*<0.001 *vs.* DMSO) and DMSO+NRG-1β: 8.8 ± 1.0 m/s). Finally, greater values were also found for the frequency parameter in the groups treated with NRG-1β protein in comparison with the cells treated only with DMSO (DMSO+NRG-1β *p*<0.01 *vs.* DMSO and NRG-1β *p*<0.01 *vs.* DMSO) (**Figure R14**).

In summary, at day 7 of differentiation iPS-derived cardiac cells reached a more mature ventricular-like phenotype when treated with the DMSO+NRG-1β, showing a shorter APD50 and APD90 values than when treated with DMSO or NRG-1β alone. By day 14 of differentiation, iPS-CMs differentiated with NRG-1β, in combination or not with DMSO, exhibited more mature properties with higher MDP, amplitude, frequency and Vmax as well as a shorter APD50 and APD90. On the other hand, iPS-CMs differentiated only with DMSO, exhibited typical properties of fetal cultivated CMs with a low MDP, frequency, amplitude and Vmax, as well as a longer APD50 and APD90 (**Figure R14**). These findings support the role of NRG-1β for cardiac differentiation and maturation of stem cells.

3. REGENERATIVE POTENTIAL OF PREDIFFERENTIATED iPS-CMs IN A MOUSE MODEL OF ACUTE MYOCARDIAL INFARCTION

3.1. Optimization of echocardiographic evaluation of left ventricular function in a mouse model of myocardial infarction

To study the *in vivo* regenerative potential of iPS-CMs, we previously optimized the acquisition and analysis protocol for the echocardiographic evaluation of LV remodeling in a mouse model of MI. To perform reliable measurements of cardiac function in a mouse model of MI, it is necessary to use high-resolution echocardiography equipment specifically designed for small animals [28], like the Vevo 770 (VisulaSonics, Toronto, ON), which has been used in this study.

3.1.1. Echocardiographic data

A complete characterization of LV post-infarction remodeling was performed in a DBA/2J mouse model of MI. In a pilot study, seventeen 8 week old female DBA/2J mice underwent permanent occlusion of the LAD coronary artery leading to MI. A sham group of fourteen 8 week old female DBA/2J mice that underwent thoracotomy but did not undergo ligation of the coronary artery was included. Four mice from the experimental group were excluded from the study: three of them died during surgery and one more 7 days after MI. Mice echocardiography was performed using a VEVO 770 before infarction and 7, 14, 30, 60, 90 and 120 days after ligation.

3.1.2. Measurement of left ventricular remodeling and cardiac function

LV systolic function was evaluated by measuring the fractional shorthening (FS%), the ejection fraction (EF%), fractional area change (FAC%), stroke volume (SV), volume in diastole (VD) and volume in systole (VS) parameters. The EF% was calculated by Teicholz and Simpson methods and the FAC% parameter was calculated in short-axis and long-axis views to visualize better the localization of the ventricular infarction.

3.1.2.1. LV structural analysis

LV diastolic average internal diameter at baseline (Dbvi), middle (Dmvi) and apical (Davi) levels were calculated before MI and 7, 14, 30, 60 and 90 days post-infarction (**Table R2**). These values increased after MI, revealing progressive post-infarction remodeling of the left ventricle. Namely, at the basal level (Dbvi), the LV diameter significantly increased ($p<0.001$) 90 days post-infarction. At middle level (Dmvi), a significant enlargment ($p<0.01$) was detected starting 14 days post-infarction and becoming prominent 30 days post-infarction ($p<0.001$). At apical level (Davi), a marked, statistically significant enlargement ($p<0.001$) appeared 7 days post-infarction that continued until the end of the study. Furthermore, the LV end-diastolic and systolic areas (Aread; Areas) (**Table R2**) significantly increased as well, starting 7 days post-infarction ($p<0.001$) and remaining at that level for the rest of the study. As it can be observed at the **Table R2** data and **Figure R15**, a progressive ventricular dilation extended from the apical origin of the infarction towards healthy myocardial areas, resulting in marked changes of both size and shape.

Table R2. Structural analysis. HR: heart rate. **Dbvi**: LV diameter (basal). **Dmvi**: LV diamter (medium). **Davi**: LV diameter (apical). **Aread**: end-diastolic area. **Areas**: end-systolic area (** indicates statistical significance *versus* day 0, with *p*<0.01) (*** indicates statistical significance *versus* day 0, with *p*<0.001). Data are mean ± SD.

Day	HR	Dbvi	Dmvi	Davi	Aread	Areas
0	364.15 ± 27.20	3.09 ± 0.38	3.36 ± 0.20	2.82 ± 0.24	18.98 ± 1.81	6.87 ± 0.93
7	366.54 ± 39.49	3.27 ± 0.35	3.63 ± 0.30	3.49 ± 0.42***	22.04 ± 2.11***	13.81 ± 2.80***
14	368.08 ± 41.21	3.09 ± 0.31	3.75 ± 0.33**	3.26 ± 0.32***	22.16 ± 2.16***	14.31 ± 2.48***
30	361.23 ± 29.31	3.49 ± 0.43	3.76 ± 0.30***	3.60 ± 0.41***	22.83 ± 2.37***	14.69 ± 2.75***
60	374.23 ± 36.31	3.35 ± 0.17	3.83 ± 0.31***	3.48 ± 0.28***	23.75 ±2.67***	15.30 ± 3.16***
90	364.23 ± 37.35	3.68 ± 0.39***	3.95 ± 0.37***	3.81 ± 0.45***	24.08 ± 2.45***	15.78 ± 3.20***

Figure R15. Visualization of the infarction. Sample images at baseline and 7, 30 and 90 days post-infarction. **Upper row**: Parasternal short-axis views. **Lower row**: Paraesternal long-axis views. The infarcted area is appreciated 7 days post-infarction and is located at the apical region. The evolution of the infarction results in progressive left ventricular remodeling.

3.1.2.2. LV functional analysis

The systolic measurements taken on short-axis views at the level of the papillary muscles (**Table R3**) did not significantly change during the experiment. This was due to the apical origin of the infarction in our model and their slow progression towards the middle and baseline levels. In view of these results, the Simpson´s rule was chosen to calculate EF% and FAC% measurements. The EF% calculated using Simpson´s rule (EF% simp) (**Table R3**) shows significant loss of systolic function starting 7 days post-

infarction ($p<0.001$). Confirming this, the LV systolic function was also evaluated using the FAC% parameter (**Figure R16**), which has been found to correlate with the EF% [30]. Namely, FAC% measured in a short-axis (FAC% short) (**Figure R16**, **Table R3**) decreased significantly ($p<0.001$) 7 days post-infarction and remained virtually unchanged. This reduction of FAC% was more evident when measured in the parasternal long-axis (FAC% long) (**Table R3**).

When the infarction affects the ventricular apex, visualizing the infarct area in a short-axis at medium and an upper level becomes difficult. Thereby, a single paraesternal long-axis view, which results in an improved visualization of the LV was also chosen to calculate FAC% in our model of MI.

Table R3. Systolic function. EF% tei: ejection fraction using Teichholz. **EF% simp**: ejection fraction using Simpson´s rule. **FS% tei**: fractional shortening using Teichholz. **VcFc**: normalized mean velocity of circumferential fiber shortening. **FAC% short**: fractional area change measured on a short-axis view**. FAC% long**: fractional area change measured on a long-axis view (*** indicates statistical significance *versus* day 0, with $p>0.001$). Data are mean ± SD.

Day	EF% tei	EF% simp	FS%	VcFc	FAC% short	FAC% long
0	62.48 ± 9.99	66.61 ± 6.42	33.59 ± 7.58	0.24 ± 0.05	65.55 ± 3.78	63.78 ± 3.87
7	65.26 ± 5.78	48.15 ± 6.21***	35.43 ± 4.75	0.25 ± 0.05	47.89 ± 3.99***	35.90 ± 6.76***
14	60.76 ± 5.56	51.69 ± 4.59***	32.19 ± 3.88	0.22 ± 0.03	50.37 ± 4.90***	35.69 ± 7.08***
30	59.70 ± 7.38	48.51 ± 6.13***	31.59 ± 5.19	0.21 ± 0.04	49.96 ± 3.74***	36.01 ± 7.69***
60	63.11 ± 3.45	45.76 ± 10.50***	33.93 ± 2.56	0.24 ± 0.03	49.26 ± 4.78***	36.16 ± 6.74***
90	59.37 ± 4.98	44.84 ± 8.30***	31.31 ± 3.44	0.22 ± 0.03	46.78 ± 3.87***	35.03 ± 8.12***

Figure R16. LV systolic funtion. FAC% measured both in paraesternal short-axis views and a long-axis views. The FAC% decreased significantly as early as 7 days after myocardial infarction (*** indicates statistically significance *versus* day 0, with $p<0.001$).

3.1.3. Tissue infarct size

In order to determine the correlation between the systolic functional changes and the heart tissue remodeling, the percentage of infarcted tissue was measured at the end-point of the experiment (90 days post-infarction). **Figure R17** shows transverse sections of one sample heart, starting at the level of the papillary muscles (leftmost) and ending at the apex (rightmost). The muscle stains in light brown-colored while the collagen appears in red, due to the Sirius red staining. Linear regression analyses demonstrated a significant correlation between the FAC% values calculated in a long-axis view and the infarct size values (r= -0.946; R^2 =0.90, *p*<0.05). However, the correlation with FAC% calculated in a short-axis view was lower (r= -0.812; R^2 =0.66), due to the difficulty for obtaining good short-axis views in this specific model, confirming the convenience to perform long-axis views for LV functional analysis.

Figure R17. Histological analysis. Transverse sections of a heart 90 days after permanent ligation of the LAD. The sections were approximately taken starting at the level the papillary muscles (left most) to the apex (right most). The anterolateral myocardium is replaced by a thin fibrous scar tissue. Scale bar: 1 mm.

In summary, mice echocardiography using Vevo 770 is a reliable method for study LV post-infarction remodeling in a DBA/2J mouse model of MI when using the Simpson's rule and FAC% LV functional parameter calculated from the parasternal short and long-axis views, which better adapted to the particular characteristics of our MI model.

Therefore, the cardiac recovery after transplantation of iPS-CMs was analyzed next following these methods in a model of acute MI.

3.2. Transplantation of predifferentiated iPS-CMs in a model of acute myocardial infarction in mice

The clone iPS-1 showed the best cardiac differentiation potential, so it was selected to study its *in vivo* regenerative cardiovascular potential in a model of acute MI in mice. iPS-CMs were transplanted on day 7 of differentiation as pre-differentiated cells might survive and proliferate better than fully mature differentiated cells. Cardiac specification was induced by treatment with DMSO+NRG-1β, which, as described above, was the treatment that induced a greater cardiac differentiation at the protein level (GFP positive areas) and a more mature ventricular-like phenotype as determinated by electrophysiological methods. LV remodeling and cardiac function were analyzed in order to evaluate the therapeutic effect of the iPS-CMs.

3.2.1. Transplantation of iPS-CMs in an acute model of MI, preserves cardiac function

In order to assess if iPS-CMs were capable of inducing an improvement in a model of acute MI, cells were transplanted in the peri-infarct area 8 week old female DBA/2J mice (n=15) after permanent LAD coronary artery occlusion. A control group (treated media animals) (n=13) and a sham group (mice that underwent thoracotomy but did not undergo ligation of the coronary artery) (n=14) were included in the study. Two animals from the iPS-CMs treated group were excluded from the study: one mouse died during surgery and another one 30 days after MI. For histological analysis, two animals per group were sacrificed at 1 and 2 weeks, one animal at 4 weeks, respectively and eight animals per group at 2 months.

Cardiac function was assessed by echocardiography 2, 30 and 60 days after cell transplantion. A statistically significant decrease was observed in EF% and FAC% values 60 days after transplant in the control animals group (treated with media) in comparison with baseline values (day 2) that indicated an adverse function of the heart (**Table R4**). Importantly, a statistically significant decrease in EF% and FAC% was not observed in iPS-CMs treated animals (**EF% Day 60**: Medium: $28.4 \pm 8.2\%$ ($p<0.05$ *vs.* day 2) and iPS-CMs: $32.6 \pm 3.9\%$ (p=n.s.); **FAC% Day 60**: Medium: $17.8 \pm 4.9\%$ ($p<0.05$ *vs.* day 2) and iPS-CMs: $20.0 \pm 3.3\%$ (p=n.s.)) which indicated that transplantation of iPS-CMs induced a preservation of the cardiac function in this model. Not significant differences in EF% and FAC% was observed at day 30 in both groups. Volume in diastole (VD) and volume in systole (VS) were also analyzed (**Table R4**) and not significant differences were observed in VD and VS parameters between 2 days and 60 days in both groups (**Table R4**).

Table R4. Echocardiographic studies. Values of EF%, FAC%, VD and VS, 2, 30 and 60 days after transplantation. Results represent the mean $\pm$ SD. *$p<0.05$, ** $p<0.01$, *** $p<0.001$ between 2 days and 30 or 60 days after iPS-CMs or Medium transplantation. A sham group was included as control of experimental procedure.

	Sham	Medium	iPS-CMs
EF (%)			
2d	63.4 ± 2.3	36.0 ± 4.5	35.5 ± 4.7
30d	61.7 ± 1.9	33.2 ± 2.3	34.7 ± 5.5
60d	62.0 ± 1.0	28.4 ± 8.2 *	32.6 ± 3.9
FAC (%)			
2d	44.0 ± 3.7	24.5 ± 6.3	24.2 ± 7.0
30d	43.1 ± 6.2	21.8 ± 3.5	21.5 ± 4.2
60d	41.0 ± 4.8	17.8 ± 4.9 *	20.0 ± 3.3
VD (µl)			
2d	56.7 ± 12.1	47.1 ± 7.1	50.6 ± 6.1
30d	60.7 ± 11.4	86.7 ± 17.8 ***	98.2 ± 22.3 ***
60d	59.0 ± 7.8	97.8 ± 26.9 ***	105.8 ± 19.9 ***
VS (µl)			
2d	20.0 ± 5.5	30.0 ± 4.5	32.7 ± 4.6
30d	22.7 ± 4.8	58.2 ± 13.3 ***	64.7 ± 16.7 ***
60d	22.0 ± 2.8	71.1 ± 23.8 ***	71.7 ± 15.2 ***

3.2.2. Transplantation of iPS-CMs induces positive tissue remodeling in infarcted hearts

To evaluate if changes in cardiac performance could be related to cell-derived effects, infarct size and infarct collagen content (fibrosis) were measured in the hearts from both experimental groups 2 months post-transplant (n=8 per group).

Transplantation of iPS-CMs induced positive remodeling of the heart in comparison with the control group (medium-treated animals), suggesting a protective effect exerted by the cells. A significant smaller infarct size (**Medium:** 36.2 ± 13.6%; **iPS-CMs:** 24.7 ± 6.3%; *p*<0.05) was detected 2 months after cells transplant in iPS-CMs treated animals (**Figure R19**). Moreover, tissue fibrosis, quantified as collagen content, was significantly reduced in the peri-infarct area in iPS-CMs treated animals (**Medium:** 43.8 ± 4.0%; **iPS-CMs:** 38.6 ± 4.1%) in comparison with the control group (**Figure R20**).
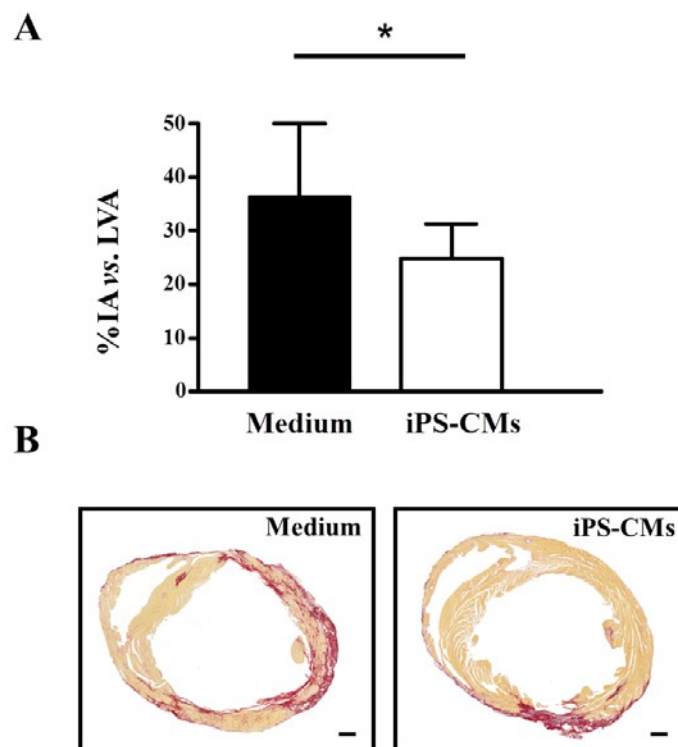
Figure R19. Infarct size. A) Heart infarct area measured 2 months post-transplantation. Black bars denote Medium treated animals (Medium) (n=8) and white bars denote iPS-CMs treated animals (iPS-CMs) (n=8). A significant smaller infarct size was detected in iPS-CMs treated animals in comparison with medium treated animals (12 serial heart sections 50 μm apart). Data indicates percentage of infarcted area (IA) *versus* total left ventricular area (LVA). Data were expressed as mean ± SD. **p*<0.05. **B)** Representative images of Sirius Red stained sections. Scale bars: 500 μm.

A

B
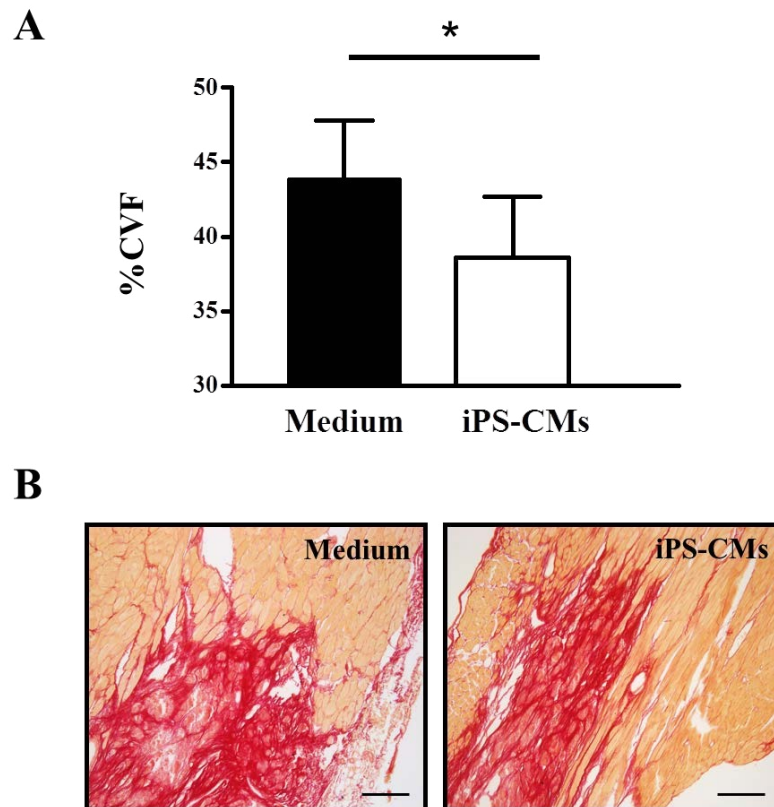
Figure R20. Cardiac tissue fibrosis. A) Percentage of collagen volume fraction (%CVF) measured in the peri-infarct area of left ventricles of the iPS-CMs treated animals (white bars) (n=8) hearts in comparison with the media treated animals (black bars) (n=8) 2 months post-transplantation. Fibrosis was significantly reduced in the iPS-CMs treated animals in comparison with medium treated animals (12 serial heart sections 50 μm apart). Data are expressed as mean ± SD. *$p<0.05$. **B)** Representative images of Sirius Red serial sections in the peri-infarct zone. Scale bars: 100 μm.

3.2.3. Transplantation of iPS-CMs induces revascularization of the cardiac tissue

Furthermore, in order to determine the potential mechanisms involved in the positive tissue remodeling and in the preservation of the cardiac function, the angiogenic effect of cell transplant was analyzed in the injured tissue.

Vascular density (arteries/arterioles) was determined 2 months after transplantation by quantification of α-SMA-positive vessels at the border zone of the infarct (n=8 per group). Tissue revascularization significantly increased in the animals treated with iPS-CMs in comparison with the media-injected ones (Medium: 12.5 ± 2.6 x 10^3 μm^2/mm^2; iPS-CMs: 17.8 ± 5.2 x 10^3 μm^2/mm^2 (**Figure R22**).
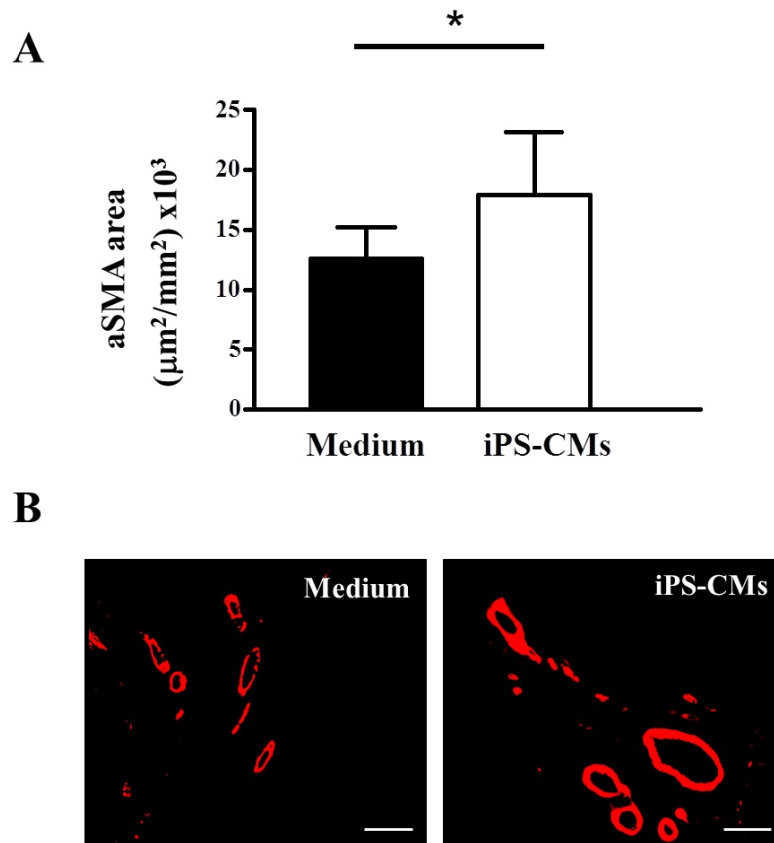
Figure R22. Cardiac tissue revascularization. A) Tissue revascularization was determined by quantifying the total area of α-SMA-positive vessels (μm^2 per mm^2) in the peri-infarct area. Black bars denote medium treated animals (Medium) (n=8) and white bars denote iPS-CMs treated animals (iPS-CMs) (n=8) (12 serial heart sections 50 μm apart). Total area of α-SMA-positive vessels was significantly higher in the iPS-CMs treated animals than in the medium treated animals. Data are expressed as mean $\pm$ SD. *$p < 0.05$. **B)** Representative images of α-SMA stained sections. Scale bars: 100 μm.

3.2.4. Cell engraftment

Finally, cell fate was analyzed at 7, 14, 30, and 60 days after transplantation by immunohistochemistry against GFP. iPS-CMs-GFP positive cells were detected 7 and 14 days post-transplantation (**Day 7:** 3.8 $\pm$ 4.6%; **Day 14:** 0.3 $\pm$ 0.4% *versus* total transplanted cells) (**Figure R21**) whereas no GFP-positive signals were detected at longer time-points (30 and 60 days after transplantation) in any of the animals.

Interestingly, ultrastructural analysis by transmission electron microscopy confirmed the presence of GFP positive iPS-CMs in the areas of cell injection one week after their transplantation (**Figure R22**) where GFP positive iPS-CMs with organized sarcomeric structure and Z bands could be detected. Importantly, the presence of

intercalated discs composed of desmosomes was also observed between the GFP positive transplanted iPS-CMs and host CMs, indicating an intercellular connection between both cell types.
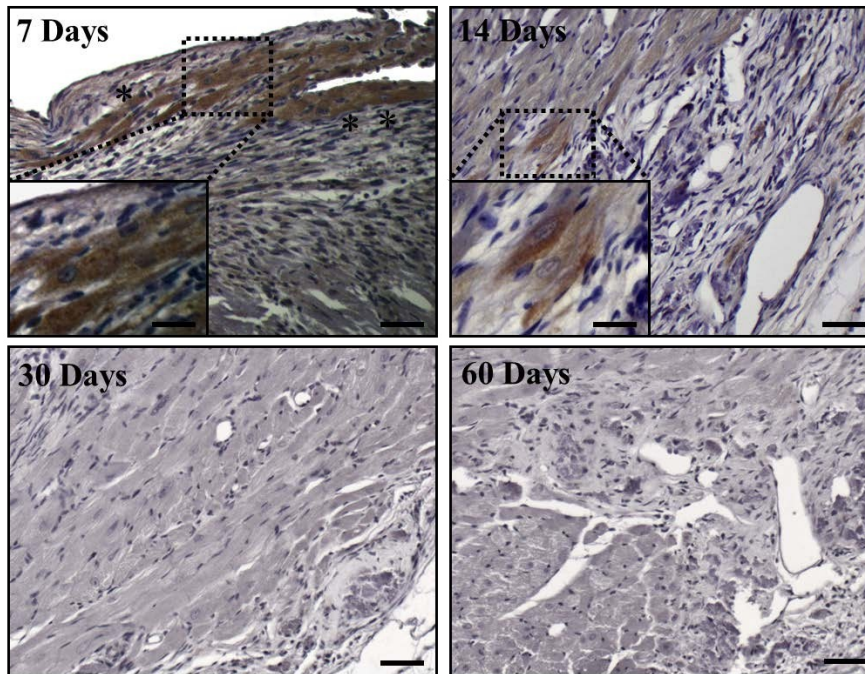
Figure R21. Analysis of cell engraftment by immunochemical detection of GFP positive cells. iPS-CMs cells were injected in the peri-infarct area after inducing an infarct. Representative areas of injured myocardium are shown 7, 14, 30 and 60 days after transplantation (day 7 and day14: n=2; day 30 and day 60: n=1) (12 serial heart sections 50 µm apart). GFP-positive areas were found 7 and 14 days after transplantation. Scale bars: 100 µm. Higher magnification: 50 µm.
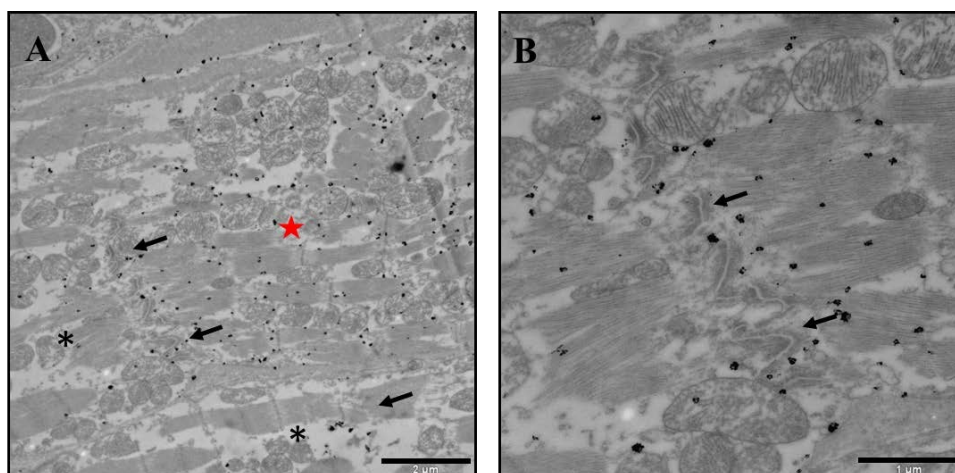
Figure R22. Transmission electron microscopy of heart transplanted iPS-CMs. Presence of GFP positive transplanted iPS-CMs was confirmed by electron microscopy after previous immunogold GFP staining (n=3). Intercalated discs composed of desmosomes (arrowheads) were detected between GFP positive iPS-CMs (red star) and host GFP negative CMs (asterisks) **(A)**. Higher magnification of desmosomes structures (arrowheads) **(B)**. Scale bars: 2 µm. Higher magnification: 1 µm.

106

Finally, the GFP positive cells were also stained for CX43 and CTNT proteins confirming the cardiac phenotype of the transplanted cells and their electro-mechanical coupling among them (**Figure R23**).
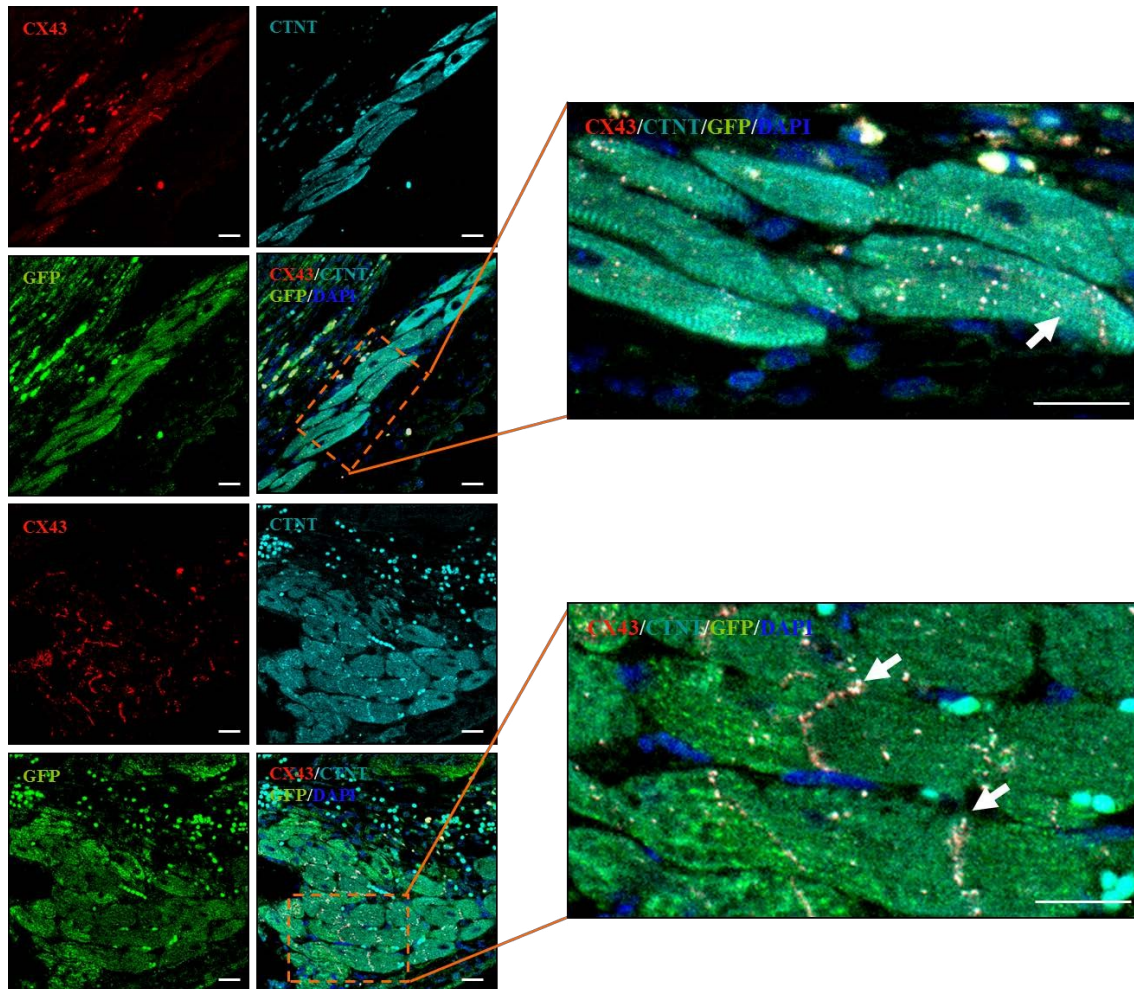
Figure R23. Immunofluorescence detection of cardiac proteins of iPS-CMs transplanted cells. iPS-CMs were detected in the injection area 7 days after their transplantation (n=2). The cells were stained for GFP (αMHC) (Alexa-488: green), CX43 (Alexa-594: red) and cardiac TROPONIN (CTNT) (Alexa-633: sky-blue). Nuclear staining was performed with DAPI (blue). Scale bars: 20 μm.

In summary, our results indicate that transplantation of iPS-CMs contributes to preserve the cardiac function and tissue viability in a model of acute MI in mice. Implanted cells exert beneficial effects by inducing a positive tissue remodeling and an increase in the damaged-tissue perfusion. The promising features of these cells require further evaluation and new strategies that potentiate their engraftment and survival in the heart tissue, contributing in a greater manner to the cardiac tissue regeneration.

DISCUSSION

Numerous studies have demonstrated the beneficial effect derived from stem cell therapy for the treatment of MI [36]. However, a direct contribution to the cardiac tissue has been only shown for few populations such as ESC, the cardiac progenitors present in the heart and the recently discovered iPS cells. Taking into account the immunogenic and ethical concerns of the ESC and the still existing technical limitations on isolating cardiac stem cells with a robust cardiac differentiation potential, the iPS cells constitute a promising cell source for cell therapy and research.

In this study, we have successfully generated iPS cells from adult mice fibroblasts by retroviral transduction of three transcription factors, *Oct3/4*, *Sox2* and *Klf4*. The protooncogene *c-Myc* was not included in the set of pluripotency factors as several reports have demonstrated that it is not essential for iPS cells generation and that its inclusion in the original set of transcription factors increases the risk of tumor formation [93]. Moreover, the negative role of *c-Myc* in the self-renewal of ESC has recently been reported showing how forced expression of *c-Myc* induced differentiation and apoptosis of hESC [304]. We generated iPS cells that presented ES-like properties, including morphology, proliferation, gene and protein expression patterns and teratoma formation capacity. Moreover, the exogenous genes over-expressed by the retrovirus were silenced in several clones, indicating that these cells were efficiently reprogrammed and did not depend on continuous expression of the transgenes for self-renewal.

Due to their embryonic-like properties, iPS cells are able to *in vitro* differentiate towards any cell type, including CMs. iPS cardiac potential has been also shown *in vivo*, after transplantation of the undifferentiated cells in an infarcted heart [156]. However, as it could be expected, a tumorigenic potential has been evidenced for iPS cells. To circumvent this problem, cardiac cells were previously derived *in vitro* to enrich the cardiac population and to eliminate residual undifferentiated cells [147, 164, 166, 167]. Still, the actual differentiation protocols present limitations and only a small percentage of the total cells differentiate towards cardiac cells. Furthermore, differentiated cardiac cells present poor levels of maturation and protocols to improve it are needed. Therefore, in the current study, we have generated iPS cells from an αMHC-GFP transgenic mouse (which allows the identification of cardiac differentiated cells) and successfully differentiated them into CMs for further selection and implantation *in vivo*. Embryoid bodies from two different iPS clones were initially differentiated by treatment with DMSO, a demethyation agent that has been shown to induce cardiac differentiation

in the P19 embryonal carcinomal cell line [305] and in hESC [205]. DMSO may exert a direct induction of CMs specification by regulation of gene expression by demethylation. By this treatment, iPS clones demonstrated early and robust *in vitro* cardiogenesis with consistent beating activity, cardiac and channel marker expression and sarcomere maturation. However, electrophysiological data revealed that DMSO-differentiated cells showed immature properties typical of fetal CMs. Our results are in concordance with previous studies where cardiac cells were *in vitro* derived from ESC or iPS cells showed also poor levels of cardiac maturation [174, 306, 307]. Many protocols have been developed to improve the cardiac specification process [51, 173, 192, 194] and recent methodological progress has enabled researchers to differentiate hESC and hiPS cells with high efficiency (more than 80%). However, despite this improvement, the cardiac cells derived continued displaying fetal phenotypes [181, 183, 308]. Thus, in an attempt to produce functionally mature CMs, we investigated the effect of the NRG-1β protein in iPS cardiac differentiation and maturation as its importance in heart development (reviewed in [208]) as well as its role in ESC cardiac differentiation [200, 201, 225] and CMs survival and proliferation [226, 228, 231] has been previously demonstrated.

The effect of NRG-1β on cardiac differentiation was analyzed by treating the cells with the protein alone or in combination with DMSO, and greater cardiac differentiation was observed when NRG-1β protein was added together with DMSO. The combined treatment significantly increased the number of GFP beating clusters of differentiated iPS cells in comparison with the treatments alone, demonstrating the synergic effect of the NRG-1β and DMSO in cardiac differentiation. Previous studies have shown that treatment with NRG-1β increased the number of beating EBs in ESC differentiation by around 50% [200] whereas in our study, NRG-1β alone induced cardiac differentiation to a lower degree (around 20%). This discrepancy between studies might reflect differences in the epigenetic/genetic characteristics of the two stem cell populations together with differences in protocol conditions for differentiating and maintaining the cardiac cells. In any case, when NRG-1β protein was combined with DMSO, similar levels of cardiac specification were reached (around 45%).

Interestingly, when the functionality of differentiated cells was analyzed, the existence of viable iPS-CMs that displayed ventricular-like action potentials was detected in all cases. It is well known that ESC-CMs form a heterogeneous population

that includes both working and nodal-type CMs [309]. This heterogeneity has been considered as a major limitation for the application of ESC-CMs for cardiac repair, as the transplantation of cardiac cells with a sustained pacemaker phenotype could promote arrhythmias [310]. In this study, we obtained a homogeneous population of ventricular-like iPS-CMs, and neither atrial or pacemaker CMs were found among the GFP populations, which indicates a specific differentiation towards a ventricular-like phenotype. More importantly, NRG-1β treated CMs exhibited functional properties that were clearly more comparable to adult host CMs than to embryonic or fetal CMs [303]. iPS-CMs showed electrophysiological maturation at day 14 of differentiation when treated with the NRG-1β protein, showing a significant shortening of APD50 and APD90 and an increase of Vmax, amplitude and MDP. On the contrary, electrophysiological maturation was not found in the cells differentiated only with DMSO, which showed a lower MDP, frequency, amplitude and Vmax, as well as a longer APD50 and APD90. Thus, we demonstrated that NRG-1β treated iPS-CMs reached a more mature phenotype in comparison to previous studies where CMs were derived from murine ESC or iPS cells [164, 166, 181, 307, 308, 311], including the studies where ESC were differentiated by NRG-1β [201]. Functional CMs with spontaneous rhythmic Ca^{2+} transients and β-adrenergic and muscarinic response were derived from iPS and ESC but multielectrode functional analysis has shown that iPS and ESC derived cardiac cells exhibited an immature phenotype that was significantly different from native ventricular tissue [174]. In a similar way, hiPS cells were differentiated towards functional CMs [164] but the cells derived exhibited typical properties of human embryonic CMs with higher values of AP duration (approximately 300 ms) but not of adult cardiac muscle [167]. Functional CMs with active response to the β-adrenergic and muscarinic agonists were also shown for ESC after NRG-1β treatment. Again, electrophysiological analysis revealed poor levels of maturation in the ESC-CMs that presented APD90 values of 200 ms (in comparison with the APD90 values of 80-90 ms we reported, closer to the APD90 values of adult CMs (83 ms) [303] [200, 201]).

As we identified an efficient cardiac differentiation protocol for mouse iPS cells and demonstrated a ventricular-like phenotype, we then studied the therapeutic benefit of the iPS-CMs cells (obtained after differentiation with dual treatment (DMSO and NRG-1β)) in a rodent model of MI. To study cardiac recovery after transplantation of

iPS-CMs in the infarcted heart, we performed ultrasound imaging, which provides a fast an inexpensive alternative to magnetic resonance imaging [25-27]. In general, the evaluation of cardiac function in mice has been hampered to date by technical issues such as the fast mouse HR, the difficulty of obtaining clear echocardiographic views of the heart and the translational motion present during the image acquisition [29, 312-314]. In this case, echocardiographic evaluation of LV remodeling was performed using the high-resolution equipment Vevo 770 (VisualSonics), specially designed for small animals. Moreover, the echocardiographic measurements and the analysis protocols were previously optimized in a pilot study where a complete structural and functional echocardiographic characterization of the LV remodeling was performed in our mouse model of MI [300]. Some technical issues were dealt with thanks to the high resolution of the equipment that provides high quality echocardiographic views of the LV. Moreover, cardiac function was initially calculated using the Teichholz and the Simpson methods as both could be theoretically used to evaluate LV function. However, our results showed that Simpson´s rule was better adapted to the particular characteristics of our MI model because unlike the Teichholz method, it does not assume that the LV cavity is an ellipse, and therefore, the post-infarct LV induced dilation is calculated in multiple slices in both systole and diastole, adjusting better to the morphometry of the heart and thereby offering a more reliable method for this *in vivo* model. Furthermore, in order to better visualize the infarct area, we acquired and performed structural measurements in both paraesternal short-axis and long-axis views. Other groups have done similar studies using the same equipment [250, 315, 316] but only using standard measurements. Given the location of the infarction, starting at the apical level and progressing towards the middle ventricle, we measured the FAC% not only using the standard short-axis views, but also a parasternal long-axis view. Both results demonstrated marked systolic dysfunction caused by LV remodeling, although a greater correlation between FAC% and infarct size (estimated from the histology) was detected in the single long-axis than in the short-axis views. This is due to the difficulty of obtaining LV short-axis views with a clear definition of the entire post-infarction endocardial border because of the orientation of the heart and the small size of the mouse rib cage [314]. Our analysis of the evolution of FAC% showed that the systolic function was directly related to the progressive dilation of the LV internal diameter and the increase of the end-systolic and end-diastolic areas. After this complete echocardiographic characterization of the heart LV remodeling, we studied the

regenerative potential of iPS derived cardiac cells in an acute mouse model of MI. Few studies have described the *in vivo* potential of iPS cells for cardiac repair [156]. Early ones showed that transplantation of undifferentiated iPS cells in acutely infarcted hearts resulted in cell engraftment, cardiac *in vivo* differentiation and an improvement in cardiac function but, as expected, they also reported tumor formation. In view of this evident limitation, we transplanted previously *in vitro* differentiated cardiac cells. At the functional level, a preservation of the cardiac function was detected in the long-term (2 months) in the iPS-CMs-treated animals that was not observed in the non-treated animals. Furthemore, iPS-CMs transplantation induced a beneficial effect in the injured hearts that resulted in a smaller infarct size and scar collagen content and an increase in the revascularization of the tissue. Moreover, no teratoma formation was observed in any animals due to the differentiation and selection method, although a more dedicated study would be needed for evaluating its safe use.

Interestingly, our *in vivo* results at the functional and tissue remodeling levels are comparable with other reports, in which a positive effect was observed after iPS-CMs transplantation [168]. In the study by *Carpenter et al.*, transplantation of hiPS-derived cardiac differentiated cells in a rat MI model attenuated scar tissue formation and, in association with this, preserved the cardiac function. In this case, the transplanted cells were detected in the peri-infarct zone 10 weeks post-transplantation (with 22% engraftment) although ten times more cells were implanted in this study than in ours. The poorer level of engraftment detected in our study could be explained by the ischemic conditions of our MI model (a permanent-ligation acute model in comparison with the ischemic-reperfusion model performed in the study by Dr. Watt), the immunogenicity against the GFP protein [259] and the cell dose. This last issue has also been previously analyzed in more detail. Interestingly, *Mummery et al.* compared the effect of injecting 1 million *vs.* 3 million cells and observed that the lower dose, despite forming smaller grafts of hESC-CMs, was associated with a better functional outcome [317]. This is consistent with other reports, which showed equal improvement of the cardiac function after transplantation with different hESC-CMs doses (10 million *vs.* 1.5 million CMs) [51, 52]. This effect must be due to the fact that cells did not significantly contribute to the regeneration of the tissue as they survived poorly in it [318]. In fact, the initial presence of large clusters of cells could cause structural disruption of adjacent host CMs [319] as it has been described for skeletal myoblasts, which when injected at

high doses disrupted the electrical coupling between the host CMs (reviewed in [320]). Clusters of cells may also secrete more extracellular matrix, increasing the fibrotic area between transplanted cells and host cells and therefore isolating the graft [50, 51].

On the other hand, although we have shown that at day 14 of differentiation cardiac cells exhibited more mature properties, iPS-CMs were transplanted at day 7 of differentiation as pre-differentiated cells might survive and proliferate better than fully mature differentiated cells. Previous studies have shown that transplanted fetal CMs integrate and survive in the myocardium better than primary adult CMs as they present a greater capacity for proliferation [321]. Moreover, it has been reported by our group that due to their high sensitivity to hypoxia, mature differentiated CMs derived from the adipose tissue did not survive in heart tissue for up to a week and thereby, failed to improve heart function [322]. In our study, we detected engrafted cardiac cells for up to two weeks, which importantly, presented a sarcomeric organization with developed Z bands. Interestingly, intercalated discs composed by desmosomes were observed connecting the transplanted CMs to adjacent host CMs, demonstrating *in vivo* maturation of the predifferentiated CMs. In comparison with our results, *Mauritz el al.* have also reported that iPS cell-derived Flk1^{+} cardiovascular progenitors are capable of engrafting on the heart tissue improving the heart function [177]. However, structured sarcomeric organization and alignment of these cells could not be detected, suggesting that these cells had an early and immature cardiac phenotype. Moreover, in other reports, pre-differentiated CMs derived from hESC have also been shown to engraft on injured rat hearts [323]. Mummery and colleagues were the first ones to demonstrate the long-term fate of hESC-CMs when transplanted in a model of MI in immmunodeficient mice [50]. hESC-CMs survived, integrated and matured in the host myocardium for at least 3 months. A maturation of hESC-CMs was observed over time, showing an improved sarcomeric organization and alignment within the host myocardium, downregulation of cardiac immature markers (*Sma* and *Mlc2a*) and upregulation of mature markers (*Mlc2v* and *Cx43*) together with the establishment of intercellular contacts such as desmosomes and gap junctions structures among the CMs. Moreover, early cardiovascular progenitors not only might not only survive and engraft better in the ischemic heart tissue but also contribute directly to the cardiovascular lineages. A stable engraftment and robust cardiac differentiation was detected for transplanted ESC-derived Nkx2.5+ cardiac progenitors following MI, which established gap junctions

with the host cells [324]. Similar results have also been demonstrated after ESC-derived cardiovascular progenitor transplantation in a murine MI model [51, 190]. *Yang et al.* described a population derived from hESC phenotypically characterized by the expression of KDR^{low}/c-kit^{-} that displayed *in vitro* and *in vivo* cardiac and vascular potential. Furthermore, mESC-derived Flk-1^{+} progenitors proliferated and differentiated into CMs *in vivo*, contributing to improve cardiac function in a dilated cardiomyopathy mouse model [325]. Mouse and human iPS cell-derived Flk-1^{+} progenitor cells have also been derived *in vitro* [147] and have exerted beneficial effects after their transplantation *in vivo*, differentiating into cardiovascular lineages and improving cardiac function in a mouse model of acute MI [177]. Finally, a population of cardiac derived cells enriched for Isl1+ progenitor cells have been shown not only to survive long-term after their transplantation into the infarcted hearts but also to differentiate into CMs, ECs and SMC, promoting endogenous angiogenesis, reducing cardiac apoptosis and infarct size and improving cardiac function [46, 326, 327].

Importantly, despite the fact that histological analysis has demonstrated the presence of electromechanically coupled iPS-CMs in the heart tissue, it can be suggested that the positive benefit observed at the functional and remodeling level is for the most part due to the trophic effect of the cells. In fact, many (stem) cells have demonstrated their therapeutic potential through paracrine mechanisms. Blood, bone marrow (BM) and adipose tissue derived progenitor cells like BM-derived mononuclear cells (BM-MNCs), SVF [328], mesenchymal stem cells [322, 329, 330] and endothelial progenitor cells (EPCs) [331] have been shown to release angiogenic factors such as bFGF, VEGF, and hepatocyte growth factor (HGF), protecting the heart from ischemia, activating revascularization of the damaged tissue, improving contractility and attenuating fibrosis following MI (reviewed in [257]). Importantly, adult CMs also release angiogenic factors in response to hypoxia [332] and mechanical stress [333, 334] promoting angiogenesis, cell survival and regulating the CMs function too [335]. Interestingly, the role of the mesenchymal cells has been described at the hemodynamic level: transplantation of autologous MSC in a non-ischemic rabbit model of heart failure led to an improvement in cardiac contractility by a decrease in catecholamine levels and a subsequent attenuation in β-adrenoceptor downregulation [336]. Also, a positive effect in cardiac post-infarction remodeling can be exerted by MSC by promoting host-derived myofibroblasts proliferation [337, 338] and by attenuating expression of collagen types

I and II, tissue inhibitor of MMP-1 (TIMP1) [339] TGF-β [340] and pro-inflammatory cytokines, which are known to regulate LV remodeling [339].

All these results demonstrate that CMs can engraft into the heart tissue, although they do not survive long-term and disappear with time. Thus, new strategies to potentiate cell delivery, engraftment and survival of the cells are essential for improving repair of infarcted hearts. Scar tissue formation after MI creates a hypoxic environment that severely compromises CM survival. Therefore, co-tranplantation of CMs with other cell populations such as the ECs and SMC that can contribute to new blood vessel formation to supply oxygen and nutrients, and stromal cells (fibroblasts) or mesenchymal cells for ECM support, could be a good option to improve cardiac cell survival. In fact, mixed populations of differentiating ESC cultures have already been used. A matrix composed of non-human primate ESC derived-SSEA1+ cardiac progenitors combined with ADSC provided new differentiated CMs and exerted trophic support after their transplantation in a primate MI model [267]. Interestingly, *Templin et al.* were the first to demonstrate long-term survival (visualized for up to 15 weeks) and differentiation after the co-administration of hiPS with MSC in a large-animal model of MI [261]. Interestingly, it has also been shown that cell patches comprising only hESC derived-CMs and the matrix that they secreted, survived poorly after their transplantation. However, the addition of endothelial and stromal cells greatly enhanced cell survival and induced tissue revascularization [269]. Similar positive effects have recently been reported using tissue patches prepared with cardiac cells derived from iPS cells. Two interesting studies have been published to date in a mouse and a pig model of MI respectively, showing the functional benefit derived from the transplanted iPS-derived cell sheets [272, 273]. Moreover, a significantly higher engraftment of CMs was demonstrated when cells were transplanted as a tricell patch composed of iPS-derived CMs, ECs and MEFs [272].

Regardless of the cell source, survival of the injected cells in the injured heart has been very limited, due not only to the injection methods, but also to the ischemic environment and the lack of cell-to-cell and cell-to matrix contact with the following loss of survival signals (reviewed in [341]). Early studies have shown how cells implanted into the infarcted heart that were previously adhered to solid scaffolds, presented greater engraftment and as a consequence, induced a much greater benefit than when injected as a cell suspension [342]. Also, transplantation of hESC derived-

CMs within bioengineered scaffolds has shown a functional improvement, increasing the tissue vascularization and survival of the cells after their transplantation into the injured hearts [266, 268-270]. Interestingly, *Levenberg et al.* showed that ESC-ECs, seeded in biodegradable polymer scaffolds could engraft long-term and form new vessels [343]. Moreover, a 3D human cardiac tissue composed by collagen type I and hiPS-CMs also showed a functional benefit after its transplantation into immunodeficient rat hearts [271]. Furthermore, *Caspi et al.* seeded hESC-derived CMs and vascular cells onto poly-L-lactic acid scaffolds, with an enhancement of CMs proliferation due to presence of ECs and the scaffold support [266]. All these data strongly suggests that engineered tissue rather than direct cell transplantation could be a more efficient approach for therapeutic purposes [344].

However, although these studies suggest a direct contribution of the transplanted iPS derived cells, further experiments will be necessary to assess the mechanisms of action of the transplanted cells as well as their functional integration and electrophysiological behavior *in vivo*. The mechanical integration of hESC-CMs in a pig model of MI [274] has been recently reported, demonstrating cell integration with the host cardiac tissue, as late as one month after their transplantation. *In vivo* functional integration of iPS-CMs should be determined to confirm their potential for cardiac repair.

Thus, although we have reported the beneficial effect derived from the transplantation of NRG-1β differentiated iPS-CMs, their poor survival and integration in the tissue constitutes the principal limitation of this study. Other strategies to improve the survival of the cells in the tissue and induce their differentiation and maturation more strongly are therefore necessary. Further studies could be proposed in which stem cells could be treated with different cytokines before or after their transplantation to enhance their survival in the tissue and therefore their therapeutic efficacy. For instance, transplantation of MSC pre-treated with FGF-2, IGF-1 and BMP2 and transplanted in a rat model of MI showed better survival in the tissue and exerted greater cytoprotective effects on neighboring CMs, which translated into a reduced infarct size and an improvement of the LV function [345]. Moreover, MSC transfected with adenovirus expressing human VEGF and SDF-1 also survived at greater levels and therefore, enhanced their trophic effect, inducing greater benefit in terms of tissue revascularization and remodeling, and thereby improving cardiac function [346].

The role that trophic factors released by the transplanted cells exert in cardiac repair is noteworthy, so it could be argued that injection of key factors/cytokines could induce a similar paracrine effect. However, it has to be taken into account that the injection of soluble factors in ischemia models has been associated with limited success, mainly due to the short-lived effect of the cytokines (reviewed in [35]). In this context, the use of controlled release systems that could allow sustained cytokine release could significantly prolong their biological effect. Several studies have developed therapeutic controlled delivery systems to release angiogenic cytokines such as VEGF, bFGF and FGF. Sustained and localized release of VEGF through PLGA microparticles has recently been reported by our group [347] which, when injected in the rat hearts after MI, induced an increase in the revascularization of the tissue and positive remodeling of the heart. The preparation of porous alginate scaffolds with the capacity to deliver bFGF with a controlled pattern has also been reported [348]. Interestingly, when the scaffold was transplanted into the mesenteric membrane of the rat peritoneum, an increased capillary density was observed. Other studies have reported efficient tissue revascularization after administration of VEGF-loaded nanoparticle-fibrin gel complexes in a rabbit model of ischemic hind limb [349] or after injection of matrigel constructs loaded with FGF9 in ischemic heart mouse models [350]. Also, local delivery of insulin-like growth factor 1 (IGF-1) with biotinylated peptide nanofibers improved cell therapy for MI [351]. In this experiment, when neonatal CMs were transplanted together with the IGF-1 nanofibers they survived better and an improved systolic function was detected. Interestingly, we have demonstrated by using a PLGA-MP system, that NRG-1β-sustained treatment induces a functional benefit that is associated with an induction of tissue revascularization and positive remodeling in an acute rat model of MI. Furthermore, induction of host CMs proliferation was also observed (data not published). Therefore, the combination of a sustained NRG-1β protein release system with iPS-CMs could represent an attractive strategy to boost survival, proliferation, differentiation and maturation of the transplanted iPS-CMs could be potentiated.

Other interesting strategies are the possibility of inducing partial or direct reprogramming of somatic cells towards CMs by overexpression of different sets of cardiac reprogramming factors like *Gata4*, *Hand2*, *Mef2c* and *Tbx5* [249, 251]. Direct *in vitro* conversion of adult cells into cardiomyocyte-like cells has been shown although

it still seems to be a rather inefficient process that needs to be optimized. Initial studies have shown that the generated CMs failed in the expression of some typical cardiac genes, showed incomplete functional maturation and poor survival after transplantation in a mouse model of MI [254]. Interestingly, this reprogramming phenomenon has been also reported *in vivo* [250]. However, even though a functional benefit was induced in a MI model, the level of transduced cells that remained with time is not clear, nor is the mechanism of this functional improvement. Also, the induction of cardiomyocyte-like cells in infarcted hearts has not been so successfully achieved by other groups that performed gene transfer of the same factors by using a polycistronic retrovirus [252]. Thus, further studies will be needed in future research in order to improve these protocols and better understand the underlying mechanisms (**See scheme D1**).

In summary, our results indicate that transplantation of iPS-CMs provides a long-term beneficial effect, helping to preserve the cardiac function and tissue viability in a model of acute MI in mice. Implanted in an acute ischemic environment, these cells survive and form connections with each other and with adjacent host CMs, exerting beneficial effects that include positive cardiac remodeling and an induction of tissue perfusion. Furthermore, we have demonstrated for the first time that NRG-1β protein significantly induces cardiac specification of miPS cells towards a mature ventricular-like cardiac phenotype. A greater effect regarding the percentage of differentiated cells was detected when cells were treated with NRG-1β in combination with DMSO. Thus, iPS cells differentiated with NRG-1β and DMSO could represent a useful source to produce a sufficient number of mature CMs for cellular transplantation and also for drug screening and target validation. The promising features of these cells require further evaluation and new strategies that help to boost their engraftment and survival into the heart tissue, contributing to a greater degree to cardiac tissue regeneration.
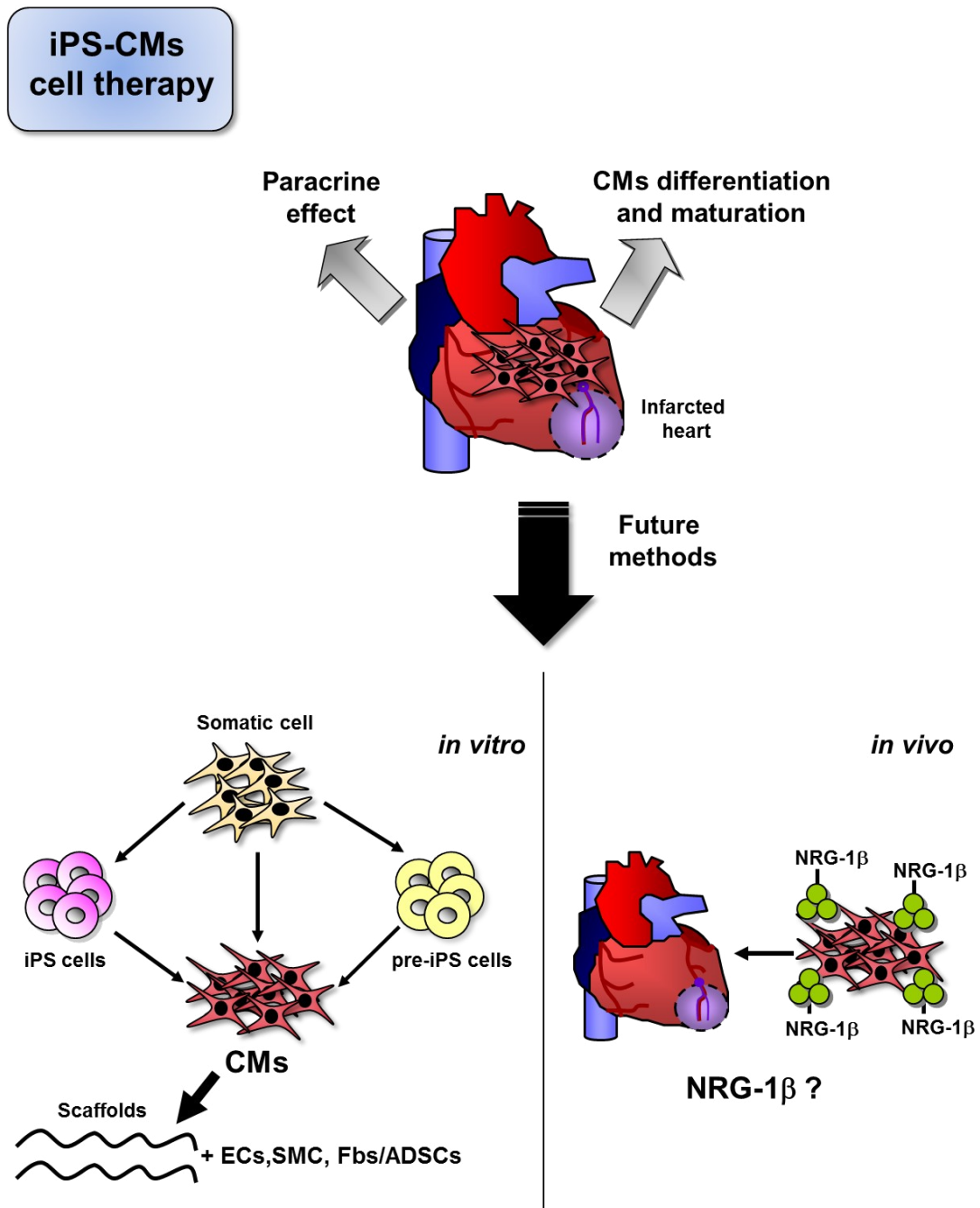
Scheme D1. iPS-CMs therapy in cardiac repair. Transplanted iPS-CMs engrafted and matured in the damaged heart tissue exerting a positive benefit including the preservation of cardiac remodeling and tissue viability. However, the poor engraftment of the cells represents the principal limitation for the therapeutical application of cardiac iPS cells. Thus, further studies such as the combination of CMs with other (stem) cell populations and bioengineered scaffolds are being assayed to improve the engraftment and survival of the transplanted cells. Finally, transplantation of iPS-CMs together with NRG-1 microparticles could represent an alternative strategy to promote *in vivo* differentiation and maturation of CMs.

CONCLUSIONS

1. Adult tail fibroblasts derived from αMHC-GFP transgenic mice can be reprogrammed into embryonic stem-like cells by retroviral over-expression of the specific pluripotency transcription factors *Oct3/4*, *Klf4* and *Sox2*.

2. All the generated and analyzed mouse iPS clones share the defining features of ESC, according to the standard tests of pluripotency. At the cell culture level, the iPS clones, exhibit typical mouse ESC morphology, present unlimited growth capacity and spontaneously form embryoid bodies when grown in suspension in the presence of serum. iPS clones activate the expression of the core ESC gene regulatory network *Nanog*, *Oct3/4*, *Klf4*, *Sox2*, *Eras*, *Ecat1*, *Fbx15* and *Rex1* pluripotent genes. OCT3/4 and NANOG protein expression and Alkaline Phosphatase activity have also been detected in the reprogrammed cells. *In vivo*, iPS cells subcutaneously injected into immunodeficient mice generate teratomas.

3. Among the six derived iPS clones, clones 1 and 2 exhibit the most robust cardiac differentiation potential. *In vitro,* treatment with a demethylation agent, dymethyl sulfoxide (DMSO), induces up-regulation of early and late specific cardiac genes and proteins, whereas no or very low levels of endothelial and smooth muscle genes expression are detected, indicating the iPS cells specification towards a cardiac phenotype. *In vitro* differentiated cells present sarcomeric organization and spontaneous contraction with action potentials typical of fetal cardiomyocytes.

4. Combination of DMSO with the recombinant NRG-1β protein induces a more robust differentiation of iPS cells towards a cardiac phenotype with larger beating GFP positive areas than DMSO alone. Also, a greater differentiation induction is achieved with the combined treatment than with the NRG-1β protein alone, demonstrating the synergistic effect of both factors.

5. iPS-derived cardiomyocytes also achieve a more mature cardiac phenotype when they are differentiated with the NRG-1β protein and show a ventricular-like action potential with shorter APD50 and APD90 and higher MDP, amplitude, frequency and Vmax values. On the contrary, iPS-CMs differentiated only with DMSO, exhibit typical properties of fetal CMs with longer APD50 and APD90 and lower MDP, amplitude, frequency and Vmax values.

6. The high resolution equipment for echocardiography, VEVO 770, allows a reliable evaluation of the left ventricular post-infarction heart remodeling in an acute DBA/2J model of MI. Measurements performed by following Simpson´s method and images taken in the heart with short but also long-axis views are required for optimal analysis.

7. Transplantation of iPS-derived cardiomyocytes in a model of acute MI in DBA/2J mice contributes to preserve the cardiac function and tissue viability. A long-lasting functional effect is associated with a smaller infarct size and scar collagen content together with higher tissue revascularization.

8. Injected in an acute ischemic environment, the cardiac cells are able to engraft, establish gap junctions among them and couple to the host cardiomyocytes through desmosomes. In global terms, contribution to the cardiac tissue is, however, minimal, suggesting a paracrine effect as the main mechanism for the observed benefits.

9. Altogether, these findings show the potential of NRG-1β protein and DMSO as a treatment for inducing a specific iPS cells differentiation towards ventricular-like cardiomyocytes. iPS-derived cardiac cells could represent an interesting cell source for cardiac regenerative therapy as they contribute to the regeneration of the ischemic tissue and provide a long-term functional preservation and positive tissue remodeling in a mouse model of acute MI.

REFERENCES

[1] Go AS, Mozaffarian D, Roger VL, Benjamin EJ, Berry JD, Borden WB, *et al.* Heart Disease and Stroke Statistics--2013 Update: A Report From the American Heart Association. Circulation 2013;127:e6-e245.

[2] Thygesen K, Alpert JS, Jaffe AS, Simoons ML, Chaitman BR, White HD. Third universal definition of myocardial infarction. Nat Rev Cardiol 2012;9:620-633.

[3] Libby P, Ridker PM, Hansson GK. Progress and challenges in translating the biology of atherosclerosis. Nature 2011;473:317-325.

[4] Jennings RB, Murry CE, Steenbergen C, Jr., Reimer KA. Development of cell injury in sustained acute ischemia. Circulation 1990;82:II2-12.

[5] Rossen RD, Michael LH, Kagiyama A, Savage HE, Hanson G, Reisberg MA*, et al.* Mechanism of complement activation after coronary artery occlusion: evidence that myocardial ischemia in dogs causes release of constituents of myocardial subcellular origin that complex with human C1q in vivo. Circ Res 1988;62:572-584.

[6] Deten A, Volz HC, Briest W, Zimmer HG. Cardiac cytokine expression is upregulated in the acute phase after myocardial infarction. Experimental studies in rats. Cardiovasc Res 2002;55:329-340.

[7] Frangogiannis NG, Smith CW, Entman ML. The inflammatory response in myocardial infarction. Cardiovasc Res 2002;53:31-47.

[8] Mann DL. Mechanisms and models in heart failure: A combinatorial approach. Circulation 1999;100:999-1008.

[9] Heusch G, Schulz R, Rahimtoola SH. Myocardial hibernation: a delicate balance. Am J Physiol Heart Circ Physiol 2005;288:H984-999.

[10] Cleutjens JP, Kandala JC, Guarda E, Guntaka RV, Weber KT. Regulation of collagen degradation in the rat myocardium after infarction. J Mol Cell Cardiol 1995;27:1281-1292.

[11] Ertl G, Frantz S. Healing after myocardial infarction. Cardiovasc Res 2005;66:22-32.

[12] Nian M, Lee P, Khaper N, Liu P. Inflammatory cytokines and postmyocardial infarction remodeling. Circ Res 2004;94:1543-1553.

[13] Nahrendorf M, Swirski FK, Aikawa E, Stangenberg L, Wurdinger T, Figueiredo JL*, et al.* The healing myocardium sequentially mobilizes two monocyte subsets with divergent and complementary functions. J Exp Med 2007;204:3037-3047.

[14] Bujak M, Frangogiannis NG. The role of TGF-beta signaling in myocardial infarction and cardiac remodeling. Cardiovasc Res 2007;74:184-195.

[15] Frangogiannis NG, Mendoza LH, Lindsey ML, Ballantyne CM, Michael LH, Smith CW*, et al.* IL-10 is induced in the reperfused myocardium and may modulate the reaction to injury. J Immunol 2000;165:2798-2808.

[16] Mann DL, Spinale FG. Activation of matrix metalloproteinases in the failing human heart: breaking the tie that binds. Circulation 1998;98:1699-1702.

[17] Sun Y, Kiani MF, Postlethwaite AE, Weber KT. Infarct scar as living tissue. Basic Res Cardiol 2002;97:343-347.

[18] Sutton MG, Sharpe N. Left ventricular remodeling after myocardial infarction: pathophysiology and therapy. Circulation 2000;101:2981-2988.

[19] Lang RM, Bierig M, Devereux RB, Flachskampf FA, Foster E, Pellikka PA*, et al.* Recommendations for chamber quantification: a report from the American Society of Echocardiography's Guidelines and Standards Committee and the Chamber Quantification Writing Group, developed in conjunction with the European Association of Echocardiography, a branch of the European Society of Cardiology. J Am Soc Echocardiogr 2005;18:1440-1463.

[20] Feigenbaum H. Role of echocardiography in acute myocardial infarction. Am J Cardiol 1990;66:17H-22H.

[21] Mor-Avi V, Lang RM, Badano LP, Belohlavek M, Cardim NM, Derumeaux G*, et al.* Current and evolving echocardiographic techniques for the quantitative evaluation of cardiac mechanics: ASE/EAE consensus statement on methodology and indications endorsed by the Japanese Society of Echocardiography. J Am Soc Echocardiogr 2011;24:277-313.

[22] Kanno S, Lerner DL, Schuessler RB, Betsuyaku T, Yamada KA, Saffitz JE*, et al.* Echocardiographic evaluation of ventricular remodeling in a mouse model of myocardial infarction. J Am Soc Echocardiogr 2002;15:601-609.

[23] Takagawa J, Zhang Y, Wong ML, Sievers RE, Kapasi NK, Wang Y*, et al.* Myocardial infarct size measurement in the mouse chronic infarction model: comparison of area- and length-based approaches. J Appl Physiol 2007;102:2104-2111.

[24] Scherrer-Crosbie M, Kurtz B. Ventricular remodeling and function: insights using murine echocardiography. J Mol Cell Cardiol 2009;48:512-517.

[25] Chin BB, Metzler SD, Lemaire A, Curcio A, Vemulapalli S, Greer KL*, et al.* Left ventricular functional assessment in mice: feasibility of high spatial and temporal resolution ECG-gated blood pool SPECT. Radiology 2007;245:440-448.

[26] Voelkl JG, Haubner BJ, Kremser C, Mayr A, Klug G, Loizides A*, et al.* Cardiac imaging using clinical 1.5 t MRI scanners in a murine ischemia/reperfusion model. J Biomed Biotechnol 2010;2011:185683.

[27] Tournoux F, Petersen B, Thibault H, Zou L, Raher MJ, Kurtz B*, et al.* Validation of noninvasive measurements of cardiac output in mice using echocardiography. J Am Soc Echocardiogr 2011;24:465-470.

[28] Foster FS, Zhang MY, Zhou YQ, Liu G, Mehi J, Cherin E*, et al.* A new ultrasound instrument for in vivo microimaging of mice. Ultrasound Med Biol 2002;28:1165-1172.

[29] Rottman JN, Ni G, Brown M. Echocardiographic evaluation of ventricular function in mice. Echocardiography 2007;24:83-89.

[30] Domanski MJ, Cunnion RE, Roberts WC. Analysis of fractional area change at various levels in the normal left ventricle. Am J Cardiol 1992;70:1367-1368.

[31] Teichholz LE, Cohen MV, Sonnenblick EH, Gorlin R. Study of left ventricular geometry and function by B-scan ultrasonography in patients with and without asynergy. N Engl J Med 1974;291:1220-1226.

[32] Ino T, Benson LN, Mikalian H, Freedom RM, Rowe RD. Determination of left ventricular volumes by Simpson's rule in infants and children with congenital heart disease. Br Heart J 1989;61:182-185.

[33] Gao XM, Dart AM, Dewar E, Jennings G, Du XJ. Serial echocardiographic assessment of left ventricular dimensions and function after myocardial infarction in mice. Cardiovasc Res 2000;45:330-338.

[34] Gaffney MM, Hynes SO, Barry F, O'Brien T. Cardiovascular gene therapy: current status and therapeutic potential. Br J Pharmacol 2007;152:175-188.

[35] Formiga FR, Tamayo E, Simon-Yarza T, Pelacho B, Prosper F, Blanco-Prieto MJ. Angiogenic therapy for cardiac repair based on protein delivery systems. Heart Fail Rev 2011;17:449-473.

[36] Passier R, van Laake LW, Mummery CL. Stem-cell-based therapy and lessons from the heart. Nature 2008;453:322-329.

[37] Yamada Y, Wang XD, Yokoyama S, Fukuda N, Takakura N. Cardiac progenitor cells in brown adipose tissue repaired damaged myocardium. Biochem Biophys Res Commun 2006;342:662-670.

[38] Schenke-Layland K, Strem BM, Jordan MC, Deemedio MT, Hedrick MH, Roos KP, et al. Adipose tissue-derived cells improve cardiac function following myocardial infarction. J Surg Res 2009;153:217-223.

[39] Martin-Puig S, Wang Z, Chien KR. Lives of a heart cell: tracing the origins of cardiac progenitors. Cell Stem Cell 2008;2:320-331.

[40] Beltrami AP, Barlucchi L, Torella D, Baker M, Limana F, Chimenti S, et al. Adult cardiac stem cells are multipotent and support myocardial regeneration. Cell 2003;114:763-776.

[41] Dawn B, Stein AB, Urbanek K, Rota M, Whang B, Rastaldo R, et al. Cardiac stem cells delivered intravascularly traverse the vessel barrier, regenerate infarcted myocardium, and improve cardiac function. Proc Natl Acad Sci U S A 2005;102:3766-3771.

[42] Rota M, Padin-Iruegas ME, Misao Y, De Angelis A, Maestroni S, Ferreira-Martins J, et al. Local activation or implantation of cardiac progenitor cells rescues scarred infarcted myocardium improving cardiac function. Circ Res 2008;103:107-116.

[43] Oh H, Bradfute SB, Gallardo TD, Nakamura T, Gaussin V, Mishina Y, et al. Cardiac progenitor cells from adult myocardium: homing, differentiation, and fusion after infarction. Proc Natl Acad Sci U S A 2003;100:12313-12318.

[44] Martin CM, Meeson AP, Robertson SM, Hawke TJ, Richardson JA, Bates S, et al. Persistent expression of the ATP-binding cassette transporter, Abcg2, identifies cardiac SP cells in the developing and adult heart. Dev Biol 2004;265:262-275.

[45] Laugwitz KL, Moretti A, Lam J, Gruber P, Chen Y, Woodard S, et al. Postnatal isl1+ cardioblasts enter fully differentiated cardiomyocyte lineages. Nature 2005;433:647-653.

[46] Bu L, Jiang X, Martin-Puig S, Caron L, Zhu S, Shao Y, et al. Human ISL1 heart progenitors generate diverse multipotent cardiovascular cell lineages. Nature 2009;460:113-117.

[47] Messina E, De Angelis L, Frati G, Morrone S, Chimenti S, Fiordaliso F, et al. Isolation and expansion of adult cardiac stem cells from human and murine heart. Circ Res 2004;95:911-921.

[48] Lee ST, White AJ, Matsushita S, Malliaras K, Steenbergen C, Zhang Y, et al. Intramyocardial injection of autologous cardiospheres or cardiosphere-derived cells preserves function and minimizes adverse ventricular remodeling in pigs with heart failure post-myocardial infarction. J Am Coll Cardiol 2011;57:455-465.

[49]   Planat-Benard V, Menard C, Andre M, Puceat M, Perez A, Garcia-Verdugo JM, *et al.* Spontaneous cardiomyocyte differentiation from adipose tissue stroma cells. Circ Res 2004;94:223-229.

[50]   van Laake LW, Passier R, Monshouwer-Kloots J, Verkleij AJ, Lips DJ, Freund C, *et al.* Human embryonic stem cell-derived cardiomyocytes survive and mature in the mouse heart and transiently improve function after myocardial infarction. Stem Cell Res 2007;1:9-24.

[51]   Laflamme MA, Chen KY, Naumova AV, Muskheli V, Fugate JA, Dupras SK, *et al.* Cardiomyocytes derived from human embryonic stem cells in pro-survival factors enhance function of infarcted rat hearts. Nat Biotechnol 2007;25:1015-1024.

[52]   Caspi O, Huber I, Kehat I, Habib M, Arbel G, Gepstein A, *et al.* Transplantation of human embryonic stem cell-derived cardiomyocytes improves myocardial performance in infarcted rat hearts. J Am Coll Cardiol 2007;50:1884-1893.

[53]   Takahashi K, Yamanaka S. Induction of pluripotent stem cells from mouse embryonic and adult fibroblast cultures by defined factors. Cell 2006;126:663-676.

[54]   Takahashi K, Tanabe K, Ohnuki M, Narita M, Ichisaka T, Tomoda K, *et al.* Induction of pluripotent stem cells from adult human fibroblasts by defined factors. Cell 2007;131:861-872.

[55]   Park IH, Zhao R, West JA, Yabuuchi A, Huo H, Ince TA, *et al.* Reprogramming of human somatic cells to pluripotency with defined factors. Nature 2008;451:141-146.

[56]   Aasen T, Raya A, Barrero MJ, Garreta E, Consiglio A, Gonzalez F, *et al.* Efficient and rapid generation of induced pluripotent stem cells from human keratinocytes. Nat Biotechnol 2008;26:1276-1284.

[57]   Yu J, Vodyanik MA, Smuga-Otto K, Antosiewicz-Bourget J, Frane JL, Tian S, *et al.* Induced pluripotent stem cell lines derived from human somatic cells. Science 2007;318:1917-1920.

[58]   Maherali N, Sridharan R, Xie W, Utikal J, Eminli S, Arnold K, *et al.* Directly reprogrammed fibroblasts show global epigenetic remodeling and widespread tissue contribution. Cell Stem Cell 2007;1:55-70.

[59]   Okita K, Ichisaka T, Yamanaka S. Generation of germline-competent induced pluripotent stem cells. Nature 2007;448:313-317.

[60]   Wernig M, Lengner CJ, Hanna J, Lodato MA, Steine E, Foreman R, *et al.* A drug-inducible transgenic system for direct reprogramming of multiple somatic cell types. Nat Biotechnol 2008;26:916-924.

[61]   Chin MH, Mason MJ, Xie W, Volinia S, Singer M, Peterson C, *et al.* Induced pluripotent stem cells and embryonic stem cells are distinguished by gene expression signatures. Cell Stem Cell 2009;5:111-123.

[62]   Deng J, Shoemaker R, Xie B, Gore A, LeProust EM, Antosiewicz-Bourget J, *et al.* Targeted bisulfite sequencing reveals changes in DNA methylation associated with nuclear reprogramming. Nat Biotechnol 2009;27:353-360.

[63]   Feng Q, Lu SJ, Klimanskaya I, Gomes I, Kim D, Chung Y, *et al.* Hemangioblastic derivatives from human induced pluripotent stem cells exhibit limited expansion and early senescence. Stem Cells 2010;28:704-712.

[64]   Lowry WE, Richter L, Yachechko R, Pyle AD, Tchieu J, Sridharan R, *et al.* Generation of human induced pluripotent stem cells from dermal fibroblasts. Proc Natl Acad Sci U S A 2008;105:2883-2888.

[65] Liu H, Zhu F, Yong J, Zhang P, Hou P, Li H, *et al.* Generation of induced pluripotent stem cells from adult rhesus monkey fibroblasts. Cell Stem Cell 2008;3:587-590.

[66] Esteban MA, Xu J, Yang J, Peng M, Qin D, Li W, *et al.* Generation of induced pluripotent stem cell lines from Tibetan miniature pig. J Biol Chem 2009;284:17634-17640.

[67] Ezashi T, Telugu BP, Alexenko AP, Sachdev S, Sinha S, Roberts RM. Derivation of induced pluripotent stem cells from pig somatic cells. Proc Natl Acad Sci U S A 2009;106:10993-10998.

[68] Li W, Wei W, Zhu S, Zhu J, Shi Y, Lin T, *et al.* Generation of rat and human induced pluripotent stem cells by combining genetic reprogramming and chemical inhibitors. Cell Stem Cell 2009;4:16-19.

[69] Liao J, Cui C, Chen S, Ren J, Chen J, Gao Y, *et al.* Generation of induced pluripotent stem cell lines from adult rat cells. Cell Stem Cell 2009;4:11-15.

[70] Honda A, Hirose M, Hatori M, Matoba S, Miyoshi H, Inoue K, *et al.* Generation of induced pluripotent stem cells in rabbits: potential experimental models for human regenerative medicine. J Biol Chem 2010;285:31362-31369.

[71] Shimada H, Nakada A, Hashimoto Y, Shigeno K, Shionoya Y, Nakamura T. Generation of canine induced pluripotent stem cells by retroviral transduction and chemical inhibitors. Mol Reprod Dev 2009;77:2.

[72] Wu Y, Zhang Y, Mishra A, Tardif SD, Hornsby PJ. Generation of induced pluripotent stem cells from newborn marmoset skin fibroblasts. Stem Cell Res 2010;4:180-188.

[73] Bao L, He L, Chen J, Wu Z, Liao J, Rao L, *et al.* Reprogramming of ovine adult fibroblasts to pluripotency via drug-inducible expression of defined factors. Cell Res 2011;21:600-608.

[74] Lu Y, West FD, Jordan BJ, Mumaw JL, Jordan ET, Gallegos-Cardenas A, *et al.* Avian-induced pluripotent stem cells derived using human reprogramming factors. Stem Cells Dev 2011;21:394-403.

[75] Stadtfeld M, Brennand K, Hochedlinger K. Reprogramming of pancreatic beta cells into induced pluripotent stem cells. Curr Biol 2008;18:890-894.

[76] Eminli S, Utikal J, Arnold K, Jaenisch R, Hochedlinger K. Reprogramming of neural progenitor cells into induced pluripotent stem cells in the absence of exogenous Sox2 expression. Stem Cells 2008;26:2467-2474.

[77] Kim JB, Zaehres H, Wu G, Gentile L, Ko K, Sebastiano V, *et al.* Pluripotent stem cells induced from adult neural stem cells by reprogramming with two factors. Nature 2008;454:646-650.

[78] Kim J, Lengner CJ, Kirak O, Hanna J, Cassady JP, Lodato MA, *et al.* Reprogramming of postnatal neurons into induced pluripotent stem cells by defined factors. Stem Cells 2011;29:992-1000.

[79] Hanna J, Markoulaki S, Schorderet P, Carey BW, Beard C, Wernig M, *et al.* Direct reprogramming of terminally differentiated mature B lymphocytes to pluripotency. Cell 2008;133:250-264.

[80] Maherali N, Ahfeldt T, Rigamonti A, Utikal J, Cowan C, Hochedlinger K. A high-efficiency system for the generation and study of human induced pluripotent stem cells. Cell Stem Cell 2008;3:340-345.

[81] Aoi T, Yae K, Nakagawa M, Ichisaka T, Okita K, Takahashi K, *et al.* Generation of pluripotent stem cells from adult mouse liver and stomach cells. Science 2008;321:699-702.

[82] Li C, Zhou J, Shi G, Ma Y, Yang Y, Gu J, *et al.* Pluripotency can be rapidly and efficiently induced in human amniotic fluid-derived cells. Hum Mol Genet 2009;18:4340-4349.

[83] Loh YH, Agarwal S, Park IH, Urbach A, Huo H, Heffner GC, *et al.* Generation of induced pluripotent stem cells from human blood. Blood 2009;113:5476-5479.

[84] Ye Z, Zhan H, Mali P, Dowey S, Williams DM, Jang YY, *et al.* Human-induced pluripotent stem cells from blood cells of healthy donors and patients with acquired blood disorders. Blood 2009;114:5473-5480.

[85] Haase A, Olmer R, Schwanke K, Wunderlich S, Merkert S, Hess C, *et al.* Generation of induced pluripotent stem cells from human cord blood. Cell Stem Cell 2009;5:434-441.

[86] Giorgetti A, Montserrat N, Aasen T, Gonzalez F, Rodriguez-Piza I, Vassena R, *et al.* Generation of induced pluripotent stem cells from human cord blood using OCT4 and SOX2. Cell Stem Cell 2009;5:353-357.

[87] Utikal J, Maherali N, Kulalert W, Hochedlinger K. Sox2 is dispensable for the reprogramming of melanocytes and melanoma cells into induced pluripotent stem cells. J Cell Sci 2009;122:3502-3510.

[88] Ohta S, Imaizumi Y, Okada Y, Akamatsu W, Kuwahara R, Ohyama M, *et al.* Generation of human melanocytes from induced pluripotent stem cells. PLoS One 2011;6:e16182.

[89] Sun N, Panetta NJ, Gupta DM, Wilson KD, Lee A, Jia F, *et al.* Feeder-free derivation of induced pluripotent stem cells from adult human adipose stem cells. Proc Natl Acad Sci U S A 2009;106:15720-15725.

[90] Tat PA, Sumer H, Jones KL, Upton K, Verma PJ. The efficient generation of induced pluripotent stem (iPS) cells from adult mouse adipose tissue-derived and neural stem cells. Cell Transplant 2010;19:525-536.

[91] Liu H, Ye Z, Kim Y, Sharkis S, Jang YY. Generation of endoderm-derived human induced pluripotent stem cells from primary hepatocytes. Hepatology 2010;51:1810-1819.

[92] Yan X, Qin H, Qu C, Tuan RS, Shi S, Huang GT. iPS cells reprogrammed from human mesenchymal-like stem/progenitor cells of dental tissue origin. Stem Cells Dev 2009;19:469-480.

[93] Nakagawa M, Koyanagi M, Tanabe K, Takahashi K, Ichisaka T, Aoi T, *et al.* Generation of induced pluripotent stem cells without Myc from mouse and human fibroblasts. Nat Biotechnol 2008;26:101-106.

[94] Huangfu D, Osafune K, Maehr R, Guo W, Eijkelenboom A, Chen S, *et al.* Induction of pluripotent stem cells from primary human fibroblasts with only Oct4 and Sox2. Nat Biotechnol 2008;26:1269-1275.

[95] Tsai SY, Clavel C, Kim S, Ang YS, Grisanti L, Lee DF, *et al.* Oct4 and klf4 reprogram dermal papilla cells into induced pluripotent stem cells. Stem Cells 2009;28:221-228.

[96] Zhao HX, Li Y, Jin HF, Xie L, Liu C, Jiang F, *et al.* Rapid and efficient reprogramming of human amnion-derived cells into pluripotency by three factors OCT4/SOX2/NANOG. Differentiation 2010;80:123-129.

[97] Stadtfeld M, Nagaya M, Utikal J, Weir G, Hochedlinger K. Induced pluripotent stem cells generated without viral integration. Science 2008;322:945-949.

[98] Sommer CA, Stadtfeld M, Murphy GJ, Hochedlinger K, Kotton DN, Mostoslavsky G. Induced pluripotent stem cell generation using a single lentiviral stem cell cassette. Stem Cells 2009;27:543-549.

[99] Woltjen K, Michael IP, Mohseni P, Desai R, Mileikovsky M, Hamalainen R, *et al.* piggyBac transposition reprograms fibroblasts to induced pluripotent stem cells. Nature 2009;458:766-770.

[100] Kaji K, Norrby K, Paca A, Mileikovsky M, Mohseni P, Woltjen K. Virus-free induction of pluripotency and subsequent excision of reprogramming factors. Nature 2009;458:771-775.

[101] Somers A, Jean JC, Sommer CA, Omari A, Ford CC, Mills JA, *et al.* Generation of transgene-free lung disease-specific human induced pluripotent stem cells using a single excisable lentiviral stem cell cassette. Stem Cells 2010;28:1728-1740.

[102] Zhou W, Freed CR. Adenoviral gene delivery can reprogram human fibroblasts to induced pluripotent stem cells. Stem Cells 2009;27:2667-2674.

[103] Okita K, Nakagawa M, Hyenjong H, Ichisaka T, Yamanaka S. Generation of mouse induced pluripotent stem cells without viral vectors. Science 2008;322:949-953.

[104] Fusaki N, Ban H, Nishiyama A, Saeki K, Hasegawa M. Efficient induction of transgene-free human pluripotent stem cells using a vector based on Sendai virus, an RNA virus that does not integrate into the host genome. Proc Jpn Acad Ser B Phys Biol Sci 2009;85:348-362.

[105] Yu J, Hu K, Smuga-Otto K, Tian S, Stewart R, Slukvin, II, *et al.* Human induced pluripotent stem cells free of vector and transgene sequences. Science 2009;324:797-801.

[106] Kim D, Kim CH, Moon JI, Chung YG, Chang MY, Han BS, *et al.* Generation of human induced pluripotent stem cells by direct delivery of reprogramming proteins. Cell Stem Cell 2009;4:472-476.

[107] Zhou H, Wu S, Joo JY, Zhu S, Han DW, Lin T, *et al.* Generation of induced pluripotent stem cells using recombinant proteins. Cell Stem Cell 2009;4:381-384.

[108] Cho HJ, Lee CS, Kwon YW, Paek JS, Lee SH, Hur J, *et al.* Induction of pluripotent stem cells from adult somatic cells by protein-based reprogramming without genetic manipulation. Blood 2010;116:386-395.

[109] Warren L, Manos PD, Ahfeldt T, Loh YH, Li H, Lau F, *et al.* Highly efficient reprogramming to pluripotency and directed differentiation of human cells with synthetic modified mRNA. Cell Stem Cell 2010;7:618-630.

[110] Miyoshi N, Ishii H, Nagano H, Haraguchi N, Dewi DL, Kano Y, *et al.* Reprogramming of mouse and human cells to pluripotency using mature microRNAs. Cell Stem Cell 2011;8:633-638.

[111] Anokye-Danso F, Trivedi CM, Juhr D, Gupta M, Cui Z, Tian Y, *et al.* Highly efficient miRNA-mediated reprogramming of mouse and human somatic cells to pluripotency. Cell Stem Cell 2011;8:376-388.

[112] Silva J, Barrandon O, Nichols J, Kawaguchi J, Theunissen TW, Smith A. Promotion of reprogramming to ground state pluripotency by signal inhibition. PLoS Biol 2008;6:e253.

[113] Kim JB, Greber B, Arauzo-Bravo MJ, Meyer J, Park KI, Zaehres H, *et al.* Direct reprogramming of human neural stem cells by OCT4. Nature 2009;461:649-643.

[114] Okita K, Matsumura Y, Sato Y, Okada A, Morizane A, Okamoto S, *et al.* A more efficient method to generate integration-free human iPS cells. Nat Methods 2011;8:409-412.

[115] Si-Tayeb K, Noto FK, Nagaoka M, Li J, Battle MA, Duris C, *et al.* Highly efficient generation of human hepatocyte-like cells from induced pluripotent stem cells. Hepatology 2009;51:297-305.

[116] Mali P, Ye Z, Hommond HH, Yu X, Lin J, Chen G, *et al.* Improved efficiency and pace of generating induced pluripotent stem cells from human adult and fetal fibroblasts. Stem Cells 2008;26:1998-2005.

[117] Bodnar AG, Ouellette M, Frolkis M, Holt SE, Chiu CP, Morin GB, *et al.* Extension of life-span by introduction of telomerase into normal human cells. Science 1998;279:349-352.

[118] Hahn WC, Counter CM, Lundberg AS, Beijersbergen RL, Brooks MW, Weinberg RA. Creation of human tumour cells with defined genetic elements. Nature 1999;400:464-468.

[119] Zhao Y, Yin X, Qin H, Zhu F, Liu H, Yang W, *et al.* Two supporting factors greatly improve the efficiency of human iPSC generation. Cell Stem Cell 2008;3:475-479.

[120] Nishimoto M, Fukushima A, Okuda A, Muramatsu M. The gene for the embryonic stem cell coactivator UTF1 carries a regulatory element which selectively interacts with a complex composed of Oct-3/4 and Sox-2. Mol Cell Biol 1999;19:5453-5465.

[121] Zhang X, Zhang J, Wang T, Esteban MA, Pei D. Esrrb activates Oct4 transcription and sustains self-renewal and pluripotency in embryonic stem cells. J Biol Chem 2008;283:35825-35833.

[122] van den Berg DL, Zhang W, Yates A, Engelen E, Takacs K, Bezstarosti K, *et al.* Estrogen-related receptor beta interacts with Oct4 to positively regulate Nanog gene expression. Mol Cell Biol 2008;28:5986-5995.

[123] Feng B, Jiang J, Kraus P, Ng JH, Heng JC, Chan YS, *et al.* Reprogramming of fibroblasts into induced pluripotent stem cells with orphan nuclear receptor Esrrb. Nat Cell Biol 2009;11:197-203.

[124] Marson A, Foreman R, Chevalier B, Bilodeau S, Kahn M, Young RA, *et al.* Wnt signaling promotes reprogramming of somatic cells to pluripotency. Cell Stem Cell 2008;3:132-135.

[125] Sato N, Meijer L, Skaltsounis L, Greengard P, Brivanlou AH. Maintenance of pluripotency in human and mouse embryonic stem cells through activation of Wnt signaling by a pharmacological GSK-3-specific inhibitor. Nat Med 2004;10:55-63.

[126] Cai L, Ye Z, Zhou BY, Mali P, Zhou C, Cheng L. Promoting human embryonic stem cell renewal or differentiation by modulating Wnt signal and culture conditions. Cell Res 2007;17:62-72.

[127] Cole MF, Johnstone SE, Newman JJ, Kagey MH, Young RA. Tcf3 is an integral component of the core regulatory circuitry of embryonic stem cells. Genes Dev 2008;22:746-755.

[128] Chen J, Liu J, Yang J, Chen Y, Ni S, Song H, *et al.* BMPs functionally replace Klf4 and support efficient reprogramming of mouse fibroblasts by Oct4 alone. Cell Res 2010;21:205-212.

[129] Mikkelsen TS, Hanna J, Zhang X, Ku M, Wernig M, Schorderet P, *et al.* Dissecting direct reprogramming through integrative genomic analysis. Nature 2008;454:49-55.

[130] Huangfu D, Maehr R, Guo W, Eijkelenboom A, Snitow M, Chen AE, *et al.* Induction of pluripotent stem cells by defined factors is greatly improved by small-molecule compounds. Nat Biotechnol 2008;26:795-797.

[131] Shi Y, Desponts C, Do JT, Hahm HS, Scholer HR, Ding S. Induction of pluripotent stem cells from mouse embryonic fibroblasts by Oct4 and Klf4 with small-molecule compounds. Cell Stem Cell 2008;3:568-574.

[132] Shi Y, Do JT, Desponts C, Hahm HS, Scholer HR, Ding S. A combined chemical and genetic approach for the generation of induced pluripotent stem cells. Cell Stem Cell 2008;2:525-528.

[133] Feldman N, Gerson A, Fang J, Li E, Zhang Y, Shinkai Y, *et al.* G9a-mediated irreversible epigenetic inactivation of Oct-3/4 during early embryogenesis. Nat Cell Biol 2006;8:188-194.

[134] Zhu S, Li W, Zhou H, Wei W, Ambasudhan R, Lin T, *et al.* Reprogramming of human primary somatic cells by OCT4 and chemical compounds. Cell Stem Cell 2010;7:651-655.

[135] Yoshida Y, Takahashi K, Okita K, Ichisaka T, Yamanaka S. Hypoxia enhances the generation of induced pluripotent stem cells. Cell Stem Cell 2009;5:237-241.

[136] Esteban MA, Wang T, Qin B, Yang J, Qin D, Cai J, *et al.* Vitamin C enhances the generation of mouse and human induced pluripotent stem cells. Cell Stem Cell 2009;6:71-79.

[137] Judson RL, Babiarz JE, Venere M, Blelloch R. Embryonic stem cell-specific microRNAs promote induced pluripotency. Nat Biotechnol 2009;27:459-461.

[138] Doi A, Park IH, Wen B, Murakami P, Aryee MJ, Irizarry R, *et al.* Differential methylation of tissue- and cancer-specific CpG island shores distinguishes human induced pluripotent stem cells, embryonic stem cells and fibroblasts. Nat Genet 2009;41:1350-1353.

[139] Lister R, Pelizzola M, Kida YS, Hawkins RD, Nery JR, Hon G, *et al.* Hotspots of aberrant epigenomic reprogramming in human induced pluripotent stem cells. Nature 2011;471:68-73.

[140] Wilson KD, Venkatasubrahmanyam S, Jia F, Sun N, Butte AJ, Wu JC. MicroRNA profiling of human-induced pluripotent stem cells. Stem Cells Dev 2009;18:749-758.

[141] Marchetto MC, Yeo GW, Kainohana O, Marsala M, Gage FH, Muotri AR. Transcriptional signature and memory retention of human-induced pluripotent stem cells. PLoS One 2009;4:e7076.

[142] Ghosh Z, Wilson KD, Wu Y, Hu S, Quertermous T, Wu JC. Persistent donor cell gene expression among human induced pluripotent stem cells contributes to differences with human embryonic stem cells. PLoS One 2010;5:e8975.

[143] Newman AM, Cooper JB. Lab-specific gene expression signatures in pluripotent stem cells. Cell Stem Cell 2010;7:258-262.

[144] Chin MH, Pellegrini M, Plath K, Lowry WE. Molecular analyses of human induced pluripotent stem cells and embryonic stem cells. Cell Stem Cell 2010;7:263-269.

[145] Zhao T, Zhang ZN, Rong Z, Xu Y. Immunogenicity of induced pluripotent stem cells. Nature 2011;474:212-215.

[146] Araki R, Uda M, Hoki Y, Sunayama M, Nakamura M, Ando S, *et al.* Negligible immunogenicity of terminally differentiated cells derived from induced pluripotent or embryonic stem cells. Nature 2013;494:100-104.

[147] Narazaki G, Uosaki H, Teranishi M, Okita K, Kim B, Matsuoka S, *et al.* Directed and systematic differentiation of cardiovascular cells from mouse induced pluripotent stem cells. Circulation 2008;118:498-506.

[148] Schenke-Layland K, Rhodes KE, Angelis E, Butylkova Y, Heydarkhan-Hagvall S, Gekas C, *et al.* Reprogrammed mouse fibroblasts differentiate into cells of the cardiovascular and hematopoietic lineages. Stem Cells 2008;26:1537-1546.

[149] Choi KD, Yu J, Smuga-Otto K, Salvagiotto G, Rehrauer W, Vodyanik M, *et al.* Hematopoietic and endothelial differentiation of human induced pluripotent stem cells. Stem Cells 2009;27:559-567.

[150] Tashiro K, Inamura M, Kawabata K, Sakurai F, Yamanishi K, Hayakawa T, *et al.* Efficient adipocyte and osteoblast differentiation from mouse induced pluripotent stem cells by adenoviral transduction. Stem Cells 2009;27:1802-1811.

[151] Senju S, Haruta M, Matsunaga Y, Fukushima S, Ikeda T, Takahashi K, *et al.* Characterization of dendritic cells and macrophages generated by directed differentiation from mouse induced pluripotent stem cells. Stem Cells 2009;27:1021-1031.

[152] Song Z, Cai J, Liu Y, Zhao D, Yong J, Duo S, *et al.* Efficient generation of hepatocyte-like cells from human induced pluripotent stem cells. Cell Res 2009;19:1233-1242.

[153] Buchholz DE, Hikita ST, Rowland TJ, Friedrich AM, Hinman CR, Johnson LV, *et al.* Derivation of functional retinal pigmented epithelium from induced pluripotent stem cells. Stem Cells 2009;27:2427-2434.

[154] Karumbayaram S, Novitch BG, Patterson M, Umbach JA, Richter L, Lindgren A, *et al.* Directed differentiation of human-induced pluripotent stem cells generates active motor neurons. Stem Cells 2009;27:806-811.

[155] Kobayashi T, Yamaguchi T, Hamanaka S, Kato-Itoh M, Yamazaki Y, Ibata M, *et al.* Generation of rat pancreas in mouse by interspecific blastocyst injection of pluripotent stem cells. Cell 2010;142:787-799.

[156] Nelson TJ, Martinez-Fernandez A, Yamada S, Perez-Terzic C, Ikeda Y, Terzic A. Repair of acute myocardial infarction by human stemness factors induced pluripotent stem cells. Circulation 2009;120:408-416.

[157] Polo JM, Liu S, Figueroa ME, Kulalert W, Eminli S, Tan KY, *et al.* Cell type of origin influences the molecular and functional properties of mouse induced pluripotent stem cells. Nat Biotechnol 2010;28:848-855.

[158] Kim K, Doi A, Wen B, Ng K, Zhao R, Cahan P, *et al.* Epigenetic memory in induced pluripotent stem cells. Nature 2010;467:285-290.

[159] Hu Q, Friedrich AM, Johnson LV, Clegg DO. Memory in induced pluripotent stem cells: reprogrammed human retinal-pigmented epithelial cells show tendency for spontaneous redifferentiation. Stem Cells 2010;28:1981-1991.

[160] Bar-Nur O, Russ HA, Efrat S, Benvenisty N. Epigenetic memory and preferential lineage-specific differentiation in induced pluripotent stem cells derived from human pancreatic islet beta cells. Cell Stem Cell 2011;9:17-23.

[161] Lohle M, Hermann A, Glass H, Kempe A, Schwarz SC, Kim JB, *et al.* Differentiation efficiency of induced pluripotent stem cells depends on the number of reprogramming factors. Stem Cells 2012;30:570-579.

[162] Martinez-Fernandez A, Nelson TJ, Ikeda Y, Terzic A. c-MYC independent nuclear reprogramming favors cardiogenic potential of induced pluripotent stem cells. J Cardiovasc Transl Res 2010;3:13-23.

[163] Mummery CL, Zhang J, Ng ES, Elliott DA, Elefanty AG, Kamp TJ. Differentiation of human embryonic stem cells and induced pluripotent stem cells to cardiomyocytes: a methods overview. Circ Res 2012;111:344-358.

[164] Zwi L, Caspi O, Arbel G, Huber I, Gepstein A, Park IH, *et al.* Cardiomyocyte differentiation of human induced pluripotent stem cells. Circulation 2009;120:1513-1523.

[165] Montserrat N, Bahima EG, Batlle L, Hafner S, Rodrigues AM, Gonzalez F, *et al.* Generation of pig iPS cells: a model for cell therapy. J Cardiovasc Transl Res 2010;4:121-130.

[166] Mauritz C, Schwanke K, Reppel M, Neef S, Katsirntaki K, Maier LS, *et al.* Generation of functional murine cardiac myocytes from induced pluripotent stem cells. Circulation 2008;118:507-517.

[167] Zhang J, Wilson GF, Soerens AG, Koonce CH, Yu J, Palecek SP, *et al.* Functional cardiomyocytes derived from human induced pluripotent stem cells. Circ Res 2009;104:e30-41.

[168] Carpenter L, Carr C, Yang CT, Stuckey DJ, Clarke K, Watt SM. Efficient differentiation of human induced pluripotent stem cells generates cardiac cells that provide protection following myocardial infarction in the rat. Stem Cells Dev 2011;21:977-986.

[169] Kang NY, Yun SW, Ha HH, Park SJ, Chang YT. Embryonic and induced pluripotent stem cell staining and sorting with the live-cell fluorescence imaging probe CDy1. Nat Protoc 2011;6:1044-1052.

[170] Hattori F, Chen H, Yamashita H, Tohyama S, Satoh YS, Yuasa S, *et al.* Nongenetic method for purifying stem cell-derived cardiomyocytes. Nat Methods 2009;7:61-66.

[171] Van Hoof D, Dormeyer W, Braam SR, Passier R, Monshouwer-Kloots J, Ward-van Oostwaard D, *et al.* Identification of cell surface proteins for antibody-based selection of human embryonic stem cell-derived cardiomyocytes. J Proteome Res 2010;9:1610-1618.

[172] Dubois NC, Craft AM, Sharma P, Elliott DA, Stanley EG, Elefanty AG, *et al.* SIRPA is a specific cell-surface marker for isolating cardiomyocytes derived from human pluripotent stem cells. Nat Biotechnol 2011;29:1011-1018.

[173] Uosaki H, Fukushima H, Takeuchi A, Matsuoka S, Nakatsuji N, Yamanaka S, *et al.* Efficient and scalable purification of cardiomyocytes from human embryonic and induced pluripotent stem cells by VCAM1 surface expression. PLoS One 2011;6:e23657.

[174] Xi J, Khalil M, Shishechian N, Hannes T, Pfannkuche K, Liang H, *et al.* Comparison of contractile behavior of native murine ventricular tissue and cardiomyocytes derived from embryonic or induced pluripotent stem cells. FASEB J 2010;24:2739-2751.

[175] Kaichi S, Hasegawa K, Takaya T, Yokoo N, Mima T, Kawamura T, *et al.* Cell line-dependent differentiation of induced pluripotent stem cells into cardiomyocytes in mice. Cardiovasc Res 2010;88:314-323.

[176] Moretti A, Bellin M, Jung CB, Thies TM, Takashima Y, Bernshausen A, *et al.* Mouse and human induced pluripotent stem cells as a source for multipotent Isl1+ cardiovascular progenitors. FASEB J 2009;24:700-711.

[177] Mauritz C, Martens A, Rojas SV, Schnick T, Rathert C, Schecker N, *et al.* Induced pluripotent stem cell (iPSC)-derived Flk-1 progenitor cells engraft, differentiate, and improve heart function in a mouse model of acute myocardial infarction. Eur Heart J 2011;32:2634-2641.

[178] Burridge PW, Keller G, Gold JD, Wu JC. Production of de novo cardiomyocytes: human pluripotent stem cell differentiation and direct reprogramming. Cell Stem Cell 2012;10:16-28.

[179] Mummery C, Ward-van Oostwaard D, Doevendans P, Spijker R, van den Brink S, Hassink R, *et al.* Differentiation of human embryonic stem cells to cardiomyocytes: role of coculture with visceral endoderm-like cells. Circulation 2003;107:2733-2740.

[180] Burridge PW, Anderson D, Priddle H, Barbadillo Munoz MD, Chamberlain S, Allegrucci C, *et al.* Improved human embryonic stem cell embryoid body homogeneity and cardiomyocyte differentiation from a novel V-96 plate aggregation system highlights interline variability. Stem Cells 2007;25:929-938.

[181] Burridge PW, Thompson S, Millrod MA, Weinberg S, Yuan X, Peters A, *et al.* A universal system for highly efficient cardiac differentiation of human induced pluripotent stem cells that eliminates interline variability. PLoS One 2011;6:e18293.

[182] Elliott DA, Braam SR, Koutsis K, Ng ES, Jenny R, Lagerqvist EL, *et al.* NKX2-5(eGFP/w) hESCs for isolation of human cardiac progenitors and cardiomyocytes. Nat Methods 2011;8:1037-1040.

[183] Zhang J, Klos M, Wilson GF, Herman AM, Lian X, Raval KK, *et al.* Extracellular matrix promotes highly efficient cardiac differentiation of human pluripotent stem cells: the matrix sandwich method. Circ Res 2012;111:1125-1136.

[184] Blin G, Nury D, Stefanovic S, Neri T, Guillevic O, Brinon B, *et al.* A purified population of multipotent cardiovascular progenitors derived from primate pluripotent stem cells engrafts in postmyocardial infarcted nonhuman primates. J Clin Invest 2010;120:1125-1139.

[185] Chan SS, Li HJ, Hsueh YC, Lee DS, Chen JH, Hwang SM*, et al.* Fibroblast growth factor-10 promotes cardiomyocyte differentiation from embryonic and induced pluripotent stem cells. PLoS One 2011;5:e14414.

[186] Yuasa S, Itabashi Y, Koshimizu U, Tanaka T, Sugimura K, Kinoshita M*, et al.* Transient inhibition of BMP signaling by Noggin induces cardiomyocyte differentiation of mouse embryonic stem cells. Nat Biotechnol 2005;23:607-611.

[187] Gessert S, Kuhl M. The multiple phases and faces of wnt signaling during cardiac differentiation and development. Circ Res 2010;107:186-199.

[188] Tran TH, Wang X, Browne C, Zhang Y, Schinke M, Izumo S*, et al.* Wnt3a-induced mesoderm formation and cardiomyogenesis in human embryonic stem cells. Stem Cells 2009;27:1869-1878.

[189] Lian X, Hsiao C, Wilson G, Zhu K, Hazeltine LB, Azarin SM*, et al.* Robust cardiomyocyte differentiation from human pluripotent stem cells via temporal modulation of canonical Wnt signaling. Proc Natl Acad Sci U S A 2012;109:E1848-1857.

[190] Yang L, Soonpaa MH, Adler ED, Roepke TK, Kattman SJ, Kennedy M*, et al.* Human cardiovascular progenitor cells develop from a KDR+ embryonic-stem-cell-derived population. Nature 2008;453:524-528.

[191] Hudson J, Titmarsh D, Hidalgo A, Wolvetang E, Cooper-White J. Primitive cardiac cells from human embryonic stem cells. Stem Cells Dev 2011;21:1513-1523.

[192] Willems E, Spiering S, Davidovics H, Lanier M, Xia Z, Dawson M*, et al.* Small-molecule inhibitors of the Wnt pathway potently promote cardiomyocytes from human embryonic stem cell-derived mesoderm. Circ Res 2011;109:360-364.

[193] Ren Y, Lee MY, Schliffke S, Paavola J, Amos PJ, Ge X*, et al.* Small molecule Wnt inhibitors enhance the efficiency of BMP-4-directed cardiac differentiation of human pluripotent stem cells. J Mol Cell Cardiol 2011;51:280-287.

[194] Kattman SJ, Witty AD, Gagliardi M, Dubois NC, Niapour M, Hotta A*, et al.* Stage-specific optimization of activin/nodal and BMP signaling promotes cardiac differentiation of mouse and human pluripotent stem cell lines. Cell Stem Cell 2011;8:228-240.

[195] Kitamura R, Takahashi T, Nakajima N, Isodono K, Asada S, Ueno H*, et al.* Stage-specific role of endogenous Smad2 activation in cardiomyogenesis of embryonic stem cells. Circ Res 2007;101:78-87.

[196] Willems E, Cabral-Teixeira J, Schade D, Cai W, Reeves P, Bushway PJ*, et al.* Small molecule-mediated TGF-beta type II receptor degradation promotes cardiomyogenesis in embryonic stem cells. Cell Stem Cell 2012;11:242-252.

[197] Nemir M, Croquelois A, Pedrazzini T, Radtke F. Induction of cardiogenesis in embryonic stem cells via downregulation of Notch1 signaling. Circ Res 2006;98:1471-1478.

[198] Kwon C, Cordes KR, Srivastava D. Wnt/beta-catenin signaling acts at multiple developmental stages to promote mammalian cardiogenesis. Cell Cycle 2008;7:3815-3818.

[199] Jang J, Ku SY, Kim JE, Choi K, Kim YY, Kim HS*, et al.* Notch inhibition promotes human embryonic stem cell-derived cardiac mesoderm differentiation. Stem Cells 2008;26:2782-2790.

[200] Wang Z, Xu G, Wu Y, Guan Y, Cui L, Lei X, *et al.* Neuregulin-1 enhances differentiation of cardiomyocytes from embryonic stem cells. Med Biol Eng Comput 2009;47:41-48.

[201] Zhu WZ, Xie Y, Moyes KW, Gold JD, Askari B, Laflamme MA. Neuregulin/ErbB signaling regulates cardiac subtype specification in differentiating human embryonic stem cells. Circ Res 2010;107:776-786.

[202] Hao J, Daleo MA, Murphy CK, Yu PB, Ho JN, Hu J, *et al.* Dorsomorphin, a selective small molecule inhibitor of BMP signaling, promotes cardiomyogenesis in embryonic stem cells. PLoS One 2008;3:e2904.

[203] Takahashi T, Lord B, Schulze PC, Fryer RM, Sarang SS, Gullans SR, *et al.* Ascorbic acid enhances differentiation of embryonic stem cells into cardiac myocytes. Circulation 2003;107:1912-1916.

[204] Cao N, Liu Z, Chen Z, Wang J, Chen T, Zhao X, *et al.* Ascorbic acid enhances the cardiac differentiation of induced pluripotent stem cells through promoting the proliferation of cardiac progenitor cells. Cell Res 2011;22:219-236.

[205] Xu C, Police S, Rao N, Carpenter MK. Characterization and enrichment of cardiomyocytes derived from human embryonic stem cells. Circ Res 2002;91:501-508.

[206] Shimoji K, Yuasa S, Onizuka T, Hattori F, Tanaka T, Hara M, *et al.* G-CSF promotes the proliferation of developing cardiomyocytes in vivo and in derivation from ESCs and iPSCs. Cell Stem Cell 2010;6:227-237.

[207] Fujiwara M, Yan P, Otsuji TG, Narazaki G, Uosaki H, Fukushima H, *et al.* Induction and enhancement of cardiac cell differentiation from mouse and human induced pluripotent stem cells with cyclosporin-A. PLoS One 2011;6:e16734.

[208] Odiete O, Hill MF, Sawyer DB. Neuregulin in cardiovascular development and disease. Circ Res 2012;111:1376-1385.

[209] Lemmens K, Doggen K, De Keulenaer GW. Role of neuregulin-1/ErbB signaling in cardiovascular physiology and disease: implications for therapy of heart failure. Circulation 2007;116:954-960.

[210] Meyer D, Yamaai T, Garratt A, Riethmacher-Sonnenberg E, Kane D, Theill LE, *et al.* Isoform-specific expression and function of neuregulin. Development 1997;124:3575-3586.

[211] Falls DL. Neuregulins: functions, forms, and signaling strategies. Exp Cell Res 2003;284:14-30.

[212] Cote GM, Miller TA, Lebrasseur NK, Kuramochi Y, Sawyer DB. Neuregulin-1alpha and beta isoform expression in cardiac microvascular endothelial cells and function in cardiac myocytes in vitro. Exp Cell Res 2005;311:135-146.

[213] Gassmann M, Casagranda F, Orioli D, Simon H, Lai C, Klein R, *et al.* Aberrant neural and cardiac development in mice lacking the ErbB4 neuregulin receptor. Nature 1995;378:390-394.

[214] Lee KF, Simon H, Chen H, Bates B, Hung MC, Hauser C. Requirement for neuregulin receptor erbB2 in neural and cardiac development. Nature 1995;378:394-398.

[215] Meyer D, Birchmeier C. Multiple essential functions of neuregulin in development. Nature 1995;378:386-390.

[216] Zhao YY, Sawyer DR, Baliga RR, Opel DJ, Han X, Marchionni MA*, et al.* Neuregulins promote survival and growth of cardiac myocytes. Persistence of ErbB2 and ErbB4 expression in neonatal and adult ventricular myocytes. J Biol Chem 1998;273:10261-10269.

[217] Kuramochi Y, Cote GM, Guo X, Lebrasseur NK, Cui L, Liao R*, et al.* Cardiac endothelial cells regulate reactive oxygen species-induced cardiomyocyte apoptosis through neuregulin-1beta/erbB4 signaling. J Biol Chem 2004;279:51141-51147.

[218] Fukazawa R, Miller TA, Kuramochi Y, Frantz S, Kim YD, Marchionni MA*, et al.* Neuregulin-1 protects ventricular myocytes from anthracycline-induced apoptosis via erbB4-dependent activation of PI3-kinase/Akt. J Mol Cell Cardiol 2003;35:1473-1479.

[219] Okoshi K, Nakayama M, Yan X, Okoshi MP, Schuldt AJ, Marchionni MA*, et al.* Neuregulins regulate cardiac parasympathetic activity: muscarinic modulation of beta-adrenergic activity in myocytes from mice with neuregulin-1 gene deletion. Circulation 2004;110:713-717.

[220] Seguchi O, Takashima S, Yamazaki S, Asakura M, Asano Y, Shintani Y*, et al.* A cardiac myosin light chain kinase regulates sarcomere assembly in the vertebrate heart. J Clin Invest 2007;117:2812-2824.

[221] Xu Y, Li X, Liu X, Zhou M. Neuregulin-1/ErbB signaling and chronic heart failure. Adv Pharmacol 2010;59:31-51.

[222] Lemmens K, Fransen P, Sys SU, Brutsaert DL, De Keulenaer GW. Neuregulin-1 induces a negative inotropic effect in cardiac muscle: role of nitric oxide synthase. Circulation 2004;109:324-326.

[223] Iivanainen E, Paatero I, Heikkinen SM, Junttila TT, Cao R, Klint P*, et al.* Intra- and extracellular signaling by endothelial neuregulin-1. Exp Cell Res 2007;313:2896-2909.

[224] Xu G, Watanabe T, Iso Y, Koba S, Sakai T, Nagashima M*, et al.* Preventive effects of heregulin-beta1 on macrophage foam cell formation and atherosclerosis. Circ Res 2009;105:500-510.

[225] Rentschler S, Zander J, Meyers K, France D, Levine R, Porter G*, et al.* Neuregulin-1 promotes formation of the murine cardiac conduction system. Proc Natl Acad Sci U S A 2002;99:10464-10469.

[226] Liu X, Gu X, Li Z, Li X, Li H, Chang J*, et al.* Neuregulin-1/erbB-activation improves cardiac function and survival in models of ischemic, dilated, and viral cardiomyopathy. J Am Coll Cardiol 2006;48:1438-1447.

[227] Li J, Gu XH, Duan JC, Zeng L, Li Y, Wang L. [Effects of recombined human neuregulin on the contractibility of cardiac muscles of rhesus monkeys with pacing-induced heart failure]. Sichuan Da Xue Xue Bao Yi Xue Ban 2007;38:105-108.

[228] Bersell K, Arab S, Haring B, Kuhn B. Neuregulin1/ErbB4 signaling induces cardiomyocyte proliferation and repair of heart injury. Cell 2009;138:257-270.

[229] Gu X, Liu X, Xu D, Li X, Yan M, Qi Y*, et al.* Cardiac functional improvement in rats with myocardial infarction by up-regulating cardiac myosin light chain kinase with neuregulin. Cardiovasc Res 2010;88:334-343.

[230] Guo YF, Zhang XX, Liu Y, Duan HY, Jie BZ, Wu XS. Neuregulin-1 attenuates mitochondrial dysfunction in a rat model of heart failure. Chin Med J (Engl) 2012;125:807-814.

[231] Hedhli N, Huang Q, Kalinowski A, Palmeri M, Hu X, Russell RR, *et al.* Endothelium-derived neuregulin protects the heart against ischemic injury. Circulation 2011;123:2254-2262.

[232] Gao R, Zhang J, Cheng L, Wu X, Dong W, Yang X, *et al.* A Phase II, randomized, double-blind, multicenter, based on standard therapy, placebo-controlled study of the efficacy and safety of recombinant human neuregulin-1 in patients with chronic heart failure. J Am Coll Cardiol 2010;55:1907-1914.

[233] Jabbour A, Hayward CS, Keogh AM, Kotlyar E, McCrohon JA, England JF, *et al.* Parenteral administration of recombinant human neuregulin-1 to patients with stable chronic heart failure produces favourable acute and chronic haemodynamic responses. Eur J Heart Fail 2010;13:83-92.

[234] Efe JA, Hilcove S, Kim J, Zhou H, Ouyang K, Wang G, *et al.* Conversion of mouse fibroblasts into cardiomyocytes using a direct reprogramming strategy. Nat Cell Biol 2011;13:215-222.

[235] Kim J, Efe JA, Zhu S, Talantova M, Yuan X, Wang S, *et al.* Direct reprogramming of mouse fibroblasts to neural progenitors. Proc Natl Acad Sci U S A 2011;108:7838-7843.

[236] Matsui T, Takano M, Yoshida K, Ono S, Fujisaki C, Matsuzaki Y, *et al.* Neural stem cells directly differentiated from partially reprogrammed fibroblasts rapidly acquire gliogenic competency. Stem Cells 2012;30:1109-1119.

[237] Davis RL, Weintraub H, Lassar AB. Expression of a single transfected cDNA converts fibroblasts to myoblasts. Cell 1987;51:987-1000.

[238] Xie H, Ye M, Feng R, Graf T. Stepwise reprogramming of B cells into macrophages. Cell 2004;117:663-676.

[239] Laiosa CV, Stadtfeld M, Xie H, de Andres-Aguayo L, Graf T. Reprogramming of committed T cell progenitors to macrophages and dendritic cells by C/EBP alpha and PU.1 transcription factors. Immunity 2006;25:731-744.

[240] Feng R, Desbordes SC, Xie H, Tillo ES, Pixley F, Stanley ER, *et al.* PU.1 and C/EBPalpha/beta convert fibroblasts into macrophage-like cells. Proc Natl Acad Sci U S A 2008;105:6057-6062.

[241] Vierbuchen T, Ostermeier A, Pang ZP, Kokubu Y, Sudhof TC, Wernig M. Direct conversion of fibroblasts to functional neurons by defined factors. Nature 2010;463:1035-1041.

[242] Han DW, Tapia N, Hermann A, Hemmer K, Hoing S, Arauzo-Bravo MJ, *et al.* Direct reprogramming of fibroblasts into neural stem cells by defined factors. Cell Stem Cell 2012;10:465-472.

[243] Szabo E, Rampalli S, Risueno RM, Schnerch A, Mitchell R, Fiebig-Comyn A, *et al.* Direct conversion of human fibroblasts to multilineage blood progenitors. Nature 2010;468:521-526.

[244] Sekiya S, Suzuki A. Direct conversion of mouse fibroblasts to hepatocyte-like cells by defined factors. Nature 2011;475:390-393.

[245] Huang P, He Z, Ji S, Sun H, Xiang D, Liu C, *et al.* Induction of functional hepatocyte-like cells from mouse fibroblasts by defined factors. Nature 2011;475:386-389.

[246] Marro S, Pang ZP, Yang N, Tsai MC, Qu K, Chang HY, *et al.* Direct lineage conversion of terminally differentiated hepatocytes to functional neurons. Cell Stem Cell 2011;9:374-382.

[247] Margariti A, Winkler B, Karamariti E, Zampetaki A, Tsai TN, Baban D, *et al.* Direct reprogramming of fibroblasts into endothelial cells capable of angiogenesis and reendothelialization in tissue-engineered vessels. Proc Natl Acad Sci U S A 2012;109:13793-13798.

[248] Takeuchi JK, Bruneau BG. Directed transdifferentiation of mouse mesoderm to heart tissue by defined factors. Nature 2009;459:708-711.

[249] Ieda M, Fu JD, Delgado-Olguin P, Vedantham V, Hayashi Y, Bruneau BG, *et al.* Direct reprogramming of fibroblasts into functional cardiomyocytes by defined factors. Cell 2010;142:375-386.

[250] Qian L, Huang Y, Spencer CI, Foley A, Vedantham V, Liu L, *et al.* In vivo reprogramming of murine cardiac fibroblasts into induced cardiomyocytes. Nature 2012;485:593-598.

[251] Song K, Nam YJ, Luo X, Qi X, Tan W, Huang GN, *et al.* Heart repair by reprogramming non-myocytes with cardiac transcription factors. Nature 2012;485:599-604.

[252] Inagawa K, Miyamoto K, Yamakawa H, Muraoka N, Sadahiro T, Umei T, *et al.* Induction of cardiomyocyte-like cells in infarct hearts by gene transfer of Gata4, Mef2c, and Tbx5. Circ Res 2012;111:1147-1156.

[253] Srivastava D, Ieda M, Fu J, Qian L. Cardiac repair with thymosin beta4 and cardiac reprogramming factors. Ann N Y Acad Sci 2012;1270:66-72.

[254] Chen JX, Krane M, Deutsch MA, Wang L, Rav-Acha M, Gregoire S, *et al.* Inefficient reprogramming of fibroblasts into cardiomyocytes using Gata4, Mef2c, and Tbx5. Circ Res 2012;111:50-55.

[255] Jayawardena TM, Egemnazarov B, Finch EA, Zhang L, Payne JA, Pandya K, *et al.* MicroRNA-mediated in vitro and in vivo direct reprogramming of cardiac fibroblasts to cardiomyocytes. Circ Res 2012;110:1465-1473.

[256] Puymirat E, Geha R, Tomescot A, Bellamy V, Larghero J, Trinquart L, *et al.* Can mesenchymal stem cells induce tolerance to cotransplanted human embryonic stem cells? Mol Ther 2009;17:176-182.

[257] Mirotsou M, Jayawardena TM, Schmeckpeper J, Gnecchi M, Dzau VJ. Paracrine mechanisms of stem cell reparative and regenerative actions in the heart. J Mol Cell Cardiol 2010;50:280-289.

[258] Numasawa Y, Kimura T, Miyoshi S, Nishiyama N, Hida N, Tsuji H, *et al.* Treatment of human mesenchymal stem cells with angiotensin receptor blocker improved efficiency of cardiomyogenic transdifferentiation and improved cardiac function via angiogenesis. Stem Cells;29:1405-1414.

[259] Mazo M, Gavira JJ, Abizanda G, Moreno C, Ecay M, Soriano M, *et al.* Transplantation of mesenchymal stem cells exerts a greater long-term effect than bone marrow mononuclear cells in a chronic myocardial infarction model in rat. Cell Transplant 2009;19:313-328.

[260] Le Blanc K. Mesenchymal stromal cells: Tissue repair and immune modulation. Cytotherapy 2006;8:559-561.

[261] Templin C, Zweigerdt R, Schwanke K, Olmer R, Ghadri JR, Emmert MY, *et al.* Transplantation and tracking of human-induced pluripotent stem cells in a pig model of myocardial infarction: assessment of cell survival, engraftment, and distribution by hybrid single photon emission computed tomography/computed tomography of sodium iodide symporter transgene expression. Circulation 2012;126:430-439.

[262] Rane AA, Christman KL. Biomaterials for the treatment of myocardial infarction: a 5-year update. J Am Coll Cardiol 2011;58:2615-2629.

[263] Matsuura K, Wada M, Shimizu T, Haraguchi Y, Sato F, Sugiyama K, *et al.* Creation of human cardiac cell sheets using pluripotent stem cells. Biochem Biophys Res Commun 2012;425:321-327.

[264] Piao H, Kwon JS, Piao S, Sohn JH, Lee YS, Bae JW, *et al.* Effects of cardiac patches engineered with bone marrow-derived mononuclear cells and PGCL scaffolds in a rat myocardial infarction model. Biomaterials 2007;28:641-649.

[265] Jin J, Jeong SI, Shin YM, Lim KS, Shin H, Lee YM, *et al.* Transplantation of mesenchymal stem cells within a poly(lactide-co-epsilon-caprolactone) scaffold improves cardiac function in a rat myocardial infarction model. Eur J Heart Fail 2009;11:147-153.

[266] Caspi O, Lesman A, Basevitch Y, Gepstein A, Arbel G, Habib IH, *et al.* Tissue engineering of vascularized cardiac muscle from human embryonic stem cells. Circ Res 2007;100:263-272.

[267] Bel A, Planat-Bernard V, Saito A, Bonnevie L, Bellamy V, Sabbah L, *et al.* Composite cell sheets: a further step toward safe and effective myocardial regeneration by cardiac progenitors derived from embryonic stem cells. Circulation 2010;122:S118-123.

[268] Xiong Q, Hill KL, Li Q, Suntharalingam P, Mansoor A, Wang X, *et al.* A fibrin patch-based enhanced delivery of human embryonic stem cell-derived vascular cell transplantation in a porcine model of postinfarction left ventricular remodeling. Stem Cells 2011;29:367-375.

[269] Stevens KR, Kreutziger KL, Dupras SK, Korte FS, Regnier M, Muskheli V, *et al.* Physiological function and transplantation of scaffold-free and vascularized human cardiac muscle tissue. Proc Natl Acad Sci U S A 2009;106:16568-16573.

[270] Masumoto H, Matsuo T, Yamamizu K, Uosaki H, Narazaki G, Katayama S, *et al.* Pluripotent stem cell-engineered cell sheets reassembled with defined cardiovascular populations ameliorate reduction in infarct heart function through cardiomyocyte-mediated neovascularization. Stem Cells 2012;30:1196-1205.

[271] Tulloch NL, Muskheli V, Razumova MV, Korte FS, Regnier M, Hauch KD, *et al.* Growth of engineered human myocardium with mechanical loading and vascular coculture. Circ Res 2011;109:47-59.

[272] Dai B, Huang W, Xu M, Millard RW, Gao MH, Hammond HK, *et al.* Reduced collagen deposition in infarcted myocardium facilitates induced pluripotent stem cell engraftment and angiomyogenesis for improvement of left ventricular function. J Am Coll Cardiol 2011;58:2118-2127.

[273] Kawamura M, Miyagawa S, Miki K, Saito A, Fukushima S, Higuchi T, *et al.* Feasibility, safety, and therapeutic efficacy of human induced pluripotent stem cell-derived cardiomyocyte sheets in a porcine ischemic cardiomyopathy model. Circulation 2012;126:S29-37.

[274] Shiba Y, Fernandes S, Zhu WZ, Filice D, Muskheli V, Kim J, *et al.* Human ES-cell-derived cardiomyocytes electrically couple and suppress arrhythmias in injured hearts. Nature 2012;489:322-325.

[275] Wernig M, Zhao JP, Pruszak J, Hedlund E, Fu D, Soldner F, *et al.* Neurons derived from reprogrammed fibroblasts functionally integrate into the fetal brain and improve symptoms of rats with Parkinson's disease. Proc Natl Acad Sci U S A 2008;105:5856-5861.

[276] Tsuji O, Miura K, Okada Y, Fujiyoshi K, Mukaino M, Nagoshi N, *et al.* Therapeutic potential of appropriately evaluated safe-induced pluripotent stem cells for spinal cord injury. Proc Natl Acad Sci U S A 2010;107:12704-12709.

[277] Darabi R, Arpke RW, Irion S, Dimos JT, Grskovic M, Kyba M, *et al.* Human ES- and iPS-derived myogenic progenitors restore DYSTROPHIN and improve contractility upon transplantation in dystrophic mice. Cell Stem Cell 2012;10:610-619.

[278] Hanna J, Wernig M, Markoulaki S, Sun CW, Meissner A, Cassady JP, *et al.* Treatment of sickle cell anemia mouse model with iPS cells generated from autologous skin. Science 2007;318:1920-1923.

[279] Xu D, Alipio Z, Fink LM, Adcock DM, Yang J, Ward DC, *et al.* Phenotypic correction of murine hemophilia A using an iPS cell-based therapy. Proc Natl Acad Sci U S A 2009;106:808-813.

[280] Raya A, Rodriguez-Piza I, Guenechea G, Vassena R, Navarro S, Barrero MJ, *et al.* Disease-corrected haematopoietic progenitors from Fanconi anaemia induced pluripotent stem cells. Nature 2009;460:53-59.

[281] An MC, Zhang N, Scott G, Montoro D, Wittkop T, Mooney S, *et al.* Genetic correction of Huntington's disease phenotypes in induced pluripotent stem cells. Cell Stem Cell 2012;11:253-263.

[282] Kazuki Y, Hiratsuka M, Takiguchi M, Osaki M, Kajitani N, Hoshiya H, *et al.* Complete genetic correction of ips cells from Duchenne muscular dystrophy. Mol Ther 2009;18:386-393.

[283] Liu GH, Suzuki K, Qu J, Sancho-Martinez I, Yi F, Li M, *et al.* Targeted gene correction of laminopathy-associated LMNA mutations in patient-specific iPSCs. Cell Stem Cell 2011;8:688-694.

[284] Zhang S, Chen S, Li W, Guo X, Zhao P, Xu J, *et al.* Rescue of ATP7B function in hepatocyte-like cells from Wilson's disease induced pluripotent stem cells using gene therapy or the chaperone drug curcumin. Hum Mol Genet 2011;20:3176-3187.

[285] Zou J, Mali P, Huang X, Dowey SN, Cheng L. Site-specific gene correction of a point mutation in human iPS cells derived from an adult patient with sickle cell disease. Blood 2011;118:4599-4608.

[286] Wang Y, Zheng CG, Jiang Y, Zhang J, Chen J, Yao C, *et al.* Genetic correction of beta-thalassemia patient-specific iPS cells and its use in improving hemoglobin production in irradiated SCID mice. Cell Res 2012;22:637-648.

[287] Lee G, Papapetrou EP, Kim H, Chambers SM, Tomishima MJ, Fasano CA, *et al.* Modelling pathogenesis and treatment of familial dysautonomia using patient-specific iPSCs. Nature 2009;461:402-406.

[288] Ebert AD, Yu J, Rose FF, Jr., Mattis VB, Lorson CL, Thomson JA, *et al.* Induced pluripotent stem cells from a spinal muscular atrophy patient. Nature 2009;457:277-280.

[289] Marchetto MC, Carromeu C, Acab A, Yu D, Yeo GW, Mu Y*, et al.* A model for neural development and treatment of Rett syndrome using human induced pluripotent stem cells. Cell 2010;143:527-539.

[290] Egawa N, Kitaoka S, Tsukita K, Naitoh M, Takahashi K, Yamamoto T*, et al.* Drug screening for ALS using patient-specific induced pluripotent stem cells. Sci Transl Med 2012;4:145ra104.

[291] Carvajal-Vergara X, Sevilla A, D'Souza SL, Ang YS, Schaniel C, Lee DF*, et al.* Patient-specific induced pluripotent stem-cell-derived models of LEOPARD syndrome. Nature 2010;465:808-812.

[292] Moretti A, Bellin M, Welling A, Jung CB, Lam JT, Bott-Flugel L*, et al.* Patient-specific induced pluripotent stem-cell models for long-QT syndrome. N Engl J Med 2010;363:1397-1409.

[293] Itzhaki I, Maizels L, Huber I, Zwi-Dantsis L, Caspi O, Winterstern A*, et al.* Modelling the long QT syndrome with induced pluripotent stem cells. Nature 2011;471:225-229.

[294] Yazawa M, Hsueh B, Jia X, Pasca AM, Bernstein JA, Hallmayer J*, et al.* Using induced pluripotent stem cells to investigate cardiac phenotypes in Timothy syndrome. Nature 2011;471:230-234.

[295] Lahti AL, Kujala VJ, Chapman H, Koivisto AP, Pekkanen-Mattila M, Kerkela E*, et al.* Model for long QT syndrome type 2 using human iPS cells demonstrates arrhythmogenic characteristics in cell culture. Dis Model Mech 2011;5:220-230.

[296] Sun N, Yazawa M, Liu J, Han L, Sanchez-Freire V, Abilez OJ*, et al.* Patient-specific induced pluripotent stem cells as a model for familial dilated cardiomyopathy. Sci Transl Med 2012;4:130ra147.

[297] Davis RP, Casini S, van den Berg CW, Hoekstra M, Remme CA, Dambrot C*, et al.* Cardiomyocytes derived from pluripotent stem cells recapitulate electrophysiological characteristics of an overlap syndrome of cardiac sodium channel disease. Circulation 2012;125:3079-3091.

[298] Jung CB, Moretti A, Mederos y Schnitzler M, Iop L, Storch U, Bellin M*, et al.* Dantrolene rescues arrhythmogenic RYR2 defect in a patient-specific stem cell model of catecholaminergic polymorphic ventricular tachycardia. EMBO Mol Med 2011;4:180-191.

[299] Pelacho B, Nakamura Y, Zhang J, Ross J, Heremans Y, Nelson-Holte M*, et al.* Multipotent adult progenitor cell transplantation increases vascularity and improves left ventricular function after myocardial infarction. J Tissue Eng Regen Med 2007;1:51-59.

[300] Benavides-Vallve C, Corbacho D, Iglesias-Garcia O, Pelacho B, Albiasu E, Castano S*, et al.* New strategies for echocardiographic evaluation of left ventricular function in a mouse model of long-term myocardial infarction. PLoS One 2012;7:e41691.

[301] Maherali N, Hochedlinger K. Guidelines and techniques for the generation of induced pluripotent stem cells. Cell Stem Cell 2008;3:595-605.

[302] Boyer LA, Lee TI, Cole MF, Johnstone SE, Levine SS, Zucker JP*, et al.* Core transcriptional regulatory circuitry in human embryonic stem cells. Cell 2005;122:947-956.

[303] Halbach M, Pfannkuche K, Pillekamp F, Ziomka A, Hannes T, Reppel M*, et al.* Electrophysiological maturation and integration of murine fetal cardiomyocytes after transplantation. Circ Res 2007;101:484-492.

[304] Sumi T, Tsuneyoshi N, Nakatsuji N, Suemori H. Apoptosis and differentiation of human embryonic stem cells induced by sustained activation of c-Myc. Oncogene 2007;26:5564-5576.

[305] Edwards MK, Harris JF, McBurney MW. Induced muscle differentiation in an embryonal carcinoma cell line. Mol Cell Biol 1983;3:2280-2286.

[306] Kehat I, Kenyagin-Karsenti D, Snir M, Segev H, Amit M, Gepstein A*, et al.* Human embryonic stem cells can differentiate into myocytes with structural and functional properties of cardiomyocytes. J Clin Invest 2001;108:407-414.

[307] Kuzmenkin A, Liang H, Xu G, Pfannkuche K, Eichhorn H, Fatima A*, et al.* Functional characterization of cardiomyocytes derived from murine induced pluripotent stem cells in vitro. FASEB J 2009;23:4168-4180.

[308] Zhang Q, Jiang J, Han P, Yuan Q, Zhang J, Zhang X*, et al.* Direct differentiation of atrial and ventricular myocytes from human embryonic stem cells by alternating retinoid signals. Cell Res 2010;21:579-587.

[309] Maltsev VA, Rohwedel J, Hescheler J, Wobus AM. Embryonic stem cells differentiate in vitro into cardiomyocytes representing sinusnodal, atrial and ventricular cell types. Mech Dev 1993;44:41-50.

[310] Chen HS, Kim C, Mercola M. Electrophysiological challenges of cell-based myocardial repair. Circulation 2009;120:2496-2508.

[311] Pfannkuche K, Liang H, Hannes T, Xi J, Fatima A, Nguemo F*, et al.* Cardiac myocytes derived from murine reprogrammed fibroblasts: intact hormonal regulation, cardiac ion channel expression and development of contractility. Cell Physiol Biochem 2009;24:73-86.

[312] Syed F, Diwan A, Hahn HS. Murine echocardiography: a practical approach for phenotyping genetically manipulated and surgically modeled mice. J Am Soc Echocardiogr 2005;18:982-990.

[313] Stypmann J. Doppler ultrasound in mice. Echocardiography 2007;24:97-112.

[314] Scherrer-Crosbie M, Thibault HB. Echocardiography in translational research: of mice and men. J Am Soc Echocardiogr 2008;21:1083-1092.

[315] Katare R, Caporali A, Emanueli C, Madeddu P. Benfotiamine improves functional recovery of the infarcted heart via activation of pro-survival G6PD/Akt signaling pathway and modulation of neurohormonal response. J Mol Cell Cardiol 2010;49:625-638.

[316] Meloni M, Descamps B, Caporali A, Zentilin L, Floris I, Giacca M*, et al.* Nerve growth factor gene therapy using adeno-associated viral vectors prevents cardiomyopathy in type 1 diabetic mice. Diabetes 2011;61:229-240.

[317] van Laake LW, Passier R, den Ouden K, Schreurs C, Monshouwer-Kloots J, Ward-van Oostwaard D*, et al.* Improvement of mouse cardiac function by hESC-derived cardiomyocytes correlates with vascularity but not graft size. Stem Cell Res 2009;3:106-112.

[318] Muller-Ehmsen J, Krausgrill B, Burst V, Schenk K, Neisen UC, Fries JW, *et al.* Effective engraftment but poor mid-term persistence of mononuclear and mesenchymal bone marrow cells in acute and chronic rat myocardial infarction. J Mol Cell Cardiol 2006;41:876-884.

[319] Wu EX, Wu Y, Nicholls JM, Wang J, Liao S, Zhu S, *et al.* MR diffusion tensor imaging study of postinfarct myocardium structural remodeling in a porcine model. Magn Reson Med 2007;58:687-695.

[320] Menasche P. Stem cell therapy for heart failure: are arrhythmias a real safety concern? Circulation 2009;119:2735-2740.

[321] Reinecke H, Zhang M, Bartosek T, Murry CE. Survival, integration, and differentiation of cardiomyocyte grafts: a study in normal and injured rat hearts. Circulation 1999;100:193-202.

[322] Mazo M, Planat-Benard V, Abizanda G, Pelacho B, Leobon B, Gavira JJ, *et al.* Transplantation of adipose derived stromal cells is associated with functional improvement in a rat model of chronic myocardial infarction. Eur J Heart Fail 2008;10:454-462.

[323] Laflamme MA, Gold J, Xu C, Hassanipour M, Rosler E, Police S, *et al.* Formation of human myocardium in the rat heart from human embryonic stem cells. Am J Pathol 2005;167:663-671.

[324] Christoforou N, Oskouei BN, Esteso P, Hill CM, Zimmet JM, Bian W, *et al.* Implantation of mouse embryonic stem cell-derived cardiac progenitor cells preserves function of infarcted murine hearts. PLoS One 2010;5:e11536.

[325] Baba S, Heike T, Yoshimoto M, Umeda K, Doi H, Iwasa T, *et al.* Flk1(+) cardiac stem/progenitor cells derived from embryonic stem cells improve cardiac function in a dilated cardiomyopathy mouse model. Cardiovasc Res 2007;76:119-131.

[326] Moretti A, Caron L, Nakano A, Lam JT, Bernshausen A, Chen Y, *et al.* Multipotent embryonic isl1+ progenitor cells lead to cardiac, smooth muscle, and endothelial cell diversification. Cell 2006;127:1151-1165.

[327] Ye J, Boyle A, Shih H, Sievers RE, Zhang Y, Prasad M, *et al.* Sca-1+ cardiosphere-derived cells are enriched for Isl1-expressing cardiac precursors and improve cardiac function after myocardial injury. PLoS One 2012;7:e30329.

[328] Mazo M, Cemborain A, Gavira JJ, Abizanda G, Arana M, Casado M, *et al.* Adipose stromal vascular fraction improves cardiac function in chronic myocardial infarction through differentiation and paracrine activity. Cell Transplant 2012;21:1023-1037.

[329] Gnecchi M, Zhang Z, Ni A, Dzau VJ. Paracrine mechanisms in adult stem cell signaling and therapy. Circ Res 2008;103:1204-1219.

[330] Burchfield JS, Dimmeler S. Role of paracrine factors in stem and progenitor cell mediated cardiac repair and tissue fibrosis. Fibrogenesis Tissue Repair 2008;1:4.

[331] Kawamoto A, Tkebuchava T, Yamaguchi J, Nishimura H, Yoon YS, Milliken C, *et al.* Intramyocardial transplantation of autologous endothelial progenitor cells for therapeutic neovascularization of myocardial ischemia. Circulation 2003;107:461-468.

[332] Sasaki H, Ray PS, Zhu L, Galang N, Maulik N. Oxidative stress due to hypoxia/reoxygenation induces angiogenic factor VEGF in adult rat myocardium: possible role of NFkappaB. Toxicology 2000;155:27-35.

[333] Seko Y, Takahashi N, Tobe K, Kadowaki T, Yazaki Y. Pulsatile stretch activates mitogen-activated protein kinase (MAPK) family members and focal adhesion kinase (p125(FAK)) in cultured rat cardiac myocytes. Biochem Biophys Res Commun 1999;259:8-14.

[334] Leychenko A, Konorev E, Jijiwa M, Matter ML. Stretch-induced hypertrophy activates NFkB-mediated VEGF secretion in adult cardiomyocytes. PLoS One 2011;6:e29055.

[335] Zentilin L, Puligadda U, Lionetti V, Zacchigna S, Collesi C, Pattarini L*, et al.* Cardiomyocyte VEGFR-1 activation by VEGF-B induces compensatory hypertrophy and preserves cardiac function after myocardial infarction. FASEB J 2009;24:1467-1478.

[336] Dhein S, Garbade J, Rouabah D, Abraham G, Ungemach FR, Schneider K*, et al.* Effects of autologous bone marrow stem cell transplantation on beta-adrenoceptor density and electrical activation pattern in a rabbit model of non-ischemic heart failure. J Cardiothorac Surg 2006;1:17.

[337] Ohnishi S, Sumiyoshi H, Kitamura S, Nagaya N. Mesenchymal stem cells attenuate cardiac fibroblast proliferation and collagen synthesis through paracrine actions. FEBS Lett 2007;581:3961-3966.

[338] Brown RD, Jones GM, Laird RE, Hudson P, Long CS. Cytokines regulate matrix metalloproteinases and migration in cardiac fibroblasts. Biochem Biophys Res Commun 2007;362:200-205.

[339] Guo J, Lin GS, Bao CY, Hu ZM, Hu MY. Anti-inflammation role for mesenchymal stem cells transplantation in myocardial infarction. Inflammation 2007;30:97-104.

[340] Xu X, Xu Z, Xu Y, Cui G. Effects of mesenchymal stem cell transplantation on extracellular matrix after myocardial infarction in rats. Coron Artery Dis 2005;16:245-255.

[341] Terrovitis JV, Smith RR, Marban E. Assessment and optimization of cell engraftment after transplantation into the heart. Circ Res 2010;106:479-494.

[342] Kutschka I, Chen IY, Kofidis T, Arai T, von Degenfeld G, Sheikh AY*, et al.* Collagen matrices enhance survival of transplanted cardiomyoblasts and contribute to functional improvement of ischemic rat hearts. Circulation 2006;114:I167-173.

[343] Levenberg S, Golub JS, Amit M, Itskovitz-Eldor J, Langer R. Endothelial cells derived from human embryonic stem cells. Proc Natl Acad Sci U S A 2002;99:4391-4396.

[344] Levenberg S, Rouwkema J, Macdonald M, Garfein ES, Kohane DS, Darland DC*, et al.* Engineering vascularized skeletal muscle tissue. Nat Biotechnol 2005;23:879-884.

[345] Hahn JY, Cho HJ, Kang HJ, Kim TS, Kim MH, Chung JH*, et al.* Pre-treatment of mesenchymal stem cells with a combination of growth factors enhances gap junction formation, cytoprotective effect on cardiomyocytes, and therapeutic efficacy for myocardial infarction. J Am Coll Cardiol 2008;51:933-943.

[346] Tang J, Wang J, Zheng F, Kong X, Guo L, Yang J*, et al.* Combination of chemokine and angiogenic factor genes and mesenchymal stem cells could enhance angiogenesis and improve cardiac function after acute myocardial infarction in rats. Mol Cell Biochem 2010;339:107-118.

[347] Formiga FR, Pelacho B, Garbayo E, Abizanda G, Gavira JJ, Simon-Yarza T, *et al.* Sustained release of VEGF through PLGA microparticles improves vasculogenesis and tissue remodeling in an acute myocardial ischemia-reperfusion model. J Control Release 2010;147:30-37.

[348] Perets A, Baruch Y, Weisbuch F, Shoshany G, Neufeld G, Cohen S. Enhancing the vascularization of three-dimensional porous alginate scaffolds by incorporating controlled release basic fibroblast growth factor microspheres. J Biomed Mater Res A 2003;65:489-497.

[349] Chung YI, Kim SK, Lee YK, Park SJ, Cho KO, Yuk SH, *et al.* Efficient revascularization by VEGF administration via heparin-functionalized nanoparticle-fibrin complex. J Control Release 2010;143:282-289.

[350] Frontini MJ, Nong Z, Gros R, Drangova M, O'Neil C, Rahman MN, *et al.* Fibroblast growth factor 9 delivery during angiogenesis produces durable, vasoresponsive microvessels wrapped by smooth muscle cells. Nat Biotechnol 2011;29:421-427.

[351] Davis ME, Hsieh PC, Takahashi T, Song Q, Zhang S, Kamm RD, *et al.* Local myocardial insulin-like growth factor 1 (IGF-1) delivery with biotinylated peptide nanofibers improves cell therapy for myocardial infarction. Proc Natl Acad Sci U S A 2006;103:8155-8160.

ANNEX

PLoS ONE

New Strategies for Echocardiographic Evaluation of Left Ventricular Function in a Mouse Model of Long-Term Myocardial Infarction

Carolina Benavides-Vallve[1], David Corbacho[1], Olalla Iglesias-Garcia[1], Beatriz Pelacho[1], Edurne Albiasu[1], Sara Castaño[2], Arrate Muñoz-Barrutia[1], Felipe Prosper[1], Carlos Ortiz-de-Solorzano[1]*

1 Imaging Unit, Fundación para la Investigación Médica Aplicada, University of Navarra, Pamplona, Navarra, Spain, 2 Cardiology Department, Clínica Universidad de Navarra, Pamplona, Navarra, Spain

Abstract

Background: The aim of this article is to present an optimized acquisition and analysis protocol for the echocardiographic evaluation of left ventricle (LV) remodeling in a mouse model of myocardial infarction (MI).

Methodology: 13 female DBA/2J mice underwent permanent occlusion of the left anterior descending (LAD) coronary artery leading to MI. Mice echocardiography was performed using a Vevo 770 (Visualsonics, Canada) before infarction, and 7, 14, 30, 60, 90 and 120 days after LAD ligation. LV systolic function was evaluated using different parameters, including the fractional area change (FAC%) computed in four high-temporal resolution B-mode short axis images taken at different ventricular levels, and in one parasternal long axis. Pulsed wave and tissue Doppler modes were used to evaluate the diastolic function and Tei Index for global cardiac function. The echocardiographic measurements of infarct size were validated histologically using collagen deposition labeled by Sirius red staining. All data was analyzed using Shapiro-Wilk and Student's t-tests.

Principal Findings: Our results reveal LV dilation resulting in marked remodeling an severe systolic dysfunction, starting seven days after MI (LV internal apical diameter, basal = 2.82 ± 0.24, 7d = 3.49 ± 0.42; p<0.001. End-diastolic area, basal = 18.98 ± 1.81, 7d = 22.04 ± 2.11; p<0.001). A strong statistically significant negative correlation exists between the infarct size and long-axis FAC% (r = -0.946; $R_2 = 0.90$; p<0.05). Moreover, the measured Tei Index values confirmed significant post-infarction impairment of the global cardiac function (basal = 0.46 ± 0.07, 7d = 0.55 ± 0.08, 14 d = 0.57 ± 0.06, 30 d = 0.54 ± 0.06, 60 d = 0.54 ± 0.07, 90 d = 0.57 ± 0.08; p<0.01).

Conclusions/Significance: In summary, we have performed a complete characterization of LV post-infarction remodeling in a DBA/2J mouse model of MI, using parameters adapted to the particular characteristics of the model In the future, this well characterized model will be used in both investigative and pharmacological studies that require accurate quantitative monitoring of cardiac recovery after myocardial infarction.

Introduction

Cardiovascular disease, and more specifically myocardial infarction (MI), is the first cause of morbidity and mortality in the world [1],[2],[3]. Left ventricle (LV) remodeling occurs after myocardial infarction as a result of the abrupt loss of contracting cardiomyocytes. Early expansion of the infarct zone is associated with LV dilation caused by the redistribution of the increased regional wall stress to preserve stroke volume [4]. Between one half and one third of patients experience progressive post-infarction dilatation with distortion of ventricular geometry and secondary mitral regurgitation [5].

Quantitative bi-dimensional transthoracic echocardiography is routinely used to characterize the LV remodeling associated with ischemic cardiomyopathies [6],[7]. The traditional echocardiographic measurements recommended for the evaluation of LV remodeling include estimates of LV end-diastolic and end-systolic volumes and LV mass. LV volumes have been demonstrated to predict adverse cardiovascular follow-up events, including recurrent infarction, heart failure, ventricular arrhythmias, and mitral regurgitation [7].

Several murine models of myocardial infarction exist, based on permanent occlusion of the left anterior descending coronary artery (LAD). These models have been used to elucidate mechanisms of myocardial remodeling and provide new insights into the physiology and treatment of cardiovascular disease [8],[9],[10],[11]. To perform reliable measurements of cardiac function in mouse models, high-resolution echocardiography equipment is available, specifically designed for small animal imaging [12]. This is the case of the Vevo 770 (VisualSonics, Toronto, ON), a high-resolution *in vivo* micro-imaging system, which has been used in this study. Ultrasound imaging provides a fast and inexpensive alternative to magnetic resonance imaging [13],[14],[15] when performing longitudinal follow up studies of cardiac remodeling.

The most common parameters used to evaluate the systolic function of the LV are the fractional shortening (FS%), ejection fraction (EF%) and cardiac output (CO) [16]. In the absence of regional wall motion abnormalities, FS% and EF% are predictably related. In mice however, the extent of the typical cavity obliteration and the associated error introduced in the volumetric measurements is far greater than in humans. Consequently, the use of FS% is more appropriate [16]. The FS% and EF% are routinely calculated using the Teichholz method [17], which assumes that the left ventricular cavity can be represented as a 3D ellipsoid of revolution. However, this might not be a reasonable assumption when the LV adopts the complex shapes caused by regional wall motion abnormalities that are common after MI. Therefore, an alternative approach to calculating EF% exists, based on the shape independent Simpson's rule [8],[18],[19], where the LV endocardial border is traced in multiple slices both in systole and diastole, and the volumes are computed from these tracings.

Using the above method, the LV function can also be measured as the percentage of change in left ventricular cross-sectional area between diastole and systole (fractional area change, FAC%), which has been found to correlate well with EF% both in normal and abnormal subjects [20]. The standard method to estimate FAC% uses cross-sectional area short-axis views at different ventricular levels. However, when the infarction affects the ventricular apex, visualizing the infarct area at medium and upper levels becomes difficult and so it is to visualize the entire endocardial border. In those cases, the standard FAC% measurement is hardly representative of the real damage. Instead we propose to use a single parasternal long-axis view, which results in improved visualization.

Cardiologists, beyond the standard systolic dysfunction, are starting to analyze post-infarction diastolic dysfunction, which precedes the depression of systolic function in patients of all ages suffering from both permanent and temporary ischemic cardiomyopathies. The standard approach to diagnose diastolic dysfunction uses a pulsed-wave Doppler scan of transmitral flow, although a variety of other measurements can be used [21],[22]. The accuracy with which those measurements quantify diastolic dysfunction is still open to discussion [23].

Finally, since the isolated analysis of systolic and diastolic mechanisms may not be reflective of overall cardiac dysfunction, the Tei index has been recently introduced. The Tei Index is a simple, reproducible, quantitative estimate of global dysfunction, independent from heart rate and blood pressure levels, characterized by low inter-observer and intra-observer variability [21],[24],[25],[26]. An estimate of global cardiac function can also be obtained using tissue Doppler imaging.

The aim of the present article is to present an optimized echocardiographic quantification of LV remodeling in a mouse model of myocardial infarction. All the above-described parameters have been included and compared in our evaluation, and those that have morphological significance, correlated with histological measurements.

The rest of the article is organized as follows. In Section 2, we briefly summarize our mice model of MI by LAD ligation, the image acquisition protocols and parameters used to evaluate cardiac function. The results are presented in Section 3. A final discussion (Section 4) and conclusions (Section 5) end the article.

Methods

Experimental model

Seventeen 8-week-old female DBA/2J mice (Harlan IBERICA S.L. Barcelona, Spain) underwent coronary artery ligation as described in *Pelacho et al.* [27]. Briefly, the animals were anesthetized with 2% isofluorane, intubated, connected to a ventilator for small animals and placed on a heating table in a supine position. A thoracotomy was then practiced at the left fourth intercostal space. Next the pericardium was opened and the left anterior descending coronary artery was ligated using a 7.0 absorbable suture. The pericardial incision was closed in layers with a 6.0 absorbable suture and the skin incision with 6.0 sutures. Finally, the endotracheal tube was removed and spontaneous breathing restored. The animals were kept in a cage, lying on a heating blanket for several hours until recovered from surgery. The survival rate over the course of the experiment was over 75%. A –sham- group made of fourteen 8-week-old female mice that underwent thoracotomy but did not undergo ligation of the coronary artery was used as control of the experimental group.

All experiments were performed in accordance with the principles of laboratory animal care formulated by the National Society for Medical Research and the guide for the care and use of laboratory animals of the Institute of Laboratory Animal Resources (Commission on Life Science, National Research Council). All animal procedures were approved by the University of Navarra Institutional Committee on Care and Use of Laboratory Animals.

Echocardiographic studies

Echocardiography. Echocardiography was performed using a Vevo 770 ultrasound system (Visualsonics, Toronto, Canada) equipped with a real time micro-visualization scan head probe (RMV-707B) working at a frame rate ranging between 110 and 120 frames per sec (fps). The nosepiece-transducer used has a central frequency of 30 MHz, a focal length of 12.7 mm and 55 μm of nominal spatial resolution. The Vevo 770 is equipped with ECG-gated kilohertz visualization software (EKV[TM]), which synthesizes high temporal resolution B-Mode images by combining several ECG-synchronized heart cycles. The EKV image reconstruction software produces B-mode sequences at up to 1000 frames per second.

Animal preparation. Mice were anesthetized with isoflurane (Isoflo®, ABBOTT S.A, Madrid, Spain), at a concentration of 4% (induction) and 1.5% (maintenance) in 100% Oxygen. Each animal was placed on a heating table in a supine position with the extremities tied to the table through four electrocardiography leads. The chest was shaved using a chemical hair remover (Veet, Reckitt Benckise, Granollers, Spain). Warmed ultrasound gel (Quick Eco-Gel, Lessa, Barcelona, Spain) was applied to the thorax surface to optimize the visibility of the cardiac chambers. The heart rate (HR) of the animals was recorded immediately before the echocardiographic study.

Table 1. Structural analysis.

Day	HR	Dbvi	Dmvi	Davi	Aread	Areas
0	364,15±27,20	3,09±0,38	3,36±0,20	2,82±0,24	18,98±1,81	6,87±0,93
7	366,54±39,49	3,27±0,35	3,63±0,30	3,49±0,42**	22,04±2,11**	13,81±2,80**
14	368,08±41,21	3,09±0,31	3,75±0,33*	3,26±0,32**	22,16±2,16**	14,31±2,48**
30	361,23±29,31	3,49±0,43	3,76±0,30**	3,60±0,41**	22,83±2,37**	14,69±2,75**
60	374,23±36,31	3,35±0,17	3,83±0,31**	3,48±0,28**	23,75±2,67**	15,30±3,16**
90	364,23±37,35	3,68±0,39**	3,95±0,37**	3,81±0,45**	24,08±2,45**	15,78±3,20**

HR: heart rate. **Dbvi**: LV diameter (basal). **Dmvi**: LV diameter (medium). **Davi**: LV diameter (apical). **Aread**: end-diastolic area. **Areas**: end-systolic area. (* indicates statistical significance versus day 0, with p<0.01) (** indicates statistical significance versus day 0, with p<0.001).
doi:10.1371/journal.pone.0041691.t001

Views and measurements. Echoes were acquired at baseline (before LAD ligation), and 7, 14, 30, 60 and 90 days after LAD ligation. LV remodeling was quantified according to the guidelines and standards of American Society of Echocardiology, the guide to micro-echocardiography study using the Vevo770 [28] and the Vevo 770® Protocol-Based Measurements and Calculations guide, as described in the following paragraphs.

First we quantified the LV structural analysis. To that end the LV diameters at basal (Dbvi), middle (Dmvi) and apical level (Davi), the end-diastolic (Aread) and end-systolic (Areas) areas were measured on a two-dimensional (B-mode) parasternal long-axis view.

The functional analysis of the heart was next evaluated, starting with the LV systolic function that was measured several ways:

– The ejection (EF% tei) and shortening (FS%) fractions were calculated from the LV diameters (LVID d, LVID s) measured on an M-mode examination of the LV. To obtain the classical LV M-mode tracing, the M-mode cursor was vertically positioned at a transthoracic parasternal short axis view – visualizing both papillary muscles-.

– The normalized mean velocity of circumferential fiber shortening (VcFc) was calculated as the ratio between the shortening fraction and the heart rate (HR) corrected ejection time (Et_n), namely:

$$VcFc = \frac{FS}{Et_n} = \frac{FS}{\frac{Et}{\sqrt{\frac{60}{HR}}}}$$

– The ejection fraction was also calculated using the Simpson's rule (EF% simp), from a long axis view and four short axis views at different levels of the LV

– The fractional area change (FAC%), was measured as

$$FAC\% = \frac{(Aread - Areas)}{Aread} \times 100.$$

First, we calculated the FAC% using one parasternal short-axis view at mid-ventricular level (FAC% short). Given the poor definition of the endocardial border on the short-axis view, especially at mid-ventricular and apical levels, caused by the apical location of the infarction in our model, we also calculated the FAC% in one EKV-mode parasternal long-axis view (FAC% long). Both short and long-axis views were acquired using gain settings that optimized the visualization of the endocardial and epicardial walls.

– The peak velocity of the septal basal level (S′ septal) and the posterior wall (S′ post) were measured using Tissue Doppler from a four chamber and short axis view, respectively.

Table 2. Systolic function.

Day	EF% tei	EF% simp	FS%	VcFc	FAC% short	FAC% long
0	62,48±9,99	66,61±6,42	33,59±7,58	0,24±0,05	65,55±3,78	63,78±3,87
7	65,26±5,78	48,15±6,21**	35,43±4,75	0,25±0,05	47,89±3,99**	35,90±6,76**
14	60,76±5,56	51,69±4,59**	32,19±3,88	0,22±0,03	50,37±4,90**	35,69±7,08**
30	59,70±7,38	48,51±6,13**	31,59±5,19	0,21±0,04	49,96±3,74**	36,01±7,69**
60	63,11±3,45	45,76±10,50**	33,93±2,56	0,24±0,03	49,26±4,78**	36,16±6,74**
90	59,37±4,98	44,84±8,30**	31,31±3,44	0,22±0,03	46,78±3,87**	35,03±8,12**

EF% tei: ejection fraction using Teichholz. **EF% simp**: ejection fraction using Simpson's rule. **FS% tei**: fractional shortening using Teichholz. **VcFc**: normalized mean velocity of circumferential fiber shortening. **FAC% short**: fractional area change measured on a short axis view. **FAC% long**: fractional area change measured on a long axis view. (* indicates statistical significance versus day 0, with p<0.01) (** indicates statistical significance versus day 0, with p<0.001).
doi:10.1371/journal.pone.0041691.t002

Table 3. Systolic function (cont'd).

Day	LVID d	LVID s	CO	S' post	S' septal
0	3,64±0,29	2,38±0,34	15,76±2,36	20,18±1,60	20,78±3,23
7	3,95±0,40	2,53±0,27	13,90±3,75	18,96±2,36	19,05±1,97
14	4,04±0,36*	2,72±0,31	15,40±4,20	18,96±1,79	17,91±1,23*
30	4,08±0,41*	2,80±0,43	17,18±4,95	18,81±1,31	17,41±1,09**
60	4,28±0,33*	2,85±0,32*	13,83±2,31	18,37±0,95*	17,74±2,70*
90	4,22±0,34**	2,90±0,28**	16,23±2,82	19,57±2,43	18,69±1,89

LVID d: LV internal diameter (diastole). **LVID s**: LV internal diameter (systole). **CO**: cardiac output. **S' post**: peak velocity of the posterior wall. **S' septal**: peak velocity of septal basal level. (* indicates statistical significance versus day 0, with p<0.01) (** indicates statistical significance versus day 0, with p<0.001).
doi:10.1371/journal.pone.0041691.t003

– The cardiac output (CO), was measured from the left ventricular output tract length (LVOT) and HR measured on a long axis view, and the area under the curve of a Doppler measured on the aortic valve.

The LV diastolic function was evaluated using pulsed-wave Doppler sensing of the transmitral inflow obtained from LV apical two or four chamber views. From the pulsed-wave Doppler graph, we measured the peak E wave velocity (early filling wave), peak A wave velocity (late atrial contraction wave), E/A ratio, deceleration time (MVDT), ejection time from opening to closure of the aortic valve (ET ms) and LV isovolumetric relaxation (IVRT) and contraction (IVCT) times. During the scan, the ultrasound beam was kept as parallel as possible to the blood flow. Representative Doppler curves obtained from one of the animals in all time points are included as Figure S1.

The Tei Index –an indicator of global cardiac function- was calculated from the pulsed-wave Doppler graph:

$$\text{Tei Index} = \frac{IVCT + IVRT}{ET}.$$

Finally, an estimate of both systolic and diastolic function was also obtained using tissue Doppler imaging on the LV septal basal portion of the mitral annulus, and on the LV posterior wall, taken from a parasternal short-axis view at the level of the papillary muscle. From the tissue Doppler imaging graph, we calculated the negative E' wave (early diastolic myocardial relaxation velocity), negative A' wave (late-atrial myocardial contraction velocity), and

Table 4. Diastolic function.

Day	E	A	E/A	ET ms	MVDT
0	670,38±69,46	410,55±49,86	1,58±0,23	57,79±5,36	21,25±1,48
7	614,52±78,08	317,09±73,61*	2,10±0,68	58,94±6,39	20,10±4,28
14	588,37±52,63*	411,86±88,69	1,63±0,46	58,73±5,74	19,43±1,97
30	558,02±74,43**	350,09±60,88	1,72±0,41	60,71±3,72	20,10±3,00
60	593,40±107,20	349,78±87,45	1,79±0,47	56,06±4,94	19,27±2,16
90	590,41±104,08	371,00±66,21	1,57±0,30	57,69±5,81	20,00±2,34

E: early filling wave. **A**: late atrial contraction wave. **E/A**: ratio between E and A. **ET ms**: ejection time from opening to closing of the aortic valve. **MVDT**: deceleration time. (* indicates statistical significance versus day 0, with p<0.01) (** indicates statistical significance versus day 0, with p<0.001).
doi:10.1371/journal.pone.0041691.t004

Table 5. Diastolic function (cont'd).

Day	IVCT	IVRT
0	12,50±2,93	14,23±2,26
7	13,94±2,97	18,17±2,20**
14	14,33±3,81	18,27±3,25*
30	13,56±3,14	18,75±2,60**
60	12,31±2,54	17,98±2,82*
90	12,98±3,08	17,50±2,39*

IVCT: LV isovolumetric contraction time. **IVRT**: LV isovolumetric relaxation time. (* indicates statistical significance versus day 0, with p<0.01) (** indicates statistical significance versus day 0, with p<0.001).
doi:10.1371/journal.pone.0041691.t005

the ratio E/E' (ratio of mitral peak velocity of early filling E to early diastolic mitral annular velocity E') Representative tissue Doppler curves obtained from one of the animals in all time points are included as Figure S2.

All measurements were performed offline using dedicated Vevo770 quantification software (Vevo 770 v. 3.0.0).

Tissue processing and staining

Mice were anesthetized, injected with 100 μl saline containing 0.1 mM cadmium chloride (Sigma), and perfusion-fixed for 10 min with 4% paraformaldehyde under physiological pressure. The hearts were excised, fixed overnight in 4% paraformaldehyde at 4°C, and cut in three 3.0 mm blocks (apical, mid-ventricular and basal) using a mouse heart slicer matrix (Zivic instruments, see Figure S3). Finally, hearts were dehydrated in 70% ethanol (4°C, o/n), embedded in paraffin and sectioned at 5 μm thickness. The sections were deparaffinated and stained by immersion in Picrosirius Red (Sigma) for 90 minutes, differentiated 2 minutes in HCl (Sigma) 0.01 N, dehydrated and mounted in DPX [27].

Morphometric analysis

The histological extent of the infarction was measured as the amount of collagen deposition stained by Sirius red [22]. Briefly, an average of 15 serial sections per heart were imaged at 2.5× using a Zeiss Axio Imager M1 microscope (Carl Zeiss AG, Oberkochen, Germany) equipped with and AxioCam ICc3 digital camera and Axiovision software (v 4.6.3.0). The images were acquired as image mosaics mounted by the software that controls the microscope. The infarct size was automatically measured in each section photograph, using the AnalySIS[R] software [29]. The results were calculated as percentage of infarcted area *vs.* total LV area and averaged through all the sections.

Statistical analysis

All data are expressed as mean ± standard deviation. The Shapiro-Wilk test was used to verify that the data followed a normal distribution, which justified or not the use of a parametric test. A Student's *t*-test was used for the statistical analysis of means. To calculate the correlation between infarction size and FAC% we used the Pearson correlation and linear regression analysis. For all tests, a *P* value of less than 0.01 was considered statistically significant. All statistical analysis was performed using SPSS software for windows (Version 15.0).

Table 6. Global cardiac function.

Day	Tei index	E/E′	E′ septal	E′ post	A′ septal	A′ post
0	0,46±0,07	28,45±3,53	23,82±3,21	25,20±4,30	20,07±3,61	17,00±2,99
7	0,55±0,08*	29,59±6,68	21,51±4,52	22,13±3,76	18,03±3,46	17,20±3,49
14	0,56±0,08*	28,57±4,69	20,33±2,43*	22,08±3,81	17,07±3,66*	17,32±3,90
30	0,54±0,06*	27,86±3,90	20,23±2,71*	21,38±3,98	18,00±2,47*	17,45±4,67
60	0,54±0,08*	29,50±3,68	20,22±3,20*	22,11±3,87	19,09±4,19*	16,29±3,45
90	0,58±0,08*	29,29±4,53	20,44±3,66	21,83±3,44	20,44±3,33	17,39±3,11

Tei index: index tei. **E/E′**: ratio between E and E′. **E′ septal:** early diastolic myocardial relaxation velocity (septal level). **E′ post:** early diastolic myocardial relaxation velocity (posterior wall). **A′ septal:** late-atrial myocardial relaxation velocity (septal level). **A′ post:** late-atrial myocardial relaxation velocity (posterior wall). (* indicates statistical significance versus day 0, with p<0.01) (** indicates statistical significance versus day 0, with p<0.001).
doi:10.1371/journal.pone.0041691.t006

Results

Echocardiographic data

The average study was 15 minutes long. Four mice from the experimental group were excluded from the study: Three of them died during surgery and one more 7 days after myocardial infarction. The results of the structural and functional measurements performed on the control –sham- group are included in Table S1. No significant differences between the basal and post-surgery (7 day) measurements were found in any of the measurements, thus the measurements obtained on the experimental group, summarized in Tables 1, 2, 3, 4, 5, and 6 can be considered free from artifacts caused by the surgery.

Measurement of left ventricular remodeling and cardiac function

LV structural analysis. Table 1 (HR) shows the average heart rate of the animals before MI and 7, 30 and 90 days post-infarction. There are no statistically significant changes between time points. Therefore no changes on LV-fractional area values can be attributed to changes in HR caused by non-properly controlled effects of the anesthetic.

Table 1 lists the LV diastolic average internal diameter at baseline (Dbvi), middle (Dmvi) and apical (Davi) levels before MI and 7, 30 and 90 days post-infarction. These values reveal progressive post-infarction remodeling of the left ventricle. Namely, at basal level (Dbvi), the LV diameter significantly increased (p<0.001) 90 days post-infarction. At middle level (Dmvi), a significant enlargement (p<0.01) was detected starting 14 days post-infarction and becoming prominent 30 days post-
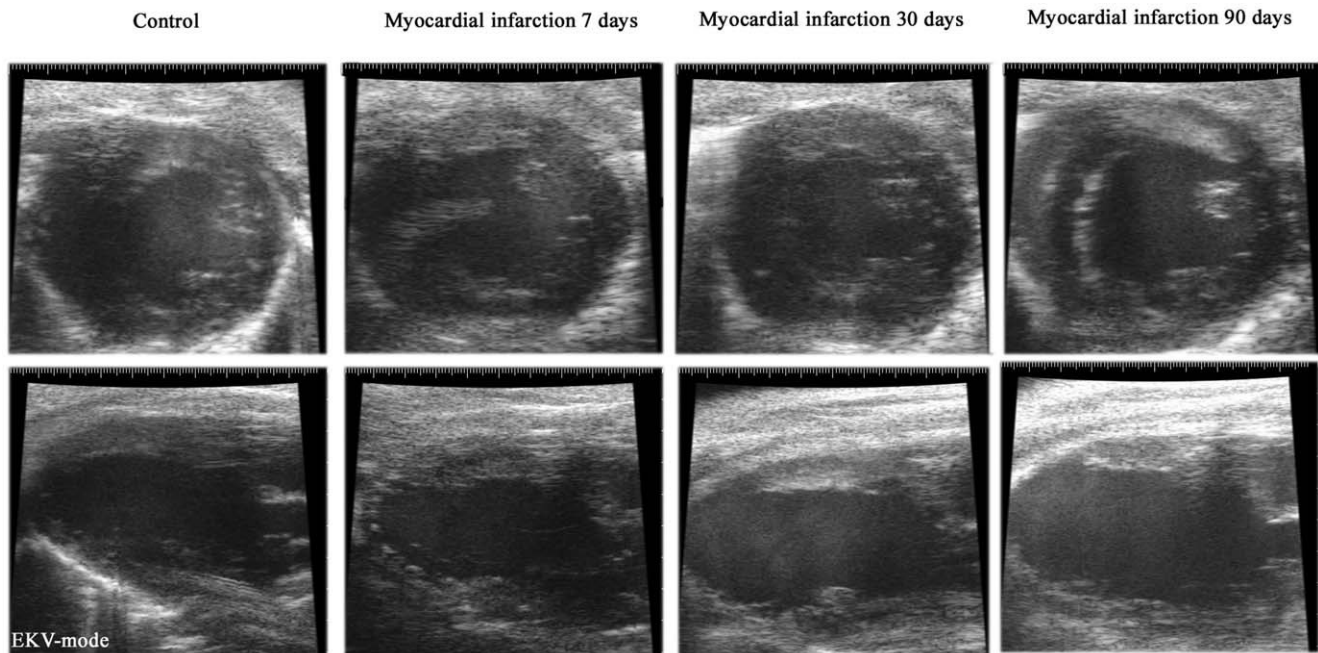
Figure 1. Visualization of the infarction. Sample EKV images at baseline and 7, 30 and 90 days post-infarction. Upper row: Parasternal short-axis views. Lower row: Parasternal long-axis views. The infarcted area is appreciated 7 days post-infarction and is located in the apical region. The evolution of the infarction results in progressive left ventricular remodeling. The videos from which the frames were selected are given as Supplementary material.
doi:10.1371/journal.pone.0041691.g001

Figure 2. LV systolic function. FAC% measured both in parasternal short-axis views and a long-axis view. The FAC% decreased significantly as early as 7 days after myocardial infarction (** indicates statistically significance versus day 0, with $p < 0.001$).
doi:10.1371/journal.pone.0041691.g002

infarction ($p < 0.001$). At apical level (Davi), a marked, statistically significant enlargement ($p < 0.001$) appeared 7 days post-in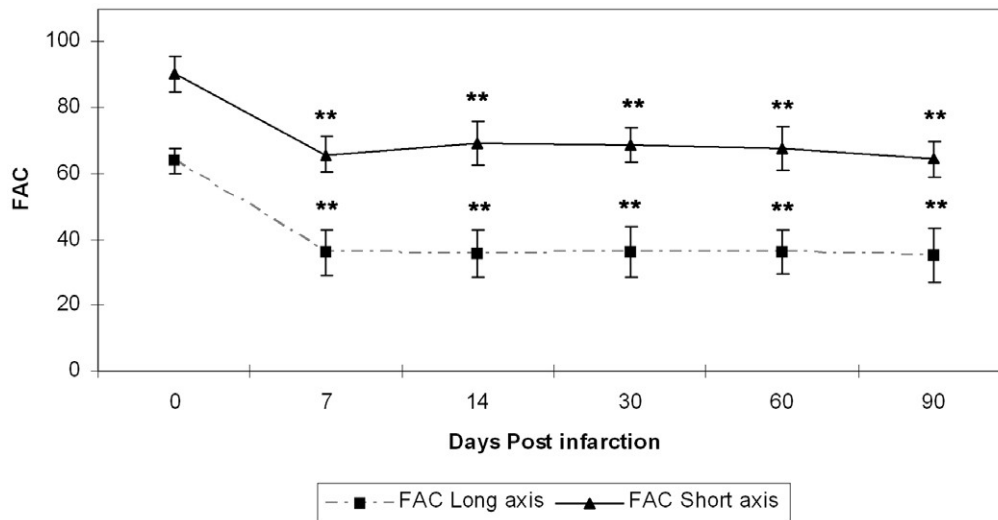farction that continued until the end of the study. Furthermore, the LV end-diastolic and systolic areas -Table 1 (Aread) & Table 1 (Areas)- increased significantly as well, starting 7 days post-infarction ($p < 0.001$) and remained at that level for the rest of the study.

These data indicate that the ventricular dilation extends progressively from the apical origin of the infarction towards healthy myocardial areas, resulting in marked changes of both size and shape. This is clearly visualized in Figure 1, which presents sample EKV images of the LV of one of the animals at baseline and 7, 30 and 90 days post-infarction, both using a mid-level short-axis and a parasternal long-axis view. The corresponding videos are given as Videos S1, S2, S3, S4, S5, S6, S7, and S8. Due to the apical location of the origin of the infarction, the progression of the infarction, i.e. LV remodeling, is not clearly appreciated on the short-axis views (Videos S1, S2, S3, and S4), while it is evident in the long-axis views (Videos S5, S6, S7, and S8).

LV functional analysis. The systolic measurements taken on short axis views at the level of the papillary muscles -Table 2 (EF%

tei, FS% & VcFc)- did not significantly change during the experiment. This is due –as already explained- to the apical origin of the infarctions in our model, and their slow progression towards the middle and baseline levels. That motivated the use of the Simpson's rule to calculate the EF% and the FAC measurements.

The EF% calculated using the Simpson's rule -Table 2 (EF% simp)- shows significant loss of systolic function starting 7 days post-infarction ($p < 0.001$). Confirming this fact, Figure 2 illustrates the evolution of the LV systolic function using the FAC%. Namely, FAC% measured in a short axis view –Table 2 (FAC% short)- decreases significantly ($p < 0.001$) 7 days post-infarction and remains virtually unchanged. This reduction of FAC% was more evident when measured in the parasternal long-axis view –Table 2 (FAC% long)-.

Finally, Table 3 (S′ septal & S′ post) contains the evolution of systolic function measured by tissue Doppler. The systolic tissue velocity S′ is degraded both at the septal basal level (S′ septal) and in the posterior wall (S′ post). This decrease is statistically
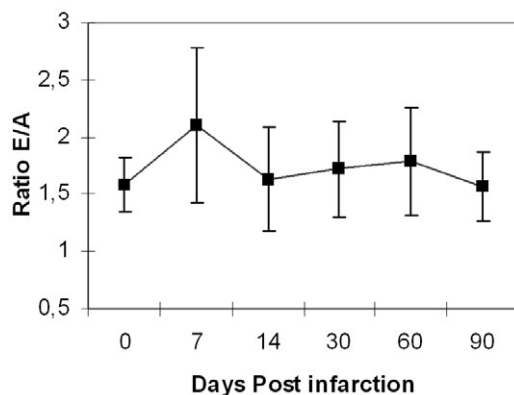

Figure 3. LV diastolic function. Evaluation of diastolic function measured as the E/A ratio calculated using the pulse Doppler wave mode at baseline and 7, 14, 30, 60 and 90 days post-infarction.
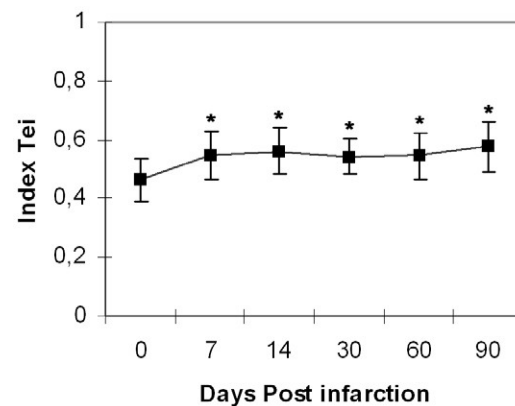doi:10.1371/journal.pone.0041691.g003

Figure 4. LV global cardiac function. Global cardiac dysfunction measured with the Tei Index at base line, 7, 14, 30, 60 and 90 days post-infarction. Changes are significant starting 7 days post-infarction until the end of the experiment (* indicates statistical significance versus day 0, with $p < 0.01$).
doi:10.1371/journal.pone.0041691.g004

significant between 14 and 60 days post-infarction when measured on the septal basal level (p<0.01), but it is only significant 60 days post-infarction when measured on the posterior wall (p = 0.01).

We used the pulsed wave Doppler of the mitral filling to measure diastolic dysfunction. We observed no significant increase of the ratio E/A -Table 4 (E/A) & Figure 3- and unchanged MVDT values (p = 0.405) during the entire duration of the study –Table 4 (MVDT)- . However, the IRVT increased significantly 7 days (p<0.001) post-infarction, and remained at that level until the end of the study (p<0.001), as seen in Table 5 (IVRT).

The Tei Index, used as an indicator of global cardiac function, -Table 6 (Index Tei) & Figure 4- increased significantly 7 days post-infarction (p<0.01) and this increase was maintained until the end of the study (p<0.01).

The tissue Doppler analysis reveals significant deterioration of the diastolic function at the septal basal velocity –Table 6 (E′ septal)-, from 14 to 60 days post infarction (p<0.01), but no significant deterioration based on the posterior velocity –Table 6 (E′ post)-. Finally, the ratio E/E′ –Table 6 (E/E′)- did not present significant changes against the basal values any time during the study.

Correlation between systolic functional changes and tissue remodeling

At the end point of the experiment −90 days post-infarction-, the percentage of infarcted tissue was measured as described in the material and methods section. Figure 5 shows transverse sections of one sample heart, starting at the level of the papillary muscles (leftmost), and ending at the apex (rightmost). The muscle appears light brown-colored while the collagen in red, due to the Sirius red staining. Linear regression analyses demonstrated that the average infarct size measured from the histological sections correlated significantly with the FAC% values calculated in a long-axis view (r = −0.946; R^2 = 0.90; p<0.05). However, the correlation with FAC% calculated in a short-axis view was lower (r = −0.812; R^2 = 0.66), due to the difficulty of obtaining good short-axis views in this specific model.

Discussion

The evaluation of cardiac function in mice has been hampered until this date by technical issues, such us the fast mouse heart rate, the difficulty to obtain clear echocardiographic views of the heart, and the translational motion present during image acquisition [16],[22],[23],[30]. In this study we present a complete structural and functional echocardiographic characterization of LV remodeling in a mouse model of long-term MI. To deal with the first two technical issues we used high-resolution ultrasound equipment dedicated for small animal imaging, which provide high-quality echocardiographic views of the LV of the mouse. In order to better visualize our apically located infarction, we have acquired and performed structural measurements in both parasternal short-axis and long-axis views. High resolution EKV mode images were used whenever necessary to improve the quality of the inherently noisy ultrasound images. Finally, the translational motion was partially compensated by the use of anesthetics.

This study has been carried out in the context of a broader effort aimed at characterizing the long-term effects of stem cell based therapies in post-infarction cardiac remodeling. We will use induced pluripotent stem (IPS) cells derived from DBA/2J cardiomyocytes, which will be injected in the infarcted myocardial areas. To avoid unwanted immunological response, the cells will be injected in infarcted hearts of DBA/2J mice. Previous studies on mouse models of MI were done mostly on C57BL mouse background [11],[19],[21],[30],[31],[32]. Since there is substantial evidence of different responses to MI due to age, sex or genetic background [10] we carried out a complete characterization of our DBA/2J MI based model. The common practice in these type of studies involves monitoring LV remodeling from 4 weeks to 9 weeks after surgery [11],[19], consistent with the general understanding that post-infarction complications can only be prevented very soon after the ischemic episode [27],[33] Instead, we monitor the cardiac function during 90 days after LAD ligation because that is the prospective duration of our cell-based therapy.

We have done a complete characterization of our myocardial infarction model by measuring the untreated progression of the LV systolic, LV diastolic and global cardiac function post MI. Other groups have done similar studies using the same equipment [34],[35],[36], but only used standard measurements. In our model, given the location of the infarction –starting at the ventricular apex and progressing towards the middle ventricle- we have measured the FAC% not only using the standard short-axis views but also in a parasternal long-axis view. Both results reflect marked systolic dysfunction caused by LV remodeling. However, the correlation between FAC% and infarct size estimated from the histology was higher for the FAC% measured in a single long-axis view than when measured in the short-axis views. This is due to the difficulty to obtain LV short-axis views with a clear definition of the entire post-infarction endocardial border, because of the orientation of the heart and the small size of the rib cage [23].

Our analysis of the evolution of FAC% with time shows that systolic dysfunction –visible as early as 7 days after MI- is directly related to the progressive dilation of the LV internal diameter and with the increase of the end-systolic and end-diastolic areas. However, changes in the diastolic function were not so evident, and were only detected using the IVRT. Contrarily, we found no
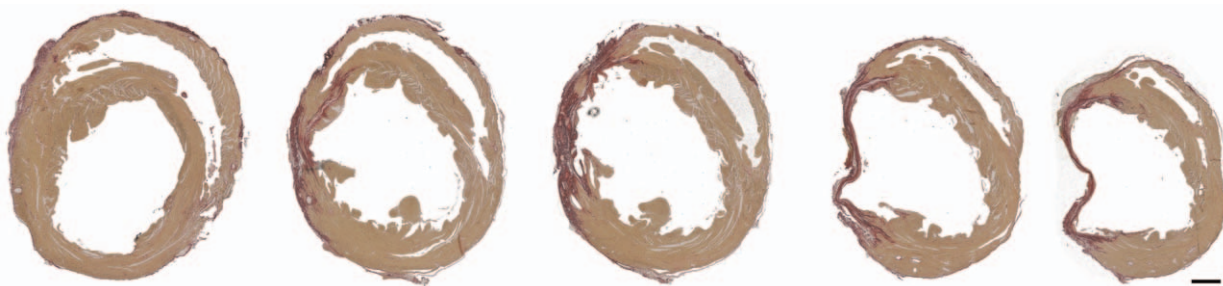

Figure 5. Histological analysis. Transverse sections of a heart 90 days after permanent ligation of the LAD. The sections were approximately taken starting at the level the papillary muscles (leftmost) to the apex (rightmost). The anterolateral myocardium is replaced by a thin fibrous scar tissue. The scale bar represents 1 mm.
doi:10.1371/journal.pone.0041691.g005

significant changes of DT and the ratio E/A, while E′ measured at the posterior wall reflected significant changes only 14 days post-infarction. This is consistent with the findings of recent studies that claim that the isolated analysis of systolic or diastolic function may not be reflective of overall cardiac function [24],[25]. Moreover, it is well know that the common parameters of systolic and diastolic function are influenced by the anesthesia used for the mouse immobilization [22],[23]. Therefore, we also computed the combined myocardial performance Tei Index, which is independent of the heart rate or blood pressure levels. Our measurements confirmed significant impairment of global cardiac function starting 7 days post-infarction.

The measurement of the infarcted area in tissue sections is the common ex-vivo approach to determine the infarct size in animal models [11]. A recent study estimated the infarct size in vivo by calculating the infarct area from sequential B-mode echocardiographic short-axis images in a mouse model of MI, demonstrating significant correlation between the estimated infarct size and the EF% [8]. Takagawa *et al.* [11] reported that infarct size derived from area, length and midline length measurements all reflect the severity of systolic dysfunction. In that line, our linear regression analysis also finds significant correlation between long-axis view FAC% and the histological infarcted size measured as the mean percentage of infarcted area vs. total LV area.

In summary, we have performed a complete characterization of LV remodeling in a mouse model of MI, establishing a valuable control for future pharmacological, cellular or tissue engineering studies of post-infarction cardiac remodeling, such as those reported by us and others [27],[29],[33],[34],[35],[36].

Supporting Information

Figure S1 Pulsed-wave Doppler analysis. Sample Doppler pulsed-wave recordings of the transmitral inflow obtained from LV apical two or four chamber views. The recordings were obtained from the same animal before infarction (top) and 7, 14, 30, 60 and 90 days (bottom) after infarction.
(TIF)

Figure S2 Tissue Doppler analysis. Sample tissue Doppler recordings of the LV septal basal portion of the mitral annulus, taken from a parasternal short-axis view at the level of the papillary muscle. The recordings were obtained from the same animal before infarction (top) and 7, 14, 30, 60 and 90 days (bottom) after infarction.
(TIF)

Figure S3 Tissue processing. A) Rodent heart slicer (Zivic Instruments). The heart is located into the slicer hole and two blades (Stanley) inserted (3 mm separated of each other). Once the blades are partially inserted, they are aligned with another one and simultaneously pressed down until the end. B) Heart blocks. The blades are raised out and the three heart blocks (apical, mid-ventricular and basal) removed.
(TIF)

Table S1 HR: heart rate. **EF% tei**: ejection fraction using Teichholz. **EF% simp**: ejection fraction using Simpson's rule. **FS% tei**: shortening fraction using Teichholz. **FAC% short**: fractional area change measured on a short axis view. **FAC% long**: fractional area change measured on a long axis view. **VcFc**: normalized mean velocity of circumferential fiber shortening. **LVID d**: LV internal diameter (diastole). **LVID s**: LV internal diameter (systole). **CO**: cardiac output. **LV vol d**: LV volume (diastole). **LV vol s**: LV volume (systole) (* indicates statistical significance versus day 0, with $p<0.01$) (** indicates statistical significance versus day 0, with $p<0.001$)
(DOCX)

Video S1 Parasternal short axis sample EKV video recording at baseline.
(AVI)

Video S2 Parasternal short axis sample EKV video recording 7 days post-infarction.
(AVI)

Video S3 Parasternal short axis sample EKV video recording 30 days post-infarction.
(AVI)

Video S4 Parasternal short axis sample EKV video recording 90 days post-infarction.
(AVI)

Video S5 Parasternal long axis sample EKV video recording at baseline.
(AVI)

Video S6 Parasternal long axis sample EKV video recording 7 days post-infarction.
(AVI)

Video S7 Parasternal long axis sample EKV video recording 30 days post-infarction.
(AVI)

Video S8 Parasternal long axis sample EKV video recording 90 days post-infarction.
(AVI)

Author Contributions

Conceived and designed the experiments: COS FP AMB BP. Performed the experiments: CBV OIG BP EA DC. Analyzed the data: CBV BP EA SC AMB DC. Wrote the paper: CBV BP AMB FP COS.

References

1. Rosamond W, Flegal K, Furie K, Go A, Greenlund K, et al. (2008) Heart disease and stroke statistics 2008 update: a report from the American Heart Association Statistics Committee and Stroke Statistics Subcommittee. Circulation 117:e25–146.
2. Roger V, Go A, Lloyd-Jones D, Adams R, Berry J, et al. (2011) Heart disease and stroke statistics 2011 update: a report from the American Heart Association. Circulation 123 (4):e18–209.
3. World Health Organization (2011) The International Journal of Public Health: media centre of cardiovascular diseases, the world health report 2011.
4. Sutton MG, Sharpe N (2000) Left Ventricular Remodeling After Myocardial Infarction: Pathophysiology and Therapy. Circulation 101: 2981–2988.
5. Lang RM, Bierig M, Devereux RB, Flachskampf FA, Foster E, et al. (2005) Recommendation for Chamber Quantification: A report from the American Society of Echocardiography's Guidelines and Standards Committee and the Chamber Quantification Writing Group, Developed in Conjunction with the European Association of Echocardiography, a Branch of the European Society of Cardiology. J Am Soc Echocardiogr 18: 1440–1463.
6. Feigenbaum H (1990) Role of Echocardiography in Acute Myocardial Infarction. Am J Cardiol 66: 17–22.
7. Mor-Avi V, Lang RM, Badano LP, Belohlavek M, Cardim NM, et al. (2011) Current and evolving echocardiographic techniques for the quantitative evaluation of cardiac mechanics: ASE/EAE consensus statement on methodology and indications. J Am Soc Echocardiogr 24: 277–313.
8. Kanno S, Lerner DL, Schuessler RB, Betsuyaku T, Yamada KA, et al. (2002) Echocardiographic evaluation of ventricular remodeling in a mouse model of myocardial infarction. J Am Soc Echocardiogr 15: 601–609.
9. Scherrer-Crosbie M, Kurtz B (2010) Ventricular remodeling and function: insights using murine echocardiography. J Mol Cell Cardiol 48: 512–517.

10. Monassier L, Theodoropoulos C, Sandler R, Constantinesco A (2004) Current mouse models for studying cardiac dysfunctions: technical and imaging aspects. Drug Discov Today 1: 235–241.

11. Takagawa J, Zhang Y, Wong M, Sievers RE, Kapasi NK, et al. (2007) Myocardial infarct size measurement in the mouse chronic infarction model: comparison of area and length –based approaches. J Appl Physiol 102: 2104–2111.

12. Foster FS, Zhang MY, Zhou YQ, Liu G, Mehi J, et al. (2002) A new ultrasound instrument for *in vivo* microimaging of mice. Ultrasound Med Biol 28: 1165–1172.

13. Chin BB, Metzler SD, Lemaire A, Curcio A, Vemulapalli S, et al. (2007) Left ventricular functional assessment in mice: Feasibility of High spatial and Temporal resolution ECG-gated blood pool SPECT. Radiology 245: 440–448.

14. Voelkl JG, Haubner BJ, Kremser C, Mayr A, Klug G, et al. (2011) Cardiac imaging using clinical 1.5T MRI scanners in a murine ischemia/reperfusion model. J Biomed Biotechnol 2011: 185683.

15. Tournoux F, Petersen B, Thibault H, Zou L, Raher MJ, et al. (2011) Validation of noninvasive measurement of cardiac output in mice using echocardiography. J Am Soc Echocardiogr 24: 465–470.

16. Rottman JN, Ni G, Brown M (2007) Echocardiographic evaluation of ventricular function in mice. Echocardiography: A Jrnl Of CV Ultrasound & Allied Tech 24: 1–7.

17. Teichholz LE, Cohen MV, Sonnenblick EH, Gorlin R (1974) Study of Left Ventricular Geometry and Function by B-scan Ultrasonography in Patients with and without Asynergy. N Engl J Med 291: 1220–1226.

18. Ino T, Benson LN, Mikalian H, Freedom RM, Rowel RD (1989) Determination of left ventricular volumes by Simpson's rule in infants and children with congenital heart disease. Br Heart J 61: 182–185.

19. Gao XM, Dart AM, Dewar E, Jennings G, Du XJ (2000) Serial echocardiographic assessment of the left ventricular dimensions and function after myocardial infarction in mice. Cardiovasc Res 45: 330–338.

20. Domanski MJ, Cunnion RE, Roberts WC (1992) Analysis of fractional area change at various levels in the normal left ventricle. Am J Cardiol 70: 1367–1368.

21. Schaefer A, Meyer GP, Hilfiker-Kleiner D, Brand B, Drexler H, et al. (2005) Evaluation of Tissue Doppler Tei Index for global left ventricular function in mice after myocardial infarction: Comparison with Pulsed Doppler Tei Index. Eur J Echocardiography 6: 367–375.

22. Stypmann J (2007) Doppler Ultrasound in Mice. Echocardiography 24: 97–112.

23. Scherrer-Crosbie, Thibault HB (2008) Echocardiography in translation research: Of mice and men. J Am Soc Echocardiogr 21: 1083–1092.

24. Parthenakis FI, Kanakaraki MK, Kanoupakis EM, Skalidis EI, et al. (2002) Value of Doppler index combining systolic and diastolic myocardial perfor-mance in predicting cardiopulmonary exercise capacity in patients with congestive heart failure: effects of Dobutamine. Chest 121: 1935–1941.

25. Tei C, Ling LH, Hodge DO, Bailey KR, Oh JK, et al. (1995) New index of combined systolic and diastolic myocardial performance: a simple and reproducible measure of cardiac function—a study in normal and dilated cardiomyopathy. J Cardiol 26: 357–366.

26. Bruch C, Schmermund A, Marin D, Katz M, Bartel T, et al. (2000) Tei-Index in patients with mild to moderate congestive heart failure. Eur Heart J 21: 1888–1895.

27. Pelacho B, Nakamura Y, Zhang J, Ross J, Heremans Y, et al. (2007) Multipoint adult progenitor cell transplantation increases vascularity and improves left ventricular function after myocardial infarction. J Tissue Eng Regen Med 1: 51–59.

28. Kiessling F, Bernd P (2011). Small Animal Imaging: Basics and Practical Guide. Berlin: Springer.

29. Formiga FR, Pelacho B, Garbayo E, Abizanda G, Gavira JJ, et al. (2010) Sustained release of VEGF through PLGA microparticles improves vasculogenesis and tissue remodeling in an acute myocardial ischemia-reperfusion model. J Control Release 147: 30–37.

30. Syed F, Diwan A, Hahn HS (2005) Murine Echocardiography: A practical approach for phenotyping genetically manipulated and surgically modeled mice. J Am Soc Echocardiogr 18: 982–990.

31. Scherrer-Crosbie M, Steudedl W, Ulrich R, Liel-Cohen N, Newell J, et al. (1999) Echocardiographic determination of risk area size in a murine model of myocardial ischemia. Am J Physiol 277: 86–92.

32. Salto-Tellez M, Yung Lim S, El-Oakley RM, Tang TP, ALmsherqi ZA, et al. (2004) Myocardial infarction in the C57BL/6J mouse. A quantifiable and highly reproducible experimental model. Cardiovasc Pathol 13: 91–97.

33. Mazo M, Gavira J, Abizanda G, Moreno C, Ecay M, et al. (2010) Transplantation of Mesenchymal Stem Cells exerts a greater long-term effect than bone marrow mononuclear cells in a chronic myocardial infarction model in rat. Cell Transplant 19: 313–328.

34. Katare R, Caporali A, Emanueli C, Madeddu P (2010) Benfotiamine improves functional recovery of the infarcted heart via activation of pro-survival G6PD/Akt signaling pathway and modulation of neurohormonal response. J Mol Cell Cardiol 49: 625–638.

35. Quian A, Huang Y, Spencer CI, Foley A, Vendatham V, et al. (2012) *In vivo* reprogramming of murine cardiac fibroblasts into induced cardiomyocytes. Nature *In Press.*

36. Meloni M, Caporali A, Graiani G, Lagrasta C, Katare R, et al. (2012) Nerve growth factor promotes cardiac repair following myocardial infarction. Circ Res 106: 1275–1284.

INDUCED PLURIPOTENT STEM CELLS AS A NEW STRATEGY FOR CARDIAC REGENERATION AND DISEASE MODELING

Olalla Iglesias-García[1], Beatriz Pelacho[1] and Felipe Prósper[1]

[1]Hematology and Cell Therapy and Foundation for Applied Medical Research, Clínica Universitaria, University of Navarra, Spain

Address for Correspondence:
Felipe Prósper MD
Hematology and Cell Therapy
Clínica Universidad de Navarra
Av. Pío XII 36, Pamplona 31008,
Navarra, Spain
Phone 34 948 255400 Fax 34 948 296500
e-mail: fprosper@unav.es

Abstract

The possibility to induce pluripotency in somatic cells or, even further, to induce cell transdifferentiation through the forced expression of reprogramming factors, has offered new attractive options for cardiovascular regenerative medicine. Thus, induced pluripotent stem cells (iPS cells) can be differentiated towards cardiomyocytes, a key cell type for cardiac regeneration, representing an ideal cell source for modeling cardiac human diseases and for a personalized regenerative cell therapy. The current article pretends to give an overview of the iPS cells features and differentiation capability, together with the methods already described for inducing their specification towards a cardiovascular phenotype. Also, *in vivo* studies performed to determine the therapeutic potential of iPS-derived cardiac cells will be discussed. Emerging studies for modeling several genetic cardiac disorders with iPS-derived cells will be finally described, as they can offer an excellent tool for drug testing and future patient-specific treatment.

1. Introduction

Cardiovascular disease is the leading cause of morbidity and mortality worldwide. It represents approximately 30% of all deaths, with nearly half resulting from myocardial infarction (MI) [1]. Fortunately, medical advances at the pharmacological, interventional, and surgical levels have significantly decreased the rate of mortality at the acute stage of the disease and have prolonged life expectancy. In spite of this remarkable progress, current treatment strategies have been unable to regenerate the diseased heart or provide a definitive cure. However, recent stem cell research has offered new hope that protective and regenerative therapies are possible (reviewed in [2]). Nevertheless, despite reports of successful *in vitro* differentiation of adult stem cells into cardiovascular lineages, only a few studies have demonstrated *in vivo* differentiation towards cardiomyocytes (CMs), particularly those derived from cardiac tissue [3, 4]. It has been hypothesized that the principal mechanism of heart tissue regeneration involves replication and differentiation of cardiac progenitor cells (CPCs). The differentiation potential of CPCs to cardiac and vascular cells (*in vitro* and *in vivo*) has been demonstrated, along with their therapeutic potential following implantation into infarcted hearts of mice, which contributed to preservation of cardiac function and tissue viability [5-7]. However, despite these positive *in vivo* effects, CPCs were found to display limited potential for self-renewal and differentiation into CMs. Thus, their therapeutic benefits have been mainly attributed to release of complementary paracrine factors. Furthermore, the regenerative role of CPCs was recently challenged after pulse-chase studies demonstrated that pre-existing adult CMs were the dominant source of heart cell replacement during myocardial homeostasis and injury [8].

Although human embryonic stem cells (ESCs) have shown the greatest cardiac differentiation potential [9], their clinical use has been hampered by important limitations, including their potential tumori- and immunogenic properties as well as ethical issues related to their origin. For this reason, the discovery of so-called induced pluripotent stem (iPS) cells [10], which closely resemble ESCs and can be easily derived from adult cells, has provided an exciting alternative for bypassing these ethical and immunogenic concerns. In this review, we provide a detailed discussion of the origin, characteristics, and differentiation potential of iPS cells.

2. Discovery and derivation of iPS cells

The cell differentiation process was once believed to be irreversible. However, in 2006, the novel generation of embryonic stem-like cells from somatic cells resulting in iPS cells, was reported by the laboratory of Dr. Yamanaka, a finding that resulted in a Nobel Prize in 2012

[10]. In order to produce iPS cells from adult mouse fibroblasts, cell de-differentiation was induced through retroviral transduction of several factors involved in pluripotency and self-renewal of ESCs. Initially, a total of 24 genes were selected and over-expressed in various combinations in order to identify those that might participate in cell reprogramming, which was ultimately found to depend on only four of the factors: Oct3/4, Klf-4, Sox-2, and c-Myc (OSKM). One year later, human iPS (hiPS) generation was also described by using the same combination of factors [11] or a different one (Oct3/4, Sox-2, Nanog, and Lin-28) [12]. Following these studies, efforts to simplify the reprogramming process and to minimize the risk of chromosomal disruption revealed that a reduced set of reprogramming factors was sufficient to generate iPS cells (reviewed in [13]). Moreover, due to safety concerns surrounding spontaneous reactivation of viral transgenes or possible oncogene activation via lentiviral insertion, alternative iPS generation strategies have been developed and tested. These have involved the use of adenoviruses, RNA-based Sendai viruses, episomal vectors, DNA plasmids, excisable vectors, mRNAs, microRNAs, or even proteins (reviewed in [14]). Recently, the use of genetic factors, chemical inhibitors, and signaling molecules that can either replace core reprogramming factors or enhance reprogramming efficiency has also been investigated (reviewed in [15]).

Collectively, *in vitro* and *in vivo* studies have indicated that, like ESCs, iPS cells have the capacity to differentiate into cell types derived from any of the three germ layers. Indeed, this wide differentiation potential was confirmed through injection of iPS cells into either immunosuppressed mice to generate teratomas or into embryos to produce chimeras [16]. Also, the protocol developed for iPS cell generation has proved to be quite reproducible. iPS cells have already been derived from many species, including humans, non-human primates, pigs, rats and mice, that share among them common pluripotency features but that similarly to ESCs and depending on the specie of origin, differ in others like phenotype, morphology and culture condition requirements. Thus, activation of the LIF-JAK-STAT pathway is required for mouse ESC and iPS self-renewal [17], being the leukemia inhibitory factor (LIF) [18] and the bone morphogenetic proteins (BMPs) [19] indispensable for cell culture and pluripotency maintenance. In contrast, fibroblast growth factor-2 (FGF2) and Nodal/Activin signaling pathways have been found to be neccesary for human ESC and iPS maintenance [11, 20], being the human iPS media usually supplemented with FGF2 for an adequate culture of the pluripotent stem cells [11, 21].

In addition, several cell types like adult β-pancreatic cells, neurons, keratinocytes and hepatocytes and hematopoietic, neural and adipose stem cells, among others, have been successfully used to produce iPS cells, demonstrating the striking plasticity of cells, independently of their origin and differentiation stage (reviewed in [13]).

3. Genetic and epigenetic profiles of iPS cells

Despite initial excitement regarding the ES-like features of iPS cells, deeper molecular analysis revealed differences between iPS cells and ESCs, mainly relating to aberrant gene expression [22]. In particular, incomplete silencing of somatic genes in reprogrammed cells, weak activation of ESC specific pluripotency genes, and non-specific aberrations (distinct from either the cell of origin or ESCs) have been detected. Also, comparison of methylation marks in ESC and iPS cell genomes revealed significant variations. Similarly, consistent differences have been observed in miRNA expression patterns between hESCs and hiPS cells [23]. Furthermore, two studies comparing global gene expression profiles in ESCs and iPS cells consistently identified the persistence of donor cell gene activation in iPS cells [24, 25]. It has been suggested that this aberrant expression could lead to immune responses even after autologous transplantation. In fact, recent work from Zhao and collaborators demonstrated that ESCs derived from C57/B6 mice induced teratoma formation without any evidence of immune responses, whereas iPS cells derived from the same mouse strain failed to form teratomas due to rapid, T cell-dependent rejection. Moreover, global gene expression analyses of ESC- and iPS cell-derived teratomas revealed overexpression of teratoma-related genes in the iPS cells, which were responsible for the immune rejection [26]. However, these findings are now controversial after a recent study observed very limited immunogenicity of skin and bone marrow-derived iPS cells transplanted into mice. It was found that the immunogenicity of ten iPS cell clones was similar to that of seven different ESC clone-derived cells, and that stable skin and bone marrow grafts derived from iPS cells formed without evidence of rejection [27].

4. Differentiation potential of iPS cells

Numerous protocols, most of them based on previous ESC techniques, have been used to differentiate iPS cells into diverse cell types *in vitro* (reviewed in [28]), demonstrating their pluripotency. Also, their *in vivo* differentiation potential has been confirmed in several animal models. For example, rat iPS cells were used to generate rat pancreas when injected into mouse blastocysts that were deficient in an essential gene required for pancreas development

[29]. Additionally, when undifferentiated iPS cells were transplanted into an ischemic rodent heart, they efficiently differentiated into cardiac and vascular cells [30]. However, despite the proven pluripotency of iPS cells, differentiation patterns can be influenced by the origin and epigenetic characteristics of the derived iPS cells, thus leading to preferential differentiation into specific cell types. Although the molecular mechanisms for this phenomenon remain ill defined, it has been proposed that iPS cells can retain residual DNA methylation signatures characteristic of their somatic tissue of origin, which can favor their differentiation towards lineages related to the donor cell [31]. In an interesting study from Dr. Polo and colleagues, it was found that iPS cells generated from tail tip fibroblasts, splenic B cells, bone marrow-derived granulocytes, and skeletal muscle precursors exhibited gene expression patterns related to their origin, suggesting that iPS cells retain a transcriptional memory of their previous state of differentiation [31]. Recently, it was demonstrated that iPS cells generated from human pancreatic islet β-cells more efficiently differentiated (*in vitro* and *in vivo*) into insulin-producing cells than ESCs and isogenic non-β-cells, corresponding with the fact that β-cell-derived iPS cells maintained open chromatin structure at key β-cell genes [32]. In light of these findings, it might be possible to optimize cell lineage differentiation based on the source of iPS cells. Thus, in order to tailor this technology to each specific application, it may be necessary to elucidate the best way to select iPS cell lines for specific differentiation procedures.

5. Cardiomyocyte differentiation from pluripotent stem cells

Efficient generation of cardiac cells represents a key goal in the therapeutic application of stem cells in cardiovascular disease. Despite the proven differentiation capacity of many stem cell populations towards different lineages (including vascular cells), a direct contribution to the cardiac tissue has been only shown for few populations, namely ESC, the cardiac progenitors present in the heart and the iPS cells. Taking into account the immunogenic and ethical concerns of the ESC and the still existing technical limitations to isolate cardiac stem cells with a robust cardiac differentiation potential, the iPS constitute a promising cell source for future myocardial regenerative therapies. Indeed, it has already been shown that mouse, human, and pig iPS cells can spontaneously differentiate into CMs that present similar gene expression patterns and functional properties as ESC-derived CMs [33]. Also, the contribution of undifferentiated iPS cells to cardiac tissue has been shown *in vivo* [30]. However, as might be anticipated, these cells also exerted a tumorigenic potential due to their embryonic characteristics [30]. To bypass this serious limitation, cardiac cells were derived from iPS

cells *in vitro* in order to enrich the cardiac population and then injected into the heart [34]. In general, these transplanted cells remained within the infarcted heart and decrease cardiac remodeling after ischemic damage. Importantly, no tumor formation has been reported; however, very careful long-term studies will be required to confirm this. Moreover, together with CMs, vascular cells can also participate in heart regeneration. By using differentiation protocols established for ESCs, recent studies have demonstrated the capacity of iPS cells to differentiate into endothelial cells (ECs) and smooth muscle cells (SMCs), contributing to heart repair by forming new blood vessels [35, 36]. On the other hand, iPS-derived cardiovascular progenitors might represent a promising alternative source for cardiac repair. Indeed, iPS cell-derived fetal liver kinase-1 (Flk-1)$^{+}$ progenitor cells have been produced *in vitro* [35, 37], and they were shown to improve cardiac function *in vivo* in a mouse model of acute MI [38]. Also, a population of iPS cell-derived progenitor cells enriched for the LIM-homeobox transcription factor islet-1 (Isl1) were shown to survive after transplantation into infarcted hearts and to differentiate into CMs, ECs, and SMCs [39]. For future clinical use, very stringent conditions for cardiovascular cell selection will need to be implemented prior to contemplating their application in patients. Also, optimization of existing *in vitro* and *in vivo* protocols for cardiac differentiation will be required, as iPS cell-derived CMs have been shown to present poor levels of maturation with high inter-line variability [40].

6. Enhancing cardiac differentiation with cytokines and small molecules

Many protocols have been used to specifically induce cardiac differentiation in ESCs, and these methods were later applied to iPS cell specification. Initially, co-culture with an endoderm-like cell line (END-2) was reported as an effective manner for deriving CMs since the endoderm plays an inductive role in the differentiation of the mesoderm-derived cardiac cells [41]. Also, to emulate embryonic development, stem cells have been sequentially treated with specific growth factors that drive the different steps of heart formation. In this regard, combinations of Activin A and FGF2 [42] or bone morphogenetic protein-4 (BMP4) and FGF2 [43] have been used to induce cardiac differentiation in hESCs and hiPS cell lines. Similarly, hiPS cells have been successfully differentiated into CMs following treatment with Activin A, BMP4, FGF2, and ascorbic acid [34]. Elliot and co-workers also demonstrated a highly efficient cardiac differentiation protocol for hESCs that used BMP4 and Activin A in combination with Wnt3a, stem cell factor (SCF or KITLG), and vascular endothelial growth factor (VEGF) [44]. In addition, sequential application of some of these factors (Activin A, BMP4, and FGF2) to a monolayer of hESCs and hiPS cells cultured over matrigel was highly

effective for inducing cardiac differentiation [45]. Also, other growth factors, such as BMP2 and FGF10, were shown to enhance cardiac differentiation in both ESCs and iPS cells [46, 47]. In contrast, inhibition of BMP signaling was also reported to induce CM differentiation from mouse ESCs [48], suggesting that transient suppression of BMP signaling might be necessary during CM specification. Furthermore, manipulation of the Wnt/β-catenin signaling pathway, which is required for mesoderm formation and heart development, can induce cardiac specification. In fact, activation of Wnt/β-catenin signaling with glycogen synthase kinase-3 (GSK3) inhibitors, such as CHIR99021 (CH), has been reported to promote cardiac differentiation of hESCs and hiPS cells [49]. Interestingly, inhibition of the Wnt pathway by late addition of the Wnt signaling inhibitors, IWR-1 or IWP-4, can also induce cardiac specification in hiPS cells [50, 51]. Distinct temporal actions of the Wnt/β-catenin pathway might explain these apparently contradictory results, with early activation required for cardiac differentiation, and inhibition needed for later specification of cardiac precursors [52-54]. The biphasic role of transforming growth factor-β (TGFβ) has also been studied. Inhibition of TGFβ/activin/Nodal and BMP signaling, using the molecules SB431542 and dorsomorphin [55], promoted cardiac differentiation in ESCs and iPS cell lines, whereas an early inhibition of TGFβ signaling produced complete inhibition of cardiac differentiation in ESCs [56, 57]. On the other hand, sustained inhibition of Notch signaling using the γ-secretase inhibitor (GSI), promoted cardiac mesoderm specification [58]. Finally, ascorbic acid [59], dimethyl sulfoxide (DMSO) [60], granulocyte colony-stimulating factor (G-CSF) [61], and cyclosporin-A [62] have all been shown to enhance the generation of CMs in mouse and human pluripotent stem cells.

7. Cardiomyocytes derivation by partial and direct reprogramming

Even though methods for safe and efficient iPS cells derivation are being rapidly developed, their tumorigenic potential remains as a major limitation for clinical applications. Overcoming this problem will require careful optimization of methods for differentiation, isolation, and/or characterization of the cells to be transplanted. In this regard, a protocol allowing differentiation of murine embryonic fibroblasts into CMs through an initial partial de-differentiation proved to be a fast and efficient manner for cardiac cell production (Figure 1), and was first described by Dr. Efe and coworkers. Briefly, fibroblasts were transduced with four reprogramming factors (OSKM) and cultured in reprogramming media (without leukemia inhibitory factor [LIF] and with an inhibitor of the JAK–STAT signaling pathway) for nine days before they were induced for cardiac differentiation via BMP4 treatment [63].

Thus, using this unique strategy, induction of a transitory or partial undifferentiated state favored cell specification towards a particular differentiated cell type. However, this method presents a potential risk for acquiring a pluripotent state with tumorigenic potential. Therefore, a third option has been tested, involving the direct reprogramming of a somatic cell into an alternative adult cell without initially inducing total or partial cell dedifferentiation. Notably, reprogramming of fibroblasts into functional ECs has also been recently reported. Human fibroblasts were transduced with OSKM reprogramming factors for four days and then treated with VEGF to induce endothelial differentiation. Interestingly, increased angiogenesis and blood flow was observed after their transplantation in a hindlimb ischemic mouse model [64]. Moreover, direct transdifferentiation of mouse mesoderm into beating CMs was achieved through over-expression of two transcription factors, Gata-4 and Tbx5, and a cardiac-specific subunit of the BAF chromatin-remodeling complex, Baf60c [65]. Additionally, a recent report has described successful *in vitro* transdifferentiation of somatic cells into functional CMs [66]. For this, Dr. Srivastava and colleagues found that over-expression of only three transcription factors (Gata-4, Mef2c, and Tbx5) in cardiac or dermal fibroblasts was sufficient for reprogramming into CMs (Figure 1). Importantly, this capacity was recently confirmed *in vivo* following local delivery of these three transcription factors in a murine model of MI [67], and the effect was enhanced by addition of thymosin β4 [68]. Fibroblast-derived cells expressed CM markers, showed sarcomeric organization, became binucleated, presented contractile potential, and were electrically coupled. Moreover, a smaller infarct size and improved cardiac function was detected in the treated animals three months post-infarction. Similarly, *in vivo* reprogramming of endogenous cardiac fibroblasts into CMs was also recently reported after overexpression of Gata-4, Hand2, Mef2c and Tbx5 [69]. Although this new approach holds promise, it might require optimization since a recent study found that CMs generated using this technique (with Gata-4, Mef2c, and Tbx5) failed to express typical cardiac genes, showed incomplete functional maturation, and displayed poor survival after transplantation in a model of MI [70]. Finally, microRNA-mediated transdifferentiation is also plausible. A single transfection of the mirRNAs 1, 133, 20, and 499 was shown to directly convert cardiac fibroblasts into CMs. Moreover, this was demonstrated both *in vitro* and *in vivo*, following delivery of these mirRNAs to ischemic mouse myocardium. The resulting CMs showed expression of typical mature cardiac markers, sarcomeric organization, and exhibited spontaneous calcium transients [71]. Taken together, these findings are extremely encouraging as they offer the possibility of reprogramming heart

endogenous fibroblasts into functional CMs. However, the efficiency of direct reprogramming remains very low and must be improved for future regenerative use.

8. iPS cells for application in cardiac disease

Despite the unquestionable scientific and therapeutic potential of iPS cells, additional research and optimization will be required to enable future clinical application of this technology. In fact, it is essential that we acquire a deeper understanding of technical and biological aspects related to iPS cells generation and differentiation and standardization of cell transdifferentiation protocols, as well as the complex genetic and epigenetic mechanisms of cell reprogramming. Furthermore, it has become clear that combining these therapies with tissue engineering techniques, allowing the creation of cell sheets and patches, can increase stem cell survival and boost therapeutic action (reviewed in [72]). Indeed, creation of human cardiac cell sheets using hiPS cells was recently reported, and hiPS derived-CM sheets displayed spontaneous and synchronous beating and electrical transmission between cell layers [73]. Moreover, transplantation of stem cell populations within bioengineered scaffolds has led to greater improvement of cardiac function in animal MI models and has even allowed for the generation of engineered human cardiac tissue. In addition, three-dimensional (3D) human cardiac tissue patches, which were generated by combining collagen type I and hESC- and hiPS-derived CMs, were recently reported [74]. Notably, CMs showed alignment and proliferation within the collagen 3D matrix when subjected to mechanical stress. Also, formation of a vascular network within the bioengineered human cardiac tissue was demonstrated when ECs and stromal cells were co-cultured with the CMs. Moreover, when cardiac constructs were transplanted into immunodeficient rat hearts, the human myocardium survived and formed grafts that closely resembled the host myocardium. The functional benefit obtained from use of iPS-derived cardiac tissue has been demonstrated in mouse [75] and pig [76] models of MI. In fact, Dai and colleagues showed the efficacy of transplanting a tricell patch containing iPS-derived CMs, ECs, and mouse embryonic fibroblasts in an infarcted mouse model, which led to improved cardiac function and attenuated the degree of adverse tissue remodeling and fibrosis [75]. Interestingly, the therapeutic benefit of hiPS cell-derived CM sheets in a porcine model of MI was also reported [76], resulting in significantly improved cardiac function and attenuated left ventricular remodeling following ischemic damage. Importantly, few surviving cells were found when hiPS cell-derived CM grafts were monitored eight weeks after transplantation, and no teratoma formation was observed. This report suggests that iPS cell-derived cardiac tissue could be therapeutically effective and safe

for use in regenerative therapy. Therefore, combining different cell populations and using tissue-engineering platforms might result in improved engraftment and survival of the transplanted cells, subsequently boosting their therapeutic effects. Further experiments will be needed to analyze the functional integration of iPS cell-derived CMs into recipient myocardium, ensuring electrophysiological compatibility of the cardiac cells and adequate microvessel development for proper perfusion. In this regard, the mechanical integration of hESC-derived CMs in a pig model of MI indicated that cell integration with host cardiac tissue was apparent at 28 days after transplantation [77]. Notably, these stable grafts partially remuscularized injured pig hearts, preserved cardiac function, and significantly reduced arrhythmia susceptibility. Moreover, the grafts were supplied by host-derived neovessels that contained erythrocytes, which indicated perfusion by host coronary circulation. Also, the presence of gap junctions between hESC-derived CMs and host CMs demonstrated their mechanical integration after transplantation.

9. iPS cells for cardiac disease modeling and drug discovery

In addition to their regenerative capacity, iPS cells constitute an important tool for modeling cardiac disease, allowing us to study the molecular mechanisms involved in cardiac syndromes and to test specific drug targets (reviewed in [78]). In fact, the generation of iPS cells from patients having genetic cardiac disorders, has already been shown. For instance, iPS cells have been derived from patients with LEOPARD syndrome, and the *in vitro*-derived CMs presented the disease phenotype [79]. Also, hiPS cell-derived CMs from patients with long-QT syndrome displayed the characteristic electrophysiological signatures of the disease [80-83]. Similar findings were observed for human iPS cell-derived CMs from patients with familial dilated cardiomyopathy and Brugada syndrome [84, 85]. Using these cells as a model, studies have analyzed the potential therapeutic efficacy of drugs or small molecules for correcting cardiac disease phenotypes. In this regard, it was reported that CMs derived from long-QT syndrome iPS cells were susceptible to catecholamine-induced tachyarrhythmia, and that the effects of isoprenaline, which exacerbated the disease phenotype, could be attenuated by treatment with β-adrenergic receptor blocker [80]. Moreover, type-II long-QT syndrome has also been modeled using iPS-derived CMs [81], which were used to evaluate the therapeutic potency of existing and new pharmacological agents. It was identified that the long-QT behavior of the CMs was aggravated by potassium channel blockers, whereas nifedipine (a calcium channel blocker) and pinacidil (an agonist of ATP-sensitive potassium channels) ameliorated the long-QT syndrome phenotype, as shown

by decreased duration of action potentials and elimination of arrhythmias. Finally, catecholaminergic polymorphic ventricular tachycardia (CPVT) was also studied using hiPS cells, and the arrhythmogenic disease phenotype could be abrogated following treatment with dantrolene, a drug effective on malignant hyperthermia [86]. Thus, important advances are likely to stem from the use of iPS cell-related disease models, which can be utilized to study mechanisms of cardiac pathogenesis, to identify cardiotoxic effects of drugs, and to characterize the protective effects or optimal doses of therapeutic agents.

10. Conclusions

The ability to induce a pluripotent state in somatic cells offers attractive new therapeutic options and provides possible tools for obtaining a deeper understanding of human disease. Although the use of iPS cells seems ideal for regenerative medicine, there are many aspects of this technology that need to be improved and assessed before clinical application becomes a reality (Figure 2). Indeed, optimization of non-integrative methods for cell reprogramming, cell differentiation/selection protocols, and *in vivo* functionality will be required prior to clinical translation of these techniques. In this regard, direct reprogramming or transdifferentiation strategies, which can allow generation of progenitors and mature cells from human somatic cells without establishing initial pluripotency, might lead to safer protocols. These approaches could avoid the danger associated with residual pluripotent stem cells that are capable of forming teratomas. In any case, greater efforts should be made to improve current standard approaches and to better understand the molecular processes involved in cell reprogramming. Furthermore, new bioengineering strategies could increase the efficacy of iPS cell-derived transplants by improving their engraftment, survival, and functionality in tissues. Also these techniques offer the possibility of creating tissue patches *in vitro* that could be transplanted into injured organs to mediate repair. Finally, this technology can be used to generate reproducible systems that model patient-specific disease, facilitating drug screening and target validation.

Taken together, the reprogramming of somatic cells into iPS cells offers exciting new tools that can be used to gain molecular insight into cardiac diseases and the potential to develop novel regenerative therapies.

DISCLOSURES

None declared

References

[1] Go AS, Mozaffarian D, Roger VL, Benjamin EJ, Berry JD, Borden WB, et al. Heart Disease and Stroke Statistics--2013 Update: A Report From the American Heart Association. Circulation. 2013 Jan 1; 127(1): e6-e245.

[2] Passier R, van Laake LW, Mummery CL. Stem-cell-based therapy and lessons from the heart. Nature. 2008 May 15; 453(7193): 322-9.

[3] Beltrami AP, Barlucchi L, Torella D, Baker M, Limana F, Chimenti S, et al. Adult cardiac stem cells are multipotent and support myocardial regeneration. Cell. 2003 Sep 19; 114(6): 763-76.

[4] Hsieh PC, Segers VF, Davis ME, MacGillivray C, Gannon J, Molkentin JD, et al. Evidence from a genetic fate-mapping study that stem cells refresh adult mammalian cardiomyocytes after injury. Nat Med. 2007 Aug; 13(8): 970-4.

[5] Winter EM, van Oorschot AA, Hogers B, van der Graaf LM, Doevendans PA, Poelmann RE, et al. A new direction for cardiac regeneration therapy: application of synergistically acting epicardium-derived cells and cardiomyocyte progenitor cells. Circ Heart Fail. 2009 Nov; 2(6): 643-53.

[6] Tang XL, Rokosh G, Sanganalmath SK, Yuan F, Sato H, Mu J, et al. Intracoronary administration of cardiac progenitor cells alleviates left ventricular dysfunction in rats with a 30-day-old infarction. Circulation. 2010 Jan 19; 121(2): 293-305.

[7] Bolli R, Chugh AR, D'Amario D, Loughran JH, Stoddard MF, Ikram S, et al. Cardiac stem cells in patients with ischaemic cardiomyopathy (SCIPIO): initial results of a randomised phase 1 trial. Lancet. 2011 Nov 26; 378(9806): 1847-57.

[8] Senyo SE, Steinhauser ML, Pizzimenti CL, Yang VK, Cai L, Wang M, et al. Mammalian heart renewal by pre-existing cardiomyocytes. Nature. 2013 Jan 17; 493(7432): 433-6.

[9] Laflamme MA, Chen KY, Naumova AV, Muskheli V, Fugate JA, Dupras SK, et al. Cardiomyocytes derived from human embryonic stem cells in pro-survival factors enhance function of infarcted rat hearts. Nat Biotechnol. 2007 Sep; 25(9): 1015-24.

[10] Takahashi K, Yamanaka S. Induction of pluripotent stem cells from mouse embryonic and adult fibroblast cultures by defined factors. Cell. 2006 Aug 25; 126(4): 663-76.

[11] Takahashi K, Tanabe K, Ohnuki M, Narita M, Ichisaka T, Tomoda K, et al. Induction of pluripotent stem cells from adult human fibroblasts by defined factors. Cell. 2007 Nov 30; 131(5): 861-72.

[12] Yu J, Vodyanik MA, Smuga-Otto K, Antosiewicz-Bourget J, Frane JL, Tian S, et al. Induced pluripotent stem cell lines derived from human somatic cells. Science. 2007 Dec 21; 318(5858): 1917-20.

[13] Stadtfeld M, Hochedlinger K. Induced pluripotency: history, mechanisms, and applications. Genes Dev. 2010 Oct 15; 24(20): 2239-63.

[14] Robinton DA, Daley GQ. The promise of induced pluripotent stem cells in research and therapy. Nature. 2012 Jan 19; 481(7381): 295-305.

[15] Feng B, Ng JH, Heng JC, Ng HH. Molecules that promote or enhance reprogramming of somatic cells to induced pluripotent stem cells. Cell Stem Cell. 2009 Apr 3; 4(4): 301-12.

[16] Okita K, Ichisaka T, Yamanaka S. Generation of germline-competent induced pluripotent stem cells. Nature. 2007 Jul 19; 448(7151): 313-7.

[17] Niwa H, Burdon T, Chambers I, Smith A. Self-renewal of pluripotent embryonic stem cells is mediated via activation of STAT3. Genes Dev. 1998 Jul 1; 12(13): 2048-60.

[18] Williams RL, Hilton DJ, Pease S, Willson TA, Stewart CL, Gearing DP, et al. Myeloid leukaemia inhibitory factor maintains the developmental potential of embryonic stem cells. Nature. 1988 Dec 15; 336(6200): 684-7.

[19]   Ying QL, Nichols J, Chambers I, Smith A. BMP induction of Id proteins suppresses differentiation and sustains embryonic stem cell self-renewal in collaboration with STAT3. Cell. 2003 Oct 31; 115(3): 281-92.

[20]   Smith AG. Embryo-derived stem cells: of mice and men. Annu Rev Cell Dev Biol. 2001; 17: 435-62.

[21]   Xiao L, Yuan X, Sharkis SJ. Activin A maintains self-renewal and regulates fibroblast growth factor, Wnt, and bone morphogenic protein pathways in human embryonic stem cells. Stem Cells. 2006 Jun; 24(6): 1476-86.

[22]   Chin MH, Mason MJ, Xie W, Volinia S, Singer M, Peterson C, et al. Induced pluripotent stem cells and embryonic stem cells are distinguished by gene expression signatures. Cell Stem Cell. 2009 Jul 2; 5(1): 111-23.

[23]   Wilson KD, Venkatasubrahmanyam S, Jia F, Sun N, Butte AJ, Wu JC. MicroRNA profiling of human-induced pluripotent stem cells. Stem Cells Dev. 2009 Jun; 18(5): 749-58.

[24]   Marchetto MC, Yeo GW, Kainohana O, Marsala M, Gage FH, Muotri AR. Transcriptional signature and memory retention of human-induced pluripotent stem cells. PLoS One. 2009; 4(9): e7076.

[25]   Ghosh Z, Wilson KD, Wu Y, Hu S, Quertermous T, Wu JC. Persistent donor cell gene expression among human induced pluripotent stem cells contributes to differences with human embryonic stem cells. PLoS One. 2010; 5(2): e8975.

[26]   Zhao T, Zhang ZN, Rong Z, Xu Y. Immunogenicity of induced pluripotent stem cells. Nature. 2011 Jun 9; 474(7350): 212-5.

[27]   Araki R, Uda M, Hoki Y, Sunayama M, Nakamura M, Ando S, et al. Negligible immunogenicity of terminally differentiated cells derived from induced pluripotent or embryonic stem cells. Nature. 2013 Feb 7; 494(7435): 100-4.

[28]   Nelson TJ, Martinez-Fernandez A, Terzic A. Induced pluripotent stem cells: developmental biology to regenerative medicine. Nat Rev Cardiol. 2010 Dec; 7(12): 700-10.

[29]   Kobayashi T, Yamaguchi T, Hamanaka S, Kato-Itoh M, Yamazaki Y, Ibata M, et al. Generation of rat pancreas in mouse by interspecific blastocyst injection of pluripotent stem cells. Cell. 2010 Sep 3; 142(5): 787-99.

[30]   Nelson TJ, Martinez-Fernandez A, Yamada S, Perez-Terzic C, Ikeda Y, Terzic A. Repair of acute myocardial infarction by human stemness factors induced pluripotent stem cells. Circulation. 2009 Aug 4; 120(5): 408-16.

[31]   Polo JM, Liu S, Figueroa ME, Kulalert W, Eminli S, Tan KY, et al. Cell type of origin influences the molecular and functional properties of mouse induced pluripotent stem cells. Nat Biotechnol. 2010 Aug; 28(8): 848-55.

[32]   Bar-Nur O, Russ HA, Efrat S, Benvenisty N. Epigenetic memory and preferential lineage-specific differentiation in induced pluripotent stem cells derived from human pancreatic islet beta cells. Cell Stem Cell. 2011 Jul 8; 9(1): 17-23.

[33]   Mauritz C, Schwanke K, Reppel M, Neef S, Katsirntaki K, Maier LS, et al. Generation of functional murine cardiac myocytes from induced pluripotent stem cells. Circulation. 2008 Jul 29; 118(5): 507-17.

[34]   Carpenter L, Carr C, Yang CT, Stuckey DJ, Clarke K, Watt SM. Efficient differentiation of human induced pluripotent stem cells generates cardiac cells that provide protection following myocardial infarction in the rat. Stem Cells Dev. 2011 Apr 10; 21(6): 977-86.

[35]   Narazaki G, Uosaki H, Teranishi M, Okita K, Kim B, Matsuoka S, et al. Directed and systematic differentiation of cardiovascular cells from mouse induced pluripotent stem cells. Circulation. 2008 Jul 29; 118(5): 498-506.

[36]   Schenke-Layland K, Rhodes KE, Angelis E, Butylkova Y, Heydarkhan-Hagvall S, Gekas C, et al. Reprogrammed mouse fibroblasts differentiate into cells of the cardiovascular and hematopoietic lineages. Stem Cells. 2008 Jun; 26(6): 1537-46.

[37]   Taura D, Sone M, Homma K, Oyamada N, Takahashi K, Tamura N, et al. Induction and isolation of vascular cells from human induced pluripotent stem cells--brief report. Arterioscler Thromb Vasc Biol. 2009 Jul; 29(7): 1100-3.

[38]   Mauritz C, Martens A, Rojas SV, Schnick T, Rathert C, Schecker N, et al. Induced pluripotent stem cell (iPSC)-derived Flk-1 progenitor cells engraft, differentiate, and improve heart function in a mouse model of acute myocardial infarction. Eur Heart J. 2011 Nov; 32(21): 2634-41.

[39]   Moretti A, Bellin M, Jung CB, Thies TM, Takashima Y, Bernshausen A, et al. Mouse and human induced pluripotent stem cells as a source for multipotent Isl1+ cardiovascular progenitors. FASEB J. 2009 Mar; 24(3): 700-11.

[40]   Xi J, Khalil M, Shishechian N, Hannes T, Pfannkuche K, Liang H, et al. Comparison of contractile behavior of native murine ventricular tissue and cardiomyocytes derived from embryonic or induced pluripotent stem cells. FASEB J. 2010 Aug; 24(8): 2739-51.

[41]   Mummery C, Ward-van Oostwaard D, Doevendans P, Spijker R, van den Brink S, Hassink R, et al. Differentiation of human embryonic stem cells to cardiomyocytes: role of coculture with visceral endoderm-like cells. Circulation. 2003 Jun 3; 107(21): 2733-40.

[42]   Burridge PW, Anderson D, Priddle H, Barbadillo Munoz MD, Chamberlain S, Allegrucci C, et al. Improved human embryonic stem cell embryoid body homogeneity and cardiomyocyte differentiation from a novel V-96 plate aggregation system highlights interline variability. Stem Cells. 2007 Apr; 25(4): 929-38.

[43]   Burridge PW, Thompson S, Millrod MA, Weinberg S, Yuan X, Peters A, et al. A universal system for highly efficient cardiac differentiation of human induced pluripotent stem cells that eliminates interline variability. PLoS One. 2011; 6(4): e18293.

[44]   Elliott DA, Braam SR, Koutsis K, Ng ES, Jenny R, Lagerqvist EL, et al. NKX2-5(eGFP/w) hESCs for isolation of human cardiac progenitors and cardiomyocytes. Nat Methods. 2011 Dec; 8(12): 1037-40.

[45]   Zhang J, Klos M, Wilson GF, Herman AM, Lian X, Raval KK, et al. Extracellular matrix promotes highly efficient cardiac differentiation of human pluripotent stem cells: the matrix sandwich method. Circ Res. 2012 Oct 12; 111(9): 1125-36.

[46]   Blin G, Nury D, Stefanovic S, Neri T, Guillevic O, Brinon B, et al. A purified population of multipotent cardiovascular progenitors derived from primate pluripotent stem cells engrafts in postmyocardial infarcted nonhuman primates. J Clin Invest. 2010 Apr; 120(4): 1125-39.

[47]   Chan SS, Li HJ, Hsueh YC, Lee DS, Chen JH, Hwang SM, et al. Fibroblast growth factor-10 promotes cardiomyocyte differentiation from embryonic and induced pluripotent stem cells. PLoS One. 2011; 5(12): e14414.

[48]   Yuasa S, Itabashi Y, Koshimizu U, Tanaka T, Sugimura K, Kinoshita M, et al. Transient inhibition of BMP signaling by Noggin induces cardiomyocyte differentiation of mouse embryonic stem cells. Nat Biotechnol. 2005 May; 23(5): 607-11.

[49]   Lian X, Hsiao C, Wilson G, Zhu K, Hazeltine LB, Azarin SM, et al. Robust cardiomyocyte differentiation from human pluripotent stem cells via temporal modulation of canonical Wnt signaling. Proc Natl Acad Sci U S A. 2012 Jul 3; 109(27): E1848-57.

[50] Willems E, Spiering S, Davidovics H, Lanier M, Xia Z, Dawson M, et al. Small-molecule inhibitors of the Wnt pathway potently promote cardiomyocytes from human embryonic stem cell-derived mesoderm. Circ Res. 2011 Aug 5; 109(4): 360-4.

[51] Ren Y, Lee MY, Schliffke S, Paavola J, Amos PJ, Ge X, et al. Small molecule Wnt inhibitors enhance the efficiency of BMP-4-directed cardiac differentiation of human pluripotent stem cells. J Mol Cell Cardiol. 2011 Sep; 51(3): 280-7.

[52] Naito AT, Shiojima I, Akazawa H, Hidaka K, Morisaki T, Kikuchi A, et al. Developmental stage-specific biphasic roles of Wnt/beta-catenin signaling in cardiomyogenesis and hematopoiesis. Proc Natl Acad Sci U S A. 2006 Dec 26; 103(52): 19812-7.

[53] Ueno S, Weidinger G, Osugi T, Kohn AD, Golob JL, Pabon L, et al. Biphasic role for Wnt/beta-catenin signaling in cardiac specification in zebrafish and embryonic stem cells. Proc Natl Acad Sci U S A. 2007 Jun 5; 104(23): 9685-90.

[54] Kwon C, Arnold J, Hsiao EC, Taketo MM, Conklin BR, Srivastava D. Canonical Wnt signaling is a positive regulator of mammalian cardiac progenitors. Proc Natl Acad Sci U S A. 2007 Jun 26; 104(26): 10894-9.

[55] Kattman SJ, Witty AD, Gagliardi M, Dubois NC, Niapour M, Hotta A, et al. Stage-specific optimization of activin/nodal and BMP signaling promotes cardiac differentiation of mouse and human pluripotent stem cell lines. Cell Stem Cell. 2011 Feb 4; 8(2): 228-40.

[56] Kitamura R, Takahashi T, Nakajima N, Isodono K, Asada S, Ueno H, et al. Stage-specific role of endogenous Smad2 activation in cardiomyogenesis of embryonic stem cells. Circ Res. 2007 Jul 6; 101(1): 78-87.

[57] Willems E, Cabral-Teixeira J, Schade D, Cai W, Reeves P, Bushway PJ, et al. Small molecule-mediated TGF-beta type II receptor degradation promotes cardiomyogenesis in embryonic stem cells. Cell Stem Cell. 2012 Aug 3; 11(2): 242-52.

[58] Jang J, Ku SY, Kim JE, Choi K, Kim YY, Kim HS, et al. Notch inhibition promotes human embryonic stem cell-derived cardiac mesoderm differentiation. Stem Cells. 2008 Nov; 26(11): 2782-90.

[59] Cao N, Liu Z, Chen Z, Wang J, Chen T, Zhao X, et al. Ascorbic acid enhances the cardiac differentiation of induced pluripotent stem cells through promoting the proliferation of cardiac progenitor cells. Cell Res. 2011 Jan; 22(1): 219-36.

[60] Xu C, Police S, Rao N, Carpenter MK. Characterization and enrichment of cardiomyocytes derived from human embryonic stem cells. Circ Res. 2002 Sep 20; 91(6): 501-8.

[61] Shimoji K, Yuasa S, Onizuka T, Hattori F, Tanaka T, Hara M, et al. G-CSF promotes the proliferation of developing cardiomyocytes in vivo and in derivation from ESCs and iPSCs. Cell Stem Cell. 2010 Mar 5; 6(3): 227-37.

[62] Fujiwara M, Yan P, Otsuji TG, Narazaki G, Uosaki H, Fukushima H, et al. Induction and enhancement of cardiac cell differentiation from mouse and human induced pluripotent stem cells with cyclosporin-A. PLoS One. 2011; 6(2): e16734.

[63] Efe JA, Hilcove S, Kim J, Zhou H, Ouyang K, Wang G, et al. Conversion of mouse fibroblasts into cardiomyocytes using a direct reprogramming strategy. Nat Cell Biol. 2011 Mar; 13(3): 215-22.

[64] Margariti A, Winkler B, Karamariti E, Zampetaki A, Tsai TN, Baban D, et al. Direct reprogramming of fibroblasts into endothelial cells capable of angiogenesis and reendothelialization in tissue-engineered vessels. Proc Natl Acad Sci U S A. 2012 Aug 21; 109(34): 13793-8.

[65] Takeuchi JK, Bruneau BG. Directed transdifferentiation of mouse mesoderm to heart tissue by defined factors. Nature. 2009 Jun 4; 459(7247): 708-11.

[66] Ieda M, Fu JD, Delgado-Olguin P, Vedantham V, Hayashi Y, Bruneau BG, et al. Direct reprogramming of fibroblasts into functional cardiomyocytes by defined factors. Cell. 2010 Aug 6; 142(3): 375-86.

[67] Qian L, Huang Y, Spencer CI, Foley A, Vedantham V, Liu L, et al. In vivo reprogramming of murine cardiac fibroblasts into induced cardiomyocytes. Nature. 2012 May 31; 485(7400): 593-8.

[68] Srivastava D, Ieda M, Fu J, Qian L. Cardiac repair with thymosin beta4 and cardiac reprogramming factors. Ann N Y Acad Sci. 2012 Oct; 1270: 66-72.

[69] Song K, Nam YJ, Luo X, Qi X, Tan W, Huang GN, et al. Heart repair by reprogramming non-myocytes with cardiac transcription factors. Nature. 2012 May 31; 485(7400): 599-604.

[70] Chen JX, Krane M, Deutsch MA, Wang L, Rav-Acha M, Gregoire S, et al. Inefficient reprogramming of fibroblasts into cardiomyocytes using Gata4, Mef2c, and Tbx5. Circ Res. 2012 Jun 22; 111(1): 50-5.

[71] Jayawardena TM, Egemnazarov B, Finch EA, Zhang L, Payne JA, Pandya K, et al. MicroRNA-mediated in vitro and in vivo direct reprogramming of cardiac fibroblasts to cardiomyocytes. Circ Res. 2012 May 25; 110(11): 1465-73.

[72] Rane AA, Christman KL. Biomaterials for the treatment of myocardial infarction: a 5-year update. J Am Coll Cardiol. 2011 Dec 13; 58(25): 2615-29.

[73] Matsuura K, Wada M, Shimizu T, Haraguchi Y, Sato F, Sugiyama K, et al. Creation of human cardiac cell sheets using pluripotent stem cells. Biochem Biophys Res Commun. 2012 Aug 24; 425(2): 321-7.

[74] Tulloch NL, Muskheli V, Razumova MV, Korte FS, Regnier M, Hauch KD, et al. Growth of engineered human myocardium with mechanical loading and vascular coculture. Circ Res. 2011 Jun 24; 109(1): 47-59.

[75] Dai B, Huang W, Xu M, Millard RW, Gao MH, Hammond HK, et al. Reduced collagen deposition in infarcted myocardium facilitates induced pluripotent stem cell engraftment and angiomyogenesis for improvement of left ventricular function. J Am Coll Cardiol. 2011 Nov 8; 58(20): 2118-27.

[76] Kawamura M, Miyagawa S, Miki K, Saito A, Fukushima S, Higuchi T, et al. Feasibility, safety, and therapeutic efficacy of human induced pluripotent stem cell-derived cardiomyocyte sheets in a porcine ischemic cardiomyopathy model. Circulation. 2012 Sep 11; 126(11 Suppl 1): S29-37.

[77] Shiba Y, Fernandes S, Zhu WZ, Filice D, Muskheli V, Kim J, et al. Human ES-cell-derived cardiomyocytes electrically couple and suppress arrhythmias in injured hearts. Nature. 2012 Sep 13; 489(7415): 322-5.

[78] Bellin M, Marchetto MC, Gage FH, Mummery CL. Induced pluripotent stem cells: the new patient? Nat Rev Mol Cell Biol. 2012 Nov; 13(11): 713-26.

[79] Carvajal-Vergara X, Sevilla A, D'Souza SL, Ang YS, Schaniel C, Lee DF, et al. Patient-specific induced pluripotent stem-cell-derived models of LEOPARD syndrome. Nature. 2010 Jun 10; 465(7299): 808-12.

[80] Moretti A, Bellin M, Welling A, Jung CB, Lam JT, Bott-Flugel L, et al. Patient-specific induced pluripotent stem-cell models for long-QT syndrome. N Engl J Med. 2010 Oct 7; 363(15): 1397-409.

[81] Itzhaki I, Maizels L, Huber I, Zwi-Dantsis L, Caspi O, Winterstern A, et al. Modelling the long QT syndrome with induced pluripotent stem cells. Nature. 2011 Mar 10; 471(7337): 225-9.

[82] Yazawa M, Hsueh B, Jia X, Pasca AM, Bernstein JA, Hallmayer J, et al. Using induced pluripotent stem cells to investigate cardiac phenotypes in Timothy syndrome. Nature. 2011 Mar 10; 471(7337): 230-4.

[83]   Lahti AL, Kujala VJ, Chapman H, Koivisto AP, Pekkanen-Mattila M, Kerkela E, et al. Model for long QT syndrome type 2 using human iPS cells demonstrates arrhythmogenic characteristics in cell culture. Dis Model Mech. 2011 Mar; 5(2): 220-30.

[84]   Sun N, Yazawa M, Liu J, Han L, Sanchez-Freire V, Abilez OJ, et al. Patient-specific induced pluripotent stem cells as a model for familial dilated cardiomyopathy. Sci Transl Med. 2012 Apr 18; 4(130): 130ra47.

[85]   Davis RP, Casini S, van den Berg CW, Hoekstra M, Remme CA, Dambrot C, et al. Cardiomyocytes derived from pluripotent stem cells recapitulate electrophysiological characteristics of an overlap syndrome of cardiac sodium channel disease. Circulation. 2012 Jun 26; 125(25): 3079-91.

[86]   Jung CB, Moretti A, Mederos y Schnitzler M, Iop L, Storch U, Bellin M, et al. Dantrolene rescues arrhythmogenic RYR2 defect in a patient-specific stem cell model of catecholaminergic polymorphic ventricular tachycardia. EMBO Mol Med. 2011 Mar; 4(3): 180-91.

FIGURE LEGENDS:

Figure 1. Strategies of regenerative therapy for cardiac tissue. Cardiomyocytes (CMs) can be successfully derived from iPS cells by *in vitro* treatment with different cytokines and cardiac growth factors. A protocol for partial somatic cell reprogramming involves over-expression of the OSKM factors (Oct4, Sox2, Klf4, and c-Myc) and culture with an inhibitor of the JAK–STAT signaling pathway (JAKi), without clonal isolation of iPS cells. This method of cardiac differentiation has been used to quickly and efficiently generate CMs. Furthermore, by over-expressing cardiac transcription factors (Gata4, Mef2c, and Tbx5), CMs can be directly obtained from somatic cells without entry into the pluripotent state. Using this technique, resident non-myocytes in the murine heart can be reprogrammed into CM-like cells *in vivo* by local delivery of these transcription factors.

Figure 2. Clinical applications of iPS cells. Generation of iPS cells from somatic cells have broadened the horizon for regenerative therapy. These cells offer the potential to model and treat human disease. Patient-specific iPS cells can be derived from somatic cells by ectopic expression of the *Oct3/4*, *Sox2*, *Klf4* and *c-Myc* transcription factors. These iPS cells can then be differentiated *in vitro* into the desired cell subtype, producing a model of the patient´s disease that can be used to screen potential drug therapies. Alternatively, iPS cells derived from a patient with a known mutation could be genetically repaired, differentiated into any desired tissue, and then transplanted into the patient. Thus, the derivation of iPS cells presents great potential for stem cell therapy. However, it will be necessary to generate a reproducible differentiation system before establishing patient-specific disease models, which could be used for drug screening, target validation, and autologous cell-replacement therapies.
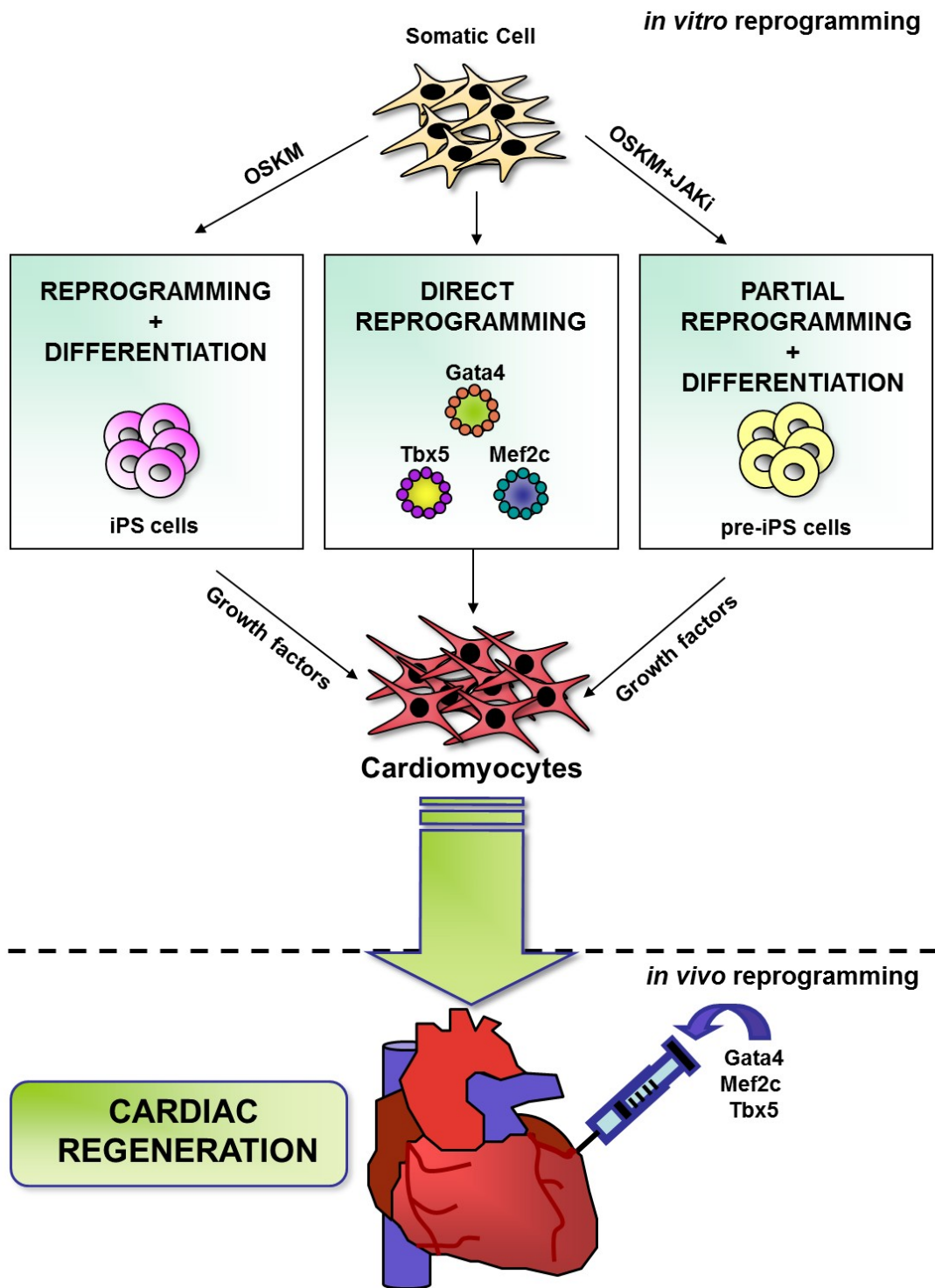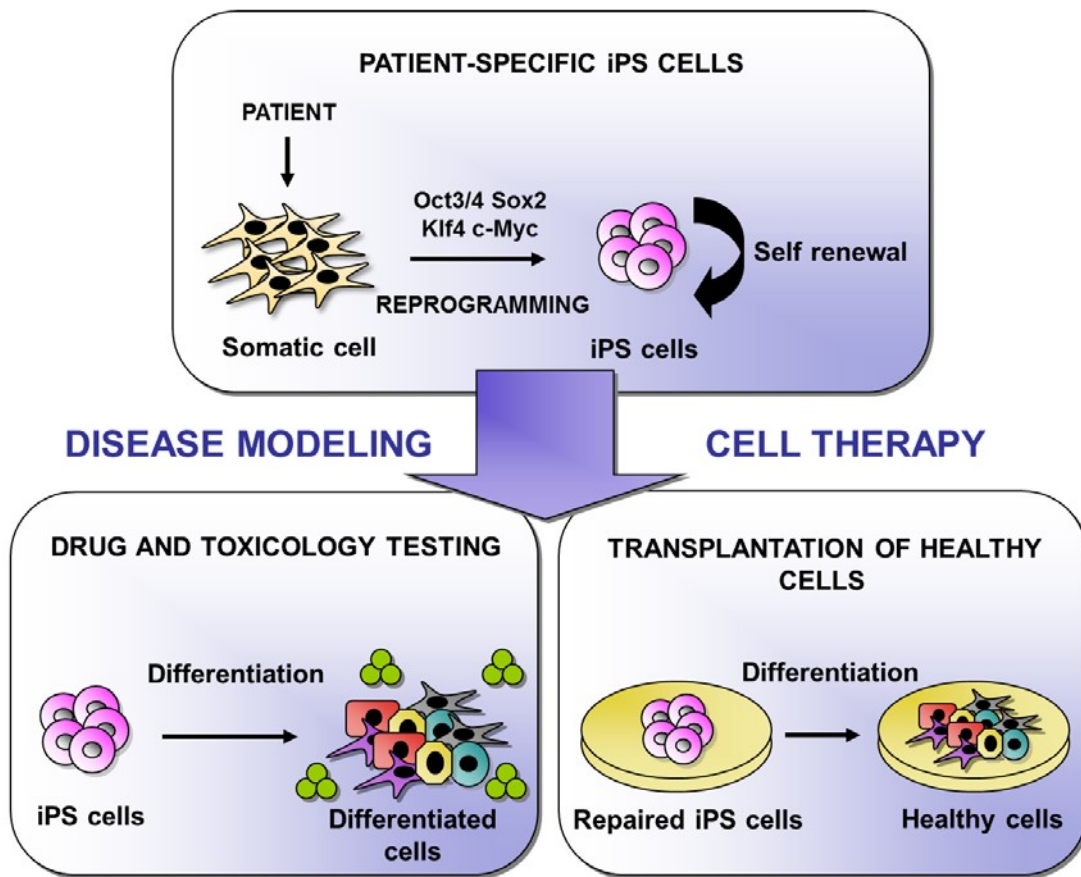
Figure 1

Figure 2